UNIVERSIDAD AUTÓNOMA DE MADRID

DEPARTAMENTO DE BIOQUÍMICA

Design and development of novel therapeutic strategies targeting K-Ras driven Pancreatic Ductal Adenocarcinoma

DOCTORAL THESIS

María Teresa Blasco Lázaro

DEPARTAMENTO DE BIOQUÍMICA

Facultad de Medicina

UNIVERSIDAD AUTÓNOMA DE MADRID

Design and development of novel therapeutic strategies targeting K-Ras driven Pancreatic Ductal Adenocarcinoma

DOCTORAL THESIS

María Teresa Blasco Lázaro

Biology B.S

Biochemistry and Biomedicine M.S

Directors:

Dr. Mariano Barbacid

Dr. Carmen Guerra

Centro Nacional de Investigaciones Oncológicas

cnio
Centro Nacional
de Investigaciones
Oncológicas

Dr. Mariano Barbacid Montalbán, director of the Experimental Oncology Group at the Spanish National Cancer Research Center (CNIO)

and

Dr. Carmen Guerra González, staff scientist of the Experimental Oncology group at the Spanish National Cancer Research Center (CNIO)

Hereby certify that the Doctoral Thesis "Design and development of novel therapeutic strategies against K-Ras driven Pancreatic Ductal Adenocarcinoma", submitted by María Teresa Blasco Lázaro for the degree of Dr. of Philosophy and carried out under of the undersigned in the Experimental Oncology Group at Spanish National Cancer Research Center (CNIO), duly meets the requirements laid out by the Spanish RD 1393/2007 and the Autonoma University of Madrid.

Madrid, April 24th 2017

Melchor Fernández Almagro, 3
E-28029 Madrid
Tel. +34 91 224 69 00
Fax +34 91 732 80 80

“En la vida no hay nada que temer, sólo hay que comprender”

“Nothing in life is to be feared, it is only to be understood”

Marie Curie

Acknowledgements

I would like to acknowledge Mariano Barbacid for giving me the opportunity to carry out my PhD in Experimental Oncology Laboratory. Especially, Carmen Guerra for her support, guidance and positivity over these years.

I am very grateful to all the people that have participated in this work and all heads and technicians of the CNIO Core Units, especially the Animal Facility, Molecular Imaging, Histopathology, Confocal Microscopy and Transgenic Mice units.

Thank you to all past and present members of Experimental Oncology group for their support and help and for making me smile everyday. It was a pleasure to do the PhD at the CNIO where I have found so many good people and friends.

And finally, I want to dedicate this thesis to my friends, Javi and my lovely family for their unwavering support. Thank you, because without you it would have been impossible to reach the end.

Y finalmente, quiero agradecer a mis amigos, a Javi y a mi querida familia su apoyo incondicional durante todos estos años. Gracias, porque sin vosotros hubiera sido imposible llegar hasta el final.

i. Summary

Summary

Genetic elimination of Egfr in a *K-Ras* driven Pancreatic Ductal Adenocarcinoma (PDAC) mouse model prevents tumor development. However, it was unknown whether the inhibition of Egfr tyrosine kinase activity could be a suitable therapy for *K-Ras* driven PDAC patients. In this thesis, we have demonstrated that Egfr catalytic activity is essential for PanIN and PDAC initiation even in the context of chronic pancreatitis and in the absence of *p16Ink4a*/*p19Arf* tumor suppressor genes. Nevertheless, inactivation of Egfr is not sufficient to inhibit tumor development of aggressive *K-Ras*^{G12V};p53-null adenocarcinomas. In this context, it has been determined that ErbB2 plays a critical role triggering Egfr phosphorylation and MAPK signaling activation.

Recently, it was demonstrated that c-Raf, a downstream mediator of K-Ras, is essential for the initiation of *K-Ras* driven PDAC. Unfortunately, in a p53 deficient background, ablation of either Egfr or c-Raf, as well as expression of an Egfr kinase dead receptor is not sufficient to inhibit tumor appearance although tumors develop with significant longer latencies. The extensive crosstalk between redundant signaling pathways in tumor cells suggests that concurrent inhibition of multiple effector pathways could be a promising therapeutic strategy to induce conclusive responses. Consistent with this, it was determined that simultaneous elimination of Egfr and c-Raf, in a p53 deficient context, completely blocks PDAC initiation.

Of note, these and other studies were performed using GEMMs that only reveal the effect of selected targets in first stages of pancreatic tumorigenesis. The development of a new PDAC therapeutic mouse model has allowed us to address the therapeutic value of Egfr inhibition and its combination with c-Raf in full-blown tumors. Elimination or inhibition of Egfr in established tumors demonstrates that its function is dispensable for PDAC maintenance and progression, whereas combined ablation of Egfr and c-Raf results in a significant therapeutic effect. Nonetheless, few tumors can progress upon target elimination, suggesting the existence of tumor heterogeneity and indicating that other signaling pathways are involved in this response. Future studies will address this issue to find better therapeutic combinations.

Resumen

La eliminación genética de Egfr en un modelo murino de Adenocarcinoma Ductal pancreático (PDAC) inducido por el oncogén *K-Ras* impide el desarrollo tumoral. Sin embargo, se desconoce si la inhibición de la actividad tirosina quinasa de Egfr podría ser una terapia adecuada para pacientes de PDAC. En esta tesis hemos demostrado que la actividad catalítica de Egfr es esencial para desarrollo de lesiones PanIN y PDAC incluso en el contexto de pancreatitis crónica y en la ausencia de los genes supresores de tumores *p16Ink4a*/*p19Arf*. Sin embargo, la inactivación de Egfr no es suficiente para inhibir el desarrollo tumoral en ausencia de p53. En este contexto, se ha determinado que ErbB2 juega un papel importante en la fosforilación de Egfr y en la activación de la vía de señalización MAPK.

Recientemente se ha demostrado que c-Raf, un intermediario de la vía de K-Ras, es esencial para la iniciación de PanIN y PDAC inducidos por el oncogén K-Ras. Lamentablemente, en ausencia de p53, la eliminación o inhibición de Egfr así como de c-Raf retrasa pero no impide la aparición de PDAC. La gran interacción y redundancia entre distintas vías de señalización en células tumorales sugiere que la inhibición simultánea de varias vías de señalización podría ser una estrategia terapéutica prometedora para inducir respuestas más concluyentes. De acuerdo con esto, se ha descubierto que la deleción simultánea de Egfr y c-Raf, en ausencia de p53, bloquea completamente la aparición de tumores.

Cabe destacar, que estos y otros estudios se han realizado utilizando modelos animales que sólo permiten estudiar el efecto de las dianas de interés durante las primeras etapas del desarrollo tumoral. La generación de un nuevo modelo de ratón terapéutico de PDAC nos ha permitido abordar el efecto de inhibir Egfr y su combinación con c-Raf en la progresión tumoral. La eliminación o inhibición de Egfr en tumores ya establecidos es prescindible para la progresión de PDAC, mientras que la eliminación simultánea de Egfr y c-Raf resulta en un efecto terapéutico significativo. No obstante, en ausencia de las dianas, algunos de los tumores continúan progresando, lo que sugiere la existencia de heterogeneidad tumoral y de otras vías de señalización implicadas en esta respuesta. Futuros estudios abordarán este problema en busca de mejores combinaciones.

ii. Contents

iii. Abbreviations

Adeno-CreGFP: Adenovirus expressing the Cre-recombinase and GFP

ADEX: Aberrantly Differentiated Endocrine exocrine tumor

ADM: Acinar to Ductal Metaplasia

ARG: Amphiregulin

ATP: Adenosine Tri-Phosphate

bp: base pair

BRCA1: Breast Cancer 1 susceptibility protein

BRCA2: Breast Cancer 2 susceptibility protein

BSA: Bovine Serum Albumin

BTC: Betacellulin

CAFs: Cancer Associated Fibroblasts

CBS: Calf Bovine Serum

Cdk4: Cyclin-dependent kinase 4

CDKN2A: Cyclin-Dependent Kinase Inhibitor 2A

cDNA : Complementary DNA

CreERT2: tamoxifen inducible Cre-Estrogen Receptor (ER) fusion protein

Crk: CT10 regulator of kinase

Ct: Comparative cycle Threshold

CTGF: Connective Tissue Growth Factor

DAG: 1,2diacilglecerol

DMEM: Dulbecco´s Modified Eagle´s Medium

DMSO: Dimethyl Sulfoxide

DNA: Deoxyribonucleic acid

DNase: Deoxyribonuclease

dNTP: Deoxynucleotide

DRS: Dual Recombinase System

DTT: Dithiothrietol

EDTA: Ethylene Diamine Tetraacetic Acid

EGF: Epidermal Growth Factor

EGFR: Epidermal Growth Factor Receptor

EGN: Epigen

EGTA: Ethylene Glycol Tetraacetic Acid

ENU: N-Ethyl-N-Nitrosourea

EPR: Epiregulin

ERK1: Extracellular signal Regulated Kinases 1

ERK2: Extracellular signal Regulated Kinases 2

ES: Embryonic Stem cells

EtOH: Ethanol

FBS: Fetal Bovine Serum

FDA: Food and Drug Administration

GAP: GTPase-Activating Protein

GAPDH: Glyceraldehyde 3-Phosphate Dehydrogenase

GBM: Glioblastoma Multiforme

GDP: Guanosine Diphosphate

GEF: Guanine nucleotide Exchange Factor

GEMM: Genetically Engineered Mouse Model

GPCR: G-Protein Coupled Receptors

Grb2: Growth Factor Receptor-bound protein 2

GTP: Guanosine Triphosphate

HB-EGF: Heparin-Binding EGF-like growth factor

HBSS: Hank´s Balanced Salt Solution

H&E: Hematoxylin and Eosin

HRP: Horseradish Peroxidase

hUBC: Human Ubiquitin C

IKBKE: IκB-related kinase

IP: Immunoprecipitation

IP_3: Inositol-1,4,5-triphosphate

IPMN: Intraductal Papillary Mucinous Neoplasms

IRES: Internal Ribosomal Entry Site

JAK: Janus Kinase

JNK: c-Jun N-terminal kinases

KDM6A: Lysine-specific Demethylase 6A

LSL: Lox-STOP-Lox

MAPK: Mitogen Activated Protein Kinase

MCN: Mucinous Cystic Neoplasms

MEF: Mouse Embryonic Fibroblast

MEK1: Mitogen Activating Protein Kinase 1

MEK2: Mitogen Activating Protein Kinase 2

MOI: Multiplicity of Infection

MTT: 3-(4,5-dimethylthiazol-2-yl)-2,5-diphenyltetrazolium bromide

Nck: Non-catalytic region of tyrosine kinase *adaptor protein*

Neo: Neomycin

NFR: Nuclear Fast Red

NSAIDs: Non-Steroidal Anti-Inflammatory Drugs

NSCLC: Non-Small Cell Lung Cancer

OCT: Optimum Cutting Temperature compound

PanIN: Pancreatic Intraepithelial Neoplasia

PBS: Phosphate Buffered Saline

PCR: Polymerase Chain Reaction

PDAC: Pancreatic Ductal Adenocarcinoma

PDX: Patient-Derived Xenografts

Pdx1: Pancreatic and Duodenal Homeobox 1

PI3K: Phosphoinositol-3-kinase

PIK3CA: Phosphatidylinositol-4,5-Bisphosphate 3-Kinase Catalytic Subunit Alpha

PKC: Protein Kinase C

PLCγ: Phospholipase C gamma

PLCε: Phospholipase C epsilon

PRSS1: Protease Serine 1

PTB: Phosphotyrosine Binding

PTEN: Phosphatase and Tensin homolog

qRT-PCR: Quantitative Reverse Transcription Polymerase Chain Reaction

RAF: Rapidly Accelerated Fibrosarcoma

RalGDS: Ral Guanine Nucleotide Dissociation Stimulator

RalGEFs: Ral Guanine Nucleotide Exchange Factor

Rb: Retinoblastoma

ROS: Reactive Oxygen Species

RNA: Ribonucleic acid

RT: Room Temperature

RTC: Rat-Tail Collagen type I

RTK: Receptor Tyrosine Kinase

RT-PCR: Reverse Transcription Polymerase Chain Reaction

SDS: Sodium Dodecyl Sulfate

SH2: Src homology 2

Shc: Src Homology 2 domain Containing protein

Shh: Sonic hedgehog

shRNA: short hairpin RNA

SSC: Saline Sodium Citrate

STAT: Signal Transducer and Activator of Transcription

STK11: Serine/Threonine Kinase 11 Interacting Protein

TAE: Tris Acetate EDTA

TAM: Tamoxifen

Taq-Polymerase: *Thermus aquaticus* DNA Polymerase

TBS: Tris Buffered Saline

TBST: Tris Buffered Saline with Tween

Tg: Transgenic

TGFα: Transforming Growth Factor α

TGFβ: Transforming Growth Factor β

TKI: Tyrosine Kinase Inhibitors

UV: Ultraviolet

WT: Wild Type

X-Gal: 5-bromo-4-chloro-3-indolyl-β-D-galactopyranoside

WCE: Whole-Cell Extracts

Yap-1: Yes-associated protein 1

4-Hydroxytamoxifen (4-OHT)

1. Introduction

1.1. Pancreatic Ductal Adenocarcinoma

1.1.1. Epidemiology and risk factors

Pancreatic ductal adenocarcinoma (PDAC) is the fourth leading cause of cancer death in developed countries. Worldwide, PDAC accounts for more than 200,000 deaths every year. Total deaths are currently increasing, and it is predicted to be the second leading cause of cancer death by 2030 (Siegel et al., 2017).

PDAC is associated with a very poor prognosis, with a 5-year survival rate of only 6% and a median survival of less than 6 months (Ying et al., 2016). This low survival rate is attributed to several factors, of which perhaps the most important is the late stage at which most of the patients are diagnosed. Most of them are asymptomatic until the disease develops to an advanced stage. Only less than 20% of the patients are eligible for initial resection. Even after potential curative resection, most patients will eventually have recurrence, and 5-year survival of completely resected patients increases only up to 25%. In addition, PDAC is an aggressive type of cancer, and 80% of patients have locally advanced or metastatic PDAC at the time of diagnosis. Tumor biology of pancreatic cancer contributes to early recurrence and metastasis, and also resistance to chemotherapy and radiotherapy (Kamisawa et al., 2016).

Minimal improvements have been made in prevention, early diagnosis and treatment in patients with advanced disease. For more than a decade, gemcitabine has been the treatment of choice (Hidalgo, 2010). This chemotherapeutic agent became the standard regimen for treating advanced PDAC patients after a clinical trial in which was shown a significant improvement in the overall survival of gemcitabine comparing with 5-fluorouracil treated patients (Burris III et al., 1997). Since then, the combination of gemcitabine with a variety of cytotoxic and targeted agents has generally shown small or no significant benefit as compared to gemcitabine alone. Only the combination of gemcitabine with erlotinib, an Epidermal Growth Factor Receptor (EGFR) inhibitor, resulted in a significant but small improvement in overall survival, coming along with uncomfortable rash in patients (Moore et al., 2007). Following a phase III clinical trial, current treatment of choice is gemcitabine plus nab-paclitaxel (nanoparticle albumin-bound paclitaxel, a novel formulation of the classical chemotherapeutic paclitaxel), which is considered the gold standard of care (Von Hoff et al., 2013). However, there is still a lot of scope in improving the treatment of pancreatic cancer. The ability of preclinical models that recapitulate the human disease and a better understanding of PDAC biology are opening newer opportunities for treatment and increasing the number of new agents that are in clinical development (Ying et al., 2016).

Several risk factors for pancreatic cancer, such as a family history, as well as cigarette smoking, chronic pancreatitis, and diabetes mellitus have been identified. On top of this, pancreatic adenocarcinoma is a disease that is associated with advancing age. PDAC is rare

before the age of 40, but it culminates in a 40-fold increased risk by the age of 80 (Bardeesy and DePinho, 2002).

Environmental factors might modulate pancreatic adenocarcinoma risk. The most well established risk factor for pancreatic cancer is cigarette smoking, causing a 75% increased risk that persists at least 10 years after smoking cessation (Iodice et al., 2008). In addition, several studies provide evidence for a strong association between chronic pancreatitis and PDAC (Lowenfels et al., 1993; Malka et al., 2002). Importantly, pancreatitis is also considered an early indicator of PDAC (Malka et al., 2002; Raimondi et al., 2010). The risk correlates with the duration of recurrent pancreatitis and chronic inflammation (Raimondi et al., 2010). An even higher risk was found in patients with rare types of pancreatitis, such as hereditary pancreatitis and tropical pancreatitis (Lowenfels et al., 1997). However, it has been described that only about 4% of chronic pancreatitis patients will develop PDAC within 20 years of diagnosis (Lowenfels et al., 1993). In PDAC mouse models, it has been illustrated that pancreatitis is an essential component for tumor development when the expression of the *K-Ras* oncogene in acinar cells starts during adulthood (Guerra et al., 2007). Due to the connection between inflammatory processes and their role in carcinogenesis and neoplastic progression, aspirin and other non-steroidal anti-inflammatory drugs (NSAIDs) have attracted interest in cancer prevention. Notably, epidemiological studies have suggested a possible protective effect for long-term NSAIDs users in pancreatic cancer risk (Bonifazi et al., 2010; Rothwell et al., 2011; Streicher et al., 2014). Likewise, NSAIDs have shown a preventative and therapeutic effect in mice (Guerra et al., 2011).

Patients with diabetes have a 30% additional risk of pancreatic cancer, which persists for more than 20 years after initial diagnosis of the disease. At the time of the diagnosis about 25% of PDAC patients suffer from diabetes mellitus, and another 40% are pre-diabetic (Chari et al., 2008). Several studies suggest that hyperglycemia, abnormal glucose metabolism, and insulin resistance are correlated with increased risk of PDAC (Stocks et al., 2009).

Although the majority of pancreatic tumors appear to be sporadic, it is estimated that 10% of pancreatic cancers are due to an inherited predisposition (Hruban et al., 2010). However, the genetic basis for most familial pancreatic cancer remains unknown. PDAC development is a feature of several genetic syndromes, but these account for a few cases of familial pancreatic cancer (Solomon et al., 2012). Germline mutations in *Breast Cancer 2* (*BRCA2*) cause increased risk of breast, ovarian, and pancreatic cancer. According to this fact, Genetically Engineered Mouse Models (GEMMs) with loss of *Brca2* in pancreas display preneoplasic ductal lesions and even PDAC tumors when *p53* is lost (Rowley et al., 2011). Germline mutations in *Cyclin-Dependent Kinase Inhibitor 2A* (*CDKN2A)* which encodes two tumor suppressors*, p16INK4A and p14ARF,* cause familial atypical mole melanoma syndrome, in which patients have increased risk of both melanoma and pancreatic cancer (Slater et al., 2010). Patients with Peutz-Jeghers syndrome, caused by germline alterations in

Serine/Threonine Kinase 11 Interacting Protein (*STK11 or LKB1*), have a markedly increased risk of pancreatic cancer (Hearle et al., 2006). In GEMMs, homozygous loss of *Lkb1* in early pancreatic precursors promotes development of pancreatic mucinous cystadenomas with very short latencies (Morton et al., 2010). Patients with hereditary pancreatitis, which is associated with germline mutations in the cationic trypsinogen *Protease Serine 1* (*PRSS1*) gene, experience a 53-fold increased incidence of pancreatic adenocarcinoma. In this case the resulting inflammation promotes tumorigenesis, in part, by producing growth factors, cytokines and reactive oxygen species (ROS), thus inducing cell proliferation, disrupting cell differentiation and selecting for oncogenic mutations (Lowenfels et al., 1997). And finally, there is also accumulating evidence linking family history with PDAC, which refers to families with two or more first-degree relatives with PDAC that do not fulfill the criteria for another inherited predisposition syndrome explained above (Hruban et al., 2010).

1.1.2. Anatomy of pancreas

The pancreas is constituted of separate functional units that regulate two different processes: digestion and glucose metabolism. The exocrine pancreas is composed of acinar, centro-acinar and ductal cells. The acinar cells, which are organized in clusters, produce digestive enzymes and constitute approximately the 95% of total cells in the pancreas. The ducts, which add mucous and bicarbonate to the enzyme mixture in the pancreas, form a network of increasing size culminating in main pancreatic ducts that empty into the duodenum in response to the intestinal hormones secretin and cholecystokinin. Centro-acinar cells are defined as specialized ductal epithelial cells located at the terminal ductal tree in the acinar-ductal cell junction. Centro-acinar cells have been proposed to be adult multipotent progenitors that proliferate in response to chronic epithelial injury (Rovira et al., 2010). The endocrine pancreas consists of specialized cells that are organized into compact islets embedded within acinar tissue, islets of Langerhans, which secrete hormones into the bloodstream. The α- and β-cells regulate the use of glucose through the production of glucagon and insulin, respectively. Pancreatic polypeptide and somatostatin, that are produced in the PP and δ-cells, regulate the secretory properties of the other pancreatic cell types (Bardeesy and DePinho, 2002).

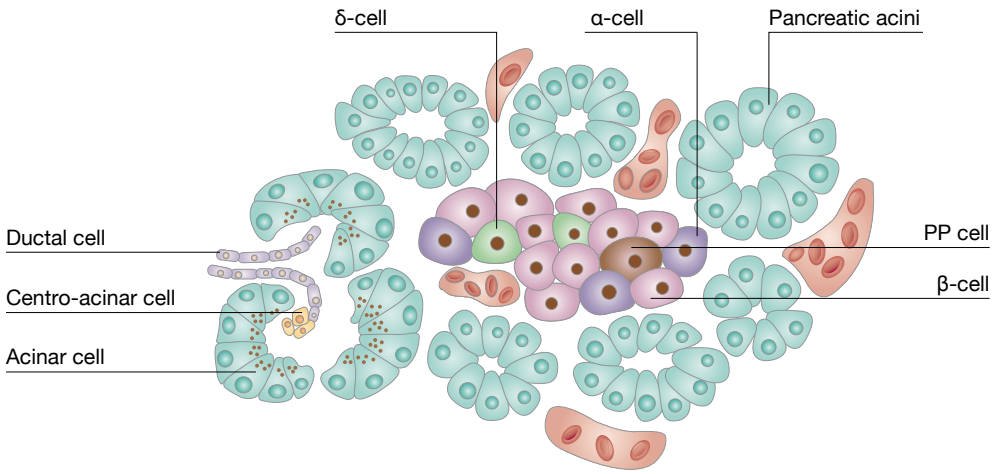

Figure 1. Anatomy of pancreas. (Adapted from Bardeesy and DePinho, 2002).

1.1.3. Histopathology and molecular pathology of Pancreatic Cancer

1.1.3.1. Histopathology of PDAC

PDAC evolves through a stepwise progression from well-defined and non-invasive precursor lesions that, in the context of their genetic features, define the genetic progression model of pancreatic carcinogenesis (Hruban et al., 2000).

Early disease histology manifests as several distinct types of precursor lesions. Most carcinomas arise from microscopic pancreatic intraepithelial neoplasia (PanIN) (Maitra and Hruban, 2008). PanIN lesions are classified into three grades according to the extent of cytological and architectural atypia: PanIN1A and PanIN1B (micropapillary type) show low-grade dysplasia; PanIN2 exhibits additional loss of polarity, nuclear crowding, cell enlargement, and hyperchromasia with frequent papillary formation; and PanIN3 (also known as *in situ* carcinoma) are advanced lesions with severe nuclear atypia, luminal necrosis, and manifest epithelial cell budding into the ductal lumen (Hruban et al., 2004; Sipos et al., 2009).

PanIN lesions are frequently associated with atrophy of acinar parenchyma followed by a reprogramming process known as acinar-to-ductal metaplasia (ADM). These structures have been proposed to be the precursors of PanIN lesions (Brune et al., 2006). Molecular analyses have demonstrated that PanIN harbors many of the same genetic alterations found in infiltrating PDAC (Hruban et al., 2007). These include activating point mutations in *K-RAS*, and inactivation of the *CDKN2A*, *TP53* and *SMAD4* genes (Hruban et al., 2007; Wilentz et al., 1998). Mutations in *K-RAS* and *CDKN2A* are early events, while *TP53* and *SMAD4* gene mutations are found in high grade lesions (PanIN3) (Figure 2) (Hruban et al., 2007; Yoshizawa et al., 2002). Interestingly, recently developed GEMMs in which a mutant *K-Ras* is expressed in the

pancreas (see section 1.1.9), develop PanIN lesions histologically identical to those found in humans, that eventually progress to invasive PDAC (Guerra et al., 2007; Hingorani et al., 2003).

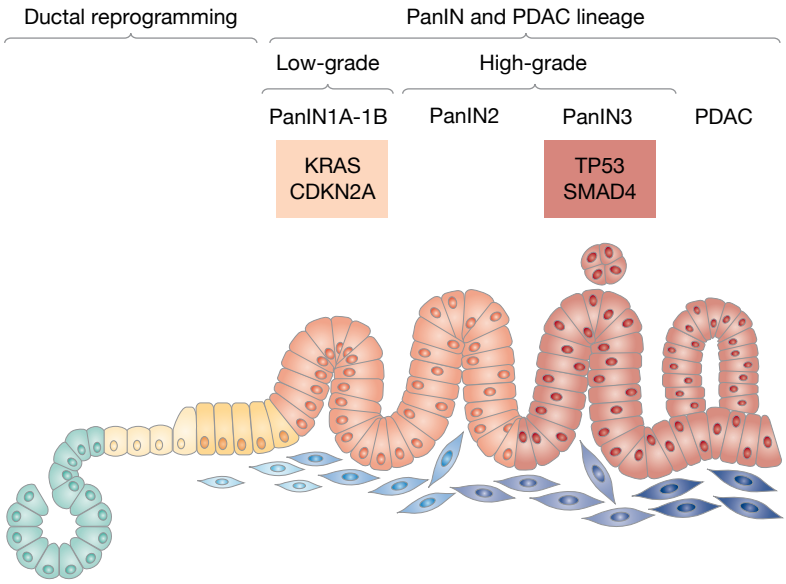

Figure 2. Histological, molecular and genetic hallmarks of human PDAC. Schematic diagram of the preneoplastic lesions and molecular changes that precede the development of PDAC (adapted from Morris et al., 2010a).

Some pancreatic ductal adenocarcinomas arise from other types of preneoplastic lesions: Intraductal Papillary Mucinous Neoplasms (IPMNs) and Mucinous Cystic Neoplasms (MCNs). IPMNs are grossly visible, non-invasive mucin-producing epithelial neoplasms, which usually form long finger-like papillae that are more than 1 cm in size. By definition, IPMNs, involve the main pancreatic duct or one of its branches and they arise, more frequently, in the head of the pancreas than in the tail (Hruban et al., 2007). A variety of molecular alterations have been reported in IPMNs. The frequency of *K-RAS* gene mutations raises with increasing degrees of dysplasia (Yoshizawa et al., 2002). The frequency of *TP53* and *CDKN2A* gene inactivation is more variable. However, *SMAD4* gene mutations are relatively uncommon (Hruban et al., 2007). In contrast, *LKB1* which is a gene associated with the Peutz-Jeghers syndrome, is biallelically inactivated in 25%, and the *Phosphatidylinositol-4,5-Bisphosphate 3-Kinase Catalytic Subunit Alpha* (*PIK3CA*) gene is mutated in 10% of IPMNs (Schönleben et al., 2006; Su et al., 1999). MCNs are far less common than IPMNs. They occur almost exclusively in women and they are much more frequent in the body and tail of the pancreas. Unlike IPMNs, MCNs do not involve the pancreatic duct system. The mucinous epithelium in MCNs is accompanied by an underlying ovarian-type stroma, a diagnostic requirement for MCNs and a key feature that distinguishes them from IPMNs. At the molecular level, activating point mutations in the *K-RAS* gene are early events in the development of MCNs, while *TP53* and *SMAD4* gene mutations represent late changes (Fukushima and Fukayama, 2007; Yoshizawa

et al., 2002). Aberrant methylation of the *CDKN2A* gene occurs in a minority of MCNs (Hruban et al., 2007).

1.1.3.2. Molecular PDAC subtypes

In 2016, Bailey et al. defined 4 molecular subtypes of PDAC based on integrated genomic analysis of 456 PDAC tumors: squamous, pancreatic progenitor, aberrantly differentiated endocrine exocrine (ADEX) and immunogenic tumors. Genomic and epigenetic features that characterize each subtype conclude in different mechanisms of molecular evolution (Bailey et al., 2016).

Squamous tumors are associated with mutations in *TP53* and *Lysine-specific demethylase 6A (KDM6A)* genes, an upregulated *TP63ΔN* transcriptional network, activated EGF signaling and downregulation of genes involved in pancreatic endodermal cell fate determination like *Pancreatic and Duodenal Homeobox* 1 (*PDX1)*, *GATA6*, etc., leading to loss of endodermal identity. Squamous subtype is associated with poor prognosis (Bailey et al., 2016).

Pancreatic progenitor tumors express genes involved in early pancreatic development like *FOXA2, FOXA 3 and PDX1* among others (Bailey et al., 2016). Especially, *PDX1* is critical for pancreas development considering that ductal, exocrine and endocrine cells derived from a progenitor that expresses *PDX1* (Hale et al., 2005).

ADEX tumors show deregulation of transcriptional pathways involved in late stages of pancreatic development and differentiation. These tumors contain highly expressed genes involved in *K-RAS* activation and upregulation of transcriptional networks associated with acinar and endocrine differentiation (Bailey et al., 2016).

Immunogenic tumors share many of the features of the pancreatic progenitor subtype, but with a significant increase in immune infiltrates. Thus, these tumors contained upregulation of immune networks pathways including B cell signaling pathways, antigen presentation, $CD4^+$ T cell, $CD8^+$ T cell and Toll-like receptor signaling (Bailey et al., 2016).

1.1.4. Molecular genetics of pancreatic adenocarcinoma

Exome sequencing of PDACs have identified, on average, more than 60 miscoding mutations per tumor (Jones et al., 2008). Moreover, all tumors examined had mutations in components of at least 12 different signaling pathways including Notch, Sonic Hedgehog (Shh) and Wnt pathways (Jones et al., 2008). More recent studies using whole-genome sequencing and copy number variation analysis have revealed frequent chromosomal rearrangements that harbor focal gene amplifications (Waddell et al., 2015). These findings make it very difficult to design rational and viable therapeutic strategies to treat advanced PDAC and may explain why most clinical trials carried out during the last two decades have made very limited

contributions to the treatment of this disease (Hidalgo, 2010).

1.1.5. Frequent mutations in oncogenes and tumor suppressor genes.

Although some (2–10%) PDACs are associated with hereditary factors (Habbe et al., 2006), most are related with high-frequency somatic mutations in a subset of genes, including the *K-RAS* oncogene, and the tumor suppressors *CKDN2A*, *TP53* (Ruggeri et al., 1992; Scarpa et al., 1993) and *SMAD4* (Hahn et al., 1996), thus modifying different signaling pathways.

K-RAS, which encodes a small GTPase that mediates downstream signaling from growth factor receptors, is the most frequently mutated oncogene in pancreatic cancer. Somatic mutations in *K-RAS* are nearly universal (>90%) in human PDAC (Jones et al., 2008; Wood and Hruban, 2012). *K-RAS* mutations found in PDAC cluster in specific hotspots (most commonly in codon 12) (Smit et al., 1988). The result is a constitutively active protein, unable to hydrolyze Guanosine Triphosphate (GTP), thus promoting persistent signaling to downstream effectors and controlling cell proliferation, survival and many other aspects of cell behavior (Downward, 2003). *K-RAS* mutations are present in most low-grade PanIN, suggesting that this event is one of the earliest alterations in pancreatic tumorigenesis (Kanda et al., 2012).

Additionally, rare somatic mutations have been reported in other members of this signaling pathway, such as *B-RAF* (Calhoun et al., 2003). *B-RAF*^{V600E} mutation is found in 3% of human PDAC. Moreover, *B-RAF* mutations are mutually exclusive with *K-RAS* mutations, and are present in 30% of the *K-RAS* wild type PDAC cases (Witkiewicz et al., 2015). Interestingly, GEMMs have illustrated that expression of *B-Raf*^{V600E} in the pancreas is sufficient to lead PanIN development (Collisson et al., 2012).

CDKN2A, which encodes an essential cell-cycle regulator, is the most frequently altered tumor suppressor gene, with loss of function in more than 90% of ductal adenocarcinomas (Wood and Hruban, 2012). This loss is mediated by several mechanisms, including intragenic mutation coupled with loss of the second allele, homozygous deletion, and promoter methylation (Maitra et al., 2006). Alterations in *CDKN2A* are also early events, with loss of *p16INK4A* expression in a subset of low-grade PanINs (Maitra et al., 2003).

Somatic mutations in the *TP53* tumor suppressor gene are present in 50-70% of PDACs. Changes in *TP53* are late events, occurring in high grade PanINs and invasive carcinoma. *TP53* inactivation occurs first through small intragenic mutation followed by loss of the wild type allele (Jones et al., 2008; Scarpa et al., 1993). The protein encoded by *TP53* plays a key role in the cellular stress response and is mutated in a wide range of tumor types (Griffin et al., 1995).

The tumor suppressor gene *SMAD4* mediates signaling downstream of the Transforming Growth Factor β (TGFβ) receptor. It is inactivated in about 55% of PDAC tumors, through

homozygous deletion or intragenic mutation followed by loss of the wild type allele. In this case, mutations also appear in late stages of tumor progression (Hahn et al., 1996). These alterations are associated with poor prognosis in pancreatic adenocarcinoma (Vogelstein and Kinzler, 2004).

1.1.6. Telomere shortening

PDAC is characterized by genomic complexity and instability. Approximately 90% of PanIN1A lesions exhibit telomere shortening, which is one of the most common early events in pancreatic tumorigenesis. As a consequence, critical shortening of telomere length in PanINs may favor these non-invasive lesions to accumulate chromosomal abnormalities and to develop into an invasive carcinoma (van Heek et al., 2002). In most cases, cells with chromosome instability are eliminated by TP53 activation. These alterations persist in those cells with *TP53* mutations (such in high-grade PanIN lesions) promoting rapid accumulation of genomic alterations (Meeker and De Marzo, 2004).

1.1.7. Sonic hedgehog, Notch and Wnt–β-catenin signaling in PDAC

Embryonic signaling pathways are typically present during fetal development, but are also frequently reactivated in cancers enhancing tumor progression and mediating resistance to chemotherapy. PDAC is characterized by frequent de-regulation of these type of pathways, including Shh, Notch and Wnt–β-catenin signaling (Morris et al., 2010a).

Paracrine signaling of Shh is not only important in gut and pancreas development, it also has a role in adult tissue homeostasis and it is an important mediator in human pancreatic carcinoma (Taipale and Beachy, 2001). Aberrant Shh ligand expression is observed at high frequency in human PDAC (~75%) and it is abnormally expressed in PanINs. There is also a high expression of Gli (transcription factor of Shh signaling pathway) in PanINs (Thayer et al., 2003). Shh ligands secreted by cancer cells act on fibroblasts promoting desmoplasia and cell motility (Bailey et al., 2008). Inhibition of Shh signaling by cyclopamine (IPI-926) in combination with gemcitabine can deplete the pancreatic stroma in GEMMs of PDAC, leading to transient stabilization of the disease (Olive et al., 2009).

Wnt–β-catenin signaling is frequently activated in PDAC and contributes to tumor cell proliferation and biology. Enhanced activation of Wnt signaling is found in 65% of PDAC (Wang et al., 2009). Shh and SMAD4 pathways induce Wnt signaling (Romero et al., 2008), thus Wnt should be considered as a combined therapeutic strategy. Wnt-β-catenin signaling in PDAC might also be involved in chemoresistance and metastasis (Cui et al., 2012), therefore representing a promising therapeutic approach.

One of the main functions of Notch signaling seems to be maintenance of pancreatic progenitor cells in an undifferentiated state by promoting their survival and self-renewal

(Apelqvist et al., 1999). Notch signaling pathway appears to be activated in human pancreatic cancer, promoting initiation, progression and maintenance of PDAC (Miyamoto et al., 2003), suggesting inhibition of Notch signaling as a promising therapeutic strategy in this malignancy. However, recent studies utilizing mouse models have revealed both oncogenic and tumor suppressor roles for Notch signaling in PDAC development (Avila and Kissil, 2013).

1.1.8. Stroma and extracellular matrix

A hallmark of PDAC is the extensive peritumoral stroma and desmoplasia, consisting of a complex array of cellular components such as Cancer Associated Fibroblasts (CAFs) and inflammatory cells, surrounded by extracellular matrix (Neesse et al., 2011). The stroma represents up to 90% of the tumor volume. Stroma has been recognized as a barrier surrounding tumor cells (Neesse et al., 2011) and was hypothesized to contribute to inefficient drug delivery and chemoresistance in PDAC (Olive et al., 2009), and more importantly to exclude cytotoxic T cells from reaching the tumor cells, a phenomenon called “immune privilege” (Fearon, 2014). Furthermore, the stroma promotes tumor growth and metastasis (Xu et al., 2012). Thus, ablation of this stromal barrier may represent a major advance in the treatment of this deadly disease. Nevertheless, recent studies have raised doubts about the role of the stroma in cancer progression since its depletion resulted in aggressive PDAC (Özdemir et al., 2014; Rhim et al., 2014). In this regard, instead of ablation of the stroma, forthcoming therapeutic strategies should focus on stromal reprogramming (Whatcott et al., 2015). In fact, transcriptional remodeling through suppression of Shh pathway (Olive et al., 2009), Connective Tissue Growth Factor (CTGF) (Neesse et al., 2011) and CXCL12 chemokine (Feig et al., 2013), as well as activation of vitamin D receptor (Sherman et al., 2014), broadly halted the capacity of CAFs to support tumor growth. Therefore, transcriptional reprogramming of PDAC stroma with tumor-directed cytotoxic and/or immunologic drugs could be a promising PDAC therapeutic strategy.

1.1.9. Use of mouse models for the study of pancreatic cancer

Mouse models provide controllable genetic systems to analyze the complexities of cancers in a physiological context. Genetic engineering has allowed us to generate mouse strains that faithfully reproduce the natural history of pancreatic human tumors, in order to understand PDAC biology and to design and test new therapeutic approaches (Guerra and Barbacid, 2013).

Due to its high frequency in PDAC, mutation of *K-RAS* was proposed as an initiating genetic event in this disease. However, initial efforts to assess the sufficiency of mutant *K-Ras* to initiate PDAC progression in mice failed because of the limitations of transgenic approaches. Expression of a transgene encoding mutant *K-Ras*^{G12D} under a ductal promoter

(Cytokeratine-19) resulted in periductal inflammation and failed to generate PDAC and even PanIN lesions (Brembeck et al., 2003).

The ability of mutant *K-Ras* to drive PDAC was not successful until the development of a Cre-inducible conditional allele Lox-stop-Lox *K-Ras*^{G12D} (*K-Ras*^{LSLG12D}) targeted to the endogenous *K-Ras* locus (Hingorani et al., 2003), thus allowing expression of constitutively active *K-Ras* under temporal and spatial control. Initially, mice expressing the *K-Ras*^{LSLG12D} allele were crossed with mice expressing the bacterial Cre-recombinase under the control of pancreatic progenitor genes promoters: *Pdx1* and *p48* (also known as *Ptf1a*), therefore targeting mutant *K-Ras* to most cells in the developing pancreas. A small number of *Pdx1-Cre; K-Ras*^{LSLG12D} and *p48-Cre;K-Ras*^{LSLG12D} mice developed PDAC over the course of 1 year. Furthermore, these strains develop, with complete penetrance, the full spectrum of PanIN lesions histologically indistinguishable from those present in human patients (Hingorani et al., 2003). Addition of mutations in loci encoding tumor suppressor genes known to be mutated or inactivated in human PDAC such as *p16Ink4a/p19Arf, p53, Lkb1* or *Smad4* accelerates the progression of these PanIN lesions, leading to the formation of invasive tumors with complete penetrance (Aguirre et al., 2003; Bardeesy et al., 2006; Hingorani et al., 2005).

There are remarkable similarities between PanIN and PDAC observed in these GEMMs (*Pdx1-Cre; K-Ras*^{LSLG12D} and *p48-Cre;K-Ras*^{LSLG12D}) with those detected in human patients. However, there are several differences to consider. PDAC is not a pediatric disease, and is likely to arise due to sporadic mutations in adult individuals. Moreover, *K-RAS* mutations appear in specific populations of cells, not in the entire pancreas. In 2007, our laboratory developed a PDAC mouse model in which a resident *K-Ras* oncogene is expressed in acinar cells (Guerra et al., 2007). This GEMM was generated by crossing a knockin *K-Ras*^{LSLG12Vgeo} with a double transgenic mouse that expresses the Cre-recombinase under the control of the *Elastase* promoter (*Elas-tTa/tetO-Cre*) following an inducible Tet-off strategy in which the expression of the enzyme is controlled by a tetracycline trans-activator (tTA). Thus, this complex model allows us to control temporally the expression of the *K-Ras* oncogene. These mice, if untreated (in absence of doxycycline), express the resident *K-Ras*^{G12Vgeo} in a limited percentage of acinar cells (20-30%) during late embryonic development (from E16.5 stage). Interestingly, they develop PanIN lesions with similar latencies and penetrance to mice expressing *K-Ras*^{G12D} in all pancreatic lineages (Guerra et al., 2007). Furthermore, a percentage of these mice develop PDAC by one year of age. Consequently suggesting that the cell of origin in PDAC tumors is likely to be an acinar cell or an acinar precursor rather than cells of ductal lineages. As indicated above, addition of mutations in *p16Ink4a/p19Arf* and *p53* tumor suppressor genes increases PDAC penetrance to 100%, and significantly reduces tumor latency (6-8 months of age) (Guerra et al., 2011).

The *Elas-tTa/tetO-Cre*;*K-Ras*^{LSLG12Vgeo} PDAC mouse model offers the possibility to turn on *K-Ras* oncogene expression during adulthood by simply providing doxycycline in the

drinking water until adult stages. Surprisingly, expression of constitutively active K-Ras in adult mice (≥ 60 days old) fails to induce pancreatic lesions (Guerra et al., 2007). Indeed, adult acinar cells are resistant to *K-Ras*^{G12V} transformation even in the presence of inactivated *p53* or *p16Ink4a*/*p19Arf* tumor suppressors (Guerra et al., 2011). However, these mice develop PanINs and PDAC in the context of chronic, acute or even sporadic events of pancreatitis, induced by exposure to cholecystokinin analog, caerulein (Guerra et al., 2007, 2011).

It is not clear how pancreatitis causes adult mice to overcome the resistance to induction of PanIN or PDAC by oncogenic *K-Ras*. Pancreatitis induces tissue damage that results in proliferation of acinar cells to repair the injured parenchyma. It is uncertain whether this proliferation is mediated by the recruitment of progenitor cells or by de-differentiation of mature acinar cells. These progenitors and/or the differentiated acinar cells become susceptible to transformation by the resident *K-Ras* oncogene leading to the acquisition of ductal-like properties as observed in the ADM and in low grade PanINs (Guerra and Barbacid, 2013). It was reported that oncogenic *K-Ras* induced differentiation of the regenerating acinar cell compartment into ductal like structures by a mechanism that involved decreased expression of β-catenin (Morris et al., 2010b).

Many GEMMs have been developed to evaluate different targets and pathways that are important for PDAC tumors, such as Egfr, Notch, Phosphoinositol-3-kinase (PI3K), etc. (Gopinathan et al., 2015; Guerra and Barbacid, 2013; Pérez-Mancera et al., 2012). For instance, two independent studies using PDAC GEMMs have illustrated that Egfr is essential for PDAC development (Ardito et al., 2012; Navas et al., 2012).

At the time of diagnosis, human PDAC patients usually present a late-stage carcinoma. However, many of these genetic studies in GEMMs have been performed with germline knockouts or Cre-dependent alleles that are expressed or deleted simultaneously with the oncogenic events. Thus, these studies should be considered only preventive strategies more than therapeutic approaches. For this reason, it would be important to assess efficacy of the targets of interest in already established tumors.

Recently, new generation models have been developed using dual recombinase system (DRS) technologies to separate temporally and physically tumor development from target deletion, using a combination of Flp-FRT and Cre-Lox systems (Schönleben et al., 2006). Schönhuber et al., used this DRS to first express *K-Ras* oncogene mutation, and after PanIN development, delete *3-phosphoinositide-dependent protein kinase 1* (*Pdk1*), an important downstream effector of PI3K, to demonstrate that deletion of this target blocks PanIN progression (Schönhuber et al., 2014).

1.2. Epidermal Growth Factor Receptor

Growth factors participate in different cellular responses by binding to cell surface

receptors. Most of these receptors are tyrosine kinase receptors (RTKs) with intrinsic kinase activity. Around 60 RTKs have been identified, and classified into more than 16 receptor families. Growth factors and RTKs interactions trigger different signaling pathways that alter gene expression and, if de-regulated, may result in alterations in the physiological state of the cell (Perona, 2006).

Epidermal growth factor (EGF) was one of the first growth factors discovered in the early 1960s. It was shown to stimulate epidermal and mesodermal cell growth and differentiation (Cohen, 1983). Subsequent studies identified the receptor and its intrinsic kinase activity. EGF was shown to bind with high affinity to a specific receptor located in the cell membrane and stimulate rapid activation of a protein kinase activity. Epidermal growth factor receptor type 1 (EGFR) was purified and characterized as a 170KDa glycoprotein, bearing ligand-inducible kinase activity (Ullrich et al., 1984).

1.2.1. ErbB family

EGFR is a member of the ErbB family, constituted by four closely related tyrosine kinase receptors: EGFR (also known as ErbB1), ErbB2, ErbB3 and ErbB4, which are expressed ubiquitously in epithelial, mesenchymal, cardiac and neuronal cells. They are involved in a variety of cellular processes, including proliferation, survival, angiogenesis and metastasis in many cancer types (Appert-Collin et al., 2015). EGFR and ErbB2 are found mutated, activated or overexpressed in a wide variety of human cancers like breast and lung cancer. These alterations result in excessive signaling that cooperates in the development and malignancy of these tumors (Burgess, 2008).

Moreover, this family of tyrosine kinase receptors is essential for embryo development. In mice, loss of signaling by any member of the ErbB family results in embryonic lethality with defects in organs, including lung, skin, heart, and brain (Table 1).

Table 1. Knockout mouse models for ErbB family receptors

ErbB family member	Discovery
Egfr knockout	(Miettinen et al., 1995; Sibilia and Wagner, 1995; Sibilia et al., 1998; Threadgill et al., 1995)
ErbB2 knockout	(Lee et al., 1995)
ErbB3 knockout	(Erickson et al., 1997)
ErbB4 knockout	(Gassmann et al., 1995)

1.2.2. Structure of EGFR

The structure of EGFR and the rest of the family members consists of a large extracellular domain, a single hydrophobic transmembrane segment, and an intracellular domain containing a juxtamembrane domain, a typical tyrosine protein kinase segment, and a tyrosine-rich carboxy-terminal tail (Ferguson, 2008). Upon receptor activation, these C-terminal tyrosines are phosphorylated. The intracellular tyrosine kinase domain of ErbB receptors is highly conserved, although the kinase domain of ErbB3 contains substitutions of critical amino acids and therefore lacks kinase activity (Guy et al., 1994). The extracellular domain is made of tandem repeat leucine-rich segments that participate in ligand binding, and cysteine-rich domains for homo- and hetero-dimer formation with ErbB family members. Extracellular domains are less conserved among the four receptors, suggesting that they have different specificity in ligand binding (Olayioye et al., 2000; Yarden and Sliwkowski, 2001).

1.2.3. Activation of EGFR

ErbB receptors are activated by binding to growth factors that are produced by the same cells that express ErbB receptors (autocrine secretion) or by surrounding cells (paracrine secretion) (Normanno et al., 2006).

EGFR is regulated by at least seven different activating ligands in humans: EGF, transforming growth factor α (TGFα), betacellulin (BTC), heparin-binding EGF-like growth factor (HB-EGF), amphiregulin (ARG), epiregulin (EPR), and epigen (EGN). Each contains an EGF-like domain that is responsible for receptor binding and activation. EGFR ligands are all produced as membrane-bound precursor proteins and are cleaved by cell-surface proteases to yield the active growth factor species (Harris et al., 2003). ErbB3 and ErbB4 are regulated by neuregulins (NRGs). NRG1 and NRG2 bind both to ErbB3 and ErbB4, whereas NRG3 and NRG4 appear to be ErbB4 specific (Falls, 2003). Three of the EGFR ligands mentioned above (BTC, EPR, and HB-EGF) also bind and activate ErbB4. For ErbB2, no soluble ligand has been identified. This orphan receptor is generally assumed to be only regulated by hetero-dimerization with other ErbB family receptors (Riese and Stern, 1998).

Binding of ligands to the extracellular domain of ErbB receptors induces the formation of receptor homo- or heterodimers, and subsequent activation of the intrinsic tyrosine kinase domain (Olayioye et al., 2000). In particular, ErbB2, which does not have known direct activating ligand, and ErbB3, which does not have kinase activity, do not form homo-dimers and they signal only through hetero-dimerization (Olayioye et al., 2000; Yarden and Sliwkowski, 2001). Dimerization leads to auto-phosphorylation of specific tyrosine residues in the carboxy-terminal tail (Heldin, 1995). Phosphorylated ErbB receptors induce the recruitment of adaptor proteins which lead to activation of intracellular signaling pathways (Shoelson, 1997) (Figure 3).

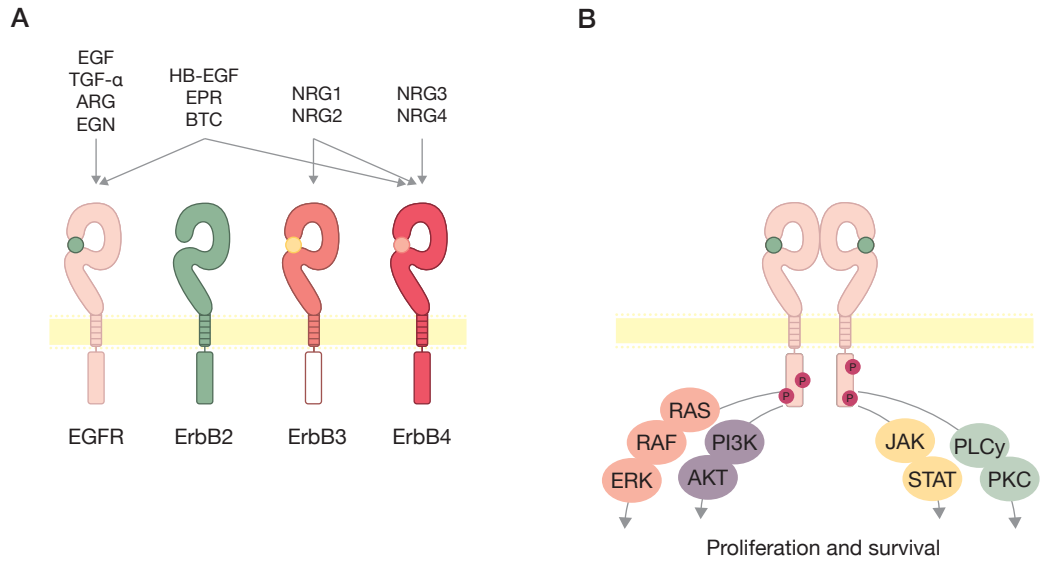

Figure 3. ErbB receptor mammalian family and their ligands. Upon ligand binding (A) the receptors form homodimers and heterodimers. The receptors then become phosphorylated on specific cytoplasmic tyrosines residues initiating downstream signaling pathways (B) (Adapted from Hynes and MacDonald, 2009).

1.2.4. EGFR signaling pathways

After ligand binding, the intracellular tyrosine kinase domain of the dimerized receptor is activated, leading to the phosphorylation of specific C-terminal tyrosine residues that serve as docking sites for adaptor proteins containing Src homology 2 (SH2) domains and phosphotyrosine binding (PTB) domains. Some of these adaptor proteins are Src Homology 2 domain Containing protein (Shc), Growth Factor Receptor-bound protein 2 (Grb2), Growth Factor Receptor-bound protein 7 (Grb7), CT10 Regulator of Kinase (Crk), Non-Catalytic region of tyrosine Kinase adaptor protein (Nck), Phospholipase C gamma (PLCγ), intracellular kinases Src, PI3K, protein tyrosine phosphatases SHP1/2 and the Cbl E3 ubiquitin ligase, among others (Normanno et al., 2006). These adaptor proteins promote the activation of several intracellular signaling pathways including the PI3K/AKT, JAK/STAT, Protein Kinase C (PKC) and Ras/Mitogen-Activated Protein Kinase (MAPK) pathways, with functions such as growth, survival, proliferation, and differentiation (Oda et al., 2005).

1.2.4.1. RAS/MAPK

RAS/MAPK pathway is one of the most widely studied signaling cascades and one of the best described in cancer. It regulates several cellular responses, of which cell proliferation is probably one of the most relevant processes (Molina and Adjei, 2006).

RAS proteins play a critical role in cell signaling both in normal cell growth and malignant transformation. They regulate proliferation, differentiation and survival in response to

extracellular stimuli (Malumbres and Barbacid, 2003). Importantly, *RAS* genes were found mutated in approximately 30% of all human tumors, thus making *RAS* the most frequently mutated oncogene in human cancer (Roberts and Der, 2007). In mammals there are three *RAS* genes that code for the four RAS isoforms: H-RAS, N-RAS and K-RAS4A and K-RAS4B (these last are splice variants of exons 4A and 4B). K-RAS4B is the principal isoform expressed in human cells (Cox and Der, 2010) and tumors (Stephen et al., 2014).

All ErbB ligands and receptors induce activation of the RAS/MAPK pathway through either Grb2 or Shc adaptor proteins (Jorissen et al., 2003). Grb2 contains an SH2 domain that binds to the phosphotyrosine residues of the active receptor. When Grb2 binds to the guanine nucleotide exchange factor (GEF) SOS, recruits it to the plasma membrane where RAS is also localized because of farnesylation. Active SOS then allows the release of bound GDP and its exchange for GTP from a member of the RAS subfamily. RAS can then bind GTP and become active. RAS-GTP complex triggers activation of downstream effectors leading to proliferation, and cell survival (Egan et al., 1993). Active RAS-GTP is converted back into the inactive RAS-GDP by GTP hydrolysis, a reaction accelerated by the interaction of RAS-GTP with GTPase-activating proteins (GAPs) (Hennig et al., 2015) (Figure 4).

Activated RAS binds to and stimulates a variety of effector proteins including: Rapidly accelerated fibrosarcoma (RAF) serine/threonine kinases, PI3K, guanine nucleotide exchanged factor for RAL (RalGEFs), and Phospolipase C epsilon (PLCε) among others (Downward, 2003). Some of these effectors are known to be involved in RAS driven oncogenesis, such as RAF serine/threonine kinases and PI3K (Davies et al., 2002; Karakas et al., 2006). The best-characterized pathway activated by RAS is the RAF/MEK/ERK pathway. RAS-GTP binds to and activates the three closely related RAF proteins, A-RAF, C-RAF and B-RAF. This interaction causes RAF to be relocalized to the plasma membrane, which is crucial for its activation by serine/threonine phosphorylation (Marais et al., 1995). When RAF proteins are active, they have the capability to phosphorylate Mitogen Activating Protein (MAP) kinase 1 and 2 (MEK1 and MEK2) which will phosphorylate and activate the Extracellular signal-Regulated Kinases 1 and 2 (ERK1 and ERK2) (Matallanas et al., 2011). These last Serine/Threonine kinases can phosphorylate more tan 150 substrates in the cytosol as well as in the nucleus where they promote the transcription of a wide variety of factors, most of them implicated in cell proliferation and survival (Yoon and Seger, 2006) (Figure 4).

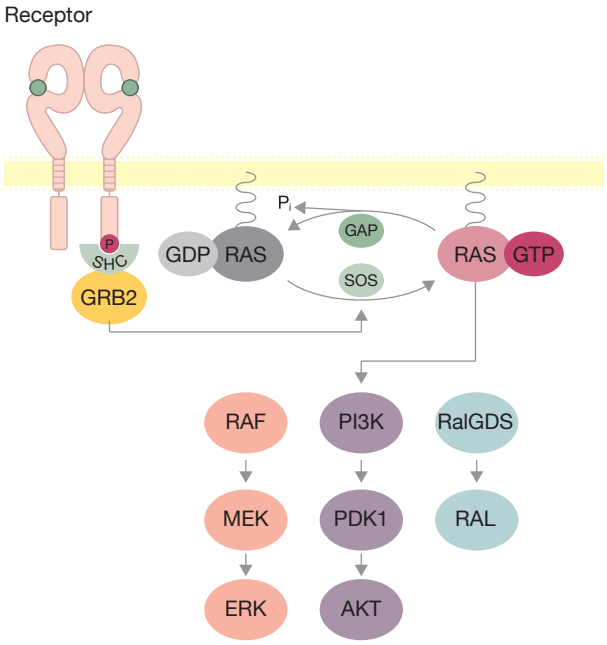

Figure 4. Ras signaling pathway

1.2.4.2. PI3K pathway

In addition to the MAPK pathway, RAS also stimulates several other effector pathways, including the PI3K and Ral guanine nucleotide dissociation stimulator (RalGDS) (Malumbres and Barbacid, 2003). As mentioned above, EGFR can also directly activate PI3K by recruitment of its p85 subunit to the activated receptors (Soltoff and Cantley, 1996).

PI3K has a key role promoting cell survival. The activation of this lipid kinase leads to the phosphorylation of phosphatidylinositol-4,5-byphosphate (PIP_2) to produce phosphatidylinositol-3,4,5-triphosphate (PIP_3). PIP_3 attracts proteins with phosphoinositide-binding domains to the plasma membrane, such as Rac-alpha serine/threonine-protein kinase (AKT) and 3-Phosphoinositide-Dependent Protein Kinase 1 (PDK1). AKT is recruited to the membrane and fully activated. Activated AKT mediates several cell responses such as growth, cell survival and resistance to apoptosis. It is know that the Phosphatase and Tensin homolog (PTEN) act as a phosphatase to dephosphorylate PIP_3, acting as a tumor suppressor negatively regulating this pathway (Downward, 2003).

Activation of the PI3K/AKT pathway is found in 59% of human PDAC cases and represents a negative prognostic factor (Yamamoto et al., 2004). Mutations in the catalytic subunit of PI3K (p110α, encoded by *PI3KCA*), in the regulatory PI3K subunit (p85α, encoded by *PIK3R1*) and amplification of AKT are commonly found in human pancreatic cancers (Witkiewicz et al., 2015; Ying et al., 2016). Furthermore, heterozygous or homozygous deletion of *PTEN* is found in 15% of human PDACs.

Although it was demonstrated that overexpression of a constitutively active *Pik3ca*^{H1047R} can induce PDAC development in GEMMs (Eser et al., 2013), *PI3KCA* mutations in human PDAC are almost always concurrent with oncogenic *K-RAS* mutations, suggesting that they both cooperate during pancreatic tumor development (Witkiewicz et al., 2015). Moreover, it has been demonstrated the role of PI3K pathway in *K-Ras* driven PDAC mouse models since the PI3K kinase subunit p110α, but not p110β, promotes PDAC growth (Baer et al., 2014) and the development of PanIN and PDAC is abolished upon deletion of *Pdk1* (Eser et al., 2013). In addition, loss of *Pten* in *K-Ras* driven PDAC GEMMs dramatically promotes highly invasive and metastatic PDAC development by a mechanism that involves *p16Ink4a/p19Arf* locus inactivation (Ying et al., 2011).

1.2.4.3. JAK/STAT

Signal Transducer and Activator of Transcription (STAT) signaling pathway participates in a wide range of cell behaviors as cell proliferation, survival, motility, invasion, angiogenesis and inflammation (Li et al., 2011). STAT tyrosine phosphorylation is mediated by Janus Kinase (JAK) family, which is activated by cytokine and growth factors receptors, such as EGFR (Darnell et al., 1994). In mammals 7 *STAT* genes have been identified, *STAT 1-4*, 5a, *5b* and *STAT 6.* Knocking out *Stat3* in the developing exocrine pancreas results in significantly reduced PanIN development, especially in high-grade lesions, and consequently, mice had lower incidence of PDAC (Fukuda et al., 2011).

1.2.4.4. PLCγ-PKC

EGFR, when phosphorylated, can bind directly to PLCγ. PLCγ is a membrane-associated enzyme that, when active, hydrolyzes PIP_2 in two molecules: 1,2diacilglecerol (DAG) and inositol-1,4,5-triphosphate (IP_3). These products are important second messengers that control different cellular processes, leading to PKC activation, which finally activates tumor promotion and c-Jun N-terminal kinases (JNK) (Wahl et al., 1990).

1.2.5. EGFR-MAPK in cancer

Deregulated expression and signaling of EGFR is a common feature of solid cancers. Several studies reported high expression of EGFR, ranging from 7% to 100% of human PDACs (Conradt et al., 2011). As mentioned above, one of the best-characterized EGFR effector pathways is the RAS-MAPK pathway and frequent mutations in RAS/RAF/MEK/ERK signaling are found in many human cancers.

1.2.5.1. Mechanisms leading to constitutive activation of EGFR

EGFR amplifications and gene mutations are frequently observed in most solid human neoplasms, like ovarian, lung, breast and pancreas cancer (Normanno et al., 2006). In many cancer types, EGFR pathway becomes hyper-activated because of mechanisms involved in ligand or receptor over-expression, or constitutive activation of the receptors (Yarden and Sliwkowski, 2001).

TGFα and EGF are commonly altered in different cancer types. Both ligands act regulating EGFR through an autocrine/paracrine secretion promoting tumor growth. Several studies in transgenic mice have shown that TGFα overexpression induces epithelial hyperplasia in liver, pancreas and gastrointestinal tract and the appearance of hepatocellular and breast carcinoma (Jhappan et al., 1990). Moreover TGFα and EGFR are co-expressed in several types of carcinomas, which correlates with poor prognosis (Salomon et al., 1995). A linkage between RAS/MAPK and EGFR receptor is mediated by the upregulation of expression of EGFR ligands by RAS signaling. One important gene target of RAS activation involves transcriptional activation of TGFα gene, which promotes persistent stimulation of EGFR. Monoclonal antibodies against EGFR, like cetuximab, were developed in order to impair ligand-receptor binding. These antibodies have an anti-proliferative effect in tumor cells expressing EGFR (Zandi et al., 2007).

EGFR overexpression in PDAC tumors is associated with poor prognosis and disease progression (Ueda et al., 2004). There are different mechanisms by which the level of EGFR is increased in tumor cells. Gene amplification has been demonstrated to occur in different tumor types such as PDAC, breast carcinomas, Non-Small Cell Lung Cancer (NSCLC) and Glioblastoma Multiforme (GBM) (Zandi et al., 2007). EGFR might also be overexpressed because of increased activity of the EGFR promoter or de-regulation at translational and post-translational levels. Wild type and mutant TP53 protein activates EGFR transcription by directly binding to specific sites in its promoter. As the level of mutant TP53 protein is usually high in tumor cells, it may lead to strong and continuous activation of *EGFR* promoter (Bykov et al., 2003). Elevated EGFR levels can also be achieved by damaged post-translational recycling, meaning that a significant portion of EGFR is recycled back to the cell surface following EGF stimulation instead of being degraded (Zandi et al., 2007).

Increased receptor signaling can also be due to *EGFR* mutations giving rise to constitutively active variants. These mutations can affect the extra- or the intracellular domain. Extracellular mutations are particularly frequent in GBM. Most of them are deletions in exons encoding all or parts of the extracellular domain. These mutations give rise to truncated receptors that are constitutively active (Zandi et al., 2007). Intracellular mutations are usually deletions and/or duplications of exons codifying for the tyrosine kinase domain. They are frequent in GBM and NSCLC (Lynch et al., 2004). Of the seven exons that encode the tyrosine kinase domain (exons 18-24) these mutations are restricted to the first four (exons 18-21)

exons. According to COSMIC database most frequent mutations are small deletions in exon 19, missense mutations (L858R en exon 21 and G719A/C in exon 18 and 3), and small duplications or insertions in exon 20. These mutations prolong the activity of ligand-activated receptors (Sordella et al., 2004). GEMMs were developed to study the role of some of these EGFR mutations. Transgenic mice harboring in type II pneumocytes a deletion of Egfr in exon 19 develop lung adenocarcinomas (Politi et al., 2006). Similar results were obtained with Egfr L858R mutant mice (Politi et al., 2006).

Aberrant EGFR signaling due to defective receptor downregulation has also been linked to neoplastic transformation. EGFR downregulation is a mechanism by which EGFR signaling is attenuated involving the internalization and subsequent degradation of the activated receptor. It was described that EGFR downregulation can be affected by overexpression of ErbB2, which can shift the formation of EGFR homodimers towards the formation of EGFR/ErbB2 heterodimers (Huang et al., 1999; Wang et al., 1999; Zandi et al., 2007). Interestingly, EGFR/ErbB2 heterodimer appears to be the strongest and the most potent inducer of cellular transformation and mitogenic signaling compared to other ErbB homo- and heterodimers (Lenferink et al., 1998; Yarden and Sliwkowski, 2001). Thus, ErbB2 overexpression is one of the mechanisms leading to potent EGFR activation (Haslekås et al., 2005).

There are other mechanisms that can induce EGFR activation through tyrosine phosphorylation and consequently stimulation of intracellular signaling pathways; this process is known as EGFR transactivation. For example, cytokines can directly activate EGFR through JAK2, which phosphorylates specific tyrosine residues in the cytoplasmic domain of EGFR and ErbB2 (Yamauchi et al., 1997, 2000). Similarly, the serine/threonine kinase PKC has also been frequently shown to be involved in EGFR signal transactivation (Fischer et al., 2003). EGFR transactivation has also been particularly well studied upon stimulation of G-protein coupled receptors (GPCR) that can have positive effects on receptor signaling through two mechanisms. First, GPCRs can stimulate matrix metalloproteinases, which induce cleavage of EGF-like ligands precursors, leading them to bind EGFR enhancing its signaling (Fischer et al., 2003; Prenzel et al., 1999). Second, GPCRs can indirectly activate Src, which phosphorylates tyrosine residues in the intracellular domains of EGFR (Dikic et al., 1996; Luttrell et al., 1997).

1.2.5.2. EGFR-MAPK inhibition

Nowadays, gemcitabine is the standard care for metastatic pancreatic cancer. However, it only confers a modest survival improvement among treated patients (Burris III et al., 1997; Li et al., 2004). For this reason, understanding the nature of PDAC biology and molecular events will permit the inhibition of key specific pathways in pancreatic tumor development.

EGFR signaling is highly upregulated in many tumor types, including PDAC. Higher EGFR expression in PDAC patients is related with metastasis and poor prognosis (Tobita et al.,

2003). Thus, EGFR has been intensively studied as a therapeutic target and specific inhibitors against the receptor have been developed. There are two types of EGFR inhibition, monoclonal antibodies and tyrosine kinase inhibitors (TKIs).

Monoclonal antibodies, like cetuximab and panitumumab, bind to the extracellular domain in order to inhibit ligand binding (Burgess et al., 2003). They interfere in receptor dimerization, phosphorylation and signal transduction, as well as they can cause receptor endocytosis (Roskoski, 2014). However, treatment of PDAC advanced patients with the combination of gemcitabine plus cetuximab did not improve the outcome compared with patients treated with gemcitabine alone (Philip et al., 2010) suggesting that combination of EGFR with alternative targets should be evaluated for new drug development.

TKIs bind to EGFR intracellular tyrosine kinase domain impairing receptor auto-phosphorylation and cell signaling (Seshacharyulu et al., 2012). Blocking EGFR with erlotinib decreases growth and metastasis of human pancreatic xenografts and improves the anticancer effect of gemcitabine (Ng et al., 2002). In 2007, a clinical trial in phase III showed that gemcitabine in combination with erlotinib significantly improved overall survival in advanced PDAC patients compared with patients only treated with gemcitabine (Moore et al., 2007). Although the benefit of the combination was minimal, it was surprising since EGFR signals upstream of K-RAS, which is mutated in most of human PDAC cases. Indeed, these results are in discrepancy with clinical data in NSCLC, in which oncogenic mutations in *EGFR* and *K-RAS* are mutually exclusive (Shigematsu et al., 2005). Similarly, oncogenic *K-RAS* mutations have shown to be detrimental in colorectal cancer patients treated with anti-EGFR therapy (Bardelli and Siena, 2010).

Nevertheless, in 2012 our laboratory and others, demonstrated using *K-Ras* driven PDAC mouse models that Egfr is essential for PDAC initiation, unlike this is not happening in colon and lung tumors. Indeed, ablation of *Egfr* in acinar cells prevents the development of preneoplastic PanIN lesions even in the context of chronic pancreatitis or in the absence of *p16Inka/p19Arf* tumor suppressors. Nevertheless, *Egfr* deletion is not sufficient to inhibit tumor development in the absence of *p53*, although tumors develop with significant longer latencies (Ardito et al., 2012; Navas et al., 2012). Tumorigenesis is a multi-step process involving several mutations that affect different pathways (Jones et al., 2008) which might explain why EGFR therapeutics has only be partially successful. Therefore, it is possible that the inhibition of EGFR in advanced PDAC tumors may not be enough because of the genetic complexity of these tumors, thus EGFR inhibition should be combined with drugs affecting other molecular pathways in order to induce conclusive responses in PDAC patients.

K-RAS is mutated in 90% of human PDAC cases, however there are no selective drugs against these tumors and the design of K-RAS inhibitors is still challenging. Nevertheless, an inducible *K-Ras*^{G12V} model has been developed to allow the conditional and reversible expression of the oncogene in the pancreas by a Tet-on strategy to study the therapeutic

benefit of inhibiting the expression of *K-Ras* mutation in already established PDAC tumors (Collins et al., 2012a; Ying et al., 2012). These mice when combined with a *p53*-mutated allele develop PDAC, but these tumors and the metastasis rapidly disappear in the absence of the oncogene. Thus, these results illustrate that continuous *K-Ras*^{G12V} expression is required for tumor maintenance (Collins et al., 2012a, 2012b; Kapoor et al., 2014). However, PDAC tumor cells can acquire alternative mechanisms to survive and proliferate in the absence of *K-Ras* oncogene. Results obtained with this model have identified *Yes-associated protein 1* (*Yap-1*) amplification, a transcriptional co-activator of the Hippo pathway that controls cell proliferation and apoptosis, as a potential bypass mechanism to overcome the dependence of PDAC on oncogenic *K-Ras* (Kapoor et al., 2014). Although this model is useful, it is important to take into account that the inducible *K-Ras* is encoded by a transgene, consequently generating an extra copy of *K-Ras* not drive by the endogenous promoter (Collins et al., 2012a; Ying et al., 2012).

Target-based therapies are widely considered to be the key of cancer treatment. While K-RAS remains an undruggable molecule, several kinase inhibitors have been generated against upstream and downstream K-RAS effectors. Due to the frequent alterations in RAF/MEK/ERK downstream kinases, this pathway is at the drug discovery vanguard. Genetically, deletion of *Mek1/2* or *Erk1/2* completely prevented oncogenic *K-Ras* driven lung adenocarcinoma development (Blasco et al., 2011). Unfortunately, systemic ablation of these targets in adult mice led to extreme toxicities resulting in the rapid death of the animals. But in addition, there was identical tumor suppression with *c-Raf* deletion, without inducing significant toxicity (Blasco et al., 2011), suggesting that c-Raf is the most suitable target to block K-Ras-mediated activation of MAPK signaling. Recently, it has been demonstrated that c-Raf is critical for PanIN and PDAC initiation. Nevertheless, in the absence of p53, *c-Raf* ablation is not sufficient to block PDAC formation (unpublished results, see appendix 8.1).

As previously mentioned, pancreatic tumors are highly heterogeneous containing multiple mutations that affect many different pathways (Jones et al., 2008). Additionally, the failure of single targeted therapies may be related to the extensive crosstalk between redundant signaling pathways in tumor cells (Huang et al., 2011), suggesting that concurrent inhibition of multiple effector pathways could be a promising therapeutic strategy. Importantly, it was recently determined that combined ablation of *Egfr* and *c-Raf* completely blocks PDAC initiation in a p53 deficient context (unpublished results, see appendix 8.2).

Taking into account all these precedents, further research is required to identify new effective targets and combination of targets for treating PDAC. This is the main goal of this thesis.

2. Objectives

Pancreatic ductal adenocarcinoma is known to be one of the most lethal cancers, mainly because patients do not benefit from current available therapeutics. Therefore, there is a substantial and urgent demand to develop novel drugs to treat pancreas cancer. GEMMs can help to design and validate new therapeutic strategies affecting selective targets at different stages of tumor development. Indeed, studies using mouse models that recapitulate the human disease, demonstrated that Egfr is essential for PDAC initiation. Nevertheless, since protein elimination cannot be achieved in the clinic, it was important to elucidate whether tyrosine kinase inhibitors could be a suitable therapy for these pancreatic tumors. Moreover, Egfr and other validated targets can be used in combination to identify new strategies that would eventually pave the way for the design of more effective therapies that will benefit PDAC patients.

Hence, the objectives of this thesis were as following:

1. Generation of a kinase dead *Egfr*^{D839A} allele and characterization of its constitutive expression during embryo development.

2. Validation of the inhibition of Egfr kinase activity as a therapeutic strategy for *K-Ras* driven PDAC.

3. Unveiling the role of Egfr and its tyrosine kinase activity in established pancreatic tumors.

4. Studying the potential therapeutic benefit of targeting Egfr and c-Raf simultaneously in full-blown PDACs. In addition, identifying the possible side effects derived from the systemic deletion of Egfr and c-Raf.

3. Materials and Methods

3.1. Generation and maintenance of mouse lines

3.1.1. Mouse lines used in this work

The PDAC mouse model was generated by crossing the knockin *K-Ras*$^{+/LSLG12Vgeo}$ (Guerra et al., 2003) with the *Elas-tTA/tetO-Cre* bitransgenic strain. In these mice, the *Elas-tTA/tetO-Cre* transgenes drive the expression of the bacterial Cre-recombinase from the *Elastase* promoter under the negative control of doxycycline (Tet-off system) (Guerra et al., 2007). *Elas-tTA* and *tetO-Cre* were provided by Dr. Grippo (Northwestern University, Chicago, IL, USA) and Dr. J.I Gordon (Washington University, St. Louis, MO, USA) respectively. The *p53*^{Lox} (Jonkers et al., 2001) and the *p16Ink4a/p19Arf*^{Lox} were generated (Krimpenfort et al., 2001) in Anton Berns´ laboratory (The Netherlands Cancer Institute, Amsterdam, The Netherlands). The *EIIa-Cre*^{T} (Lakso et al., 1996) was generated in Heiner Westphal´s laboratory (National Institute of Child Health and Human Development, Bethesda, MD, USA). The *Egfr*^{Lox} (Natarajan et al., 2007) was generated in Maria Sibilia´s laboratory (Institute for Cancer Research, Vienna, Austria). The *c-Raf*^{Lox} (Jesenberger et al., 2001) was generated in Manuela Baccarini´s laboratory (Institute of Microbiology and Genetics, Vienna, Austria). The *K-Ras*^{FSFG12V} (Drosten, unpublished) was generated in Mariano´s Barbacid Laboratory (Spanish National Cancer Centre, CNIO, Madrid, Spain). In collaboration with the CNIO Transgenic Mice Core Unit we generated the *Elas-tTA/tetO-Flp* bitransgenic strain. The *p53*^{FRT} (Lee et al., 2012) was generated in David Kirsch´s laboratory (Duke University Medical Center, Durham, NC, USA). The *Tg.hUBC-CreERT2*^{T} (Ruzankina et al., 2007) was generated in Eric. J. Brown´s laboratory (University of Pennsylvania, School of Medicine, Philadelphia, PA, USA).

By crossing the different mouse strains we generated the final genotypes used in this work.

3.1.2. Generation of Egfr$^{LmLD839A/LmLD839A}$ mutant mice

For the generation of the murine *Egfr*^{LmLD839A} allele, the genomic region encoding the murine *Egfr* gene was cloned from the BAC RP23-26C13. The D839A mutation and the LoxP-cDNA-STOP-neo-LoxP cassette were inserted in the *Egfr* genomic locus by Red/ET (“triple recombination”) (performed by Genebridges, Heidelberg, Germany), and PCR analysis confirmed correct modification of the locus. The modified *Egfr* genomic locus from the BAC was subcloned into a high-copy plasmid backbone introducing *Not*I and *Sal*I restriction recognition sites for convenient linearization of the targeting construct prior to introduction into Embryonic Stem (ES) cells.

The linearized vector was electroporated into B6129SF17/J mouse ES cells. ES cell clones having undergone proper homozygous recombination with both arms of the targeting

vector were identified by southern blot as described below (see section 2.8). Single cell suspensions of two independent and positive ES cell clones (58 and 103) were microinjected into FVB donor blastocysts, which were then implanted into pseudopregnant C57BL/6J females. The Transgenic Mice Unit at the CNIO performed the electroporation and aggregation procedures. Two male founder chimera pups were backcrossed to C57BL/6J females for germline transmission of the targeted allele.

3.1.3. Maintenance of mice

All mice used in these projects were housed in the Animal Facility of the Spanish National Cancer Research (CNIO) in accordance with Federation of European Laboratory Animal Science Association (FELASA) recommendations and following European Union legislation. All experiments described in this thesis have been approved by the Bioethics and Animal Welfare Committee of the Institute for Health Care Carlos III. Mice were subjected to light and dark cycles of 12 hours each with temperature and humidity regulated. Animals were fed *ad libitum* with a standardized diet (28018S, Tekland).

3.2. *In vivo* proceedings

3.2.1. Doxycycline and caerulein treatments

The *Elas-tTA/tetO-Cre* transgenes drive the expression of the bacterial Cre-recombinase from the *Elastase* promoter under the negative control of doxycycline (Tet-off system). In the absence of doxycycline, the expression of the Cre-recombinase starts at embryonic day 16.5 (E16.5) (*embryonic protocol* henceforth). The enzyme recognizes the LoxP sites in the *K-Ras*^{LSLG12Vgeo} locus and allows the expression of resident *K-Ras*^{G12Vgeo} oncogene in 20-30% of acinar cells (Guerra et al., 2007). To prevent the expression of the *Elastase*-driven Cre-recombinase, doxycycline is provided and the enzyme is not expressed. At 2 months of age (or P60), doxycycline is removed and the expression of the Cre-recombinase allows for the expression of the *K-Ras*^{G12Vgeo} mutation in the adulthood (*adult protocol* henceforth) (Guerra et al., 2007) (Figure 5).

Doxycycline (2mg/ml; Sigma) was provided in the drinking water as a sucrose solution (5% w/v) to pregnant mothers from the time of conception and to their offspring until the time of activated expression of the resident *K-Ras*^{G12Vgeo} oncogene (P60, at this time we considered that mice have reached adulthood). The doxycycline provided in the drinking water was changed every two days, being photolabile. In the *adult protocol* and for the appearance of tumors, chronic pancreatitis was needed. Pancreatitis was induced by caerulein (Sigma-Aldrich), a cholecystokinin analog. Caerulein was administered as a 0.1ml single daily intraperitoneal injection of 125µg/Kg, 5 days per week for 3 months (from P90 to p180).

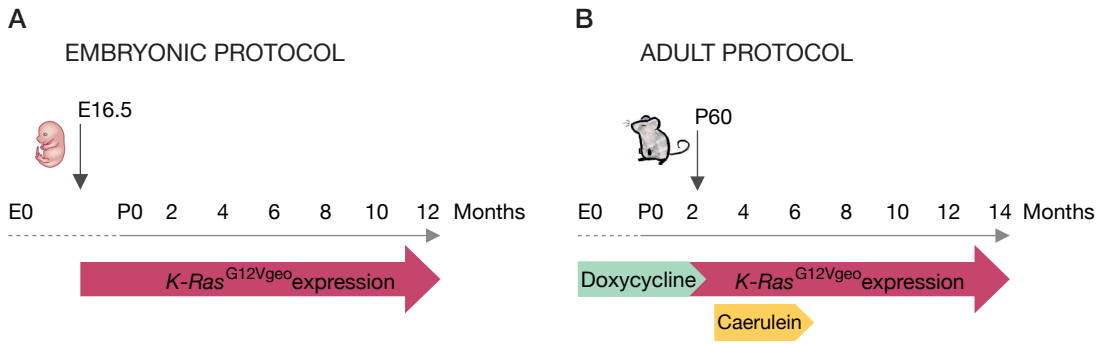

Figure 5. Schematic representation of protocols and treatments. (A) Schematic diagram of timing at which the resident knockin *K-Ras* oncogene is expressed during embryonic development. Mutated oncogene is expressed from embryonic day 16.5, animals were sacrificed and their pancreas analyzed at 1 year of age. (B) Schematic diagram of the timing at which the *K-Ras*^{G12Vgeo} is expressed in adult mice. In the *Elas-tTA/tetO-Cre; K-Ras*^{LSLG12Vgeo} strain, the mothers and their offspring were exposed to doxycycline in drinking water to prevent expression of the oncogene until the animals were 2 months old. These mice do not develop any lesions unless they underwent pancreatitis, thus pancreatitis was induced by caerulein treatment for 3 months. Mice were sacrificed and their pancreas analyzed at 14 months of age.

3.2.2. Abdominal Ultrasound

Imaging studies were done by the Molecular Imaging Core Unit at CNIO. Briefly, mice were anesthetized with 4% isoflurane (Braun Vetcare) in 100% oxygen at a rate of 1.5 liter/min. Hypothermia associated with anesthesia was avoided using a bed-heater. Abdominal hair was removed by depilation cream to prepare the examination area. Mice were screened for PDAC and tumors were measured with a micro-ultrasound system Vevo 770 (Visualsonics, Toronto, Canada) with an ultrasound transducer of 40 MHz (RMV704, Visualsonics, Toronto, Canada). PDAC size was calculated as LengthxWidth^2 /2.

3.2.3. Tamoxifen diet

Tamoxifen diet was provided to induce the activity of the modified CreERT2-recombinase (tamoxifen inducible Cre-Estrogen Receptor (ER) fusion protein expressed from the transgene *Tg.hUC-CreERT2*^{T}). Tamoxifen allows for the CreERT2 enzyme to translocate into the nucleus to achieve target deletion or expression of floxed alleles. The standardized diet (28018S, Tekland) contains natural estrogens like genistein, a phytoestrogen that belongs to the category of the isoflavones. The genistein has been shown to interact with animal and human estrogen receptors. Hence, to avoid the competition between genistein and tamoxifen for the estrogen receptor, and to eliminate them from the organism, we used a transition diet (2919S Tekland) that lacks the main sources of these compounds in rodent diet (alfalfa or soybean) for a minimum of 10 days. Afterwards, mice were fed with Tekland CRD Tam^{400}/CreER tamoxifen containing diet *ad libitum*. Tamoxifen is hydroxylated in the mouse

liver into 4-Hydroxytamoxifen (4-OHT), which is the active metabolite of tamoxifen.

3.2.4. Standard necropsy

Necropsies were performed in the dissection laboratory. Mice were euthanized in a CO_2 chamber and several tissue samples were collected either in 10% buffered formalin, embedded In Optimal Cutting Temperature compound (OCT) and/or frozen at -80ºC to be sectioned at a later time on a microtome-cryostat or directly frozen in dry ice for extraction of protein, DNA or RNA. The Comparative Pathology Core Unit at CNIO processed all the tissues samples fixed in formalin. Embryos were extracted from the uterus of the mother at different time points (E13.5 and E18.5), fixed in formalin and processed by the Comparative Pathology Core Unit at CNIO.

3.3. Genotyping

3.3.1. DNA extraction

At weaning, a piece of the tail of the mouse was cut to extract genomic DNA for genotyping. Cells were cultured, harvested and collected in pellets. Tissues and cells were incubated with a lysis buffer (20mM Tris-HCl pH 8.0, 100mM NaCl, 0.5% SDS, 10mM EDTA pH 8.0 and milliq H_2O) and 400µg/ml of proteinase K overnight at 55ºC. The next day, 300µl of saturated NaCl were added to the digested sample. After mixing vigorously by inversion, the mix was incubated on ice for 10 minutes. The samples were then centrifuged at 13,000 rpm for 10 minutes at 4ºC. The supernatant was transferred to a clean eppendorf, 800µl of isopropanol were added and the solution was mixed vigorously. Then, after incubating the mix for at least 5 minutes at room temperature to allow DNA precipitation, the samples were centrifuged at 13,000 rpm for 30 minutes at 4ºC. The supernatant was discarded and the pellets were washed twice with 500µl of 70% ethanol (EtOH). The samples were centrifuged again at 13,000 rpm for 10 minutes at 4ºC and the supernatant was discarded. Finally, the pellets were left to air dry. Dry pellets were resuspended in 100µl of Tris-EDTA buffer solution.

3.3.2. Genotyping PCR

Most of the mice were genotyped by Transnetyx (Cordoba, TN, USA). Nevertheless, occasionally for mice and always for cell lines, the genotyping was done as following.

Isolated genomic DNA from mice tails were used for genotyping by Polymerase Chain Reaction (PCR). Each reaction contained: 1µl $MgCl_2$ 25mM, 2µl Taq-Polymerase Buffer 1X, 0.25µl dNTPs 10mM, 0.2µl BSA 10 mg/ml, 0.1µl Taq-Polymerase (5U/µl EcoTaq, Ecogen), 0.75µl of each of the primers (10µM, Sigma), 1µl of DNA and up to 20µl of milli-q H_2O.

The oligonucleotides used for genotyping, and the expected bands were:

K-Ras^{LSLG12Vgeo}

K-Ras I0: 5´-CGTCCAGCGTGTCCTAGACTTTA-3´

K-Ras 3'ex1: 5´-CTCAGTCATTTTCAGCAGGC-3´

K-Ras STOP: 5´-TAGTGCCTTGACTAGAGATCA-3´

K-Ras^{LSLG12Vgeo} allele: 590bp (K-Ras STOP + K-Ras 3'ex1)

K-Ras^{+} allele: 420bp (K-Ras I0 + K-Ras 3'ex1)

K-Ras^{G12Vgeo} allele: 669bp (K-Ras I0 + K-Ras 3'ex1)

p16Ink4a/p19Arf ^{Lox}

p16/p19 forward: 5´-CCTGACTATGGTAGTAAAGTGG-3´

p16/p19 reverse: 5´-ACGTGTATGCCACCCTGACC-3´

p16Ink4a/p19Arf^{Lox} allele: 390bp

p16Ink4a/p19Arf^{+} allele: 290bp

p53^{Lox}

p53 forward: 5´-CACAAAAACAGGTTAAACCCAG-3´

p53 reverse: 5´-GAAGACAGAAAAGGGGAGGG-3´

p53^{Lox} allele: 370bp

p53^{+} allele: 288bp

Egfr^{LmLD839A}

Egfr KD forward: 5´-ACCGCATCAAGCAAAG-3´

Egfr KD 2R reverse: 5´-CGATCTTCCAGGTAGTTCA-3´

Egfr^{LmLD839A} allele: 246bp

Egfr^{D839A} allele: 282bp

Egfr^{+} allele: 189bp

K-Ras^{FSFG12V}

K-Ras 3'ex1: 5´-CTCAGTCATTTTCAGCAGGC-3´

K-Ras STOP: 5´-TAGTGCCTTGACTAGAGATCA-3´

K-Ras 2F_8B2: 5´-CCACAGGGTATAGCGTACTATGCAG-3´

K-Ras^{FSFG12V} allele: 507bp (K-Ras STOP + K-Ras 3'ex1)

K-Ras^{+} allele: 358bp (K-Ras 2F_8B2 + K-Ras 3'ex1)

K-Ras^{G12V} allele: 441bp (K-Ras 2F_8B2 + K-Ras 3'ex1)

p53^{FRT}

p53 FRT forward: 5´- CAAGAGAACTGTGCCTAAGAG-3´

p53 FRT reverse: 5´- CTTTCTAACAGCAAAGGCAAGC -3´

p53 Δ Rv: 5´-ACTCGTGGAACAGAAACAGGCAGA-3´

p53^{FRT} allele: 292bp (p53 FRT forward + p53 FRT reverse)

p53$^{\Delta}$ allele: 352bp (p53 FRT forward + p53 Δ reverse)

p53^{+} allele: 258bp (p53 FRT forward + p53 FRT reverse)

Egfr^{Lox}

Egfr forward 15C9: 5´-CTCTTGACTGCTGCCAACTTAG-3´

Egfr reverse 7B9: 5´-GAGATCTCCACACTTCCAGGTCA-3´

Egfr^{Lox} allele: 550bp

Egfr^{+} allele: 350bp

c-Raf^{Lox}

c-Raf forward 1F: 5´-CTGATTGCCCAACTGCCATAA-3´

c-Raf forward 3F: 5´-GAGTCAGCAAATGCACTGAAATG-3´

c-Raf reverse: 5´-ACTGATCTGGAGCACAGCAAT-3´

c-Raf^{Lox} allele: 196bp (c-Raf 1F forward + c-Raf reverse)

c-Raf $^{\Delta}$ allele: 270bp (c-Raf 3F forward + c-Raf reverse)

c-Raf $^{+}$ allele: 143bp (c-Raf 1F forward + c-Raf reverse)

The following PCR program was used: denaturation at 94°C for 1 minute, followed by 35 cycles of denaturation at 94°C for 30 seconds, annealing at 60°C for 30 seconds and extension at 72°C for 1 minute, and finally, followed by a long extension at 72°C for 10 minutes.

3.4. Processing of mouse tissues

3.4.1. X-Gal staining on cryosections

The *K-Ras*^{LSLG12Vgeo} allele carries an IRES-βgeo cassette within the 3´ non-translated sequences. The Internal Ribosomal Entry Site (IRES) allows for bicistronic translation of βgeo sequences from a transcript driven by the endogenous *K-Ras* promoter upon Cre-recombinase cleavage of the STOP transcriptional cassette (Guerra et al., 2003). βgeo is a bacterial gene that contains sequences from *LacZ* (the gene encoding β-galactosidase enzyme) and *neoR* (the gene that confers resistance to neomycin). This strategy allows identification of *K-Ras*^{G12Vgeo} expressing cells by X-Gal staining.

X-Gal staining provides a visual assay of β-galactosidase activity. As mentioned before, *LacZ* gene encodes the β-galactosidase enzyme that cleaves X-Gal into galactose and 5-bromo-4-chloro-3-hydroxyindole. This second compound is then oxidized into 5,5-dibromo-4,4-dichloro-indigo. Indicative of the name, this final product has a blue color.

To detect β-galactosidase activity, pancreas and PDAC tumors were embedded in OCT and frozen at -80ºC. The samples were cut at a 10µm thickness using a microtome-cryostat (Vacutomer, Dako). Sections were stored at 4ºC overnight or 1 hour at room temperature (RT). For fixing, sections were incubated for 10 minutes at RT in a solution containing 0.2% glutaraldehyde (Sigma-Aldrich), 2mM $MgCl_2$, 5mM EGTA and 0.1M phosphate buffer pH 7.2 for 15 minutes at RT. After the fixation, sections were washed three times, 10 minutes each; with a washing solution that contains 2mM $MgCl_2$, 0.1M phosphate buffer pH 7.2, 0.02% NP-40 and 0.01% sodium deoxycholate (Sigma-Aldrich). After washes, sections were incubated in a staining solution containing 2mM $MgCl_2$, 0.1M phosphate buffer pH 7.2, 0.02% NP-40, 0.01% sodium deoxycolate, 5mM $K_3Fe(CN)_6$ (Prolab), 5mM $K_4Fe(CN)_6$ (Prolab) and 1mg/ml X-Gal (Panreac) dissolved in Dimethyl Sulfoxide (DMSO) at 37ºC overnight. The following day or after 48 hours, sections were washed 3 times with washing solution and counter-stained with Nuclear Fast Red (NFR).

3.4.2. Nuclear Fast red Staining

The NFR solution was prepared as follows: 25g aluminum sulphate (Sigma) and 0.5g NFR (Sigma) were boiled in 500ml milliq H_2O and then filtered. For counter-staining, sections were washed once with distilled-water and then introduced in a coupling with NFR solution for 30 seconds. The sections were rinsed with abundant distilled-water and dehydrated by incubating them twice for 2 minutes in 70% EtOH (Panreac), twice for 2 minutes with 100% EtOH and finally 1 minute in xylol (Merck). Finally, the sections were mounted with mounting media (Dako).

3.4.3. Histopathology and immunohistochemistry

Specimens were fixed in 10% buffered formalin (Sigma-Aldrich) and embedded in paraffin. For histopathological analysis, pancreas were serially sectioned (3μm thick) and every ten sections stained with hematoxylin and eosin (H&E). Sections (3μm thick) of bone marrow, brain, heart, kidney, large intestine, liver, lung, pancreas, skin, small intestine, spleen, stomach and thymus were stained with H&E for histopathological examination.

Antibodies used for immunohistochemistry included pre-diluted rat monoclonal anti-Cytokeratin 19 (CK-19) (Monoclonal Antibodies Core Unit; CNIO) and rabbit polyclonal anti-cleaved Caspase3 (1:750; Cell Signaling #9661). Toluidine blue staining was performed in skin paraffin slides in order to detect mast cells.

3.4.4. Laser Capture Microdissection and PCR analysis

Approximately 7,000-10,000 cells were obtained by Laser Capture Microdissection (LCM) using a PALM microbeam Zeiss Axio Observer (Carl Zeiss) from pancreas cryosections (10μm thick) stained with X-Gal to identify cells expressing (blue staining) and non expressing (not stained) *K-Ras*^{G12V} oncogene, as previously described (Guerra et al., 2003). Cells from PanIN lesions were also obtained by LCM from paraffin sections (3μm thick). The cap containing captured cells was mixed with 25μl NIDD buffer (50mM KCl, 10mM Tris-HCl pH 7.5, 2mM $MgCl_2$, 0.45% NP-40, 0.45% Tween-20) containing 400μg/ml proteinase K and incubated overnight at 55ºC with gentle shaking. Samples were boiled for 10 minutes to inactivate proteinase K and 5μl of the product was submitted to PCR amplification in the presence of 1μl $MgCl_2$ 25mM, 2μl Taq-Polymerase Buffer 1X, 0.25μl dNTPs 10mM, 0.2μl BSA 10mg/ml, 0.1μl Taq-Polymerase (5u/μl EcoTaq, Ecogen), 0.75μl of each of the primers (10μM, Sigma-Aldrich), and up to 25μl of milliq H_2O.

Primers used and the expected bands were the following:

Egfr^{LmLD839A}

Egfr KD forward: 5´-ACCGCATCAAGCAAAG-3´

Egfr KD 2R reverse: 5´-CGATCTTCCAGGTAGTTCA-3´

Egfr^{LmLD839A} allele: 246bp

Egfr^{D839A} allele: 282bp

Egfr^{+} allele: 189bp

c-Raf^{Lox}

c-Raf forward 1F: 5´-CTGATTGCCCAACTGCCATAA-3´

c-Raf forward 3F: 5´-GAGTCAGCAAATGCACTGAAATG-3´

c-Raf reverse: 5´-ACTGATCTGGAGCACAGCAAT-3´

c-Raf^{Lox} allele: 196bp (c-Raf 1F Forward + c-Raf Reverse)

c-Raf$^{\Delta}$ allele: 270bp (c-Raf 3F Forward + c-Raf Reverse)

c-Raf^{+} allele: 143bp (c-Raf 1F Forward + c-Raf Reverse)

The following PCR program was used: denaturation at 94°C for 1 minute, followed by 35 cycles of denaturation at 94°C for 30 seconds, annealing at 60°C for 30 seconds and extension at 72°C for 30s, and finally, followed by a long extension at 72°C for 10 minutes.

3.5. Tissue Culture

3.5.1. Tissue culture conditions

Cells were maintained in an incubator at 37ºC with 16% O_2 and 5% CO_2. Mouse PDAC cell explants, Mouse Embryonic Fibroblasts (MEFs) and HEK293T cells (ATCC® Number CRL-11268^{TM}) were cultured in Dulbecco´s Modified Eagle´s Medium (DMEM; Gibco) with 10% (vol/vol) of Fetal Bovine Serum (FBS; Gibco) and 1% Penicillin/Streptomycin (Gibco). When specified, 10% Calf Bovine Serum (CBS; Gibco) replaced FBS.

3.5.2. PDAC cell explants

To generate mouse PDAC explants, freshly isolated tumors were minced with sterile razor blades, digested with collagenase P (1.5µg/ml) in Hank´s Balanced Salt Solution (HBSS; Gibco) for 30 minutes at 37ºC, and cultured in DMEM with 10% FBS and 1% Penicillin/Streptomycin. After 48 hours, media was supplemented with G418 (75µg/ml; Sigma-Aldrich), an analog of neomycin sulfate, to select *K-Ras*^{G12Vgeo} mutant cells, due to the presence of the neomycin resistance cassette (geo; section 3.4.1) in cells expressing the oncogene.

All studies were done on cells maintained in culture for less than 10 passages. Their corresponding genotypes were verified by PCR analysis.

3.5.3. Derivation of MEFs from mouse strains

Timed pregnancies were set up and MEFs were isolated from E13.5 embryos 13 days after the appearance of the copulation plug. Embryos were separated by slicing through the

uterus in the regions between each embryo. The yolk sac was gently pulled off with forceps. Embryos were washed by immersion in three consecutive 10 cm tissue culture plate with PBS with 1% Penicillin/Streptomycin. The head, separated from the body using forceps, was used for genotyping. After tearing out the red tissue (heart and liver), the rest of the embryo was placed in a 6 cm tissue culture plate and dissected manually with a blade to mince the tissue into pieces of 1-2mm and incubated 10 minutes with 4ml 0.25% trypsin-EDTA. The dish was removed from the incubator and cells pipetted up and down several times with a 10ml pipet, and then placed in a 37°C tissue culture incubator for another 5 minutes. The cell suspension was then transferred to a 10cm tissue culture plate with 16ml of DMEM supplemented with 10% FBS and 1% Penicillin/Streptomycin. When cells were confluent, usually after 48 hours, they were harvested by trypsinization, spun down, and the cell pellet resuspended in freezing medium (DMEM with 20% fetal bovine serum and 10% DMSO). The MEFs were aliquoted into cryovials and frozen using standard methods for mammalian cell cryopreservation.

3.5.4. Immortalization of MEFs

To immortalize cells, primary MEFs we continuously plated 1.0 x 10^6 cells in a 10cm tissue culture plate with DMEM, 10% FBS and 1% Penicillin/Streptomycin every 3 days for 15-20 passages (also known as 3T3 protocol). Cells tend to enter a crisis stage around passage 5-6, where they would not actively proliferate between passages. Once the crisis stage had passed and cells continuously proliferate to more than double the seeded density they were considered immortal and frozen down. Same protocol was followed with DMEM 10% Calf Bovine Serum (CBS; Gibco), although in this case, the crisis stage was longer.

3.5.5. Proliferation MTT assay

Cells were cultured in DMEM containing either CBS or FBS. Cells were seeded in 96 well plates at a density of 1,000 cells/well and incubated in DMEM supplemented with 10% FBS or 10% CBS and 1% Penicillin/Streptomycin. Proliferation assays were done for 8 days and proliferation rate was determined by the 3-(4,5-dimethylthiazol-2-yl)-2,5-diphenyltetrazolium bromide (MTT) assay (Roche). The resulting absorbance was measured with a microplate reader at 590 nm (EnVision 2104 Multilabel Reader, Perkin Elmer, Walthman, MA). Results represent the average of six independent experiments in which all samples were assayed in triplicate.

3.5.6. Egfr Phosphorylation Assay

MEFs were serum starved for 16 hours before ligand stimulation. Ligand stimulation was performed using 150ng/ml EGF (Sigma Aldrich) at 37ºC for 5 minutes. Cells were lysed and Egfr was immunoprecipitated from protein extracts using anti-Egfr monoclonal antibody (1:50;

Rabbit monoclonal; Abcam ab52894) bound to protein A sepharose (GE Healthcare). Proteins were separated on SDS/PAGE gel and transferred to a nitrocellulose membrane for immunoblotting with anti-Egfr antibody (1:100; Rabbit monoclonal; Abcam ab52894) and anti-Phosphotyrosine 4G10 HRP-conjugated (1:10,000; Mouse monoclonal; Millipore 16-316). For time-course and EGF-stimulation assays, $1x10^6$ MEFs or tumor cells, respectively, were seeded in p10 plates. The next day cells were rinsed twice with PBS and serum starved for 16 hours. They were stimulated with EGF (150ng/ml) during the indicated time periods and collected for Western blot.

3.5.7. Acinar to ductal metaplasia assay

Cell explants of normal adult mouse pancreas were established by modification of previously published protocols (Githens et al., 1994; De Lisle and Logsdon, 1990; Wagner et al., 2002). Whole pancreas was harvested and digested in 0.2mg/ml collagenase-P (Roche) at 37ºC. Following multiple washes with HBSS supplemented with 5% FBS, collagenase-P (Roche) digested pancreatic tissue was sequentially filtered through 100µm polypropylene mesh (Spectrum Laboratories). The filtrate was passed through a 30% FBS cushion at 1,000 rpm. The cellular pellet was resuspended in RPMI 1640 (Lonza) supplemented with 1% Penicillin/Streptomycin and 10% FBS. An equal volume of neutralized Rat-Tail Collagen type I (RTC; Discovery Labware Inc.) was added to the cellular suspension. The cellular/RTC suspension was supplemented with 0.1mg/ml soybean trypsin inhibitor (Sigma-Aldrich) and 1µg/ml dexamethasone (Sigma-Aldrich). Cellular/RTC suspension (500µl) was pipetted into each well of a 24 well plate pre-coated with 200µl of RTC. After solidification of the RTC, media supplemented with Penicillin/Streptomycin and FBS (at above mentioned concentrations) was added. Cultures were maintained at 37ºC in a 5% CO_2 incubator for 5 days with medium replaced on days 1 and 3. The first day G418 was added to the media at a final concentration of 75µg/ml to select those cells expressing the resident *K-Ras*^{G12V} oncogene (about 30% of all acinar cells). Cell explants were maintained in the presence or absence of recombinant human TGFα 50ng/ml (PrePro Tech, 100-16A) and/or EGF 50ng/ml (Sigma-Aldrich, E4127).

3.5.8. Infection of cells with Adenoviruses

Mouse PDAC cell explants were seeded at equal densities and were infected at 100 MOI (Multiplicity Of Infection) with Adeno-CreGFP (Adenovirus expressing Cre-recombinase and Green Fluorescent Protein) particles. Five days post-infection cells were screened for GFP and then seeded to assess their colony formation ability.

3.5.9. Colony formation assay

Cells were seeded in 10 cm tissue culture dishes at equal densities (2,000 and 5,000 cells). They were allowed to form colonies for approximately 2 weeks. Fresh media was added to the tissue culture plates twice a week. After 10-14 days colonies were stained with crystal violet.

3.5.10. Crystal violet staining of colonies

First, the media was removed from the plates and they were washed with PBS. Cells were fixed for 5-10 minutes with 7ml of glutaraldehyde 0.1%. Then they were rinsed with PBS and stained with crystal violet 0.5% for one hour. Afterwards the plates were washed with water several times, to remove excess dye and dried at RT overnight.

3.5.11. Production of lentivirus and infection of cells

Lentiviral supernatants were produced in HEK293T cells (70%-80% confluence). Packaging plasmids pLP1 (1.9μg), pLP2 (1.3μg), pLP/VSVG (1.64μg) (Invitrogen) and the lentiviral construct (5μg) were mixed and added to 40μl of Polyethylenimine (1mg/ml) and 500μl serum free DMEM. The mixture was vortexed for 5 seconds and incubated at RT for 15 minutes. HEK293T cells were transfected by addition of this transfection mix dropwise. Transfected cells were incubated at 37ºC overnight followed by a 24 hours incubation at 32ºC. Lentiviral supernatant was collected and filtered with 0.45μm pore size filters. Cells were infected with this filtered solution and Polybrene added at a concentration of 8μg/ml. Alternatively, filtered lentiviral supernatant could be stored at -80ºC for later use. After infection cells were selected with 2μg/ml puromycin for 48h.

Knockdown of ErbB2 was mediated with lentiviral Mission short hairpin RNA (shRNA) plasmid (Sigma TRCN0000234103). Non-target shRNA control vector was used as a negative control.

3.6. Western blot

3.6.1. Protein Extraction

Protein extraction, either from tissues or cultured cells, was performed in NP-40 lysis buffer: 50mM Tris-HCl pH 7.4, 150mM NaCl, 0.5% NP40, and a cocktail of proteases and phosphatases inhibitors (cOmplete Mini, Roche; Phosphatase Inhibitor Cocktail 2 and 3, Sigma-Aldrich). For tissue protein extraction, we used a homogenizer to mechanically breakdown the tissue samples and maximize the efficiency of lysis. Five zirconium beads were added to a 1.5ml screw capped tube together with the sample and four volumes of lysis buffer.

The samples were incubated on ice for 30 minutes. The extracts were centrifuged for 10 minutes at 13,000 rpm and 4ºC to remove the undigested membranes/DNA and the supernatant was transferred to a new tube. To quantify the amount of protein obtained, we used the Bradford method (Bio-Rad) (1µl of the protein extract was added to 1ml of 1X Bradford reagent and the absorbance was read on a spectrophotometer at 595nm). Bovine Serum Albumin (BSA) was used to generate a standard curve.

3.6.2. Protein electrophoresis

Tissue/cell extracts (25/50µg) were prepared for loading in the gel by adding 4X loading buffer and 10X reducing agent (Thermo Fisher Scientific). Samples were boiled for 5 minutes at 95ºC, spun down and loaded in Nupage Bis-Tris Midi gels (Thermo Fisher Scientific). MOPS 1X (Thermo Fisher Scientific) running buffer was used for separating large- to medium-sized proteins. In addition, we loaded 10µl of Spectra Multicolor Broad Range Protein Ladder (Thermo Fisher Scientific) for molecular weight reference.

3.6.3. Transferring the denatured proteins to a membrane

A piece of nitrocellulose transfer membrane (GE Healthcare) and Whatman 3MM (Sigma-Aldrich) paper were sized to gel and prewet in transfer buffer (Tris-Glycine 1X, Lonza; MeOH 20%, Panreac). A “transfer sandwich” was assembled in the following order: cathode, 4x Whatman paper, gel, nitrocellulose membrane 4x Whatman paper, anode. Generally wet transfers were performed, as it is recommended specially for proteins with a large molecular weight. The gel was transferred for 70 minutes at a constant current of 0.40A and maximum power. Afterwards, staining with Ponceau S solution (Sigma) was performed to check the efficiency of protein transfer.

3.6.4. Blocking and antibodies

Membranes were blocked by incubation with 5% BSA in TBST (1X Tris-Buffered Saline (TBS) solution; 0.1% of Tween-20) for phosphorylated proteins, and 5% non-fat milk in TBST buffer for the rest of the proteins, for 45 minutes at RT. Incubation with primary antibodies diluted in the blocking solution was performed overnight on a rotating platform at 4ºC. The next day, the membranes were washed three times with 1X TBST buffer for 10 minutes on a shaking platform at RT. Afterwards, blots were incubated for 1h with the appropriate secondary antibodies HRP (1:2000, Dako) or fluorescence (1:5000, Life Technologies) labeled. For HRP secondary antibodies, protein visualization was carried out with and enhanced chemiluminiscent system (ECL Plus; Amersham Biosciences) using different exposure times depending on the antibody. For the fluorescent secondary antibodies, the LICOR scanner was used.

Membranes were blotted with antibodies raised against Egfr (1:100; Rabbit monoclonal; Abcam ab52894), phospho-Egfr Tyr1068 (1:1,000; Rabbit monoclonal; Cell Signaling #3777), ErbB2 (1:500; Rabbit monoclonal; Cell Signaling #3250), Akt (1:500; Rabbit polyclonal; Cell Signaling #9272), phospho-Akt Ser473 (1:250; Rabbit polyclonal; Cell Signaling #9271), Erk1/2 (Erk1, 1:2,000 Mouse monoclonal BD Biosciences 554100; Erk2 1:1,000 Mouse monoclonal BD Biosciences 610103), phospho-Erk1/2 Thr202/Tyr204 (1:500; Rabbit polyclonal; Cell Signaling #9101), Phospho-tyrosine 4G10 HRP-conjugated (1:10,000; Mouse monoclonal; Millipore 16-316) and Gapdh (1:10,000; Mouse monoclonal; Sigma-Aldrich G8795) for loading control.

3.7. Quantitative Real Time PCR

3.7.1. RNA extraction

Total RNA was extracted from cells using the RNeasy Mini Kit (Qiagen). Briefly, cells were washed with cold PBS and scrapped with RLT lysis buffer. Lysates were transferred to a QIAshredder column in order to shred tissue finely. After centrifuging at maximum speed for 2 minutes at 4ºC, one volume of 70% EtOH was added to the flow-through and mixed by pipetting. Then, up to 700µl was transferred to an RNeasy spin column. Columns were centrifuged for 30 seconds at 1,000 rpm and flow-through was discarded. Following 350µl of RW1 buffer were added to the column and again centrifuged. Residual genomic DNA was removed from the samples by digestion with 10µl of DNAse in 70µl RDD buffer per column. Digestion was performed on column, during incubation at RT for 15 minutes. To stop the digestion, 350µl of RW1 buffer were added to the column followed by centrifugation. Flow-through was discarded and 500µl of RPE buffer were added to wash the column, it was discarded after centrifuging for 2 minutes at 10,000 rpm. Residual alcohol was removed by doing a dry spin at maximum speed for 1 min. RNA was then eluted in 30-50µl of RNase free H_2O. Finally, RNA was quantified using a Nanodrop spectrophotometer.

3.7.2. cDNA synthesis: Reverse Transcription PCR (RT-PCR)

cDNA synthesis was performed using SuperScript II Reverse Transcription kit (Thermo Fisher Scientific) following manufacture´s protocol. For each sample 1µg of RNA in 6µl of H_2O was incubated for 2 minutes at 65ºC followed by 2 minutes on ice. Afterwards, the following mix was added: 4µl of 5X buffer, 2µl of 0.1M DTT, 2µl of 10mM dNTPs, 0.5µl of RNAse inhibitor (400U/µl), 5µl of random primers (previously diluted 1:30) and 0.5µl of the SII polymerase (200U/µl). The mixture was incubated for 10 minutes at RT and then 1 hour at 42ºC. The reaction was stopped by heating at 98ºC for 5 minutes. Finally, 80µl of H_2O were added to the

reaction and samples were frozen at -20ºC.

3.7.3. Real Time PCR

Designed primers had a melting temperature between 58ºC-61ºC, length of 100-200bp, and when possible cover an exon-exon junction (to avoid the problem of possible residual genomic DNA contamination). Primers were ordered to Sigma-Aldrich with standard desalting purification.

Primers used were the following:

Egfr

Egfr forward: 5´-GCCATCTGGGCCAAAGATACC- 3´

Egfr reverse: 5´-GTCTTCGCATGAATAGGCCAAT- 3´

Gapdh

Gapdh forward: 5´-CCCACTAACATCAAATGGGG- 3´

Gapdh reverse: 5´-CCTTCCACAATGCCAAAGTT- 3´

Quantitative RT-PCR assays were performed with the AB 7900 Fast Real Time PCR System using Power SYBR Green PCR Master Mix (Applied Biosystems). For each sample the following mix was added: 10µl SYBR Green Mix (Roche), 0.5µl of 10µM primer forward, 0.5µl of 10µM primer reverse, 1µl of cDNA template and 8µl of H_2O. Samples were prepared in a 96-well plate, sealed with optical adhesive film.

3.7.4. Data analysis

The relative mRNA expression was calculated using the comparative cycle threshold (Ct) method:

$\Delta\Delta Ct = \Delta Ct$ sample $- \Delta Ct$ reference

ΔCt sample is the Ct value for any sample normalized to the endogenous housekeeping gene and ΔCt reference is the Ct value for the calibrator also normalized to the endogenous housekeeping gene (*Gapdh*).

3.8. Southern blot

3.8.1. DNA extraction

A phenol-chloroform protocol was followed in order to obtain DNA pure enough for southern application. Cells were lysed overnight at 55ºC in lysis buffer (20mM Tris-HCl pH 8.0, 100mM NaCl, 0.5% SDS, 10mM EDTA pH 8.0 and milli-q H_2O) with 400µg/ml of proteinase K. The next day, 500µl of phenol were added and mixed vigorously by vortexing to create an emulsion. The mix was centrifuged for 5 minutes at 13,000 rpm at 4ºC. The upper aqueous phase was transferred to a new 1.5ml tube. 500µl of phenol-chloroform were added and mixed vigorously by vortexing to create an emulsion. The mix was centrifuged for 5 minutes at 13,000 rpm and 4ºC. The upper aqueous phase was transferred to a new 1.5ml tube. 500 µl of chloroform were added and mixed vigorously by vortexing to create an emulsion. The mix was centrifuged for 5 minutes at 13000 rpm and 4ºC. The upper aqueous phase was transferred to a new 1.5ml tube. 700µl of isopropanol were added and mixed by inverting the tube 15 times. To allow for precipitation the mix was incubated 10 minutes at RT. The mix was centrifuged for 15 minutes at 13,000rpm and 4ºC. The supernatant was discarded avoiding disruption of the pellet. The pellet was cleaned with 1ml of 70% ethanol. The mix was centrifuged for 5 minutes at 13,000rpm and 4ºC. Again, the supernatant was discarded avoiding disruption of the pellet. The pellet was dried and finally dissolved in Tris-EDTA buffer solution.

3.8.2. DNA digestion with restriction enzymes

DNA (30-50µg) was prepared in a 26µl volume. To perform digestion the following was added to each DNA sample: 3µl of restriction enzyme of interest, 1µl RNase DNase-free, 4µl of spermidine, 4µl of 10X restriction enzyme buffer and 2µl of 100X BSA. The final mix of 40µl was mixed well and incubated at 37°C overnight. The digested genomic DNA was resolved in a 0.8% agarose gel to obtain enough separation of the expected bands. The gel was washed with distilled H_2O and incubated with 0.25N HCl for 15 minutes in gentle agitation to depurinate DNA fragments, break the DNA into smaller pieces that will be easily transferred from the gel to the membrane. Then, it was rinsed with distilled H_2O and incubated with denaturing solution (0.5 M NaOH, 1.5 M NaCl) for 20 minutes with gentle agitation to denature the double-stranded DNA. Afterwards, the gel was transferred to the neutralizing solution (0.5 M Tris-HCl pH 8.0, 1.5 M NaCl) for 30 minutes with gentle agitation. Finally, the gel was equilibrated with transfer buffer 10X Saline Sodium Citrate (SSC) for at least 10 minutes. Then, the DNA was transferred to a nylon membrane by capillarity with 10X SSC buffer. To this end, a “transfer sandwich” was prepared. First, 3mm Whatman blotting paper was placed on a facedown plastic gel mold within a pyrex tray filled with 10X SSC buffer. The following components were piled up in this order: the gel facing down, one nylon Hybond N+ membrane (Amersham), two pieces of Whatman paper (cut to size of gel and membrane), and finally on top a stack of paper towels.

The entire transfer was wrapped in plastic wrap to avoid evaporation of buffer. The DNA was allowed to transfer overnight. The next day, the membrane was exposed to $1.2x10^5$µJ of ultraviolet radiation using a UV Stratalinker 1800 (Stratagene) to permanently attach the DNA to the membrane by covalent crosslinking. Following which, the membrane was incubated with 10ml of pre-Hybridization buffer (5mM Polyvinylpyrrolidone, 2mM Ficoll, 0.1M Dextran Sulfate, 25mM Na_2HPO_4, 0.9M NaCl, 35mM SDS, 2.5M EDTA pH 8, 10mg/ml of salmon sperm DNA, 13M formamide) to reduce non-specific bindings, for at least 4 hours in a glass tube (with the DNA side facing inwards) in a rotating oven at 42°C.

3.8.3. Labeling the DNA probe and Hybridization

1µl of the probe (25-100ng) was added to 45µl of H_2O and the mix was boiled in water for 3 minutes to produce denaturation of the DNA. Right after that, it was put on ice during 3 minutes to avoid renaturation and thereafter added to an eppendorf of the kit Rediprime II Random Prime Labelling system (Amersham). Then 5µl of α32P-dCTP was added and everything was mixed by pipetting. The mix was incubated in a shaking thermoblock for 10 minutes at 37 °C to allow labeling of the probe. During this period, the pre-hybridation buffer in the glass tube with the membrane was replaced with new 10ml. The labeled probe was purified with a column from the G-50 Microcolums Radiolabeled Probe Purification Kit (Amersham). 1µl of a labeled probe against the lambda-HindIII DNA ladder was added to the recently labeled probe and 5µl of NaOH 5N was also added to induce chemical denaturation of the probes. The membrane was incubated with the labeled probes overnight at 42ºC in the rotating oven. The following day the membrane was washed in the glass tube in three steps of 20 minutes each: 2X SSC, 0.1% SDS; 1X SSC, 0.1% SDS and 0.1X SSC, 0.1% SDS at 42ºC. The membrane was placed in a plastic sleeve and exposed to a phosphoimager screen for at least 4 hours. The screen was then developed using the phosphoimager and its software (Molecular Dynamics).

3.9. Statistical Analyses

All statistical analyses were performed using unpaired Student t-test. *P*-value <0.05 was considered to be statistically significant (*p<0.05; **p<0.01; ***p<0.001). All the calculations were performed with the Excel software (Microsoft).

4. Results

4.1. Study of Egfr tyrosine kinase inhibition in PDAC initiation

Egfr deletion has been reported to impair PDAC initiation (Ardito et al., 2012; Navas et al., 2012). However, elimination of the protein cannot be achieved in the clinic and most of the current EGFR inhibitors are small molecules that inhibit EGFR tyrosine kinase activity. Because of this, it was important to investigate whether the therapeutic benefit observed upon ablation of *Egfr* in PDAC mouse models relied on Egfr catalytic activity and or on kinase independent functions.

We decided to generate a conditional knock-in allele that upon Cre-mediated recombination expresses a kinase dead Egfr protein to mimic the effect of selective and efficient EGFR inhibitors for PDAC treatment. These approaches should provide relevant information for the design of future clinical trials that will benefit cancer patients.

4.1.1. Generation of an inducible Egfr kinase dead allele: $Egfr^{D839A}$

We therefore designed an inducible *Egfr* kinase dead knock-in allele that expresses a catalytic inactive Egfr protein under its own regulatory elements upon Cre-mediated recombination. With this purpose and in order to ensure proper expression of both Egfr wild type and catalytic inactive proteins, we designed a targeting vector (Figure 6A) with the following elements in the specified order:

- A mouse *Egfr* cDNA encoding exons 21 to 28 (indicated as “minigene”)

- A transcriptional Stop sequence

- The PGK-Neomycin resistance gene cassette, in reverse orientation.

- LoxP sites flanking the aforementioned elements to allow their excision upon Cre-recombinase activity

- The exon 21 containing the point mutation, resulting in the substitution of the Aspartic acid D839 for an Alanine (D839A) in an essential conserved triad of amino acids constituting the HRD motif. This highly conserved Aspartic acid plays a critical role during catalysis as it serves as a catalytic base to accept the proton from the hydroxyl group of the substrate (Jura et al., 2011; Zhang et al., 2015b). Therefore, this mutation confers a kinase dead property to this protein, thus kinase dead mutants cannot stimulate cell signaling.

This allele will be referred to as $Egfr^{LmLD839A}$ where LmL accounts for LoxP-minigene-LoxP. $Egfr^{LmLD839A}$ mice express the wild type Egfr protein during embryonic and postnatal development because of the floxed minigene. When these sequences are removed by the Cre-recombinase, the kinase dead isoform is expressed from the targeted endogenous locus. This strategy has been successfully used earlier to express isoforms of other genes (Dankort et al., 2007).

Briefly, for the generation of the *Egfr*^{LmLD839A} allele, ES cells were electroporated with the targeting vector and homologous recombination events were identified by Southern blot (figure 6B). Mice were generated from clones (58 and 103), with the help of the Transgenic Mice Core Unit at the CNIO, and a breeding colony was established in a mixed B6;129Sf17/J background.

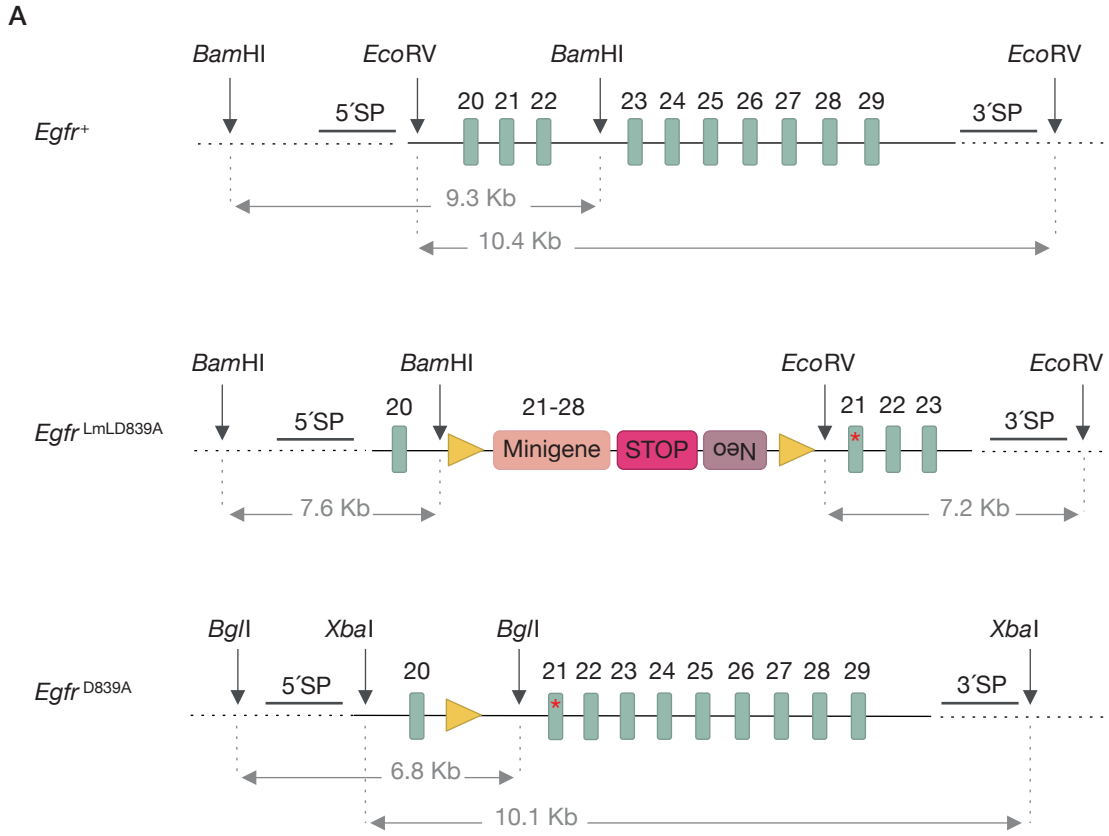

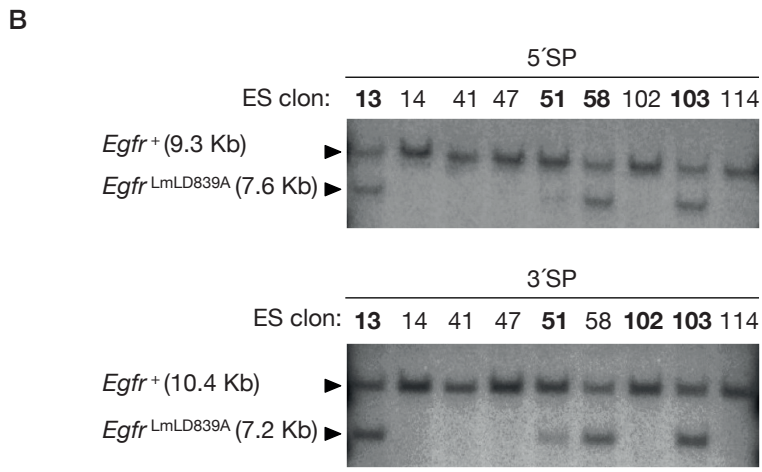

Figure 6. Schematic representation of *Egfr*$^{+}$, *Egfr*^{LmLD839A} and *Egfr*^{D839A} alleles. (A) The mouse genomic *Egfr* wild type locus (*Egfr*$^{+}$), the inducible (*Egfr*^{LmLD839A}) and the catalytic inactive (*Egfr*^{D839A}) knock-in alleles are represented. External 5´ and 3´ Southern blot probes (5´SP and 3´SP, respectively) and the size of restriction fragments are indicated. Exons (boxes), LoxP sites (triangles), Minigene (cDNA

from exon 21 to 28), Neomycin resistance cassette gene (Neo) and transcriptional Stop cassette (STOP) are depicted. The modified exon 21 encoding the D839A mutation is indicated (*). (B) Southern blot analysis for both homology arms was performed with DNA isolated from ES cell clones electroporated with the targeting vector and selected with G418. DNA was digested with *Bam*HI (for the 5´SP) and *Eco*RV (for the 3´SP). Diagnostic bands for each allele are indicated. ES homologous recombinant clones are indicated in bold.

4.1.2. Egfr kinase activity is essential for mouse embryo development

All members of the ErbB family are essential for embryo development since loss of signaling of any of them is associated with early lethality in mice. *ErbB2* null mice die at mid-gestation due to neural crest and motor nerve defects and trabecular malformation in the heart, similar to *ErbB4* deficient mice (Gassmann et al., 1995; Lee et al., 1995). *ErbB3* knockout embryos die at later stages because they lack the Schwann cell precursors, which result in the death of motor and sensory neurons (Erickson et al., 1997). *Egfr* is normally required for embryo implantation, development and appropriate maturation of central nervous system. *Egfr* knockout mice ($Egfr^{-/-}$) die at different stages of development depending on the genetic background: CF1 background results in peri-implantation death, 129/Sv mice reach mid-gestation, C57Bl/6J mice die just after birth and MF1 and CD1 mice can live for up to 20 days after birth (Miettinen et al., 1995; Sibilia and Wagner, 1995; Sibilia et al., 1998; Threadgill et al., 1995). Suggesting that this signaling cascade is differently regulated in various mouse strains and that there are other pathways capable of partially compensate Egfr signaling in the embryo. All surviving *Egfr* knockout mice suffer from neurodegeneration and defects in skin, liver, kidney and lung (Sibilia et al., 1998). Additionally, two *Egfr* mutant alleles with reduced receptor signaling have been described in mice. $Egfr^{wa2}$ mutation alters the kinase domain reducing by 80-95% the activity of the receptor (Luetteke et al., 1994). Homozygous $Egfr^{wa2}$ mice are viable but they develop impaired maternal lactation (Fowler et al., 1995). $Egfr^{wa5}$ allele encodes an entire kinase dead receptor that results from an Aspartate to a Glycine change that alters the DFG domain of the Egfr catalytic domain. $Egfr^{wa5}$ homozygotes mice die perinatally and display placental defects identical to those observed in *Egfr* knockout mice (Du et al., 2004; Lee et al., 2004).

To address the effect of the constitutive expression of the $Egfr^{D839A}$ catalytic inactive receptor, we crossed $Egfr^{+/LmLD839A}$ mice with a transgenic mouse strain expressing the Cre-recombinase under the control of the *EIIa* promoter. This strain carries a *Cre*-transgene under the control of the adenovirus *EIIa* promoter that targets expression of the Cre-recombinase in the early mouse embryo, driving recombination prior to implantation in the uterine wall (Lakso et al., 1996). Cre-mediated recombination occurs in a wide range of tissues, including germ cells that transmit $Egfr^{D839A}$ mutation to the progeny. Indeed, genotyping of the pups confirmed that the $Egfr^{D839A}$ allele was transmitted. $Egfr^{+/D839A}$ mice were crossed with C57BL/6J mice to eliminate the *EIIa-Cre* transgene. Finally, crosses between $Egfr^{+/D839A}$ mice were set up.

Egfr$^{+/D839A}$ mice reached adulthood without any apparent defect, whereas homozygous *Egfr*$^{D839A/D839A}$ mice died during embryonic development. Few *Egfr*$^{D839A/D839A}$ embryos survive until E13.5 and E18.5 (Table 2). At E18.5 mutant embryos were slightly reduced in size and weight compared to their wild type littermates. They showed open eyelids, immature lungs with poorly inflated regions and increased amount of cells in the alveolar area, and skin abnormalities with almost absent keratinization of the epidermis and poor differentiated hair follicles (Figure 7). Death in-utero probably resulted from a defect in the spongiotrophoblast layer of the placenta (the part of the placenta where maternal and fetal tissues come in closest contact); it was reduced in size, with only a thin layer of cells (Figure 7B). These results recapitulate the defects observed in *Egfr*$^{-/-}$ and *Egfr*$^{wa5/wa5}$ mice (Du et al., 2004; Lee et al., 2004; Sibilia and Wagner, 1995)

As was previously described (Sibilia and Wagner, 1995; Threadgill et al., 1995), genetic background plays an important role in regulating Egfr signaling. For this reason, we backcrossed the *Egfr*^{D839A} allele to the C57BL/6J genetic background for 7 generations to reproduce previous results (Sibilia and Wagner, 1995). However, in contrast to *Egfr*$^{-/-}$ mice that died just after birth, *Egfr*$^{D839A/D839A}$ embryos died during gestation (Table 3).

In conclusion, Egfr catalytic activity is required for embryonic development since expression of the *Egfr*$^{D839A/D839A}$ alleles resulted in embryonic lethality in both mixed and C57BL/6J pure genetic backgrounds likely due to placental defects.

Table 2. Offspring from matings between *Egfr*$^{+/D839A}$ mice (mixed background).

Stage	n	*Egfr*$^{+/+}$	*Egfr*$^{+/D839A}$	*Egfr*$^{D839A/D839A}$
E13.5	69	18 (26%)	42 (61%)	9 (13%)
E.18.5	102	25 (24.5%)	73 (71.6%)	4 (3.9%)
P0	130	46 (35%)	84 (65%)	0 (0%)

Table 3. Offspring from matings between *Egfr*$^{+/D839A}$ mice in C57BL/6J genetic background.

Stage	n	*Egfr*$^{+/+}$	*Egfr*$^{+/D839A}$	*Egfr*$^{D839A/D839A}$
E13.5	38	14 (36.9%)	20 (52.6%)	4 (10.5%)
E.18.5	68	30 (44.1.%)	38 (55.9%)	0 (0%)
P0	92	30 (32.6%)	62 (67.4%)	0 (0%)

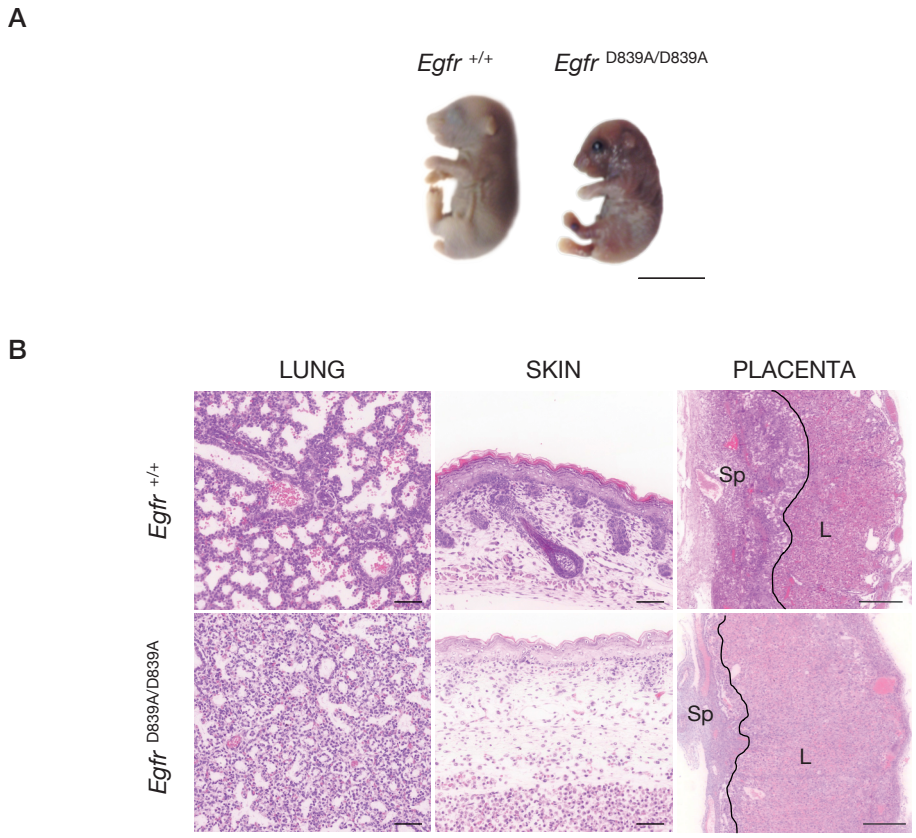

Figure 7. Constitutive expression of Egfr^{D839A} leads to embryonic lethality. (A) Representative images of wild type and *Egfr*$^{D839A/D839A}$ embryos at E18.5. *Egfr*$^{D839A/D839A}$ embryos were smaller than their wild type littermates and showed open eyelids. Scale bar represents 1cm. (B) Lung, skin and placenta H&E staining obtained from *Egfr*$^{+/+}$ and *Egfr*$^{D839A/D839A}$ embryos at E18.5. Sp: Spongiotrophoblast. L: Labyrinth. Scale bar represents 100μm (lung and skin) and 500μm (placenta).

4.1.3. Egfr^{D839A} protein has impaired kinase activity

4.1.3.1. Egfr^{D839A} shows impaired ligand-dependent phosphorylation

In order to study the role of Egfr^{D839A} *in vitro*, crosses between *Egfr*$^{+/D839A}$ mice were set up and MEFs were extracted at embryonic day E13.5. As previously mentioned, *Egfr*$^{D839A/D839A}$ embryos were not obtained at Mendelian ratios (Tables 2 and 3).

Firstly, the expression of the catalytic inactive receptor was verified by Quantitative Real time PCR (qRT-PCR) and Western blot. As expected, there were no significant differences comparing Egfr expression levels between *Egfr*$^{+/+}$, *Egfr*$^{LmLD839A/LmLD839A}$ and *Egfr*$^{D839A/D839A}$ alleles, indicating that the genetic modifications of the allele were neither affecting the expression nor the stability of the protein in primary MEFs (Figure 8A, B).

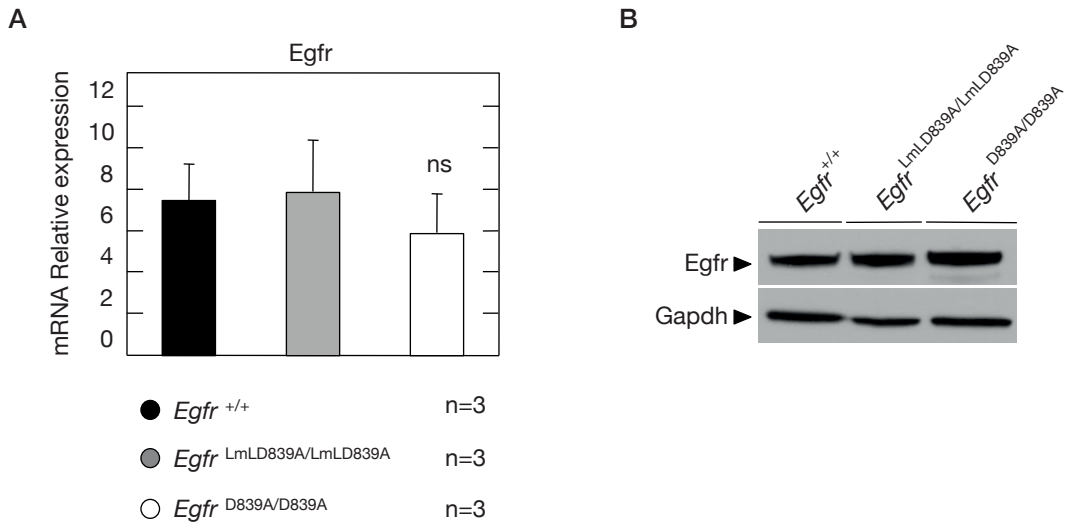

Figure 8. Analysis of the expression of the Egfr catalytic inactive receptor in MEFs. (A) qRT-PCR analysis of the relative expression levels of *Egfr* in $Egfr^{+/+}$, $Egfr^{LmLD839A/LmLD839A}$ and $Egfr^{D839A/D839A}$ MEFs (n=3). Gapdh expression levels were used for normalization. Data are represented as mean ± SD. (B) Western blot analysis of Egfr expression in whole cells extracts obtained from $Egfr^{+/+}$, $Egfr^{LmLD839A/LmLD839A}$ and $Egfr^{D839A/D839A}$ MEFs. Gapdh expression served as loading control. Migration of the indicated proteins is shown by arrowheads.

Ligand binding leads to the formation of EGFR homo- and/or heterodimers with other ErbB family members. Subsequently, the EGFR intracellular C-terminal region is phosphorylated and the catalytic domain is activated. Active EGFR recruits and phosphorylates signaling proteins, such as Grb2, which links cell surface receptors to the RAS/MAPK signaling cascade (Jorissen et al., 2003).

To evaluate Egfr catalytic activity, phosphorylation status of the receptor was assessed in response to EGF stimulation in MEFs. After Egfr immunoprecipitation we could observe that EGF-dependent phosphorylation was markedly reduced in $Egfr^{D839A/D839A}$ MEFs and consequently $Egfr^{D839A}$ protein has impaired catalytic activity (Figure 9A).

In addition, to evaluate the contribution of Egfr on ligand-induced signal transduction, phosphorylation levels of the main downstream targets were assessed at different time points in response to EGF stimulation. We analyzed by Western blot the phosphorylation status of Erk1/2 (as a readout of the MAPK pathway) and Akt (as a readout of the PI3K pathway). $Egfr^{D839A/D839A}$ mutant MEFs failed to trigger MAPK and PI3K signaling and both pathways were downregulated compared to wild type MEFs (Figure 9B). Furthermore, phosphorylation of Egfr (Tyr 1068) in $Egfr^{D839A/D839A}$ mutant MEFs was absent, which is in accordance with the immunoprecipitation results.

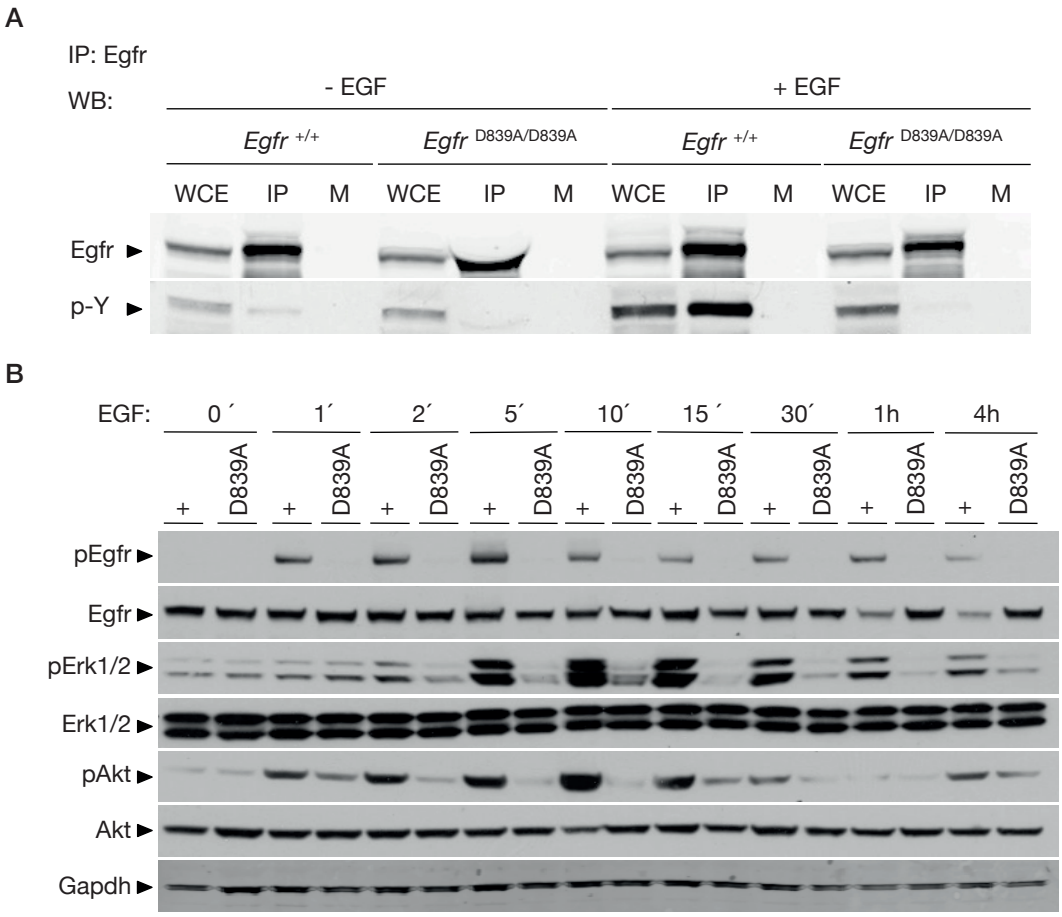

Figure 9. Egfr^{D839A} protein has impaired kinase activity. (A) *Egfr*$^{+/+}$ and *Egfr*$^{D839A/D839A}$ MEFs were serum starved for 16 hours and then stimulated with EGF (150ng/ml). Following EGF stimulation (5 min), whole-cell extracts were prepared and Egfr proteins were immunoprecipitated. The presence of phosphorylated Egfr was detected by Western blotting with the anti-phosphotyrosine antibody. Lanes WCE: whole-cell extract at a 1:10 dilution before immunoprecipitation (IP), M: mock immunoprecipitate. (B) *Egfr*$^{+/+}$ and *Egfr*$^{D839A/D839A}$ MEFs were serum starved for 16 hours and then stimulated with EGF (150ng/ml). Whole-cell extracts were prepared at the indicated times following EGF stimulation. Western blot analysis of Egfr, Erk1/2 and Akt phosphorylated proteins. Gapdh expression served as loading control. Arrowheads show migration of the indicated proteins. Lanes +: whole-cell extract from *Egfr*$^{+/+}$ MEFs. Lanes D839A: whole-cell extract from *Egfr*$^{D839A/D839A}$ MEFs.

4.1.3.2. Characterization of Egfr kinase dead MEFs

We next determined the impact of *Egfr* kinase dead mutation on spontaneous immortalization of MEFs following a 3T3 protocol (Figure 10A, B). In standard media conditions (10% FBS) there were no detectable differences between mutant homozygous and wild type MEFs. In contrast, under restricted growth factor conditions (10% CBS), mutant MEFs did not overcome the crisis stage even after 40 passages, thus indicating, that under these circumstances, Egfr^{D839A} has an impact on immortalization process (Figure 10B). We also found significant differences between the proliferation rates of *Egfr*$^{D839A/D839A}$ MEFs and wild type MEFs over 12 days in culture either in media containing FBS or CBS. Consequently, *Egfr*^{D839A}

mutation has an inhibitory effect in proliferation and *Egfr*$^{D839A/D839A}$ MEFs display a significant limited proliferation capability (Figure 10C, D).

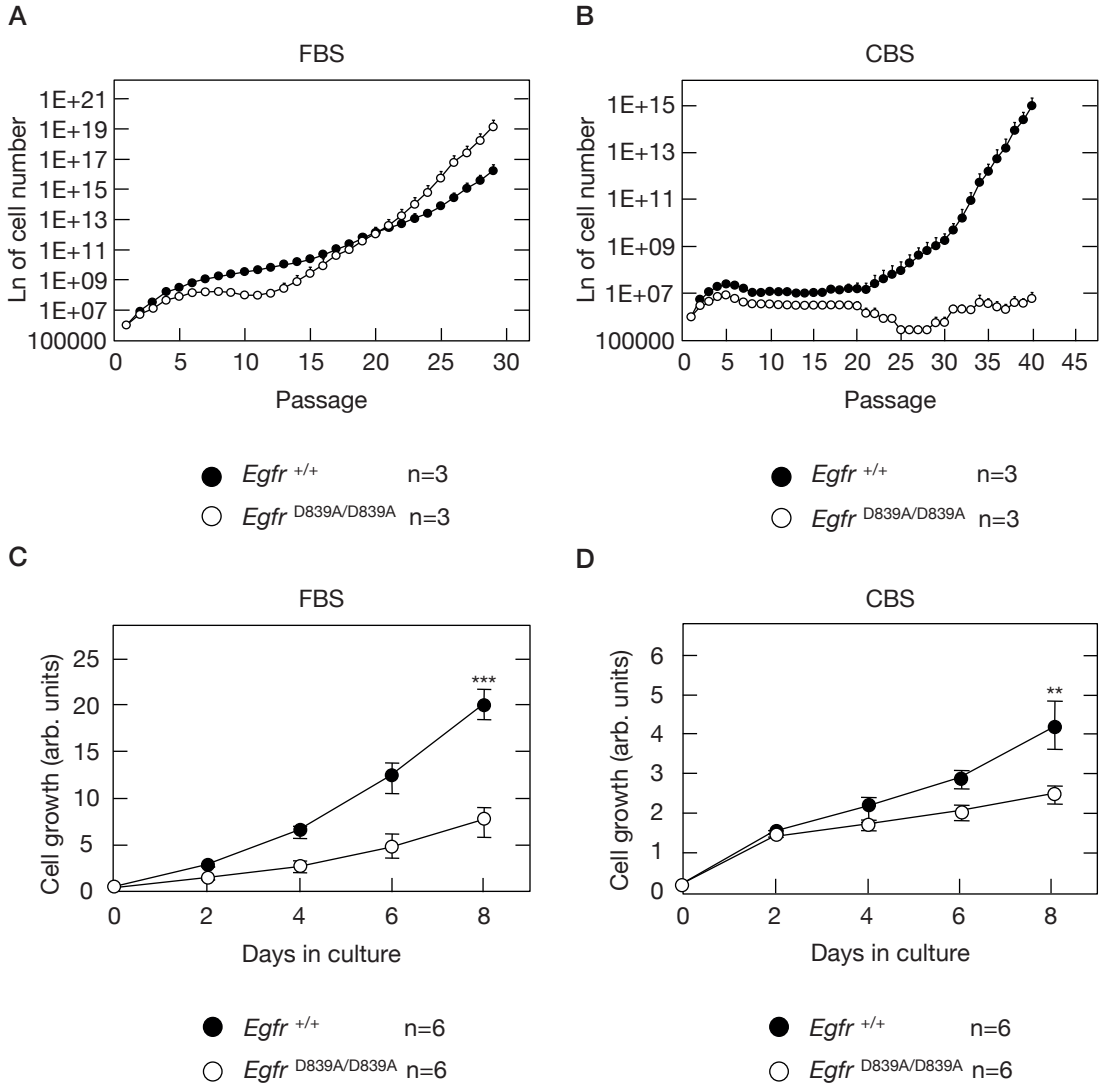

Figure 10. Egfr kinase activity is required for MEFs immortalization and proliferation *in vitro*. (A, B) Immortalization of primary *Egfr*$^{+/+}$ (n=3) and *Egfr*$^{D839A/D839A}$ (n=3) MEFs following a 3T3 protocol. Cells were cultivated in DMEM supplemented with 10% FBS (A) or alternatively 10% CBS (B). Error bars indicate mean ± SD. (C, D) Proliferation curves of primary *Egfr*$^{+/+}$ (n=6) and *Egfr*$^{D839A/D839A}$ (n=6) MEFs cultivated in DMEM supplemented with 10% FBS (C) or 10% CBS (D). Proliferation was determined by MTT. Error bars indicate mean ± SD. P-values at day 8 **p<0.01, ***p<0.001.

4.1.4. Egfr^{D839A} impairs PDAC tumor initiation

As previously mentioned, our PDAC mouse model was generated by crossing a knock-in *K-Ras*^{LSLG12Vgeo} allele with a double transgenic mice *Elas-tTA;tetO-Cre* (from now on *ElasK-Ras*^{G12Vgeo}) allowing the expression of the *K-Ras*^{G12Vgeo} in acinar cells, following an inducible Tet-Off strategy in which the expression of the Cre-recombinase is under the control of the *Elastase* promoter (Guerra et al., 2007).

One of the main objectives of this thesis was to investigate whether the elimination of Egfr catalytic activity was able to recapitulate the results obtained with the elimination of Egfr protein in PDAC initiation. To this end, we carried out the same studies performed earlier (Navas et al., 2012).

We generated the *ElasK-Ras*^{G12Vgeo};*Egfr*$^{LmLD839A/LmLD839A}$ mouse strain. Since *K-Ras*^{LSLG12Vgeo} and *Egfr*$^{LmLD839A/LmLD839A}$ inducible knock-in alleles are based on the Cre-mediated recombination system, expression of the *K-Ras*^{G12Vgeo} oncogene and the *Egfr*^{D839A} kinase dead form was concomitant in acinar cells

4.1.4.1. Egfr catalytic activity is essential for *K-Ras* oncogene-driven ADM *in vitro*

Acinar to ductal metaplasia (ADM) is the described precursor of PanIN lesions (Brune et al., 2006; Parsa et al., 1985). Lineage tracing experiments in PDAC mouse models demonstrated that PanIN lesions are mainly derived from acinar cells undergoing acinar to ductal metaplasia (Kopp et al., 2012), suggesting that ADM might be an early event that promotes *K-Ras* driven tumorigenesis. Moreover, it was previously shown that generation of ductal-like structures *in vitro* from wild type acinar cells is largely dependent on activation of Egfr by EGF (Means et al., 2005). Acinar cells isolated from *ElasK-Ras*^{G12Vgeo} mice efficiently transdifferentiated *in vitro* into metaplastic ductal-like cells and this process was largely dependent on activation of Egfr considering that ADM was highly reduced in the absence of this receptor (Navas et al., 2012). The very same approach was done in *ElasK-Ras*^{G12Vgeo};*Egfr*$^{LmL839A/LmLD839A}$ isolated acinar cells. Inhibition of Egfr catalytic activity significantly reduced the capability of acinar cells to generate ductal-like structures, but did not block completely the competence of acinar cell explants to generate metaplastic structures (Figure 11). These observations suggest that ADM requires Egfr signaling in the presence of a mutant *K-Ras* oncogene but also that EGF and TGFα may contribute to ADM by activating additional signaling pathways, at least *in vitro*.

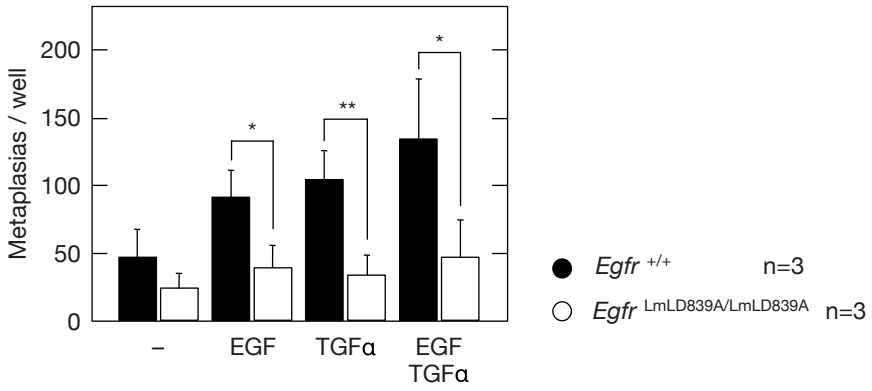

Figure 11. Acinar cells expressing the endogenous *K-Ras* oncogene require Egfr catalytic activity to undergo metaplasia *in vitro*. Acinar cell explants were isolated from pancreas of dox-untreated (in absence of doxycycline) 6 to 8 weeks-old *ElasK-Ras*^{G12Vgeo};*Egfr*$^{+/+}$ (solid bars, n=3) mice and *ElasK-Ras*^{G12Vgeo};*Egfr*$^{LmLD839A/LmLD839A}$ (open bars, n=3) mice. Acinar cells were incubated in the absence (-) or presence of the indicated growth factors at a final concentration of 50ng/ml. G418 (75µg/ml) was added to the culture media to select *K-Ras*^{G12Vgeo} expressing cells. The number of metaplasias was determined after five days in culture. Data shown represent mean ± SD, *p<0.05, **p<0.01.

4.1.4.2. Egfr catalytic activity is essential for *K-Ras* oncogene-driven PanIN lesions

We performed histological examination of the pancreas in mice not exposed to doxycycline to allow expression of the *Elastase*-driven Cre-recombinase from late embryonic development (E16.5) (*embryonic protocol*). One-year-old control *ElasK-Ras*^{G12Vgeo};*Egfr*$^{+/+}$ mice (n=12) exhibited abundant low- and high-grade PanIN lesions (average of 6.4 and 2.5 per pancreas, respectively) (Figure 12A). In contrast, analysis of serial sections of pancreas from one-year-old *ElasK-Ras*^{G12Vgeo};*Egfr*$^{LmLD839A/LmLD839A}$ mice (n=14) only revealed the presence of a limited number of PanIN lesions in three of the mice. Importantly, analysis of all these lesions disclosed incomplete recombination of the *Egfr*^{LmLD839A} allele (Figure 12B). These observations indicate that Egfr catalytic activity is essential for the induction of PanIN lesions by *K-Ras* oncogene.

A

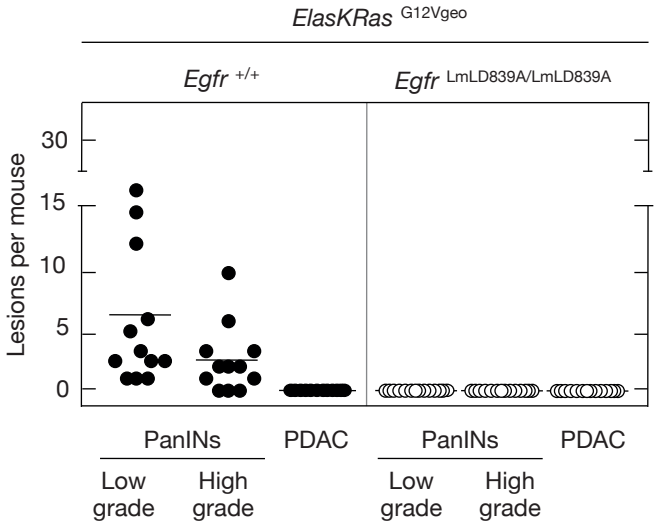

B

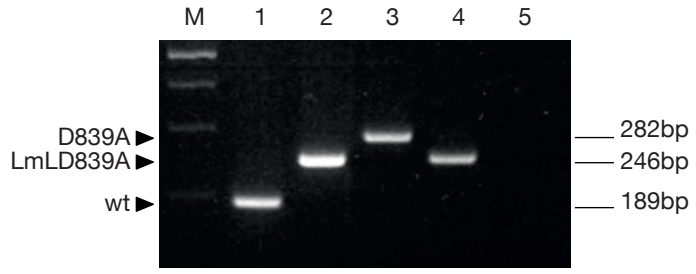

Figure 12. Induction of PanIN lesions by an endogenous *K-Ras* oncogene requires Egfr catalytic activity. (A) Number of low- and high-grade PanIN lesions and PDAC per mouse in the *embryonic protocol* carrying the indicated alleles. *ElasK-Ras*^{G12Vgeo};*Egfr*$^{+/+}$ (solid circles, n=12) and *ElasK-Ras*^{G12Vgeo};*Egfr*$^{LmLD839A/LmLD839A}$ (open circles, n=14). Horizontal bars indicate the average number of lesions per mouse for each genotype. (B) PCR analysis of *Egfr* alleles from PanIN lesions obtained by LCM. Lanes 1, 2 and 3: *Egfr*$^{+/+}$ (wt), *Egfr*$^{LmLD839A/LmLD839A}$ and *Egfr*$^{D839A/D839A}$ controls, respectively. Lane 4: DNA extracted from PanIN lesions of *ElasK-Ras*^{G12Vgeo};*Egfr*$^{LmLD839A/LmLD839A}$ mice revealed the presence of the unrecombined *Egfr*^{LmLD839A} allele. Lane 5: blank. Lane M: DNA ladder. Expected fragments for each allele are depicted.

The absence of PanIN lesions in *ElasK-Ras*^{G12Vgeo};*Egfr*$^{LmLD839A/LmLD839A}$ mice could be due to a reduction in the number of cells expressing the *K-Ras* oncogene. However, X-Gal staining of pancreatic cryosections of *ElasK-Ras*^{G12Vgeo};*Egfr*$^{LmLD839A/LmLD839A}$ mice demonstrated β-galactosidase activity (blue staining) in 20-30% of the acinar cells, the same percentage as in *ElasK-Ras*^{G12Vgeo};*Egfr*$^{+/+}$ pancreatic sections (Figure 13A). Furthermore, PCR analysis from DNA of X-Gal positive cells isolated by LCM, demonstrated complete recombination of *Egfr*^{LmLD839A} allele in acinar cells expressing the *K-Ras*^{G12Vgeo} oncogene (Figure 13B).

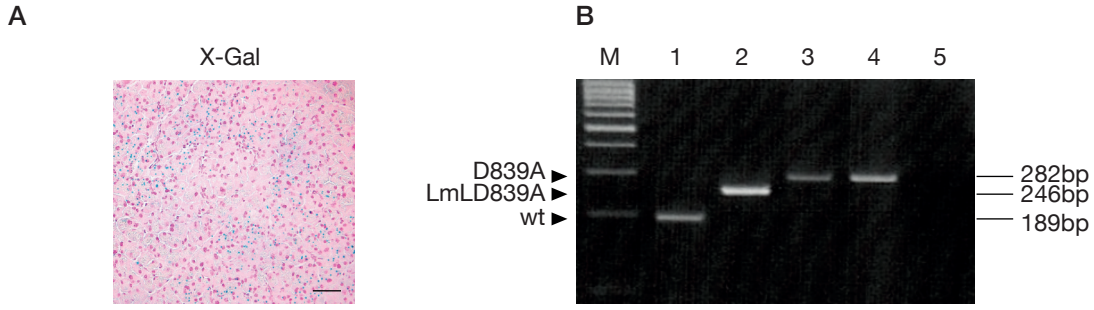

Figure 13. Acinar cells expressing the *K-Ras*^{G12Vgeo}, identified by β-galactosidase activity, exhibit complete recombination of the Egfr^{LmLD839A} allele. (A) Identification of *K-Ras*^{G12Vgeo} expressing acinar cells by X-Gal staining (blue spots) in cryosections from pancreas of *ElasK-Ras*^{G12Vgeo};*Egfr*$^{LmLD839A/LmLD839A}$ mice. Scale bar represents 100μm. (B) PCR analysis of *Egfr* alleles from X-Gal positive acinar cells. Lane 1, 2 and 3: *Egfr*$^{+/+}$ (wt), *Egfr*$^{LmLD839A/LmLD839A}$ and *Egfr*$^{D839A/D839A}$ controls, respectively. Lane 4: DNA extracted from X-Gal positive acinar cells of *ElasK-Ras*^{G12Vgeo};*Egfr*$^{LmLD839A/LmLD839A}$ mice revealed complete recombination of the *Egfr*^{LmLD839A} allele. Lane 5: blank. Lane M: DNA ladder. Expected fragments for each allele are depicted.

4.1.4.3. Adult mice also require Egfr catalytic activity for PanIN formation

We exposed *ElasK-Ras*^{G12Vgeo};*Egfr*$^{+/+}$ and *ElasK-Ras*^{G12Vgeo};*Egfr*$^{LmLD839A/LmLD839A}$ littermates to doxycycline from conception until adulthood (P60) to prevent expression of the Cre-recombinase. As previously reported (Guerra et al., 2007), in the *adult protocol* it is necessary the cooperation of the pancreatitis for PanIN and PDAC induction. Hence, mice were treated with caerulein for 3 months (P90-P180) and pancreas were analyzed at 14 month of age (1 year after turning on the expression of the resident *K-Ras* oncogene). *ElasK-*

Ras^{G12Vgeo};*Egfr*$^{LmLD839A/LmLD839A}$ mice (n=10) revealed complete absence of low- and high grade PanIN lesions and PDAC (Figure 14). Only four mice carried PanIN lesions, all of which still retained the expression of the Egfr wild type protein (data not shown). As expected, *ElasK-Ras*^{G12Vgeo};*Egfr*$^{+/+}$ control littermates exhibited multiple lesions (Guerra et al., 2011; Navas et al., 2012). *Egfr* wild type mice (n=13) developed low grade PanINs (average of 17 per pancreas) and more than 90% (12 out of 13) of displayed high-grade PanINs (average of 13 per pancreas), only one mouse developed PDAC.

The expression of a catalytic inactive form of Egfr blocked tumor initiation in the *adult* and in the *embryonic protocol*. Therefore, the inhibition of Egfr tyrosine kinase activity recapitulates the results of the Egfr conditional knockout (Navas et al., 2012).

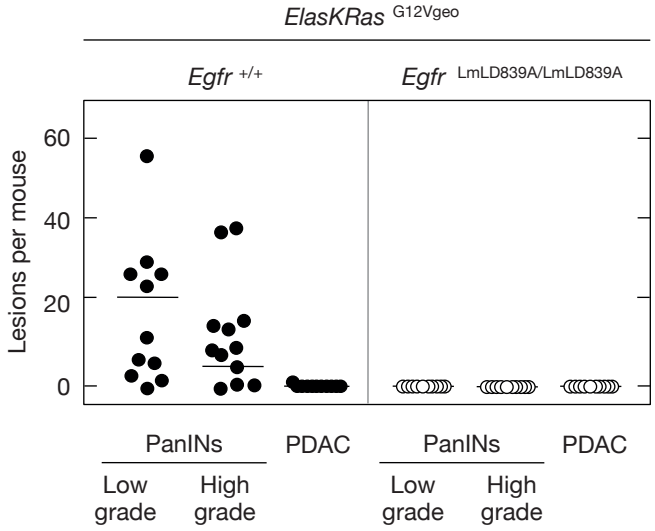

Figure 14. Induction of PanIN lesions by an endogenous *K-Ras*^{G12Vgeo} oncogene requires Egfr catalytic activity in the *adult protocol.* Number of low- and high-grade PanIN lesions and PDAC per mouse in 14-month-old *ElasK-Ras*^{G12Vgeo} mice carrying the indicated alleles. *ElasK-Ras*^{G12Vgeo};*Egfr*$^{+/+}$ (solid circles, n=13) and *ElasK-Ras*^{G12Vgeo};*Egfr*$^{LmLD839A/LmLD839A}$ (open circles, n=10). These mice were exposed to doxycycline from conception until P60. At that time, Cre-recombinase leads the concomitant expression of the resident *K-Ras*^{G12Vgeo} oncogene and the catalytic inactive form of Egfr in acinar cells. Mice were treated with caerulein from P90 to P180. Horizontal bars indicate the average number of lesions per mouse for each genotype.

4.1.5. Lack of Egfr kinase activity blocks PDAC tumor initiation in a p16Ink4a/p19Arf deficient background

In addition to *K-RAS* mutations, most human PanINs and PDAC display inactivation of the *p16INK4a/p14ARF* locus (Wood and Hruban, 2012). In mice, it has been described that loss of *p16Ink4a/p19Arf* in combination with the expression of the mutated *K-Ras* oncogene results in an earlier appearance of PanIN lesions that rapidly progress to highly invasive and metastatic PDAC (Aguirre et al., 2003; Guerra et al., 2011). These studies indicate that loss of

p16Ink4a/p19Arf contributes to pancreatic cancer in mice.

Conditional floxed *p16Ink4a/p19Arf* alleles were introduced into *ElasK-Ras*^{G12Vgeo} mice carrying either wild type or *Egfr*^{LmLD839A} alleles. Mice were allowed to age and were sacrificed at humane end point or at 1 year of age. These mice were not exposed to doxycycline to allow for the expression of the resident *K-Ras*^{G12Vgeo} oncogene during late embryonic development (E16.5, *embryonic protocol*). Littermates carrying wild type *Egfr* alleles in homozygosis (n=7) or heterozygosis (n=10) succumbed to the disease (Figure 15A). All mice displayed PDAC, which occasionally metastasized to several organs. In contrast, *ElasKRas*^{G12Vgeo};*Egfr*$^{LmLD839A/LmLD839A}$ mice (n=7) were alive at 1 year of age, time at which they were sacrificed and their pancreas analyzed. Interestingly, the few PanIN lesions detected still expressed the wild type receptor from the *Egfr*^{LmLD839A} allele (Figure 15B). These observations indicate that upon inactivation of *p16Ink4a/p19Arf* alleles, *K-Ras* mutant acinar cells still need Egfr catalytic activity for PDAC initiation, similar to the results obtained with the *Egfr* conditional knockout (Navas et al., 2012).

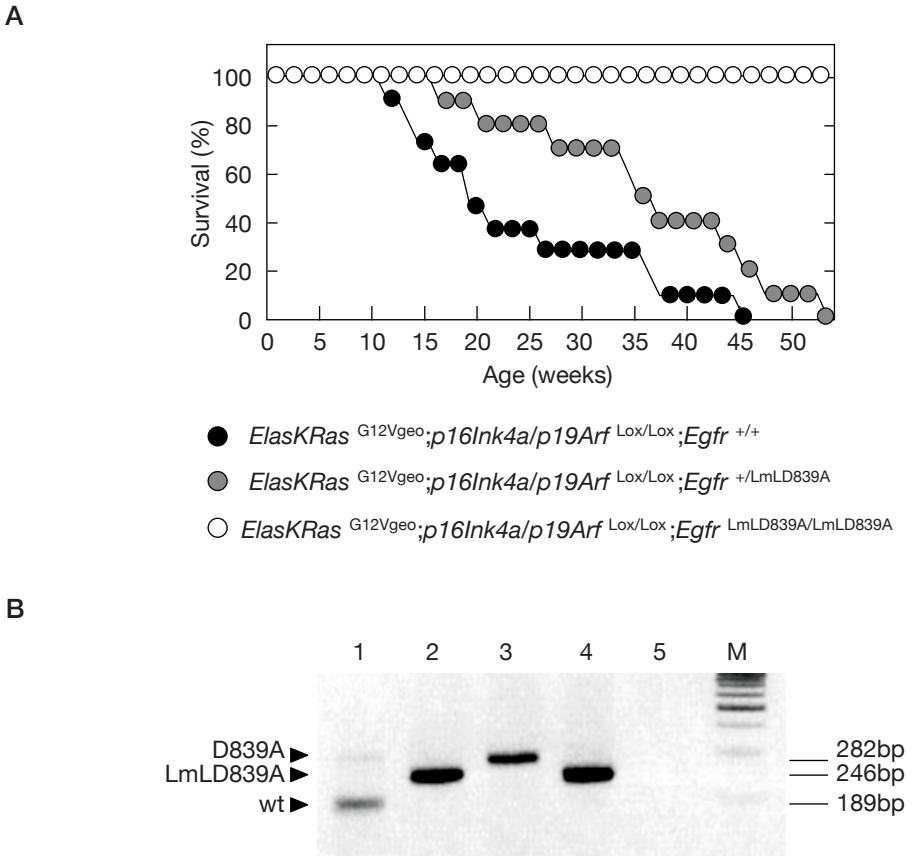

Figure 15. Loss of *p16Ink4a/p19Arf* tumor suppressors does not abrogate the need of Egfr catalytic activity for PanIN/PDAC initiation. (A) Survival curve of dox-untreated *ElasK-Ras*^{G12Vgeo}; *p16Ink4a/p19Arf*$^{Lox/Lox}$;*Egfr*$^{+/+}$ (solid circles, n=7) mice, *ElasK-Ras*^{G12Vgeo}; *p16Ink4a/p19Arf*$^{Lox/Lox}$; *Egfr*$^{+/LmLD839A}$ mice (grey circles, n=10) and *ElasK-Ras*^{G12Vgeo}; *p16Ink4a/p19Arf*$^{Lox/Lox}$;*Egfr*$^{LmLD839A/LmLD839A}$ mice (open circles, n=7). (B) PCR analysis of *Egfr* alleles from PanIN lesions isolated by LCM. Lanes 1, 2 and 3: *Egfr*$^{+/+}$ (wt), *Egfr*$^{LmLD839A/LmLD839A}$ and *Egfr*$^{D839A/D839A}$ controls, respectively. Lane 4: DNA extracted

from PanIN lesions of *ElasK-Ras*^{G12Vgeo};*p16Ink4a/p19Arf*$^{Lox/Lox}$;*Egfr*$^{LmLD839A/LmLD839A}$ mice revealed the presence of the unrecombined floxed allele. Lane 5: blank. Lane M: DNA ladder. Expected fragments for each allele are depicted.

4.1.6. Lack of Egfr kinase activity does not impair tumor initiation in a p53 deficient background.

Most PDAC tumors are associated with mutations in tumor suppressor genes including *CKDN2A*, *TP53* (Ruggeri et al., 1992; Scarpa et al., 1993) and *SMAD4* (Hahn et al., 1996). Mutations in *TP53* and *SMAD4* are often associated with progression of PanIN-3 lesions to invasive PDAC tumors (Guerra and Barbacid, 2013). In GEMMs, addition of mutations in *p53* accelerates the progression of PanIN lesions towards invasive PDAC that results in reduced survival (Guerra et al., 2007; Hingorani et al., 2005).

In order to study the effect of inhibiting Egfr kinase activity in the absence of p53, we introduced the *p53*$^{Lox/Lox}$ alleles in the *ElasK-Ras*^{G12Vgeo} strain in the presence of the wild type or the inactive form of Egfr.

Ten weeks-old dox-untreated mice (before mice show signs of over tumor development) carrying *Egfr*$^{+/+}$ alleles (n=10) displayed abundant low- and high-grade PanIN lesions and PDAC (average of 9 high-grade PanINs and 4 PDAC per mouse). Interestingly, mice carrying conditional *Egfr* kinase dead alleles (n=9) also displayed neoplastic lesions but with significantly reduced incidence (average of 2 high-grade lesions and 0.2 PDAC per mouse) (Figure 16A). This observed difference in tumor development affected survival. When we allowed these mice to age, animals carrying *Egfr*$^{+/+}$ alleles (n=7) displayed an average survival of 17 weeks of age, similar to heterozygous mice (n=10). Nonetheless, mice carrying conditional *Egfr*$^{LmLD839A/LmLD839A}$ alleles (n=7) display an average survival of 24 weeks of age. Thus, impaired Egfr catalytic activity promotes a significant 41% increase in survival (17 versus 24 weeks) (Figure 16B). Tumor development was not due to incomplete recombination of *Egfr*^{LmLD839A} alleles, since all tumors analyzed by PCR expressed the inactive form of Egfr (Figure 16C). Similar results were previously described with the *Egfr* conditional knockout, although the increase of median survival was slightly higher (Navas et al., 2012).

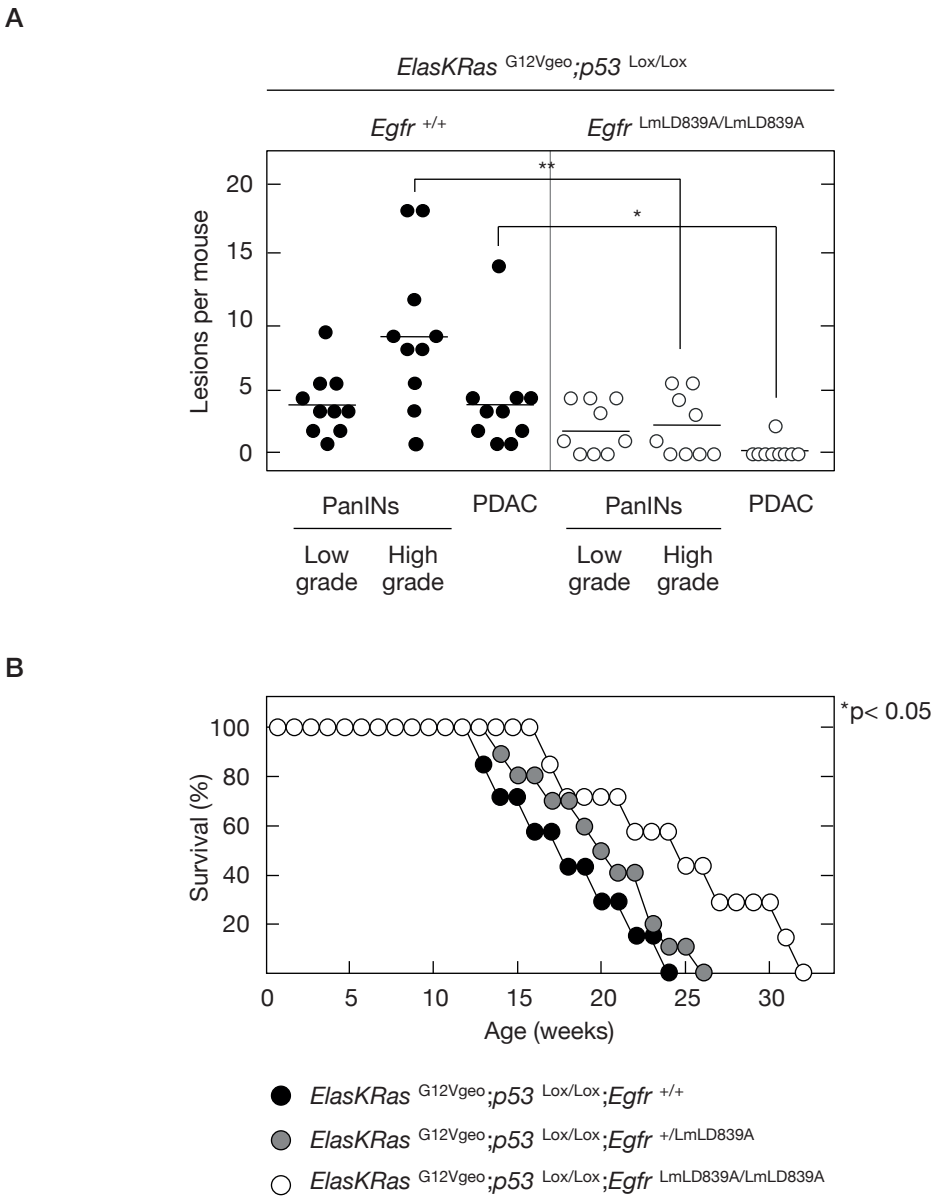

Figure 16. Inhibition of Egfr catalytic activity delays but does not prevent PanIN and PDAC initiation in the absence of *p53* tumor suppressor gene during the *embryonic protocol*. (A) Number of low- and high-grade PanIN lesions and PDACs per mouse in dox-untreated 10 weeks–old *ElasK-Ras*^{G12Vgeo};*p53*$^{Lox/Lox}$;*Egfr*$^{+/+}$ (solid circles, n=10) mice, and *ElasK-Ras*^{G12Vgeo};*p53*$^{Lox/Lox}$;*Egfr*$^{LmLD839A/LmLD839A}$ (open circles, n=9) mice. In these mice, expression of the Cre-recombinase in pancreatic acinar cells during late embryonic development results in the concomitant expression of the endogenous *K-Ras*^{G12Vgeo} and the inactive form of Egfr, together with the ablation of

p53 conditional alleles. Horizontal bars indicate the average number of lesions per mouse for each genotype. *p<0.05, **p<0.01 are indicated. (B) Survival of dox-untreated *ElasK-Ras*^{G12Vgeo};*p53*$^{Lox/Lox}$;*Egfr*$^{+/+}$ (solid circles, n=7) mice, *ElasK-Ras*^{G12Vgeo};*p53*$^{Lox/Lox}$;*Egfr*$^{+/LmLD839A}$ (grey circles, n=10) mice and *ElasK-Ras*^{G12Vgeo};*p53*$^{Lox/Lox}$;*Egfr*$^{LmLD839A/LmLD839A}$ (open circles, n=7) mice. *p<0.05 is indicated. (C) PCR analysis of *Egfr* alleles from PDAC-derived cell explants. Lanes 1, 2 and 3: *Egfr*$^{+/+}$ (wt), *Egfr*$^{LmLD839A/LmLD839A}$ and *Egfr*$^{D839A/D839A}$ controls respectively. Lanes 4, 5, 6: DNA extracted from three different PDAC-derived cell explants obtained from *ElasK-Ras*^{G12Vgeo};*p53*$^{Lox/Lox}$;*Egfr*$^{LmLD839A/LmLD839A}$ mice revealed complete recombination of the *Egfr*^{LmLD839A} allele. Lane 7: blank. Lane M: DNA ladder. Expected fragments for each allele are depicted.

A similar approach was followed with mice expressing the resident *K-Ras*^{G12Vgeo} oncogene during adulthood. These mice were treated with doxycycline and later treated with caerulein for 3 months. Whereas in the *embryonic protocol* there is a significant increase in survival in mice expressing *Egfr* kinase dead alleles, in the *adult protocol*, *ElasK-Ras*^{G12Vgeo};*p53*$^{Lox/Lox}$; *Egfr*$^{LmLD839A/LmLD839A}$ (open circles, n=14) mice died with a median survival of 40 weeks, and control *ElasK-Ras*^{G12Vgeo};*p53*$^{Lox/Lox}$;*Egfr*$^{+/+}$ (solid circles, n=7) mice died with a median survival of 36 weeks. As illustrated in the survival curve in figure 17, lack of Egfr kinase activity neither impaired nor delayed tumor development. Mice died after 45 to 50 weeks irrespective of the *Egfr* genotype. In contrast, ablation of *Egfr* resulted in an increased survival time of 40% (Navas et al., 2012). As previously observed in the *embryonic protocol*, tumors expressed the inactive form of Egfr when analyzed by PCR (data not shown). Consequently, inhibition of the Egfr catalytic activity did not impair or delay PDAC formation during adulthood in p53 deficient tumors.

Together, these results indicate that loss of p53 triggers oncogenic pathways that bypass the requirement of Egfr signaling for tumor initiation.

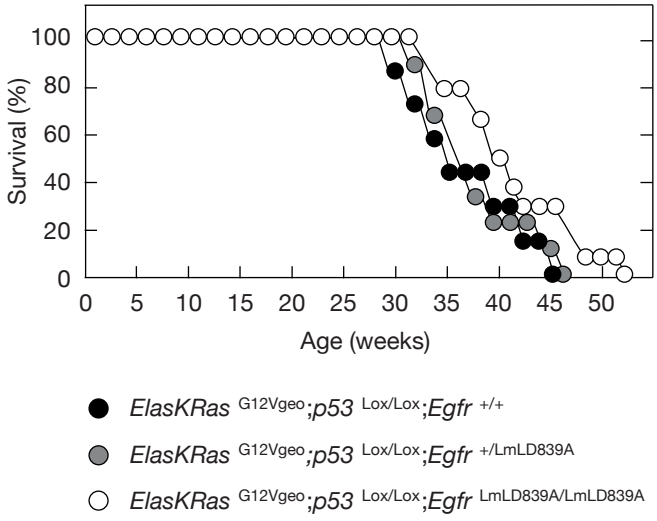

Figure 17. Inhibition of Egfr catalytic activity during adulthood did not impair PDAC tumor formation in the absence of p53. Survival of *ElasK-Ras*^{G12Vgeo};*p53*$^{Lox/Lox}$;*Egfr*$^{+/+}$ (solid circles, n=7) mice, *ElasK-Ras*^{G12Vgeo};*p53*$^{Lox/Lox}$;*Egfr*$^{+/LmLD839A}$ (grey circles, n=9) mice and *ElasK-Ras*^{G12Vgeo};

p53$^{Lox/Lox}$;*Egfr*$^{LmLD839A/LmLD839A}$ (open circles, n=14) mice. Mice were exposed to doxycycline from conception until P60. At that time, Cre-recombinase leads the concomitant expression of the resident *K-Ras*^{G12Vgeo} oncogene, the catalytic inactive form of Egfr and the ablation of *p53* conditional alleles. Mice were treated with caerulein from P90 to P180. There are not statistically significant differences.

4.1.6.1. ErbB2 is responsible of Egfr^{D839A} phosphorylation and MAPK signaling activation in a p53 deficient background

Egfr is responsible for the activation of some of the pathways that have been shown to be important in pancreas tumorigenesis, including PI3K and MAPK. Unexpectedly, *ElasK-Ras*^{G12Vgeo};*p53*$^{-/-}$;*Egfr*$^{D839A/D839A}$ PDAC cell explants exhibited phosphorylation of the inactive receptor and consequently, activation of downstream signaling cascades (Figure 18A). To asses whether other members of the ErbB family were compensating the lack of Egfr tyrosine kinase activity, we knocked down ErbB2 with a specific shRNA in *ElasK-Ras*^{G12Vgeo};*p53*$^{-/-}$;*Egfr*$^{+/+}$ and *ElasK-Ras*^{G12Vgeo};*p53*$^{-/-}$;*Egfr*$^{D839A/D839A}$ PDAC cell explants. As illustrated in figure 18B, knockdown of ErbB2 led to substantial inhibition of Egfr^{D839A} phosphorylation together with inhibition of MAPK signaling pathway (as shown by reduced levels of Erk1/2 phosphorylation), whereas these effects were not observed in cells expressing the wild type form of Egfr. However, the effect of ErbB2 knockdown in the PI3K pathway was inconclusive, since phosphorylation of Akt was only reduced in two out of three cell explants analyzed.

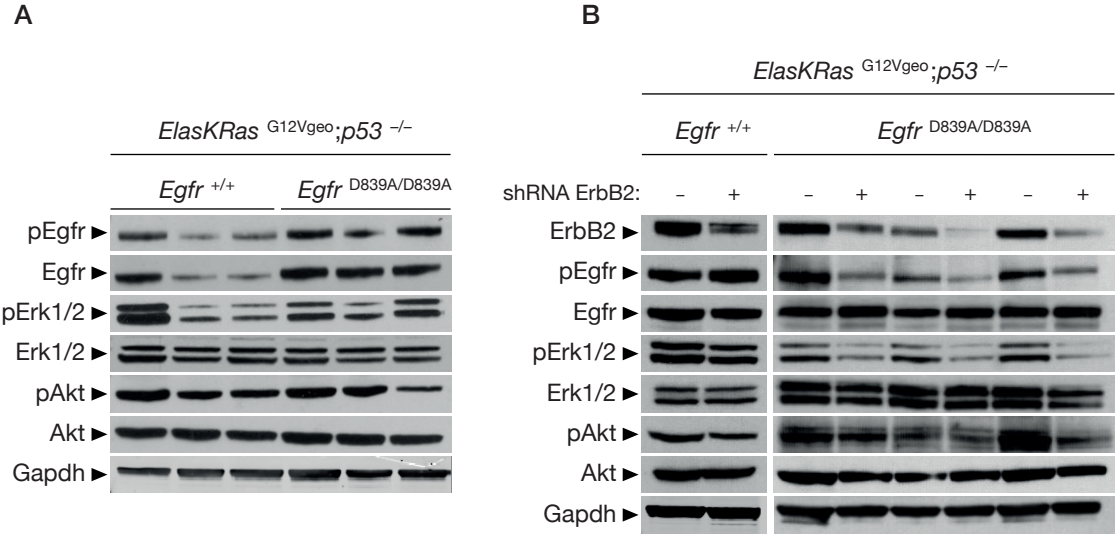

Figure 18. ErbB2 triggers Egfr kinase dead phosphorylation and activation of downstream signaling pathways. (A) Western blot analysis of Egfr, Erk1/2 and Akt phosphorylated proteins in *ElasK-Ras*^{G12Vgeo};*p53*$^{-/-}$;*Egfr*$^{+/+}$ (n=3) and *ElasK-Ras*^{G12Vgeo};*p53*$^{-/-}$;*Egfr*$^{D839A/D839A}$ (n=3) PDAC-derived cell explants. Gapdh expression served as loading control. Arrowheads show migration of the indicated proteins. (B) *ElasK-Ras*^{G12Vgeo};*p53*$^{-/-}$;*Egfr*$^{+/+}$ (n=3, representative Western blot from one explant is shown) and *ElasK-Ras*^{G12Vgeo};*p53*$^{-/-}$;*Egfr*$^{D839A/D839A}$ PDAC cell explants (n=3) were infected with lentiviral particles expressing either a shRNA against ErbB2 (+) or a control shRNA (–). Phosphorylation levels of Egfr,

Erk1/2 and Akt proteins and total ErbB2 expression were analyzed by Western blot. Gapdh expression served as loading control. Arrowheads show migration of the indicated proteins.

4.2. Analyzing the potential therapeutic benefit of targeting Egfr and c-Raf in established PDAC

It is known that EGFR, and all ErbB family members, are capable of activating the RAS/MAPK and PI3K pathways (Jorissen et al., 2003), which are essential in cell cycle regulation, differentiation and proliferation and are commonly deregulated in cancer (Malumbres and Barbacid, 2003). However, as previously shown in this thesis, Egfr inhibition is not sufficient to block PDAC tumorigenesis and it should be used in cooperation with targets affecting other signaling pathways to induce better responses.

Moreover, these and previous results were obtained using our initiation PDAC mouse model, in which ablation or inhibition of the target of interest was concomitant with *K-Ras*^{G12V} expression and *p53* deletion. Consequently, these results only disclose the effects of selected targets during the first stages of tumorigenesis, thus they should be considered as only preventative strategies rather than therapeutic. For this reason, we decided to develop a new PDAC mouse model to assess the therapeutic value of Egfr and its combination with c-Raf in already established PDAC.

4.2.1. Generation of the PDAC therapeutic strain

To address the therapeutic value of the *Egfr* deletion/inhibition and its combination with other targets of interest in full-blown tumors, we developed a PDAC mouse model in which we can separate, spatially and temporally, tumor induction from target ablation/inactivation using two independent recombinases. Development of PDAC was initiated by the Flp/Frt recombinase system, whereas the Cre/LoxP system was used to ablate the potential therapeutic targets to be validated.

In collaboration with the Transgenic Mice Core Unit at CNIO we generated the *tetO-Flp* transgenic strain, which in combination with the *Elas-tTA* strain (*Elas-tTA/tetO-Flp*), allows the expression of the yeast Flp-recombinase in cells expressing the *Elastase* promoter under the negative control of doxycycline (Tet-off system). Additionally, we took advantage of the *K-Ras*$^{+/FSFG12V}$ mice (Drosten et al., unpublished) and *p53*$^{Frt/Frt}$ mice (Lee et al., 2012), in which the expression of the *K-Ras* mutation and the deletion of *p53* takes place upon Flp-mediated recombination of Frt sites. By crossing the *K-Ras*^{FSFG12V};*p53*$^{Frt/Frt}$ strain with the *Elas-tTA/tetO-Flp* we allowed for concomitant expression of the *K-Ras*^{G12V} oncogene and *p53* deletion in acinar cells during late embryonic development (E16.5). The resulting strain, *Elas-tTA/tetO-Flp;K-Ras*^{FSFG12V};*p53*$^{Frt/Frt}$ developed PDAC tumors with complete penetrance and similar latencies to those observed in *Elas-tTA/tetO-Cre;K-Ras*^{LSLG12Vgeo};*p53*$^{Lox/Lox}$ mice (data not shown).

Besides, the modified Cre-recombinase (CreERT2) was introduced as a transgene (*Tg.hUBC-CreERT2*$^{+/T}$) together with floxed target alleles. The CreERT2 recombinase is ubiquitously expressed under the human Ubiquitin C promoter (Ruzankina et al., 2007). Exposure of the resulting tumor-bearing mice (as determined by non-invasive ultrasound techniques) to a tamoxifen-containing diet resulted in the translocation of the CreERT2 enzyme into the nucleus and in the systemic deletion/inactivation of floxed alleles. This approach allowed us to assess both the therapeutic efficacy of ablation/inactivation of target genes in already established PDAC tumors, and the systemic toxicity associated to the lack or inhibition of studied proteins in the whole body (Figure 19).

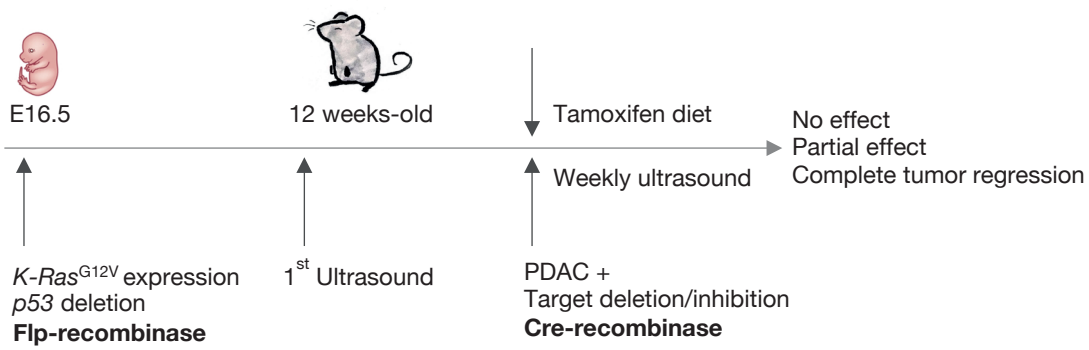

Figure 19. Timeline for the therapeutic approach. The expression of the resident *K-Ras*^{G12V} and the ablation of the *p53* tumor suppressor started at E16.5 by the Flp-recombinase in the absence of doxycycline (Tet-off system). The screening by ultrasound techniques started at 12 weeks of age. Positive PDAC animals were exposed to a tamoxifen-containing diet, which resulted in the ubiquitous activation of the Cre-recombinase and as a result, deletion/inactivation of floxed targets genes. Once the tumor was detected, tumor size was assessed by ultrasound weekly.

4.2.2. Egfr elimination or inactivation does not affect PDAC progression *in vivo*

With the purpose of investigating the role of Egfr in tumor progression, we introduced *Egfr*^{Lox} (to eliminate Egfr) and *Egfr*^{LmLD839A} (to inhibit Egfr tyrosine kinase activity) alleles in our PDAC therapeutic strain.

Elas-tTA/tetO-Flp;K-Ras^{FSFG12V};*p53*$^{Frt/Frt}$;*Egfr*$^{+/+}$;*Tg.hUBC-CreERT2*$^{+/T}$ control mice (10 mice/15 tumors), *Elas-tTA/tetO-Flp;K-Ras*^{FSFG12V};*p53*$^{Frt/Frt}$;*Egfr*$^{Lox/Lox}$;*Tg.hUBC-CreERT2*$^{+/T}$ mice (6 mice/8 tumors) and *Elas-tTA/tetO-Flp;K-Ras*^{FSFG12V};*p53*$^{Frt/Frt}$;*Egfr*$^{LmLD839A/LmLD839A}$; *Tg.hUBC-CreERT2*$^{+/T}$ mice (8 mice/22 tumors) were monitored by ultrasound in order to detect established pancreatic tumors. Mice with established and comparable PDAC were subjected to tamoxifen treatment and tumor progression was monitored weekly. Unfortunately, neither deletion nor inhibition of Egfr affects tumor growth or survival. As a consequence, tumor volume fold change did not decrease in tumors lacking Egfr or its kinase activity in comparison with control tumors (Figure 20A, B).

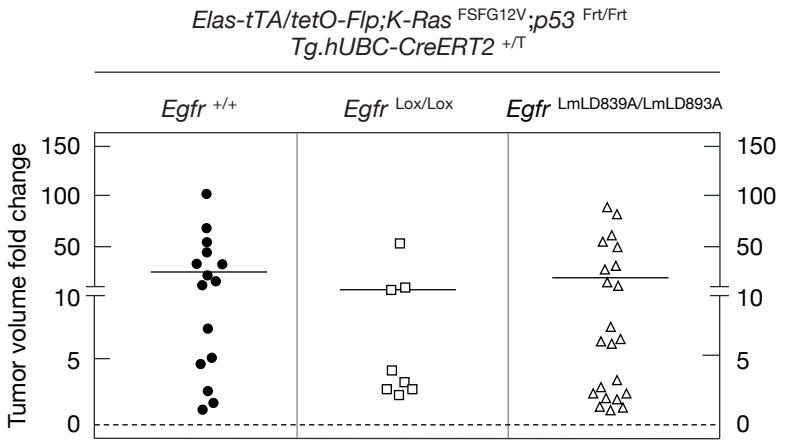

Figure 20. Egfr elimination or inhibition of its catalytic activity does not impair PDAC progression. Tumor volume fold change of tumors from *Elas-tTA/tetO-Flp;K-Ras*^{FSFG12V};*p53*$^{Frt/Frt}$;*Egfr*$^{+/+}$;*Tg.hUBC-CreERT2*$^{+/T}$ mice (10 mice/15 tumors, solid circles), *Elas-tTA/tetO-Flp;K-Ras*^{FSFG12V};*p53*$^{Frt/Frt}$;*Egfr*$^{Lox/Lox}$;*Tg.hUBC-CreERT2*$^{+/T}$ mice (6 mice/8 tumors, open squares) and *Elas-tTA/tetO-Flp;K-Ras*^{FSFG12V};*p53*$^{Frt/Frt}$;*Egfr*$^{LmLD839A/LmLD839A}$;*Tg.hUBC-CreERT2*$^{+/T}$ mice (8 mice/22 tumors, open triangles). Changes in tumor volume were calculated for each individual tumor based on ultrasound scans performed at the beginning and at the end of tamoxifen treatment. Horizontal bars indicate the average tumor fold change. There are not statistically significant differences.

4.2.3. Combined deletion of Egfr and c-Raf as a multi-targeted therapy against PDAC

Our laboratory has previously shown that c-Raf is essential for initiation (Blasco et al., 2011) and progression (unpublished data) of *K-Ras*^{G12V} driven lung adenocarcinoma. Moreover, we determined that c-Raf was also essential for PanIN and PDAC initiation in a p53 proficient background (unpublished results, see appendix 8.1).

Unfortunately, in a p53 deficient background, ablation of either *Egfr* (Navas et al., 2012) or *c-Raf* (unpublished results, see appendix 8.1), as well as expression of an Egfr kinase dead isoform, delays but does not prevent tumor appearance in PDAC mouse models. These already validated targets can be used in combination leading to the identification of therapeutic strategies that could be uncovered for future clinical trials. Accordingly to these observations, our laboratory demonstrated that, in the absence of p53, concomitant ablation of *Egfr* and *c-Raf* target genes completely blocked PDAC initiation (unpublished results, see appendix 8.2).

These results obtained by simultaneous deletion of *Egfr* and *c-Raf* in our initiation PDAC mouse model were surprising and promising. However, *Egfr* and *c-Raf* were deleted at the initiation stages and not in already established tumors. Consequently, this approach interferes in the first stages of tumorigenesis and do not reveal the therapeutic value of a genetic target. For this reason, we decided to assess the efficacy of *Egfr* and *c-Raf* deletion in already established PDAC tumors. Hence, we introduced *Egfr*^{Lox} together with *c-Raf*^{Lox} alleles in our PDAC therapeutic strain, generating the *Elas-tTA/tetO-Flp;K-Ras*^{FSFG12V}; *p53*$^{Frt/Frt}$;*Egfr*$^{Lox/Lox}$;*c-*

Raf$^{Lox/Lox}$;*Tg.hUBC-CreERT2*$^{+/T}$ final genotype.

4.2.3.1. Combined elimination of *Egfr* and *c-Raf* affects proliferation of PDAC cell explants *in vitro*

We took advantage of PDAC cell explants derived from *Elas-tTA/tetO-Flp;K-Ras*^{FSFG12V};*p53*$^{Frt/Frt}$;*Egfr*$^{+/+}$;*c-Raf*$^{+/+}$ mice (n=3) and *Elas-tTA/tetO-Flp;K-Ras*^{FSFG12V};*p53*$^{Frt/Frt}$;*Egfr*$^{Lox/Lox}$;*c-Raf*$^{Lox/Lox}$ mice (n=3) which were subjected to a colony formation assay. Clones were seeded at equal densities and infected with adenovirus particles expressing GFP-Cre at a MOI of 100. Cells were seeded 5 days post-infection to assess their colony formation capability.

Simultaneous elimination of *Egfr* and *c-Raf* target genes induced arrest in proliferation, as illustrated by a decrease in the number of established colonies, in two out of three studied cell lines. Importantly, there was one cell line that continued growing after the genetic ablation of the targets (Figure 21A, B). Of note, expression of both Egfr and c-Raf was undetectable by Western blot, confirming complete recombination of floxed alleles since expression of both Egfr and c-Raf was undetectable by Western blot (Figure 21C). Characterization of these resistant PDAC cell explants is currently ongoing. We are performing RNA-seq analysis, phospho-receptor tyrosine kinase arrays and drug screenings in order to identify signaling pathways involved in this response.

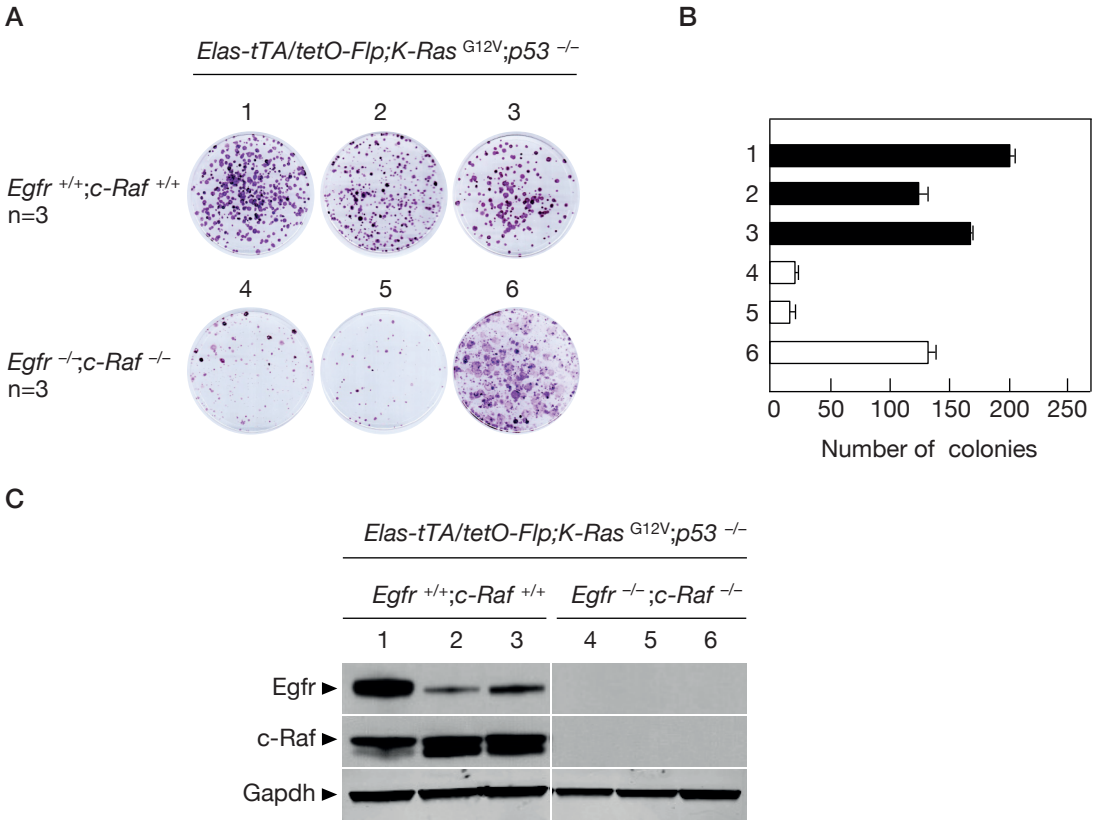

Figure 21. Elimination of *Egfr* and *c-Raf* causes changes in proliferation of PDAC-derived cell lines. (A) Representative plates from colony formation assays. *Elas-tTA/tetO-Flp;K-Ras*^{FSFG12V}; *p53*$^{Frt/Frt}$;*Egfr*$^{+/+}$;*c-Raf*$^{+/+}$ PDAC-derived cell lines (used as controls; numbers 1, 2 and 3) and *Elas-tTA/tetO-Flp;K-Ras*^{FSFG12V};*p53*$^{Frt/Frt}$;*Egfr*$^{Lox/Lox}$;*c-Raf*$^{Lox/Lox}$ PDAC-derived cell lines (numbers 4, 5 and 6) were infected with Adeno-CreGFP particles. After 5 days, they were seeded at equal densities and allowed to form colonies for 12 days. Cells were fixed with glutaraldehyde and stained with crystal violet. (B) Quantification of the number of colonies that grew 12 days after the Adeno-CreGFP infection. (C) Western blot analysis of Egfr and c-Raf protein expression in whole cell extracts obtained from colonies that grew after Adeno-CreGFP infection. All colonies growing from *Elas-tTA/tetO-Flp;K-Ras*^{G12V};*p53*$^{-/-}$;*Egfr*$^{-/-}$;*c-Raf*$^{-/-}$ did not express the targets of interest. Gapdh expression served as a loading control. Arrowheads show migration of the indicated proteins.

4.2.3.2. *In vivo* concomitant deletion of Egfr and c-Raf alleles results in a positive outcome in established pancreatic tumors

In order to investigate *Egfr* and *c-Raf* genes as potential therapeutic targets we decided to delete simultaneously both alleles in already established tumors. With this aim, we generated *Elas-tTA/tetO-Flp;K-Ras*^{FSFG12V};*p53*$^{Frt/Frt}$;*Egfr*$^{+/+}$;*c-Raf*$^{+/+}$;*Tg.hUBC-CreERT2*$^{+/T}$ and *Elas-tTA/tetO-Flp;K-Ras*^{FSFG12V};*p53*$^{Frt/Frt}$;*Egfr*$^{Lox/Lox}$;*c-Raf*$^{Lox/Lox}$;*Tg.hUBC-CreERT2*$^{+/T}$ strains. We monitored PDAC formation by high-resolution ultrasound starting at 12 weeks of age. Mice with established tumors of comparable size (tumor larger than 2 mm in diameter) were enrolled and fed *ad libitum* with a tamoxifen-containing diet activating the Cre-recombinase and therefore deleting systemically *Egfr* and *c-Raf* floxed alleles. To investigate whether tamoxifen or activation of CreERT2 itself affects PDAC growth, control (*Elas-tTA/tetO-Flp;K-Ras*^{FSFG12V}; *p53*$^{Frt/Frt}$;*Egfr*$^{+/+}$;*c-Raf*$^{+/+}$;*Tg.hUBC-CreERT2*$^{+/T}$) mice were also subjected to tamoxifen treatment.

Deletion of floxed *Egfr* and *c-Raf* alleles was efficient. In fact, we confirmed by Western blot that Egfr and c-Raf proteins were not expressed in several tissues of *Elas-tTA/tetO-Flp;K-Ras*^{FSFG12V};*p53*$^{Frt/Frt}$;*Egfr*$^{Lox/Lox}$;*c-Raf*$^{Lox/Lox}$;*Tg.hUBC-CreERT2*$^{+/T}$ mice after 3 weeks of tamoxifen treatment (Figure 22).

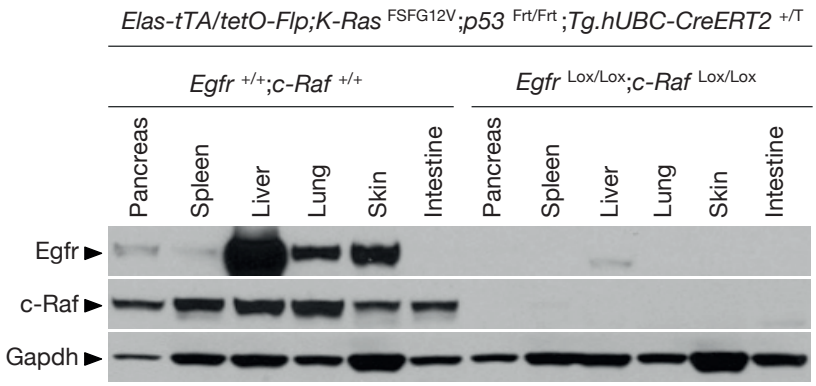

Figure 22. Systemic ablation of *Egfr* and *c-Raf* alleles is effective in mice exposed to a tamoxifen diet. Representative Western blot analysis of Egfr and c-Raf protein levels in tissues obtained from *Elas-*

tTA/tetO-Flp;K-Ras^{FSFG12V};*p53*$^{Frt/Frt}$;*Egfr*$^{+/+}$;*c-Raf*$^{+/+}$;*Tg.hUBC-CreERT2*$^{+/T}$ and *Elas-tTA/tetO-Flp;K-Ras*^{FSFG12V};*p53*$^{Frt/Frt}$;*Egfr*$^{Lox/Lox}$;*c-Raf*$^{Lox/Lox}$;*Tg.hUBC-CreERT2*$^{+/T}$ mice treated with tamoxifen for 3 weeks. Gapdh expression served as a loading control. Arrowheads show migration of the indicated proteins.

Combined ablation of *Egfr* and *c-Raf* in established pancreatic tumors impaired tumor growth as revealed by significant differences in tumor volume fold change at time of necropsy. Tumor volume fold change was 4.99 in *Egfr* and *c-Raf* deleted tumors (9 mice/10 tumors) whereas in wild type tumors corresponded to 24.09 (10 mice/15 tumors) (Figure 23A). Tumors in *Elas-tTA/tetO-Flp;K-Ras*^{FSFG12V};*p53*$^{Frt/Frt}$;*Egfr*$^{+/+}$;*c-Raf*$^{+/+}$;*Tg.hUBC-CreERT2*$^{+/T}$ control mice (10 mice/15 tumors) increased in size during the period under tamoxifen treatment (Figure 23A, B, C, D). In contrast, about 60% of tumors in *Elas-tTA/tetO-Flp;K-Ras*^{FSFG12V};*p53*$^{Frt/Frt}$;*Egfr*$^{Lox/Lox}$;*c-Raf*$^{Lox/Lox}$;*Tg.hUBC-CreERT2*$^{+/T}$ mice (9 mice/10 tumors) either partially regressed (1 out of 10) or completely disappeared (5 out of 10) (Figure 23A, B, C, F). Furthermore, the majority of the tumors that progressed (4 out of 10) grew less than the control cohort (Figure 23A, C, E).

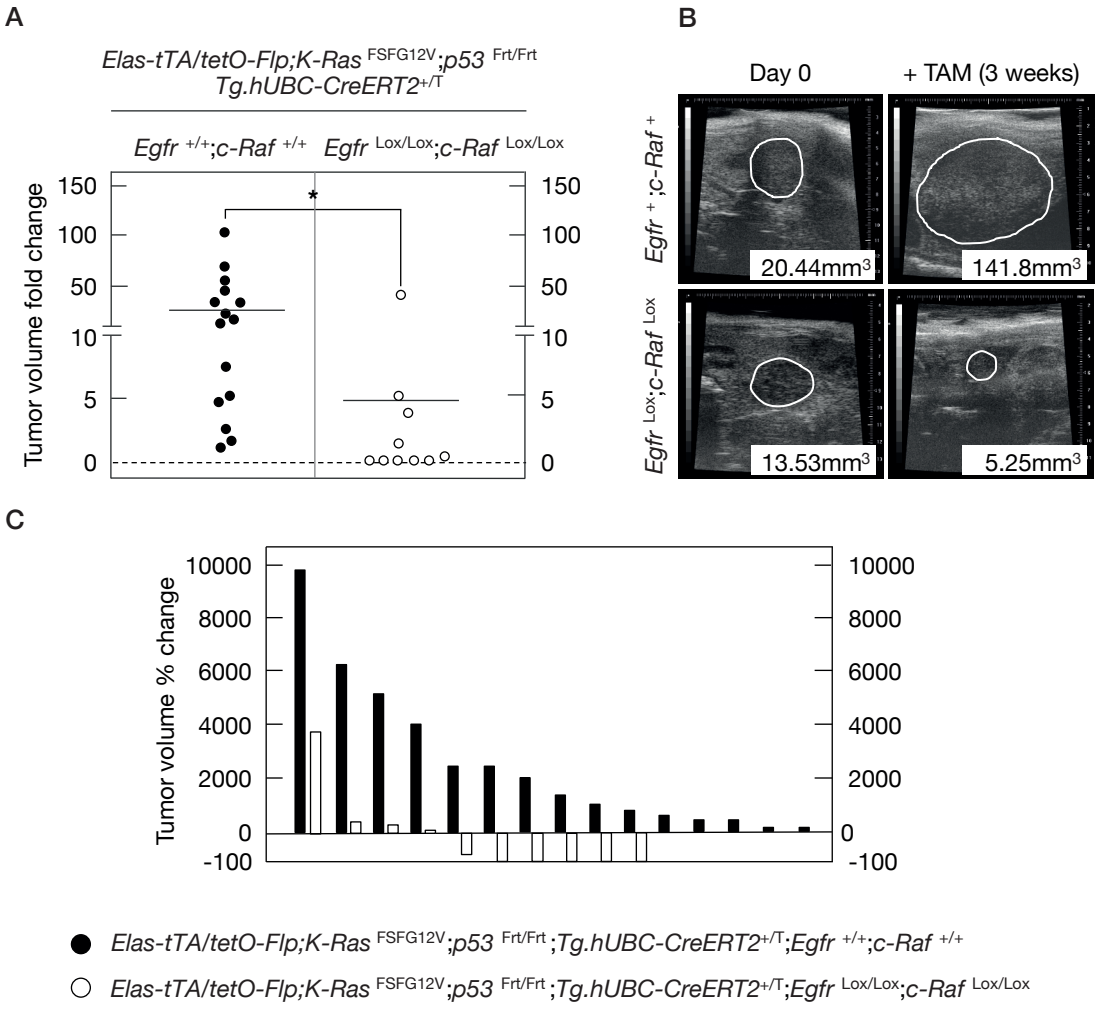

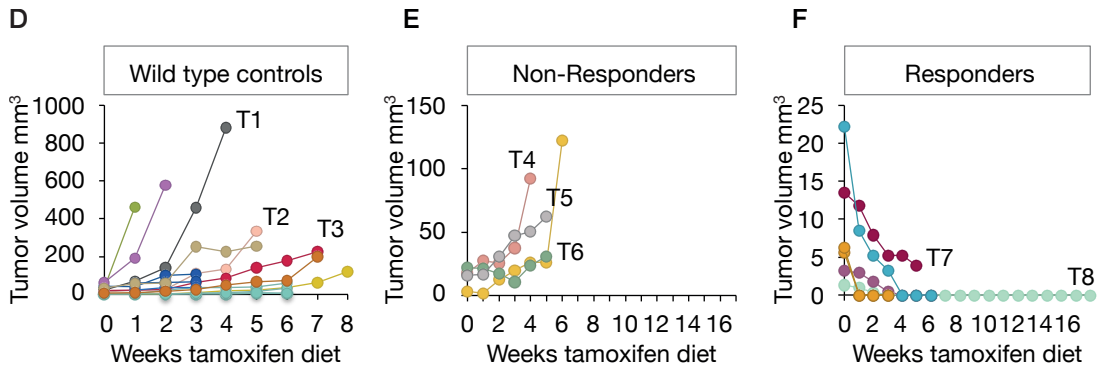

Figure 23. Egfr and c-Raf are essential for PDAC progression. (A) Tumor volume fold change of tumors from *Elas-tTA/tetO-Flp;K-Ras*^{FSFG12V};*p53*$^{Frt/Frt}$;*Egfr*$^{+/+}$;*c-Raf*$^{+/+}$;*Tg.hUBC-CreERT2*$^{+/T}$ mice (10 mice/15 tumors, solid circles) and from *Elas-tTA/tetO-Flp;K-Ras*^{FSFG12V};*p53*$^{Frt/Frt}$;*Egfr*$^{Lox/Lox}$;*c-Raf*$^{Lox/Lox}$;*Tg.hUBC-CreERT2*$^{+/T}$ mice (9 mice/10 tumors, open circles). Changes in tumor volume were calculated for each individual tumor based on ultrasound scans performed at the beginning and at the time of necropsy. *p<0.05 is indicated. (B) Tumor growth was monitored by high-resolution ultrasound in *Elas-tTA/tetO-Flp;K-Ras*^{FSFG12V};*p53*$^{Frt/Frt}$;*Egfr*$^{Lox/Lox}$;*c-Raf*$^{Lox/Lox}$;*Tg.hUBC-CreERT2*$^{+/T}$ and in *Elas-tTA/tetO-Flp;K-Ras*^{FSFG12V};*p53*$^{Frt/Frt}$;*Egfr*$^{+/+}$;*c-Raf*$^{+/+}$;*Tg.hUBC-CreERT2*$^{+/T}$ control mice. Pictures show tumor growth at day 0 and 3 weeks after treatment with tamoxifen (+TAM). Visible lesions are outlined in white. Tumor volumes are indicated. (C) Waterfall plot representing the percentage of change in tumor volume of individual PDACs detected by ultrasound in *Elas-tTA/tetO-Flp;K-Ras*^{FSFG12V};*p53*$^{Frt/Frt}$;*Egfr*$^{+/+}$;*c-Raf*$^{+/+}$;*Tg.hUBC-CreERT2*$^{+/T}$ mice (10 mice/15 tumors, solid bars) and *Elas-tTA/tetO-Flp;K-Ras*^{FSFG12V};*p53*$^{Frt/Frt}$;*Egfr*$^{Lox/Lox}$;*c-Raf*$^{Lox/Lox}$;*Tg.hUBC-CreERT2*$^{+/T}$ mice (9 mice/10 tumors, open bars). Changes in tumor volume were calculated for each individual tumor based on ultrasound scans performed at the beginning and at the time of necropsy. (D) Quantification of tumor volume in tamoxifen-treated *Elas-tTA/tetO-Flp;K-Ras*^{FSFG12V};*p53*$^{Frt/Frt}$;*Egfr*$^{+/+}$;*c-Raf*$^{+/+}$;*Tg.hUBC-CreERT2*$^{+/T}$ control mice (n=10 mice, n=15 tumors). Each color represents a different mouse. (E) Quantification of tumor volume in tamoxifen-treated *Elas-tTA/tetO-Flp;K-Ras*^{FSFG12V};*p53*$^{Frt/Frt}$;*Egfr*$^{Lox/Lox}$;*c-Raf*$^{Lox/Lox}$;*Tg.hUBC-CreERT2*$^{+/T}$ mice (n= 4 mice, n=4 tumors) which harbored tumors that progressed upon target ablation. Each color represents a different mouse. (F) Quantification of tumor volume in tamoxifen-treated *Elas-tTA/tetO-Flp;K-Ras*^{FSFG12V};*p53*$^{Frt/Frt}$;*Egfr*$^{Lox/Lox}$;*c-Raf*$^{Lox/Lox}$;*Tg.hUBC-CreERT2*$^{+/T}$ mice (n= 5 mice, n=6 tumors) that responded to target elimination. We could appreciate how tumors regressed or even disappeared. Each color represents a different mouse. T1-T8 represents different tumors.

As illustrated in Figure 24A, expression of both Egfr and c-Raf proteins were completely absent in tumor tissue after tamoxifen treatment. Remarkably, those tumors that progressed upon target elimination retained normal levels of phospho-Erk1/2 and phospho-Akt, suggesting that other signaling pathways compensated the absence of Egfr and c-Raf to sustain proliferation during tumor progression (Figure 24A, tumors T4, T5 and T6). Moreover, the histopathological analysis revealed that these tumors (T4, T5), as well as tumors that regressed (T7, T8), still expressed PDAC markers, such as the ductal marker CK19 (Figure 24B).

These facts suggest that targeting Egfr and c-Raf simultaneously impairs progression in about 60% of established PDACs. Nevertheless, there are tumors that can progress upon target elimination, suggesting the presence of tumor heterogeneity and the contribution of

alternative signaling pathways. It remains to be determined which other cascades are relevant for the maintenance of these tumor cells.

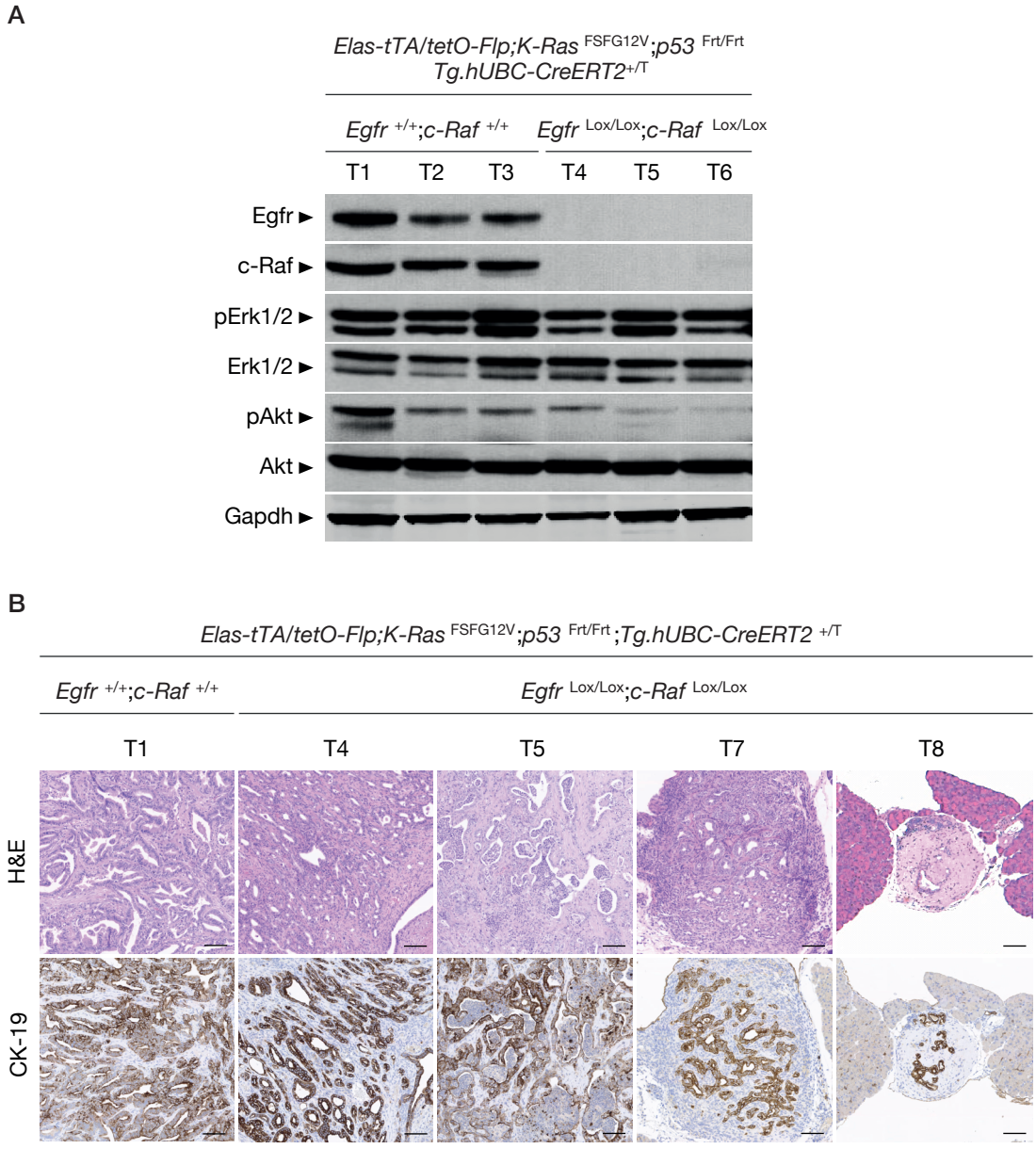

Figure 24. Tumors lacking Egfr and c-Raf expression still show CK-19 positive cells and active downstream signaling pathways. (A) Western blot analysis of Egfr and c-Raf expression in PDAC lysates derived from *Elas-tTA/tetO-Flp;K-Ras*^{FSFG12V};*p53*$^{Frt/Frt}$;*Egfr*$^{+/+}$;*c-Raf*$^{+/+}$;*Tg.hUBC-CreERT2*$^{+/T}$ control mice (n=3, T1, T2 and T3) and *Elas-tTA/tetO-Flp;K-Ras*^{FSFG12V};*p53*$^{Frt/Frt}$;*Egfr*$^{Lox/Lox}$;*c-Raf*$^{Lox/Lox}$;*Tg.hUBC-CreERT2*$^{+/T}$ (n=3, T4, T5 and T6) mice treated with tamoxifen. Phosphorylation levels of Erk1/2 and Akt were analyzed. Gapdh expression served as a loading control. Arrowheads show migration of the indicated proteins. (B) H&E and CK19 staining of PDAC sections from tumors of the indicated genotypes sacrificed at humane end point. Scale bar represents 100µm. T1-T8 represents different tumors (see figure XD, XE, XF).

4.2.3.3. Toxicity and side effects derived from systemic ablation of Egfr and c-Raf

One of the greatest challenges in oncology is to develop therapeutic strategies that diminish oncogenic signaling without affecting normal homeostasis. Importantly, due to the fact that human Ubiquitin C promoter led to the ubiquitous expression of the Cre-recombinase, *Egfr* and *c-Raf* were deleted systemically. Therefore, this approach also allowed us to evaluate the possible side effects associated with the combined treatment of Egfr and c-Raf inhibitors. However, observations derived from these genetic approaches need to be taken into consideration when targeting Egfr and c-Raf in the clinic, since pharmacologic therapeutic strategies are unlikely to result in irreversible loss of Egfr and c-Raf expression.

In order to study the possible side effects of combined elimination of the targets, *Egfr*$^{+/+}$;*c-Raf*$^{+/+}$;*Tg.hUBC-CreERT2*$^{+/T}$ and *Egfr*$^{Lox/Lox}$;*c-Raf*$^{Lox/Lox}$;*Tg.hUBC-CreERT2*$^{+/T}$ mice were continuously fed with a tamoxifen-containing diet starting at 12 weeks of age. As illustrated in Figure XA, mice carrying *Egfr* and *c-Raf* floxed alleles lost weight at the beginning of the treatment to thereafter maintain it constant or almost recover it. A similar effect was observed in control mice (Figure 25A). However, *Egfr*$^{Lox/Lox}$;*c-Raf*$^{Lox/Lox}$;*Tg.hUBC-CreERT2*$^{+/T}$ mice developed skin alterations (mostly associated with loss of Egfr expression, given that the same defects were observed in mice only lacking Egfr protein whereas these alterations were not present in mice with deletion of *c-Raf).* Mice exhibited hyperplasia and disorganization in the epidermis, hyperkeratosis, folliculitis, and inflammation with an increased number in mast cells (confirmed with toluidine-blue staining), apart from ulcers and scabs (Figure 25B, C).

Approximately 50-100% patients treated with EGFR inhibitors develop acneiform rash and folliculitis (Owczarczyk-Saczonek et al., 2013), indicating that the defects observed in mice could be comparable with those observed in treated patients. Tamoxifen-treated mice also showed slight disorganization in the crypts of the small intestine with an increased number of apoptotic cells (confirmed by cleaved Caspase-3 immunohistoquemistry), but despite these alterations, the intestine maintained its architecture and functionality (Figure 25D). Apart from these alterations, mice survived without major health problems for several months. Nevertheless, mainly due to the described skin alterations, the first *Elas-tTA/tetO-Flp;K-Ras*^{FSFG12V};*p53*$^{Frt/Frt}$;*Egfr*$^{Lox/Lox}$;*c-Raf*$^{Lox/Lox}$;*Tg.hUBC-CreERT2*$^{+/T}$ mice enrolled in the therapeutic studies were prematurely sacrificed. No defects incompatible with life were observed after histopathological examination. In fact, we have maintained mice for at least 17-18 weeks under tamoxifen treatment. We are currently trying to increase the number of mice and to prolong their time under tamoxifen treatment to deeply investigate tumor behavior.

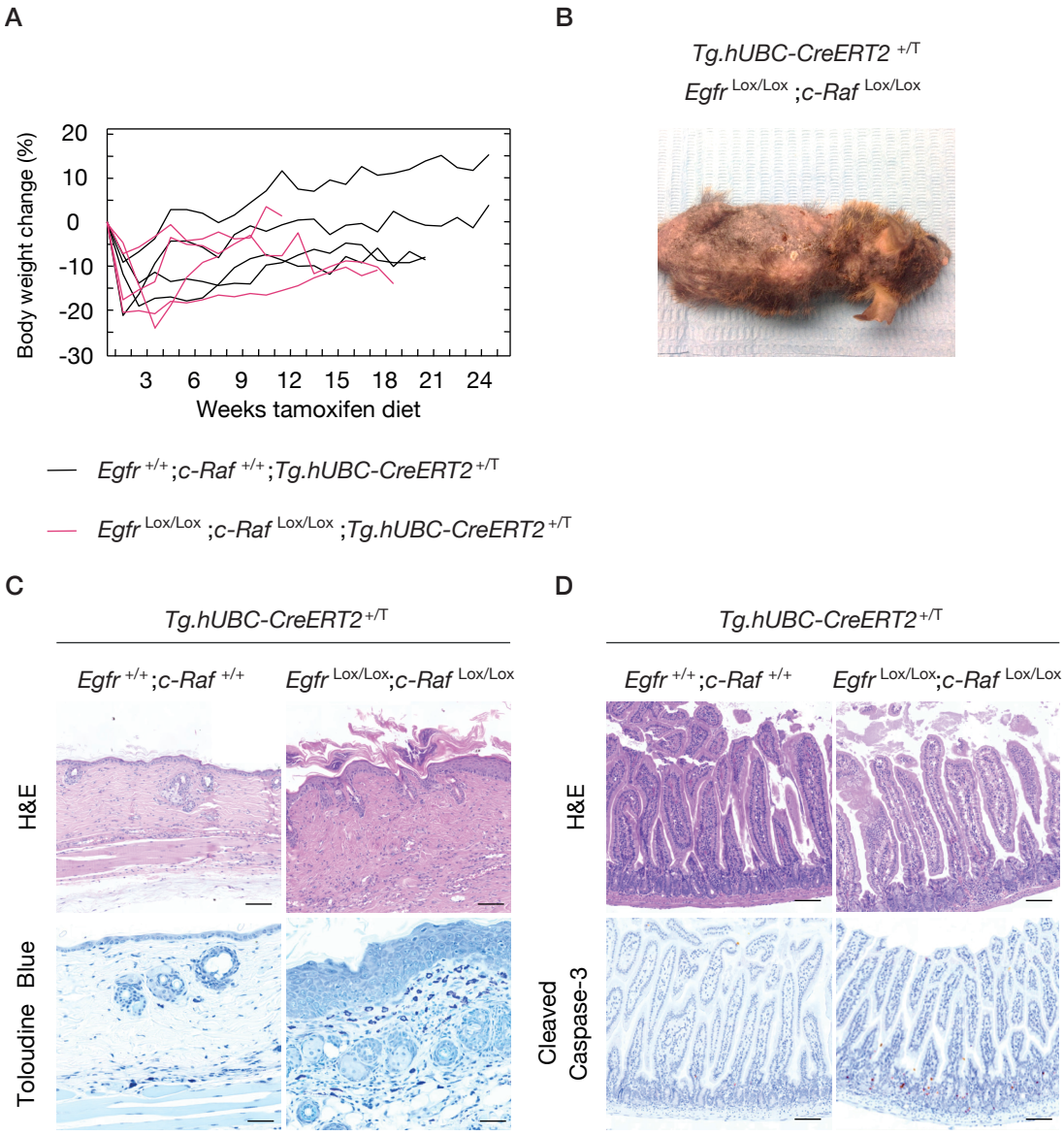

Figure 25. Body weight, skin and intestinal defects associated with concomitant *Egfr* and *c-Raf* deletion. (A) Representation of the percentage of change in body weight in *Egfr*$^{+/+}$;*c-Raf*$^{+/+}$;*Tg.hUBC-CreERT2*$^{+/T}$ (n=4) and *Egfr*$^{Lox/Lox}$;*c-Raf*$^{Lox/Lox}$;*Tg.hUBC-CreERT2*$^{+/T}$ mice (n=4) exposed to tamoxifen. Body weight was weekly recorded. (B) Aspect of *Egfr*$^{Lox/Lox}$;*c-Raf*$^{Lox/Lox}$;*Tg.hUBC-CreERT2*$^{+/T}$ mice and macroscopic skin defects that have been observed after 18 weeks of treatment with tamoxifen diet. (C) Representative H&E and Toluidine-blue staining in skin sections of *Egfr*$^{+/+}$;*c-Raf*$^{+/+}$;*Tg.hUBC-CreERT2*$^{+/T}$ and *Egfr*$^{Lox/Lox}$;*c-Raf*$^{Lox/Lox}$;*Tg.hUBC-CreERT2*$^{+/T}$ tamoxifen-treated mice. Scale bar represents 100µm (H&E) and 50µm (toluidine-blue). (D) Representative H&E and cleaved Caspase-3 staining in intestine sections of *Egfr*$^{+/+}$;*c-Raf*$^{+/+}$;*Tg.hUBC-CreERT2*$^{+/T}$ and *Egfr*$^{Lox/Lox}$;*c-Raf*$^{Lox/Lox}$;*Tg.hUBC-CreERT2*$^{+/T}$ tamoxifen-treated mice. Scale bar represents 100µm.

5. Discussion

Despite its low incidence, PDAC is one of the deadliest carcinomas due to the lack of effective treatments available. Furthermore, the first stages of tumor development are asymptomatic and diagnosis almost always occurs at late stages with a high incidence of metastasis. The development of GEMMs that closely recapitulate the natural history of human disease could help scientists design and validate newer and better therapeutic strategies.

The most frequent genetic alteration in PDAC is an activating mutation in the *K-RAS* oncogene (Almoguera et al., 1988; Biankin et al., 2012). Several strategies to target K-RAS directly have been developed. However, these targeted therapies have been inefficient, in part because K-RAS itself has remained difficult to inhibit with small molecules. Hence, attempts to target this oncogene in the clinic have focused on the inhibition of upstream and downstream molecules of RAS signaling pathway.

PDAC GEMMs that recapitulate the human disease have been developed to evaluate the therapeutic value of different targets and pathways. Using PDAC mouse models it was shown that Egfr has a key role in pancreas tumorigenesis impairing tumor initiation (Ardito et al., 2012; Navas et al., 2012). Nevertheless, genetic ablation cannot be achieved in the clinic and this could explain why EGFR therapeutics have only been partially successful (Moore et al., 2007). Moreover, pancreatic tumorigenesis involves several mutations affecting different pathways (Jones et al., 2008), thus EGFR inhibition in advanced PDAC patients will not be sufficient and it should be combined with drugs targeting different pathways with an important role in PDAC progression and maintenance.

Along with this, it was recently demonstrated that the RAF/MEK/ERK pathway has a key role in *K-Ras* driven NSCLC and PDAC. Previous studies from our laboratory have illustrated that c-Raf is essential for lung (Blasco et al., 2011) and pancreas tumor initiation (unpublished, see appendix 8.1) without affecting normal homeostasis, suggesting that it is a suitable target to block the MAPK pathway. Interestingly, combined elimination of Egfr and c-Raf entirely blocks PDAC initiation in a p53 deficient context (unpublished, see appendix 8.2).

Considering these results, the main aim of the current thesis was to investigate the potential therapeutic benefit of inhibiting Egfr and its combination with c-Raf as a multi-targeted therapy in the context of *K-Ras* driven PDAC.

5.1. Validation of Egfr tyrosine kinase inhibition in *K-Ras* driven PDAC

5.1.1. Generation of a conditional *Egfr* kinase dead allele

In order to study the inhibition of Egfr tyrosine kinase activity in pancreatic tumorigenesis and to elucidate whether the benefit previously described (Ardito et al., 2012; Navas et al., 2012) relied on Egfr catalytic activity, we designed a mouse model that expressed a catalytic inactive form of the receptor ($Egfr^{D839A}$) to mimic the effect of efficient and selective Egfr inhibitors.

As previously reported in this thesis, there are two Egfr mutant alleles that result in reduced signaling of the receptor, the recessive hypomorphic *Egfr*^{wa2} (Fowler et al., 1995; Luetteke et al., 1994) and the dominant antimorphic *Egfr*^{wa5} (Du et al., 2004; Lee et al., 2004). The *Egfr*^{wa2} allele is a spontaneously arising point mutation causing a V743G substitution in the ATP binding motif of the tyrosine kinase domain, presumably altering the structure of the active site. The mutated receptor has an 80-95% reduction in Egfr activity (Luetteke et al., 1994). Homozygous *Egfr*^{wa2} mice are viable and healthy, however females develop impaired maternal lactation (Fowler et al., 1995). The *Egfr*^{wa5} strain was developed using N-Ethyl-N-Nitrosourea (ENU) mutagenesis. The ENU treatment induced an adenine to guanine transition leading to an amino acid change from Aspartic acid to Glycine (D833G). This mutation results in an alteration in the DFG domain of the Egfr catalytic loop, which plays a role in chelating Mg^{2+} and stabilizing ATP binding, encoding a completely inactive form of the receptor since no phosphorylation of Egfr^{wa5} is detected following stimulation with ligands. *Egfr*^{wa5} homozygous mice die during gestation with phenotypes indistinguishable to those observed in *Egfr* knockout mice (Du et al., 2004; Lee et al., 2004).

In our *Egfr*^{D839A} mice, an Alanine replaces the Aspartic acid of the HRD domain (D839A), which acts as a proton acceptor that is critical for catalysis. Constitutive homozygous expression of *Egfr*^{D839A} resulted in embryonic lethality, reproducing the defects developed by the *Egfr* knockout and *Egfr*^{wa5} homozygous mice, illustrating that Egfr catalytic activity is essential for mouse embryo development. Egfr^{D839A} protein stability was verified by Western blot and the phosphorylation assay revealed that Egfr^{D839A} catalytic activity was impaired. Therefore, we can affirm that Egfr^{D839A} protein lacked kinase activity without being affected in terms of protein expression or stability. Moreover, *Egfr*^{D839A} MEFs showed impaired proliferation and they could not stimulate MAPK and PI3K signaling pathways in the presence of its ligands. Both cascades are essential for cell proliferation, survival and migration and consequently for mouse development.

We generated an *Egfr*^{LmLD839A} conditional allele that encodes an inducible catalytic inactive receptor upon Cre-mediated recombination. Using this conditional knockin approach we avoided the embryonic lethality associated with this mutation and we were able of exploring its role in tumor initiation and progression.

5.1.2. Egfr kinase activity in *K-Ras*^{G12V} driven PDAC initiation

5.1.2.1. Egfr catalytic activity is essential for PDAC initiation

As previously reported, Egfr is expressed in pancreatic lesions and tumors, in mouse and human samples (Navas et al., 2012). Additionally, the presence of Egfr is essential for ADM *in vitro* and for PDAC development *in vivo* (Ardito et al., 2012; Navas et al., 2012). In order to investigate whether the therapeutic benefit observed upon *Egfr* ablation in *K-Ras*^{G12V} driven

PDAC relied on Egfr catalytic activity or on its kinase independent functions, we introduced the *Egfr*^{LmLD839A} conditional strain in our PDAC initiation mouse model.

In the *embryonic protocol*, the absence of pancreatic lesions in *ElasK-Ras*^{G12Vgeo};*Egfr*$^{LmLD839A/LmLD839A}$ mice suggests that the inhibition of Egfr catalytic activity concomitantly with *K-Ras*^{G12Vgeo} expression is impairing pancreatic tumorigenesis. Furthermore, we confirmed that upon *K-Ras*^{G12Vgeo} expression, Egfr signaling plays an important role in ADM, a key event for PanIN and PDAC initiation. It was previously shown that ADM is largely dependent on activation of Egfr considering that addition of its ligands, such as EGF and TGFα, highly increased the number of metaplasias (Means et al., 2005). As consequence, this process was significantly reduced in the absence of Egfr (Navas et al., 2012). Upon expression of a catalytic inactive Egfr, ADM was significantly reduced but not completely blocked, suggesting that the generation of ductal-like structures requires Egfr signaling in the presence of *K-Ras*^{G12V}, but also that EGF and TGFα may contribute to ADM by activating additional signaling pathways, at least *in vitro*.

Nevertheless, since PDAC is not a pediatric disease we studied the role of Egfr kinase activity during the adulthood. In the *adult protocol*, *K-Ras*^{G12Vgeo} expression started at 2 months of age and mice were treated with caerulein for three months to induce chronic pancreatitis. Control mice showed low- and high-grade lesions (more than 90% of mice displayed high-grade PanIN lesions); however none of them were found in mice expressing the kinase inactive receptor. Thus, Egfr tyrosine kinase activity and its signaling are essential for *K-Ras*^{G12V} driven PanIN and PDAC initiation both in the *embryonic* and in the *adult protocol*.

Although these studies have been done in our tumor initiation PDAC model, they suggest that EGFR tyrosine kinase inhibitors could be useful in the clinical scenario, especially for patients carrying the wild type form of *TP53*. Hence, the use of GEMMs could provide essential information for patient stratification that could be translated into a meaningful contribution for patient benefit.

5.1.2.2. Egfr catalytic activity is essential for PDAC initiation in the absence of p16Ink4/p19Arf tumor suppressor genes, but loss of p53 triggers activation of other signaling pathways.

Somatic mutations in tumor suppressor genes are highly associated with PDAC. Loss of *p16INK4A/p14ARF* appears during early stages (PanIN1-2) affecting more than 90% of pancreatic tumors (Wood and Hruban, 2012) whereas mutations in *TP53* are late events (PanIN-3) present in 50-70% of PDAC cases (Scarpa et al., 1993).

GEMMs have allowed the study of cooperation between *K-Ras* and loss of a wide range of tumor suppressor genes such as *p53*, *p16Ink4a/p19Arf*, *Smad4*, *Pten*, among others, which significantly resulted in rapid tumor development, leading in some cases to the acquisition of a metastatic phenotype (Gopinathan et al., 2015).

In the *embryonic protocol, ElasK-Ras*^{G12V};*p16Ink4a/p19Arf*$^{Lox/Lox}$;*Egfr*$^{LmLD839A/LmLD839A}$ mice at 1 year of age did not show any PanIN lesion nor PDAC. On the contrary, control mice developed PDAC tumors that implied their sacrifice at humane end point. These results indicate that in the absence of *p16Ink4a/p19Arf* tumor suppressor genes, Egfr signaling is essential for PDAC initiation. Patients with these types of genetic alterations could benefit from drugs inhibiting EGFR tyrosine kinase activity. Nevertheless, as previously pointed out, caution should be taken, considering that our PDAC model is useful to genetically investigate the role of different targets at initiation stages but not in established pancreatic tumors.

During the *embryonic protocol,* in a p53 deficient context, loss of Egfr catalytic activity did not block the appearance of pancreatic tumors, although mice increased their lifespan by 41% with respect to their wild type littermates. Whilst elimination of *Egfr* in the *adult protocol* delayed tumor formation in the absence of p53 (Navas et al., 2012), inhibition of its kinase activity did not show any survival benefit. This observation is the only difference between the expression of an Egfr kinase dead receptor and the complete elimination of the protein in the *K-Ras*^{G12V} driven PDAC model, which may be related with the poor response in PDAC patients treated with the combination of erlotinib plus gemcitabine (Moore et al., 2007).

All together, these results indicate that in the absence of p53 other signaling pathways are involved in tumor growth conferring resistance to Egfr inhibition. Notably, analysis of PDAC cell lines derived from *ElasK-Ras*^{G12V};*p53*$^{-/-}$;*Egfr*$^{D839A/D839A}$ pancreatic tumors revealed Egfr^{D839A} tyrosine phosphorylation and activation. These observations suggest that there are other molecules regulating Egfr phosphorylation and consequently, persistent activation of MAPK and PI3K signaling in the absence of p53.

It is important to note that ligand binding induces formation of receptor homo- and heterodimers, and subsequent activation of the intrinsic tyrosine domain. All possible homo- and heterodimeric receptor complexes between members of the ErbB family have been identified in different systems (Normanno et al., 2006). ErbB2 represents the preferred dimerization partner among all other ErbB receptors (Olayioye et al., 2000). Heterodimerization of EGFR with ErbB2 inhibits downregulation of EGFR, and thereby, prolongs growth factor signaling (Huang et al., 1999; Wang et al., 1999; Zandi et al., 2007). Remarkably, defective downregulation of ErbB2-EGFR heterodimers results in a more potent signaling than EGFR homodimers (Lenferink et al., 1998; Yarden and Sliwkowski, 2001). This raises the possibility that ErbB2 represents a mechanism for the increase of EGFR levels on the cell surface and prolongation of growth factor signaling (Hendriks et al., 2003).

Besides dimerization with other ErbB family members, several other Egfr-related heterodimerizations could be important for therapeutic resistance. For instance, using lung cancer cell lines, it was shown that acquired resistance to TKIs was mediated by dimerization between Met (hepatocyte growth factor receptor) and ErbB3, driving activation of PI3K and Src and completely replacing signals from the inhibited Egfr (Engelman et al., 2007).

In an effort to elucidate whether other members of the ErbB family were compensating the loss of Egfr catalytic activity, we systematically knocked down ErbB2 with a specific shRNA in *ElasK-Ras*^{G12Vgeo};*p53*$^{-/-}$;*Egfr*$^{+/+}$ and *ElasK-Ras*^{G12Vgeo};*p53*$^{-/-}$;*Egfr*$^{D839A/D839A}$ PDAC-derived cell explants. We found that ErbB2 was responsible for Egfr^{D839A} phosphorylation and that Egfr/ErbB2 heterodimers were sustaining, at least in part, MAPK activation. Consequently, ErbB2 could be maintaining Egfr signaling and promoting PDAC development in the absence of p53.

Interestingly, the first dual-specificity inhibitor, lapatinib, which targets both EGFR and ErbB2, was approved for the treatment of ErbB2 overexpressing breast cancer (Geyer et al., 2006). During the last few years several other dual-specificity inhibitors, as afatinib have been developed (Li et al., 2008). Afatinib is a selective, potent and irreversible ErbB family blocker. Unlike erlotinib, afatinib covalently binds to and irreversibly blocks signaling from all homo- and heterodimers formed by the ErbB family members (Li et al., 2008). This drug received the Food and Drug Administration (FDA) approval in 2013 for treating EGFR-mutated NSCLC (Soria et al., 2015). Based on preclinical evidences in PDAC cell lines (Huguet et al., 2016; Ioannou et al., 2011), afatinib, is under current evaluation in an ongoing phase II trial in combination with gemcitabine (NCT01728818), and in a phase I trial, in combination with gemcitabine and nab-paclitaxel (NCT02975141) to treat PDAC patients. In order to investigate the role of Egfr/ErbB2 inhibition in PDAC GEMMs, we are also currently performing afatinib treatment in tumor-bearing mice.

It is important to highlight that the in effect on PI3K/Akt pathway activation after ErbB2 knockdown in three different PDAC-derived cell lines was inconclusive. This may reflect tumor heterogeneity and extensive genetic diversity that needs further analysis. Likewise, tumor explants lacking p53 and Egfr displayed Akt phosphorylation that could explain for Egfr-independent mechanism, that in the absence of p53, promote PanIN and PDAC initiation (Navas et al., 2012). Moreover, these tumor explants are sensitive to the combined inhibition of PI3K and STAT3 (Navas et al., 2012). Thus, successful treatment of advanced human pancreatic tumors may require inhibition of distinct signaling cascades.

5.2. Targeting Egfr and c-Raf in *K-Ras* driven PDAC progression

5.2.1. Generation of the therapeutic PDAC mouse model

Our group and others have identified several candidate genes involved in K-Ras signaling with potential therapeutic value. For instance, Egfr and c-Raf are essential for PanIN and PDAC initiation. Similarly, targets of the PI3K pathway such as Pdk1 and p110α (Baer et al., 2014; Eser et al., 2013; Wu et al., 2014) were shown to be indispensable for pancreas tumorigenesis. Inhibition of NF-κB pathway by genetic ablation of IKKβ or the loss of non-canonical IκB-related kinase (IKBKE) reduced the development of PanIN and PDAC (Ling et al.,

2012; Rajurkar et al., 2017). However, all these studies were carried out in PDAC GEMMs in which the alleles of interest were deleted at the same time when the initiating oncogenic events were expressed. Consequently, this approach does not allow to genetically validate targets in established PDACs, nor genetic investigation of resistance mechanisms or manipulation of tumor microenvironment.

Therefore, to mimic a clinical scenario in which the therapeutic intervention occurs after diagnosis of PDAC, we have developed a novel PDAC model based in a dual recombinase system (DRS) that enables sequential manipulation of PDAC. This new model combines the Flp-FRT recombination system for tumor development with the Cre-LoxP system for a second genetic manipulation. PDAC development is induced by concomitant expression of the oncogenic *K-Ras*^{G12V} mutation and *p53* deletion with the *Elas-tTA/tetO-Flp* system. Target ablation or inactivation in established tumors (detected by ultrasound) is achieved by a CreERT2 system. Importantly, when CreERT2 is ubiquitously expressed, leads to systemic ablation of the target, allowing evaluation of possible side effects associated with target elimination or inhibition.

Another recently described PDAC model has made use of the DRS (Schönhuber et al., 2014). This *Pdx1-Flp;*FSF-*K-Ras*$^{G12D/+}$;FSF-Rosa26$^{CAG-CreERT2/+}$ strain was used to eliminate *Pdk1* upon tamoxifen treatment of mice at three months of age. Interestingly, *Pdk1* ablation in PanINs blocked tumor progression almost completely (Schönhuber et al., 2014). Nevertheless, this study was performed in a p53 proficient background and *Pdk1* ablation was not done in full-blown tumors. Additionally, in this model, the Cre-recombinase is only expressed in cells that have undergone Flp-recombination (in cells expressing the *K-Ras* oncogene) and not systemically, thus they could not study the possible related side effects derived from *Pdk1* ablation.

This new genetic strategy has allowed us to study the therapeutic value of eliminating (conditional knockout alleles) or inhibiting (conditional knockin kinase dead alleles) Egfr as an individual target, or in combination with c-Raf as a multi-targeted therapy. Furthermore, we have evaluated the toxic side effects of systemic target ablation or inhibition.

5.2.2. Deletion or inhibition of Egfr in full-blown tumors do not impair PDAC progression

Aforementioned results obtained in this thesis demonstrated that, in aggressive p53-null adenocarcinomas, Egfr signaling inhibition is dispensable for PDAC initiation. Nevertheless, in order to determine the potential therapeutic benefit of Egfr in already established PDAC, we introduced *Egfr*^{Lox} alleles as well as *Egfr*^{LmLD839A} alleles (to mimic the effect of efficient Egfr inhibitors) in our PDAC therapeutic strain (*Elas-tTA/tetO-Flp;K-Ras*^{FSFG12V};*p53*$^{Frt/Frt}$;*Tg.hUBC-CreERT2*$^{+/T}$). Unfortunately, neither Egfr ablation nor inhibition of its kinase activity, exhibited a significant beneficial effect in PDAC progression. Tumors progressed, independently of Egfr

status without a significant difference in tumor fold change, likely due to activation of alternative pathways upon *p53* deletion that still need to be elucidated. The molecular analysis and the histopathological characterization of these tumors are currently ongoing.

These results in mice are in accordance to the observations derived from PDAC patients treated with erlotinib in combination with gemcitabine (Moore et al., 2007). The failure of Egfr targeted therapy may be related to the extensive crosstalk between redundant proliferation signaling pathways in tumor cells (Huang et al., 2011), which results in cancer cell survival even though some pathways are blocked by targeted therapy. This suggests, that dual pathway inhibition could be a promising therapeutic strategy. In addition, related intratumor heterogeneity could be an added complication that needs to be addressed (Burrell et al., 2013).

5.2.3. Combined elimination of Egfr and c-Raf in established *K-Ras* driven PDAC

It has been recently shown that c-Raf is essential for *K-Ras* induced NSCLC (Blasco et al., 2011; Karreth et al., 2011) and PDAC (unpublished results). Ablation of *c-Raf* in acinar cells of *ElasK-Ras*^{G12Vgeo} mice completely prevented PanIN formation both in the *embryonic* and in the *adult protocol*. However, elimination of this target in a p53 deficient background did not block PDAC initiation (unpublished results, see appendix 8.1).

Unfortunately, in a p53 deficient background, ablation of either Egfr (Navas et al., 2012) or c-Raf (unpublished results) as well as expression of an Egfr kinase dead receptor, delays but does not prevent development of PDAC. Importantly, loss of p53 can sustain proliferation in the absence of Ras proteins via Ras-independent activation of the MAPK signaling pathway (Drosten et al., 2014). The mechanism is still unknown, but it raises the possibility of the MAPK activation by a Ras independent mechanism when *p53* is mutated. These observations may have an important implication in cancer treatment because mutations in *Ras* oncogenes and *p53* are frequent events in human tumors (Griffin et al., 1995; Roberts and Der, 2007). In this scenario, loss of p53 would emphasize activation of the MAPK pathway by mutant Ras, which may cause stronger MAPK activation and increased tumor cell proliferation.

Furthermore, human pancreatic tumors contain multiple mutations affecting different signaling pathways (Jones et al., 2008). Thus, it is presumably, that complete inhibition of tumor development requires inactivation of two or even more signaling cascade to induce better responses. Indeed, our previous results have demonstrated that simultaneous genetic ablation of *Egfr* and *c-Raf* results in complete inhibition of PDAC initiation (unpublished results, see appendix 8.2). These observations suggest that, in the absence of p53, both targets are critical during initial steps of PDAC formation such as ADM. Although these results look promising, it is important to note that they were obtained using GEMMs in which both *Egfr* and *c-Raf* were ablated during the first stages of tumorigenesis and not in full-blown tumors. Nevertheless, these observations suggest a promising value for this therapeutic combination.

Thus, to fully validate these findings we introduced *Egfr* and *c-Raf* floxed alleles in the PDAC therapeutic strain to investigate the combination of these targets in established PDACs.

5.2.3.1. Combined deletion of *Egfr* and *c-Raf* in established PDACs results in a significant therapeutic effect

Conventional chemotherapy has limited effect in pancreatic cancer and several signaling pathways, including MAPK and PI3K, represent exciting new targets for a possible therapeutic intervention, especially because known inhibitors are already clinical available.

The crosstalk between redundant proliferation pathways, such as MAPK and PI3K cascades, in tumor cells appears to be particularly important clinically. Indeed, several preclinical studies have revealed that dual pathway inhibition shows promising effects. The combined inhibition of MEK and PI3K has been shown to be effective in *K-Ras* driven NSCLC (Engelman et al., 2008) as well as in other Ras mutant cancers (Roberts et al., 2012). Nevertheless, although combined targeting of MEK and PI3K provided clinically significant responses in a mouse model of PDAC, the treatment did not produce a durable response (Alagesan et al., 2015), indicating differences in the requirements of different types of tumors, and suggesting that alternative therapeutic strategies will be required. Combined FGFR1 and MEK inhibition (Manchado et al., 2016) and inhibition of DDR1 together with Notch signaling (Ambrogio et al., 2016) also shown a significant effect in a model of *K-Ras* driven lung adenocarcinoma. The first clinical studies to evaluate the efficacy of dual pathway inhibition in patients also showed promising effects in tumor growth targeting PI3K/AKT and MAPK pathways. However, multi-targeted inhibition was significantly more toxic than single-agent therapy (Shimizu et al., 2012).

Most of these studies were done using different combinations of MEK inhibitors, but it is important to take into consideration that *Mek* and *Erk* genetic ablation caused multi-organ failure leading to the rapid death of the animals (Blasco et al., 2011). Furthermore, the use of MEK inhibitors is very limited in the clinic due to the associated toxicities. Fortunately, *c-Raf* elimination does not affect tissue homeostasis (Blasco et al., 2011).

Simultaneous genetic ablation of *Egfr* and *c-Raf* in full-blown PDAC (*Elas-tTA/tetO-Flp;K-Ras*^{FSFG12V};*p53*$^{Frt/Frt}$;*Egfr*$^{Lox/Lox}$;*c-Raf*$^{Lox/Lox}$;*Tg.hUBC-CreERT2*$^{+/T}$) results in a significant therapeutic effect. About 60% of PDACs displayed partial or even complete regression. However, there are still tumors that can progress upon target elimination. Moreover, in these tumors, lack of Egfr and c-Raf does not affect Erk1/2 and Akt phosphorylation, suggesting that resistant mechanisms lead to cell signaling activation compensating the deficiency of these proteins. Paraffin sections of pancreas from mice that responded to target ablation, presented few PanIN lesions (undetectable by ultrasound). It remains to be determined whereas these PanINs retain both Egfr and c-Raf expression (we are currently performing LCM to analyze them by PCR). Pancreatic tumors are extremely heterogeneous exhibiting a wide range of

mutations (Jones et al., 2008), which could explain different responses upon target elimination. In order to identify differentially expressed genes and the transcription programs involved in different tumor responses we will consequently perform DNA- and RNA-seq analysis.

These results underscore the value of this therapeutic combination. Therefore, to validate our findings in a relevant preclinical setting we are using cell lines derived from PDAC patient-derived xenografts (PDX) that harbor *K-RAS* and *TP53* mutations. With the help of CRISPR/Cas9 editing technology we are trying to concomitant ablate *Egfr* and *c-Raf* genes. Moreover, specific shRNAs against both targets are being used to promote simultaneous *Egfr* and *c-Raf* knockdown. PDX cell lines will be subcutaneously and/or orthotopically implanted in the pancreas of immunocompromised mice to monitor tumor growth in the presence or absence of the targets of interest.

The use of drug combinations to target Egfr and c-Raf in GEMMs and PDX tumor models will be helpful to determine tumor behavior. As previously reported there are several specific EGFR inhibitors, but unfortunately, there are no specific drugs against C-RAF. One of the first-generation RAF inhibitors, sorafenib, was developed as a C-RAF inhibitor to treat RAS mutant cancers (Lyons et al., 2001). Although it was approved by the FDA for a variety of cancers, its efficacy remains unknown due to its multi-kinase inhibitory effects. Vemurafenib and dabrafenib are small molecules that were shown to potently inhibit B-RAF^{V600E} (Gibney and Zager, 2013; Tsai et al., 2008). In PDAC, *B-RAF* mutations are mutually exclusive with *K-RAS* mutations and are present in 30% of *K-RAS* wild type PDAC cases (Witkiewicz et al., 2015). In mice, mutant *B-Raf* is sufficient to induce PDAC development (Collisson et al., 2012) implicating the utility of B-RAF inhibitors in PDAC. However, it should be stressed that any clinical trial with RAF inhibitors should be restricted to patients with confirmed *B-RAF* mutation, since targeting wild type B-RAF with RAF inhibitors can lead to paradoxical activation of ERK signaling through transactivation of C-RAF, triggering an accelerating tumor growth (Heidorn et al., 2010; Poulikakos et al., 2010). This observation led to the development of a second-generation of RAF inhibitors (also known as “paradox breakers”), which do not activate MAPK in the presence of RAS mutations. They are pan-RAF dimer inhibitors; they bind all RAF members with similar affinity inhibiting their kinase activity without activating MAPK in the presence of RAS mutations, indicating that the activity of the dimers was effectively blocked (Peng et al., 2015; Zhang et al., 2015a).

As available RAF inhibitors are not selective against C-RAF, we are generating a new *c-Raf* conditional kinase dead allele to introduce it into the therapeutic PDAC strain. We will finally combine it with the already described *Egfr*^{LmLD839A} to genetically model the outcome of Egfr and c-Raf selective inhibitors in PDAC. For the pharmacological validation *in vivo*, either in GEMMs or in PDX models, trametinib (Mek inhibitor) and afatinib will be used to inhibit the MAPK and Egfr signaling pathway, respectively.

As already described, combined ablation of *Egfr* and *c-Raf* results in a significant

therapeutic response. Nonetheless, there are few tumors that can progress upon target elimination, suggesting that Egfr and c-Raf may not be sufficient to provide optimal therapeutic benefit and they will have to be combined with other therapies. It was described that c-Raf can phosphorylate other proteins apart from Mek. Among them, Retinoblastoma protein (Rb) is phosphorylated and inactivated by c-Raf in the nucleus, which is necessary for cell cycle entry (Wang et al., 1998). Rb phosphorylation correlates with poor overall survival in PDAC (Trevino et al., 2013). Moreover, inhibitors of the complex c-Raf-Rb have been reported to inhibit proliferation, migration and invasion of pancreatic cell lines, including metastatic cells that are resistant to gemcitabine. The same effect was observed in preventing *in vivo* growth and metastasis of pancreatic cancer cells introduced in immunocompromised mice (Trevino et al., 2013). Additionally, the absence of the Cyclin-dependent kinase 4 (Cdk4) protein, a well-known cell cycle regulator, has been reported to impair lung tumor initiation and progression in *K-Ras* driven lung adenocarcinoma (Puyol et al., 2010). Whereas Rb phosphorylation by c-Raf is considered as a preparing step for cell cycle entry (Wang et al., 1998), Rb mediated phosphorylation by Cdk4 promotes G1-S transition in cell division (Kato et al., 1993). Thus, concomitant genetic elimination of *c-Raf* and *Cdk4* together with *Egfr* would be an interesting therapeutic strategy to assess whether this multi-targeted therapy could have a synergistic effect in *K-Ras* driven PDAC.

5.2.3.2. Side effects associated with the systemic elimination of Egfr and c-Raf

Loss of Egfr expression in adult mice is associated with skin side effects. Mice presented rashes together with ulcers, inflammation, hyperkeratosis and hyperplasia, similar to those alterations observed in patients treated with EGFR inhibitors (Owczarczyk-Saczonek et al., 2013). Germline loss of Egfr causes lung and neuronal defects (Sibilia and Wagner, 1995; Sibilia et al., 1998). Nevertheless, upon detailed examination none of these alterations were found in adult mice lacking the receptor.

In human patients, acneiform rash is the most common side effect of EGFR inhibitors treatments. It is a follicular papulopustular eruption that affects skin areas with a high density of sebaceous glands, such as the face, scalp, chest and upper back (Fabbrocini et al., 2015). Likewise, adult mice lacking Egfr protein show primary symptoms around the snout, face, ears, scalp and upper back. Inhibition of EGFR in keratinocytes induces apoptosis, cell arrest, reduced cell migration and increased cell adhesively and differentiation. All these processes induce keratinocytes to release inflammatory chemokines promoting inflammatory cell infiltration (Paul et al., 2014). In mice, we have observed an increased amount of mast cells, which secrete numerous vasoactive and pro-inflammatory mediators (Theoharides et al., 2012) that could be related with the observed inflammatory processes in patients.

It is known that monoclonal antibodies like cetuximab more frequently trigger acneiform rash than tyrosine kinase inhibitors like erlotinib (Thomas and Grandis, 2004). In accordance

with these observations, adult mice expressing $Egfr^{D839A}$ (the tyrosine kinase inactive form of Egfr) do not seem to develop skin alterations as severe as when the receptor is absent. This could be due to the fact that using tyrosine kinase inhibitors, EGFR signaling could be compensated by EGFR/ErbB2 heterodimers (Huang et al., 1999; Wang et al., 1999; Zandi et al., 2007), whereas monoclonal antibodies inhibit EGFR ligand binding and induce receptor endocytosis and degradation (Roskoski, 2014), probably blocking EGFR heterodimerization and consequently its signaling.

Egfr and *c-Raf* combined ablation (apart from skin problems) resulted in increased apoptosis in intestinal crypts that did not compromise intestinal structure and/or functionality. We did not observe a significant weight loss or other obvious defects upon detailed examination of relevant tissues.

All these observations need to be taken into consideration when targeting Egfr and c-Raf in the clinic, although clinical treatments do not result in irreversible loss of target expression.

Unfortunately, most of the mice enrolled in our therapeutic studies were sacrificed due to ethical recommendations because of their aspect due to the dermatitis. In spite of this, mice under tamoxifen treatment can survive several months and we are currently maintaining them for longer periods of time to better understand tumor behavior.

Together, these observations underscore the complexity of oncogenic K-Ras signaling and the need for an in-depth genetic analysis of the role and requirement of RAF/MEK/MAPK and other signaling pathway components in *K-Ras* driven PDAC progression and maintenance.

6. Conclusions

The conclusions obtained in this thesis were the following:

1. Egfr catalytic activity is indispensable for mouse development. Germline expression of a catalytic inactive Egfr mutant is associated with skin, lung and placental defects leading to perinatal lethality.

2. Elimination of Egfr kinase activity impairs PanIN and PDAC development even in the context of chronic pancreatitis or in the absence of the *p16Ink4/p19Arf* tumor suppressor genes.

3. Inhibition of Egfr catalytic activity is not sufficient to inhibit tumor development in the absence of p53. In this context, ErbB2 is important triggering Egfr phosphorylation and MAPK signaling activation.

4. Elimination or inhibition of Egfr results in limited therapeutic effect in K-Ras^{G12V} PDAC maintenance and progression.

5. Simultaneous deletion of *Egfr* and *c-Raf* in full-blown PDAC results in a significant therapeutic effect in approximately 60% of the tumors, with very low associated toxicity.

6. Nevertheless, there are tumors that can progress upon target elimination, suggesting the existence of tumor heterogeneity and the contribution of alternative signaling pathways. Therefore, Egfr and c-Raf may not be sufficient to provide optimal therapeutic benefit and further research is required to identify effective therapeutic strategies.

Las conclusiones obtenidas en esta tesis son las siguientes:

1. La actividad catalítica de Egfr es indispensable para el desarrollo del ratón. La expresión constitutiva de un mutante de Egfr catalíticamente inactivo está asociada con defectos en la piel, pulmones y placenta, que conllevan a una letalidad perinatal.

2. La eliminación de la actividad quinasa de Egfr impide el desarrollo de PanIN y PDAC incluso en el contexto de pancreatitis crónica y en ausencia de los genes supresores de tumores *p16Ink4/p19Arf.*

3. La inhibición de las actividad catalítica de Egfr no es suficiente para impedir el desarrollo tumoral en ausencia de p53. En este contexto, ErbB2 juega un papel importante en la fosforilación de Egfr y en la activación de la vía de señalización MAPK.

4. La eliminación o inhibición de Egfr tiene un efecto terapéutico limitado en el mantenimiento y progresión de tumores de páncreas inducidos por el oncogén *K-Ras*^{G12V}.

5. La deleción simultánea de Egfr y c-Raf en tumores avanzados resulta en un efecto terapéutico significativo en aproximadamente el 60% de los tumores, con una toxicidad asociada baja.

6. Sin embargo, hay tumores que pueden progresar tras la eliminación de las dianas, lo que sugiere la existencia de heterogeneidad tumoral y la contribución de otras vías de señalización. Por lo tanto, Egfr y c-Raf pueden no ser suficientes para proporcionar un efecto terapéutico óptimo y se requiere más investigación para identificar estrategias más eficaces.

7. References

Aguirre, A.J., Bardeesy, N., Sinha, M., Lopez, L., Tuveson, D.A., Horner, J., Redston, M.S., and DePinho, R.A. (2003). Activated Kras and Ink4a/Arf deficiency cooperate to produce metastatic pancreatic ductal adenocarcinoma. Genes Dev. *17*, 3112–3126.

Alagesan, B., Contino, G., Guimaraes, A.R., Corcoran, R.B., Deshpande, V., Wojtkiewicz, G.R., Hezel, A.F., Wong, K., Loda, M., Weissleder, R., et al. (2015). Combined MEK and PI3K inhibition in a mouse model of pancreatic cancer. Clin. Cancer Res. *21*, 396–404.

Almoguera, C., Shibata, D., Forrester, K., Martin, J., Arnheim, N., and Perucho, M. (1988). Most human carcinomas of the exocrine pancreas contain mutant c-K-ras genes. Cell *53*, 549–554.

Ambrogio, C., Gómez-López, G., Falcone, M., Vidal, A., Nadal, E., Crosetto, N., Blasco, R.B., Fernández-Marcos, P.J., Sánchez-Céspedes, M., Ren, X., et al. (2016). Combined inhibition of DDR1 and Notch signaling is a therapeutic strategy for KRAS-driven lung adenocarcinoma. Nat. Med. *22*, 270–277.

Apelqvist, a, Li, H., Sommer, L., Beatus, P., Anderson, D.J., Honjo, T., Hrabe de Angelis, M., Lendahl, U., and Edlund, H. (1999). Notch signalling controls pancreatic cell differentiation. Nature *400*, 877–881.

Appert-Collin, A., Hubert, P., Crémel, G., and Bennasroune, A. (2015). Role of ErbB receptors in cancer cell migration and invasion. Front. Pharmacol. *6*, 1–10.

Ardito, C.M., Grüner, B.M., Takeuchi, K.K., Lubeseder-Martellato, C., Teichmann, N., Mazur, P.K., DelGiorno, K.E., Carpenter, E.S., Halbrook, C.J., Hall, J.C., et al. (2012). EGF Receptor Is Required for KRAS-Induced Pancreatic Tumorigenesis. Cancer Cell *22*, 304–317.

Avila, J.L., and Kissil, J.L. (2013). Notch signaling in pancreatic cancer: Oncogene or tumor suppressor? Trends Mol. Med. *19*, 320–327.

Baer, R., Cintas, C., Dufresne, M., Cassant-Sourdy, S., Schunhuber, N., Planque, L., Lulka, H., Couderc, B., Bousquet, C., Garmy-Susini, B., et al. (2014). Pancreatic cell plasticity and cancer initiation induced by oncogenic Kras is completely dependent on wild-type PI 3-kinase p110?? Genes Dev. *28*, 2621–2635.

Bailey, J.M., Swanson, B.J., Hamada, T., Eggers, J.P., Singh, P.K., Caffery, T., Ouellette, M.M., and Hollingsworth, M.A. (2008). Sonic hedgehog promotes desmoplasia in pancreatic cancer. Clin. Cancer Res. *14*, 5995–6004.

Bailey, P., Chang, D.K., Nones, K., Johns, A.L., Patch, A.-M., Gingras, M.-C., Miller, D.K., Christ, A.N., Bruxner, T.J.C., Quinn, M.C., et al. (2016). Genomic analyses identify molecular subtypes of pancreatic cancer. Nature *531*, 47–52.

Bardeesy, N., and DePinho, R. a (2002). Pancreatic cancer biology and genetics. Nat. Rev. Cancer *2*, 897–909.

Bardeesy, N., Cheng, K.H., Berger, J.H., Chu, G.C., Pahler, J., Olson, P., Hezel, A.F., Horner, J., Lauwers, G.Y., Hanahan, D., et al. (2006). Smad4 is dispensable for normal pancreas development yet critical in progression and tumor biology of pancreas cancer. Genes Dev. *20*, 3130–3146.

Bardelli, A., and Siena, S. (2010). Molecular mechanisms of resistance to cetuximab and panitumumab in colorectal cancer. J. Clin. Oncol. *28*, 1254–1261.

Biankin, A. V., Waddell, N., Kassahn, K.S., Gingras, M.-C., Muthuswamy, L.B., Johns, A.L., Miller, D.K., Wilson, P.J., Patch, A.-M., Wu, J., et al. (2012). Pancreatic cancer genomes reveal aberrations in axon guidance pathway genes. Nature *491*, 399–405.

Blasco, R.B., Francoz, S., Santamaría, D., Cañamero, M., Dubus, P., Charron, J., Baccarini, M., and Barbacid, M. (2011). C-Raf, but Not B-Raf, Is Essential for Development of K-Ras Oncogene-Driven Non-Small Cell Lung Carcinoma. Cancer Cell *19*, 652–663.

Bonifazi, M., Gallus, S., Bosetti, C., Polesel, J., Serraino, D., Talamini, R., Negri, E., and La Vecchia, C. (2010). Aspirin use and pancreatic cancer risk. Eur. J. Cancer Prev. *19*, 352–354.

Brembeck, F.H., Schreiber, F.S., Deramaudt, T.B., Craig, L., Rhoades, B., Swain, G., Grippo, P., Stoffers, D.A., Silberg, D.G., and Rustgi, A.K. (2003). The mutant K-ras oncogene causes pancreatic periductal lymphocytic infiltration and gastric mucous neck cell hyperplasia in transgenic mice. Cancer Res. *63*, 2005–2009.

Brune, K., Abe, T., Canto, M., O'Malley, L., Klein, A.P., Maitra, A., Volkan Adsay, N., Fishman, E.K., Cameron, J.L., Yeo, C.J., et al. (2006). Multifocal neoplastic precursor lesions associated with lobular atrophy of the pancreas in patients having a strong family history of pancreatic cancer. Am. J. Surg. Pathol. *30*, 1067–1076.

Burgess, A.W. (2008). EGFR family: structure physiology signalling and therapeutic targets. Growth Factors *26*, 263–274.

Burgess, A.W., Cho, H.S., Eigenbrot, C., Ferguson, K.M., Garrett, T.P.J., Leahy, D.J., Lemmon, M.A., Sliwkowski, M.X., Ward, C.W., and Yokoyama, S. (2003). An open-and-shut case? Recent insights into the activation of EGF/ErbB receptors. Mol. Cell *12*, 541–552.

Burrell, R. a, McGranahan, N., Bartek, J., and Swanton, C. (2013). The causes and consequences of genetic heterogeneity in cancer evolution. Nature *501*, 338–345.

Burris III, H.A., Moore, M.J., Andersen, J., Green, M.R., Rothenberg, M.L., Modiano, M.R., Cripps, M.C., Portenoy, R.K., Storniolo, A.M., Tarassoff, P., et al. (1997). Improvements in Survival and Clinical Benefit With Gemcitabine as First-Line Therapy for Patients With Advanced Pancreas Cancer : A Randomized Trial. *15*, 2403–2413.

Bykov, V.J.N., Selivanova, G., and Wiman, K.G. (2003). Small molecules that reactivate mutant p53. Eur. J. Cancer *39*, 1828–1834.

Calhoun, E.S., Jones, J.B., Ashfaq, R., Adsay, V., Baker, S.J., Valentine, V., Hempen, P.M., Hilgers, W., Yeo, C.J., Hruban, R.H., et al. (2003). BRAF and FBXW7 (CDC4, FBW7, AGO, SEL10) mutations in distinct subsets of pancreatic cancer: potential therapeutic targets. Am. J. Pathol. *163*, 1255–1260.

Chari, S.T., Leibson, C.L., Rabe, K.G., Timmons, L.J., Ransom, J., de Andrade, M., and Petersen, G.M. (2008). Pancreatic Cancer-Associated Diabetes Mellitus: Prevalence and Temporal Association With Diagnosis of Cancer. Gastroenterology *134*, 95–101.

Cohen, S. (1983). The epidermal growth factor (EGF). Cancer *51*, 1787–1791.

Collins, M.A., Bednar, F., Zhang, Y., Brisset, J., Galbán, S., Galbán, C.J., Rakshit, S., Flannagan, K.S., Adsay, N.V., Pasca di Magliano, M., et al. (2012a). Oncogenic Kras is required for both the initiation and maintenance of pancreatic cancer in mice. J. Clin. Invest. *122*, 639–653.

Collins, M.A., Brisset, J.C., Zhang, Y., Bednar, F., Pierre, J., Heist, K.A., Galbán, C.J., Galbán, S., and di Magliano, M.P. (2012b). Metastatic Pancreatic Cancer Is Dependent on Oncogenic Kras in Mice. PLoS One *7*.

Collisson, E.A., Trejo, C.L., Silva, J.M., Gu, S., Korkola, J.E., Heiser, L.M., Charles, R.-P., Rabinovich, B.A., Hann, B., Dankort, D., et al. (2012). A Central Role for RAF→MEK→ERK Signaling in the Genesis of Pancreatic Ductal Adenocarcinoma. Cancer Discov. *2*, 685–693.

Conradt, L., Godl, K., Schaab, C., Tebbe, A., Eser, S., Diersch, S., Michalski, C.W., Kleeff, J., Schnieke, A., Schmid, R.M., et al. (2011). Disclosure of erlotinib as a multikinase inhibitor in pancreatic ductal adenocarcinoma. Neoplasia *13*, 1026–1034.

Cox, A.D., and Der, C.J. (2010). Ras history: The saga continues. Small GTPases *1*, 2–27.

Cui, J., Jiang, W., Wang, S., Wang, L., and Xie, K. (2012). Role of Wnt/β-catenin signaling in drug resistance of pancreatic cancer. Curr. Pharm. Des. *18*, 2464–2471.

Dankort, D., Filenova, E., Collado, M., Serrano, M., Jones, K., and McMahon, M. (2007). A new mouse model to explore the initiation , progression , and therapy tumors. Genes Dev. *21*, 379–384.

Darnell, J.E., Kerr, I.M., and Stark, G.R. (1994). Jak-STAT pathways and transcriptional activation in response to IFNs and other extracellular signaling proteins. Science *264*, 1415–1421.

Davies, H., Bignell, G.R., Cox, C., Stephens, P., Edkins, S., Clegg, S., Teague, J., Woffendin, H., Garnett, M.J., Bottomley, W., et al. (2002). Mutations of the BRAF gene in human cancer. Nature *417*, 949–954.

Dikic, I., Tokiwa, G., Lev, S., Courtneidge, S.A., and Schlessinger, J. (1996). A role for Pyk2 and Src in linking G-protein-coupled receptors with MAP kinase activation. Nature *383*, 547–550.

Downward, J. (2003). Targeting RAS signalling pathways in cancer therapy. Nat. Rev. *3*, 11–22.

Drosten, M., Sum, E.Y.M., Lechuga, C.G., Simon-Carrasco, L., Jacob, H.K.C., Garcia-Medina, R., Huang, S., Beijersbergen, R.L., Bernards, R., and Barbacid, M. (2014). Loss of p53 induces cell proliferation via Ras-independent activation of the Raf/Mek/Erk signaling pathway. Proc. Natl. Acad. Sci. *111*, 15155–15160.

Du, X., Tabeta, K., Hoebe, K., Liu, H., Mann, N., Mudd, S., Crozat, K., Sovath, S., Gong, X., and Beutler, B. (2004). Velvet, a Dominant Egfr Mutation that Causes Wavy Hair and Defective Eyelid Development in Mice. Genetics *166*, 331–340.

Egan, S.E., Giddings, B.W., Brooks, M.W., Buday, L., Sizeland, A.M., and Weinberg, R.A. (1993). Association of Sos Ras exchange protein with Grb2 is implicated in tyrosine kinase signal transduction and transformation. Nature *363*, 45–51.

Engelman, J. a, Zejnullahu, K., Mitsudomi, T., Song, Y., Hyland, C., Park, J.O., Lindeman, N., Gale, C.M., Zhao, X., Christensen, J., et al. (2007). MET amplification leads to gefitinib resistance in lung cancer by activating ERBB3 signaling. Science (80-.). *316*, 1039–1043.

Engelman, J. a, Chen, L., Tan, X., Crosby, K., Guimaraes, A.R., Upadhyay, R., Maira, M., McNamara, K., Perera, S. a, Song, Y., et al. (2008). Effective use of PI3K and MEK inhibitors to treat mutant Kras G12D and PIK3CA H1047R murine lung cancers. Nat. Med. *14*, 1351–1356.

Erickson, S.L., O'Shea, K.S., Ghaboosi, N., Loverro, L., Frantz, G., Bauer, M., Lu, L.H., and Moore, M.W. (1997). ErbB3 is required for normal cerebellar and cardiac development: a comparison with ErbB2-and heregulin-deficient mice. Development *124*, 4999–5011.

Eser, S., Reiff, N., Messer, M., Seidler, B., Gottschalk, K., Dobler, M., Hieber, M., Arbeiter, A., Klein, S., Kong, B., et al. (2013). Selective requirement of PI3K/PDK1 signaling for kras oncogene-driven pancreatic cell plasticity and cancer. Cancer Cell *23*, 406–420.

Fabbrocini, G., Panariello, L., Caro, G., and Cacciapuoti, S. (2015). Acneiform Rash Induced by EGFR Inhibitors: Review of the Literature and New Insights. Ski. Appendage Disord. *1*, 31–37.

Falls, D.L. (2003). Neuregulins: Functions, forms, and signaling strategies. In The EGF Receptor Family: Biologic Mechanisms and Role in Cancer, pp. 15–31.

Fearon, D.T. (2014). The carcinoma-associated fibroblast expressing fibroblast activation protein and escape from immune surveillance. Cancer Immunol Res *2*, 187–193.

Feig, C., Jones, J.O., Kraman, M., Wells, R.J.B., Deonarine, A., Chan, D.S., Connell, C.M., Roberts, E.W., Zhao, Q., Caballero, O.L., et al. (2013). Targeting CXCL12 from FAP-expressing carcinoma- associated fi broblasts synergizes with anti – PD-L1 immunotherapy in pancreatic cancer. Proc Natl Acad Sci U S A *110*, 20212–20217.

Ferguson, K.M. (2008). Structure-Based View of Epidermal Growth Factor Receptor Regulation. Annu. Rev. Biophys. *37*, 353–373.

Fischer, O.M., Hart, S., Gschwind, a., and Ullrich, a. (2003). EGFR signal transactivation in cancer cells. Biochem. Soc. Trans. *31*, 1203–1208.

Fowler, K.J., Walker, F., Alexander, W., Hibbs, M.L., Nice, E.C., Bohmer, R.M., Mann, G.B., Thumwood, C., Maglitto, R., and Danks, J.A. (1995). A mutation in the epidermal growth factor receptor in waved-2 mice has a profound effect on receptor biochemistry that results in impaired lactation. Proc. Natl. Acad. Sci. U. S. A. *92*, 1465–1469.

Fukuda, A., Wang, S.C., Morris, J.P., Folias, A.E., Liou, A., Kim, G.E., Akira, S., Boucher, K.M., Firpo, M.A., Mulvihill, S.J., et al. (2011). Stat3 and MMP7 Contribute to Pancreatic Ductal Adenocarcinoma Initiation and Progression. Cancer Cell *19*, 441–455.

Fukushima, N., and Fukayama, M. (2007). Mucinous cystic neoplasms of the pancreas: Pathology and molecular genetics. J. Hepatobiliary. Pancreat. Surg. *14*, 238–242.

Gassmann, M., Casagranda, F., Orioli, D., Simon, H., Lai, C., Klein, R., and Lemke, G. (1995). Aberrant neural and cardiac development in mice lacking the ErbB4 neuregulin receptor. Nature *378*, 390–394.

Geyer, C.E., Forster, J., Lindquist, D., Chan, S., Romieu, C.G., Pienkowski, T., Jagiello-Gruszfeld, A., Crown, J., Chan, A., Kaufman, B., et al. (2006). Lapatinib plus Capecitabine for HER2-Positive Advanced Breast Cancer. N. Engl. J. Med. *355*, 2733–2743.

Gibney, G.T., and Zager, J.S. (2013). Clinical development of dabrafenib in BRAF mutant melanoma and other malignancies. Drug Eval. *9*, 893–899.

Githens, S., Schexnayder, J.A., Moses, R.L., Denning, G.M., Smith, J.J., and Frazier, M.L. (1994). Mouse pancreatic acinar/ductlar tissue gives rise to epithelial cultures that are morphologically, biochemically, and functionally indistinguishable from interlobular duct cell cultures. Vitr. Cell. Dev. Biol. - Anim. *30*, 622–635.

Gopinathan, A., Morton, J.P., Jodrell, D.I., and Sansom, O.J. (2015). GEMMs as preclinical models for testing pancreatic cancer therapies. Dis. Model. Mech. *8*, 1185–1200.

Griffin, C.A., Hruban, R.H., Morsberger, L.A., Ellingham, T., Long, P.P., Jaffee, E.M., Hauda, K.M., Bohlander, S.K., and Yeo, C.J. (1995). Consistent Chromosome Abnormalities in Adenocarcinoma of the Pancreas. Cancer Res. *55*, 2394–2399.

Guerra, C., and Barbacid, M. (2013). Genetically engineered mouse models of pancreatic adenocarcinoma. Mol. Oncol. *7*, 232–247.

Guerra, C., Mijimolle, N., Dhawahir, A., Dubus, P., Barradas, M., Serrano, M., Campuzano, V., and Barbacid, M. (2003). Tumor induction by an endogenous K-ras oncogene is highly dependent on cellular context. Cancer Cell *4*, 111–120.

Guerra, C., Schuhmacher, A.J., Cañamero, M., Grippo, P.J., Verdaguer, L., Pérez-Gallego, L., Dubus, P., Sandgren, E.P., and Barbacid, M. (2007). Chronic Pancreatitis Is Essential for Induction of Pancreatic Ductal Adenocarcinoma by K-Ras Oncogenes in Adult Mice. Cancer Cell *11*, 291–302.

Guerra, C., Collado, M., Navas, C., Schuhmacher, A.J., Hernández-Porras, I., Cañamero, M., Rodriguez-Justo, M., Serrano, M., and Barbacid, M. (2011). Pancreatitis-induced inflammation contributes to pancreatic cancer by inhibiting oncogene-induced senescence. Cancer Cell *19*, 728–739.

Guy, P.M., Platko, J. V, Cantley, L.C., Cerione, R. a, and Carraway, K.L. (1994). Insect cell-expressed p180erbB3 possesses an impaired tyrosine kinase activity. Proc. Natl. Acad. Sci. U. S. A. *91*, 8132–8136.

Habbe, N., Langer, P., Sina-Frey, M., and Bartsch, D.K. (2006). Familial pancreatic cancer syndromes. Endocrinol Metab Clin North Am *35*, 417–30, xi.

Hahn, S. a, Schutte, M., Hoque, a T., Moskaluk, C. a, da Costa, L.T., Rozenblum, E., Weinstein, C.L., Fischer, a, Yeo, C.J., Hruban, R.H., et al. (1996). DPC4, a candidate tumor suppressor gene at human chromosome 18q21.1. Science *271*, 350–353.

Hale, M.A., Kagami, H., Shi, L., Holland, A.M., Elsässer, H.P., Hammer, R.E., and MacDonald, R.J. (2005). The homeodomain protein PDX1 is required at mid-pancreatic development for the formation of the exocrine pancreas. Dev. Biol. *286*, 225–237.

Harris, R.C., Chung, E., and Coffey, R.J. (2003). EGF receptor ligands. Exp. Cell Res. *284*, 2–13.

Haslekås, C., Breen, K., Pedersen, K.W., Johannessen, L.E., Stang, E., and Madshus, I.H. (2005). The inhibitory effect of ErbB2 on epidermal growth factor-induced formation of clathrin-coated pits correlates with retention of epidermal growth factor receptor-ErbB2 oligomeric complexes at the plasma membrane. Mol. Biol. Cell *16*, 5832–5842.

Hearle, N., Schumacher, V., Menko, F.H., Olschwang, S., Boardman, L.A., Gille, J.J.P., Keller, J.J., Westerman, A.M., Scott, R.J., Lim, W., et al. (2006). Frequency and spectrum of cancers in the Peutz-Jeghers syndrome. Clin. Cancer Res. *12*, 3209–3215.

van Heek, N.T., Meeker, A.K., Kern, S.E., Yeo, C.J., Lillemoe, K.D., Cameron, J.L., Offerhaus, G.J.A., Hicks, J.L., Wilentz, R.E., Goggins, M.G., et al. (2002). Telomere shortening is nearly universal in pancreatic intraepithelial neoplasia. Am. J. Pathol. *161*, 1541–1547.

Heidorn, S.J., Milagre, C., Whittaker, S., Nourry, A., Niculescu-Duvas, I., Dhomen, N., Hussain, J., Reis-Filho, J.S., Springer, C.J., Pritchard, C., et al. (2010). Kinase-dead BRAF and oncogenic RAS cooperate to drive tumor progression through CRAF. Cell *140*, 209–221.

Heldin, C.-H. (1995). Dimerization of cell surface receptors in signal transduction. Cell *80*, 213–223.

Hendriks, B.S., Opresko, L.K., Wiley, H.S., and Lauffenburger, D. (2003). Coregulation of epidermal growth factor receptor/human epidermal growth factor receptor 2 (HER2) levels and locations: quantitative analysis of HER2 overexpression effects. Cancer Res. *63*, 1130–1137.

Hennig, A., Markwart, R., Esparza-Franco, M.A., Ladds, G., and Rubio, I. (2015). Ras activation revisited: role of GEF and GAP systems. Biol. Chem. *396*, 831–848.

Hidalgo, M. (2010). Pancreatic Cancer. N. Engl. J. Med. *362*, 1605–1617.

Hingorani, S.R., Petricoin, E.F., Maitra, A., Rajapakse, V., King, C., Jacobetz, M.A., Ross, S., Conrads, T.P., Veenstra, T.D., Hitt, B.A., et al. (2003). Preinvasive and invasive ductal pancreatic cancer and its early detection in the mouse. Cancer Cell *4*, 437–450.

Hingorani, S.R., Wang, L., Multani, A.S., Combs, C., Deramaudt, T.B., Hruban, R.H., Rustgi, A.K., Chang, S., and Tuveson, D.A. (2005). Trp53R172H and KrasG12D cooperate to promote chromosomal instability and widely metastatic pancreatic ductal adenocarcinoma in mice. Cancer Cell *7*, 469–483.

Von Hoff, D.D., Ervin, T., Arena, F.P., Chiorean, E.G., Infante, J., Moore, M., Seay, T., Tjulandin, S.A., Ma, W.W., Saleh, M.N., et al. (2013). Increased survival in pancreatic cancer with nab-paclitaxel plus gemcitabine. N. Engl. J. Med. *369*, 1691–1703.

Hruban, R.H., Goggins, M., Parsons, J., and Kern, S.E. (2000). Progression model for pancreatic cancer. Clin. Cancer Res. *6*, 2969–2972.

Hruban, R.H., Klimstra, D.S., Adsay, N.V., Albores-Saavedra, J., Furukawa, T., Klöppel, G., Lüttges, J., and Shimizu, M. (2004). An illustrated consensus on the classification of pancreatic intraepithelial neoplasia and intraductal papillary mucinous neoplasms. Am. J. Surg. Pathol. *28*, 977–987.

Hruban, R.H., Maitra, A., Kern, S.E., and Goggins, M. (2007). Precursors to Pancreatic Cancer. Gastroenterol. Clin. North Am. *36*, 831–849.

Hruban, R.H., Canto, M.I., Goggins, M., Schulick, R., and Klein, A.P. (2010). Update on familial pancreatic cancer. Adv. Surg. *44*, 293–311.

Huang, G., Chantry, A., and Epstein, R.J. (1999). Overexpression of ErbB2 impairs ligand-dependent downregulation of epidermal growth factor receptors via a post-transcriptional mechanism. J. Cell. Biochem. *74*, 23–30.

Huang, Z.Q., Saluja, A.K., Dudeja, V., Vickers, S.M., and Buchsbaum, D.J. (2011). Molecular Targeted Approaches for Treatment of Pancreatic Cancer. 2221–2238.

Huguet, F., Fernet, M., Giocanti, N., Favaudon, V., and Larsen, A.K. (2016). Afatinib, an Irreversible EGFR Family Inhibitor, Shows Activity Toward Pancreatic Cancer Cells, Alone and in Combination with Radiotherapy, Independent of KRAS Status. Target. Oncol. *11*, 371–381.

Hynes, N.E., and MacDonald, G. (2009). ErbB receptors and signaling pathways in cancer. Curr. Opin. Cell Biol. *21*, 177–184.

Ioannou, N., Dalgleish, A.G., Seddon, A.M., Mackintosh, D., Guertler, U., Solca, F., and Modjtahedi, H. (2011). Anti-tumour activity of afatinib, an irreversible ErbB family blocker, in human pancreatic tumour cells. Br. J. Cancer *105*, 1554–1562.

Iodice, S., Gandini, S., Maisonneuve, P., and Lowenfels, A.B. (2008). Tobacco and the risk of pancreatic cancer: A review and meta-analysis. Langenbeck's Arch. Surg. *393*, 535–545.

Jesenberger, V., Procyk, K.J., Rüth, J., Schreiber, M., Theussl, H.C., Wagner, E.F., and Baccarini, M. (2001). Protective role of Raf-1 in Salmonella-induced macrophage apoptosis. J. Exp. Med. *193*, 353–364.

Jhappan, C., Stahle, C., Harkins, R.N., Fausto, N., Smith, G.H., and Merlino, G.T. (1990). TGFα overexpression in transgenic mice induces liver neoplasia and abnormal development of the mammary gland and pancreas. Cell *61*, 1137–1146.

Jones, S., Zhang, X., Parsons, D.W., Lin, J.C.-H., Leary, R.J., Angenendt, P., Mankoo, P., Carter, H., Kamiyama, H., Jimeno, A., et al. (2008). Core Signaling Pathways in Human Pancreatic Cancers Revealed by Global Genomic Analyses. Science (80-.). *321*, 1801–1806.

Jonkers, J., Meuwissen, R., van der Gulden, H., Peterse, H., van der Valk, M., and Berns, A. (2001). Synergistic tumor suppressor activity of BRCA2 and p53 in a conditional mouse model for breast cancer. Nat. Genet. *29*, 418–425.

Jorissen, R.N., Walker, F., Pouliot, N., Garrett, T.P.J., Ward, C.W., and Burgess, A.W. (2003). Epidermal growth factor receptor: Mechanisms of activation and signalling. Exp. Cell Res. *284*, 31–53.

Jura, N., Zhang, X., Endres, N.F., Seeliger, M.A., Schindler, T., and Kuriyan, J. (2011). Catalytic Control in the EGF Receptor and Its Connection to General Kinase Regulatory Mechanisms. Mol. Cell *42*, 9–22.

Kamisawa, T., Wood, L.D., Itoi, T., and Takaori, K. (2016). Pancreatic cancer. Lancet (London, England) *388*, 73–85.

Kanda, M., Matthaei, H., Wu, J., Hong, S.M., Yu, J., Borges, M., Hruban, R.H., Maitra, A., Kinzler, K., Vogelstein, B., et al. (2012). Presence of somatic mutations in most early-stage pancreatic intraepithelial neoplasia. Gastroenterology *142*.

Kapoor, A., Yao, W., Ying, H., Hua, S., Liewen, A., Wang, Q., Zhong, Y., Wu, C.J., Sadanandam, A., Hu, B., et al. (2014). Yap1 activation enables bypass of oncogenic KRAS addiction in pancreatic cancer. Cell *158*, 185–197.

Karakas, B., Bachman, K.E., and Park, B.H. (2006). Mutation of the PIK3CA oncogene in human cancers. Br. J. Cancer *94*, 455–459.

Karreth, F. a., Frese, K.K., DeNicola, G.M., Baccarini, M., and Tuveson, D. a. (2011). C-Raf is required for the initiation of lung cancer by K-Ras G12D. Cancer Discov. *1*, 128–136.

Kato, J., Matsushime, H., Hiebert, S.W., Ewen, M.E., and Sherr, C.J. (1993). Direct binding of cyclin D to the retinoblastoma gene product (pRb) and pRb phosphorylation by the cyclin D-dependent kinase CDK4. Genes Dev. *7*, 331–342.

Kopp, J.L., von Figura, G., Mayes, E., Liu, F.F., Dubois, C.L., Morris, J.P., Pan, F.C., Akiyama, H., Wright, C.V.E., Jensen, K., et al. (2012). Identification of Sox9-Dependent Acinar-to-Ductal Reprogramming as the Principal Mechanism for Initiation of Pancreatic Ductal Adenocarcinoma. Cancer Cell *22*, 737–750.

Krimpenfort, P., Quon, K.C., Mooi, W.J., Loonstra, A., and Berns, A. (2001). Loss of p16Ink4a confers susceptibility to metastatic melanoma in mice. Nature *413*, 83–86.

Lakso, M., Pichel, J.G., Gorman, J.R., Sauer, B., Okamoto, Y., Lee, E., Alt, F.W., and Westphal, H. (1996). Efficient in vivo manipulation of mouse genomic sequences at the zygote stage. Proc. Natl. Acad. Sci. U. S. A. *93*, 5860–5865.

Lee, C.-L., Moding, E.J., Huang, X., Li, Y., Woodlief, L.Z., Rodrigues, R.C., Ma, Y., and Kirsch, D.G. (2012). Generation of primary tumors with Flp recombinase in FRT-flanked p53 mice. Dis. Model. Mech. *5*, 397–402.

Lee, D., Cross, S.H., Strunk, K.E., Morgan, J.E., Bailey, C.L., Jackson, I.J., and Threadgill, D.W. (2004). Wa5 is a novel ENU-induced antimorphic allele of the epidermal growth factor receptor. Mamm Genome *15*, 525–536.

Lee, K.F., Simon, H., Chen, H., Bates, B., Hung, M.C., and Hauser, C. (1995). Requirement for neuregulin receptor erbB2 in neural and cardiac development. Nature *378*, 394–398.

Lenferink, A.E.G., Pinkas-Kramarski, R., Van De Poll, M.L.M., Van Vugt, M.J.H., Klapper, L.N., Tzahar, E., Waterman, H., Sela, M., Van Zoelen, E.J.J., and Yarden, Y. (1998). Differential endocytic routing of homo- and hetero-dimeric ErbB tyrosine kinases confers signaling superiority to receptor heterodimers. EMBO J. *17*, 3385–3397.

Li, D., Ambrogio, L., Shimamura, T., Kubo, S., Takahashi, M., Chirieac, L.R., Padera, R.F., Shapiro, G.I., Baum, A., Himmelsbach, F., et al. (2008). BIBW2992, an irreversible EGFR/HER2 inhibitor highly effective in preclinical lung cancer models. Oncogene *27*, 4702–4711.

Li, D.H., Xie, K.P., Wolff, R., and Abbruzzese, J.L. (2004). Pancreatic cancer. Lancet *363*, 1049–1057.

Li, H. dong, Huang, C., Huang, K. jian, Wu, W. dong, Jiang, T., Cao, J., Feng, Z. zhong, and Qiu, Z. jun (2011). STAT3 knockdown reduces pancreatic cancer cell invasiveness and matrix metalloproteinase-7 expression in nude mice. PLoS One *6*.

Ling, J., Kang, Y., Zhao, R., Xia, Q., Lee, D.F., Chang, Z., Li, J., Peng, B., Fleming, J.B., Wang, H., et al. (2012). Kras G12D-Induced IKK2/B/NF-kB Activation by IL-1alpha and p62 Feedforward Loops Is Required for Development of Pancreatic Ductal Adenocarcinoma. Cancer Cell *21*, 105–120.

De Lisle, R., and Logsdon, C. (1990). Pancreatic acinar cells in culture: expression of acinar and ductal antigens in a growth-related manner. Eur J Cell Biol *51*, 64–75.

Lowenfels, A.B., Maisonneuve, P., DiMagno, E.P., Elitsur, Y., Gates, L.K., Perrault, J., and Whitcomb, D.C. (1997). Hereditary Pancreatitis and the Risk of Pancreatic Cancer. JNCI J. Natl. Cancer Inst. *89*, 442–446.

Lowenfels, a B., Maisonneuve, P., Cavallini, G., Ammann, R.W., Lankisch, P.G., Andersen, J.R., Dimagno, E.P., Andrén-Sandberg, a, and Domellöf, L. (1993). Pancreatitis and the risk of pancreatic cancer. International Pancreatitis Study Group. N. Engl. J. Med. *328*, 1433–1437.

Luetteke, N.C., Phillips, H.K., Qiu, T.H., Copeland, N.G., Earp, H.S., Jenkins, N.A., and Lee, D.C. (1994). The mouse waved-2 phenotype results from a point mutation in the EGF receptor tyrosine kinase. Genes Dev. *8*, 399–413.

Luttrell, L.M., Delia Rocca, G.J., Van Biesen, T., Luttrell, D.K., and Lefkowitz, R.J. (1997). Gβγ subunits mediate Src-dependent phosphorylation of the epidermal growth factor receptor. J. Biol. Chem. *272*, 4637–4644.

Lynch, T.J., Bell, D.W., Sordella, R., Gurubhagavatula, S., Okimoto, R.A., Brannigan, B.W., Harris, P.L., Haserlat, S.M., Supko, J.G., Haluska, F.G., et al. (2004). Activating Mutations in the Epidermal Growth Factor Receptor Underlying Responsiveness of Non–Small-Cell Lung Cancer to Gefitinib. N. Engl. J. Med. *350*, 2129–2139.

Lyons, J.F., Wilhelm, S., Hibner, B., and Bollag, G. (2001). Discovery of a novel Raf kinase inhibitor. Endocr. Relat. Cancer *8*, 219–225.

Maitra, A., and Hruban, R.H. (2008). Pancreatic cancer. Annu. Rev. Pathol. *3*, 157–188.

Maitra, A., Adsay, N.V., Argani, P., Iacobuzio-Donahue, C., De Marzo, A., Cameron, J.L., Yeo, C.J., and Hruban, R.H. (2003). Multicomponent analysis of the pancreatic adenocarcinoma progression model using a pancreatic intraepithelial neoplasia tissue microarray. Mod. Pathol. *16*, 902–912.

Maitra, A., Kern, S.E., and Hruban, R.H. (2006). Molecular pathogenesis of pancreatic cancer. Best Pract. Res. Clin. Gastroenterol. *20*, 211–226.

Malka, D., Hammel, P., Maire, F., Rufat, P., Madeira, I., Pessione, F., Lévy, P., and Ruszniewski, P. (2002). Risk of pancreatic adenocarcinoma in chronic pancreatitis. Gut *51*, 849–852.

Malumbres, M., and Barbacid, M. (2003). RAS oncogenes: the first 30 years. Nat. Rev. Cancer *3*, 459–465.

Manchado, E., Weissmueller, S., Morris, J.P., Chen, C.-C., Wullenkord, R., Lujambio, A., de Stanchina, E., Poirier, J.T., Gainor, J.F., Corcoran, R.B., et al. (2016). A combinatorial strategy for treating KRAS-mutant lung cancer. Nature *534*, 647–651.

Marais, R., Light, Y., Fpaterson, H., and Marshall, C.J. (1995). Ras recruits Raf-1 to the plasma membrane for activation by tyrosine phosphorylation. EMBO J. *1413*, 3136–3145.

Matallanas, D., Birtwistle, M., Romano, D., Zebisch, A., Rauch, J., von Kriegsheim, A., and Kolch, W. (2011). Raf family kinases: old dogs have learned new tricks. Genes Cancer *2*, 232–260.

Means, A.L., Meszoely, I.M., Suzuki, K., Miyamoto, Y., Rustgi, A.K., Coffey, R.J., Wright, C.V.E., Stoffers, D. a, and Leach, S.D. (2005). Pancreatic epithelial plasticity mediated by acinar cell transdifferentiation and generation of nestin-positive intermediates. Development *132*, 3767–3776.

Meeker, A.K., and De Marzo, A.M. (2004). Recent advances in telomere biology: implications for human cancer. Curr. Opin. Oncol. *16*, 32–38.

Miettinen, P.J., Berger, J.E., Meneses, J., Phung, Y., Pedersen, R.A., Werb, Z., and Derynck, R. (1995). Epithelial immaturity and multiorgan failure in mice lacking epidermal growth factor receptor. Nature *376*, 337–341.

Miyamoto, Y., Maitra, A., Ghosh, B., Zechner, U., Argani, P., Iacobuzio-Donahue, C.A., Sriuranpong, V., Iso, T., Meszoely, I.M., Wolfe, M.S., et al. (2003). Notch mediates TGF alpha-induced changes in epithelial differentiation during pancreatic tumorigenesis. Cancer Cell *3*, 565–576.

Molina, J.R., and Adjei, A.A. (2006). The Ras/Raf/MAPK Pathway. J. Thorac. Oncol. *1*, 7.

Moore, M.J., Goldstein, D., Hamm, J., Figer, A., Hecht, J.R., Gallinger, S., Au, H.J., Murawa, P., Walde, D., Wolff, R. a., et al. (2007). Erlotinib plus gemcitabine compared with gemcitabine alone in patients with advanced pancreatic cancer: A phase III trial of the National Cancer Institute of Canada Clinical Trials Group. J. Clin. Oncol. *25*, 1960–1966.

Morris, J.P., Wang, S.C., and Hebrok, M. (2010a). KRAS, Hedgehog, Wnt and the twisted developmental biology of pancreatic ductal adenocarcinoma. Nat. Rev. Cancer *10*, 683–695.

Morris, J.P., Cano, D.A., Sekine, S., Wang, S.C., Hebrok, M., Jemal, A., Feldmann, G., Beaty, R., Hruban, R., Maitra, A., et al. (2010b). Beta-catenin blocks Kras-dependent reprogramming of acini into pancreatic cancer precursor lesions in mice. J. Clin. Invest. *120*, 508–520.

Morton, J.P., Jamieson, N.B., Karim, S.A., Athineos, D., Ridgway, R.A., Nixon, C., Mckay, C.J., Carter, R., Brunton, V.G., Frame, M.C., et al. (2010). LKB1 Haploinsufficiency Cooperates With Kras to Promote Pancreatic Cancer Through Suppression of p21-Dependent Growth Arrest. YGAST *139*, 586–597.e6.

Natarajan, A., Wagner, B., and Sibilia, M. (2007). The EGF receptor is required for efficient liver regeneration. Proc. Natl. Acad. Sci. U. S. A. *104*, 17081–17086.

Navas, C., Hernández-Porras, I., Schuhmacher, A.J., Sibilia, M., Guerra, C., and Barbacid, M. (2012). EGF receptor signaling is essential for k-ras oncogene-driven pancreatic ductal adenocarcinoma. Cancer Cell *22*, 318–330.

Neesse, A., Michl, P., Frese, K.K., Feig, C., Cook, N., Jacobetz, M.A., Lolkema, M.P., Buchholz, M., Olive, K.P., Gress, T.M., et al. (2011). Stromal biology and therapy in pancreatic cancer. Gut *60*, 861–868.

Ng, S.S.W., Tsao, M.-S., Nicklee, T., and Hedley, D.W. (2002). Effects of the epidermal growth factor receptor inhibitor OSI-774, Tarceva, on downstream signaling pathways and apoptosis in human pancreatic adenocarcinoma. Mol. Cancer Ther. *1*, 777–783.

Normanno, N., De Luca, A., Bianco, C., Strizzi, L., Mancino, M., Maiello, M.R., Carotenuto, A., De Feo, G., Caponigro, F., and Salomon, D.S. (2006). Epidermal growth factor receptor (EGFR) signaling in cancer. Gene *366*, 2–16.

Oda, K., Matsuoka, Y., Funahashi, a, and Kitano, H. (2005). A comprehensive pathway map of epidermal growth factor receptor signaling. Mol Syst Biol *1*, 2005 0010.

Olayioye, M. a, Neve, R.M., Lane, H. a, and Hynes, N.E. (2000). The ErbB signaling network: receptor heterodimerization in development and cancer. EMBO J. *19*, 3159–3167.

Olive, K.P., Jacobetz, M.A., Davidson, C.J., Gopinathan, A., McIntyre, D., Honess, D., Madhu, B., Goldgraben, M.A., Caldwell, M.E., Allard, D., et al. (2009). Inhibition of Hedgehog signaling enhances delivery of chemotherapy in a mouse model of pancreatic cancer. Science (80-.). *324*, 1457–1461.

Owczarczyk-Saczonek, A., Witmanowski, H., and Placek, W. (2013). Acneiform rash during lung cancer therapy with erlotinib (Tarceva). Postep. Dermatologii I Alergol. *30*, 195–198.

Özdemir, B.C., Pentcheva-Hoang, T., Carstens, J.L., Zheng, X., Wu, C.C., Simpson, T.R., Laklai, H., Sugimoto, H., Kahlert, C., Novitskiy, S. V., et al. (2014). Depletion of carcinoma-associated fibroblasts and fibrosis induces immunosuppression and accelerates pancreas cancer with reduced survival. Cancer Cell *25*, 719–734.

Parsa, I., Longnecker, D.S., Scarpelli, D.G., Pour, P., and Lefkowitz, M. (1985). Ductal Metaplasia of Human Exocrine Pancreas and Its Association with Carcinoma. Cancer Res. *45*, 1285–1290.

Paul, T., Schumann, C., Rüdiger, S., Boeck, S., Heinemann, V., Kächele, V., Steffens, M., Scholl, C., Hichert, V., Seufferlein, T., et al. (2014). Cytokine regulation by epidermal growth factor receptor inhibitors and epidermal growth factor receptor inhibitor associated skin toxicity in cancer patients. Eur. J. Cancer *50*, 1855–1863.

Peng, S. Bin, Henry, J.R., Kaufman, M.D., Lu, W.P., Smith, B.D., Vogeti, S., Rutkoski, T.J., Wise, S., Chun, L., Zhang, Y., et al. (2015). Inhibition of RAF Isoforms and Active Dimers by LY3009120 Leads to Anti-tumor Activities in RAS or BRAF Mutant Cancers. Cancer Cell *28*, 384–398.

Pérez-Mancera, P.A., Guerra, C., Barbacid, M., and Tuveson, D.A. (2012). What we have learned about pancreatic cancer from mouse models. Gastroenterology *142*, 1079–1092.

Perona, R. (2006). Cell signalling: Growth factors and tyrosine kinase receptors. Clin. Transl. Oncol. *8*, 77–82.

Philip, P.A., Benedetti, J., Corless, C.L., Wong, R., O'Reilly, E.M., Flynn, P.J., Rowland, K.M., Atkins, J.N., Mirtsching, B.C., Rivkin, S.E., et al. (2010). Phase III study comparing gemcitabine plus cetuximab versus gemcitabine in patients with advanced pancreatic adenocarcinoma: Southwest oncology group-directed intergroup trial S0205. J. Clin. Oncol. *28*, 3605–3610.

Politi, K., Zakowski, M.F., Fan, P., Schonfeld, E.A., Pao, W., and Varmus, H.E. (2006). Lung adenocarcinomas induced in mice by mutant EGF receptors found in human lung cancers respond to a tyrosine kinase inhibitor or to down-regulation of the receptors. 1496–1510.

Poulikakos, P.I., Zhang, C., Bollag, G., Shokat, K.M., and Rosen, N. (2010). RAF inhibitors transactivate RAF dimers and ERK signalling in cells with wild-type BRAF. Nature *464*, 427–430.

Prenzel, N., Zwick, E., Daub, H., Leserer, M., Abraham, R., Wallasch, C., and Ullrich, a (1999). EGF receptor transactivation by G-protein-coupled receptors requires metalloproteinase cleavage of proHB-EGF. Nature *402*, 884–888.

Puyol, M., Martín, A., Dubus, P., Mulero, F., Pizcueta, P., Khan, G., Guerra, C., Santamaría, D., and Barbacid, M. (2010). A synthetic lethal interaction between K-Ras oncogenes and Cdk4 unveils a therapeutic strategy for non-small cell lung carcinoma. Cancer Cell *18*, 63–73.

Raimondi, S., Lowenfels, A.B., Morselli-Labate, A.M., Maisonneuve, P., and Pezzilli, R. (2010). Pancreatic cancer in chronic pancreatitis; aetiology, incidence, and early detection. Best Pract. Res. Clin. Gastroenterol. *24*, 349–358.

Rajurkar, M., Dang, K., Fernandez-Barrena, M.G., Liu, X., Fernandez-Zapico, M.E., Lewis, B.C., and Mao, J. (2017). IKBKE Is Required during KRAS-Induced Pancreatic Tumorigenesis. Cancer Res. 1–11.

Rhim, A.D., Oberstein, P.E., Thomas, D.H., Mirek, E.T., Palermo, C.F., Sastra, S.A., Dekleva, E.N., Saunders, T., Becerra, C.P., Tattersall, I.W., et al. (2014). Stromal elements act to restrain, rather than support, pancreatic ductal adenocarcinoma. Cancer Cell *25*, 735–747.

Riese, D.J., and Stern, D.F. (1998). Specificity within the EGF family/ErbB receptor family signaling network. BioEssays *20*, 41–48.

Roberts, P.J., and Der, C.J. (2007). Targeting the Raf-MEK-ERK mitogen-activated protein kinase cascade for the treatment of cancer. Oncogene *26*, 3291–3310.

Roberts, P.J., Usary, J.E., Darr, D.B., Dillon, P.M., Pfefferle, A.D., Whittle, M.C., Duncan, J.S., Johnson, S.M., Combest, A.J., Jin, J., et al. (2012). Combined PI3K/mTOR and MEK inhibition provides broad antitumor activity in faithful murine cancer models. Clin. Cancer Res. *18*, 5290–5303.

Romero, D., Iglesias, M., Vary, C.P.H., and Quintanilla, M. (2008). Functional blockade of Smad4 leads to a decrease in Beta-catenin levels and signaling activity in human pancreatic carcinoma cells. Carcinogenesis *29*, 1070–1076.

Roskoski, R. (2014). The ErbB/HER family of protein-tyrosine kinases and cancer. Pharmacol. Res. *79*, 34–74.

Rothwell, P.M., Fowkes, F.G.R., Belch, J.F., Ogawa, H., Warlow, C.P., and Meade, T.W. (2011). Effect of daily aspirin on long-term risk of death due to cancer: Analysis of individual patient data from randomised trials. Lancet *377*, 31–41.

Rovira, M., Scott, S.-G., Liss, A.S., Jensen, J., Thayer, S.P., and Leach, S.D. (2010). Isolation and characterization of centroacinar/terminal ductal progenitor cells in adult mouse pancreas. Proc. Natl. Acad. Sci. *107*, 75–80.

Rowley, M., Ohashi, A., Mondal, G., Mills, L., Yang, L.I.N., Zhang, L., Sundsbak, R., Shapiro, V., Muders, M.H., Smyrk, T., et al. (2011). Inactivation of Brca2 Promotes Trp53-Associated but Inhibits KrasG12D-Dependent Pancreatic Cancer Development in Mice. YGAST *140*, 1303–1313.e3.

Ruggeri, B., Zhang, S.Y., Caamano, J., DiRado, M., Flynn, S.D., and Klein-Szanto, A.J. (1992). Human pancreatic carcinomas and cell lines reveal frequent and multiple alterations in the p53 and Rb-1 tumor-suppressor genes. Oncogene *7*, 1503–1511.

Ruzankina, Y., Pinzon-Guzman, C., Asare, A., Ong, T., Pontano, L., Cotsarelis, G., Zediak, V.P., Velez, M., Bhandoola, A., and Brown, E.J. (2007). Deletion of the developmentally essential gene ATR in adult mice leads to age-related phenotypes and stem cell loss. Cell Stem Cell *1*, 113–126.

Salomon, D.S., Brandt, R., Ciardiello, F., and Normanno, N. (1995). Epidermal growth factor-related peptides and their receptors in human malignancies. Crit. Rev. Oncol. Hematol. *19*, 183–232.

Scarpa, a, Capelli, P., Mukai, K., Zamboni, G., Oda, T., Iacono, C., and Hirohashi, S. (1993). Pancreatic adenocarcinomas frequently show p53 gene mutations. Am. J. Pathol. *142*, 1534–1543.

Schönhuber, N., Seidler, B., Schuck, K., Veltkamp, C., Schachtler, C., Zukowska, M., Eser, S., Feyerabend, T.B., Paul, M.C., Eser, P., et al. (2014). A next-generation dual-recombinase system for time- and host-specific targeting of pancreatic cancer. Nat. Med. *20*, 1340–1347.

Schönleben, F., Qiu, W., Ciau, N.T., Ho, D.J., Li, X., Allendorf, J.D., Remotti, H.E., and Su, G.H. (2006). PIK3CA mutations in intraductal papillary mucinous neoplasm/carcinoma of the pancreas. Clin. Cancer Res. *12*, 3851–3855.

Seshacharyulu, P., Ponnusamy, M.P., Haridas, D., Jain, M., Ganti, A.K., and Batra, S.K. (2012). Targeting the EGFR signaling pathway in cancer therapy. Expert Opin. Ther. Targets *16*, 15–31.

Sherman, M.H., Yu, R.T., Engle, D.D., Ding, N., Atkins, A.R., Tiriac, H., Collisson, E.A., Connor, F., Van Dyke, T., Kozlov, S., et al. (2014). Vitamin D receptor-mediated stromal reprogramming suppresses pancreatitis and enhances pancreatic cancer therapy. Cell *159*, 80–93.

Shigematsu, H., Lin, L., Takahashi, T., Nomura, M., Suzuki, M., Wistuba II, Fong, K.M., Lee, H., Toyooka, S., Shimizu, N., et al. (2005). Clinical and biological features associated with epidermal growth factor receptor gene mutations in lung cancers. J Natl Cancer Inst *97*, 339–346.

Shimizu, T., Tolcher, A.W., Papadopoulos, K.P., Beeram, M., Rasco, D.W., Smith, L.S., Gunn, S., Smetzer, L., Mays, T.A., Kaiser, B., et al. (2012). The clinical effect of the dual-targeting strategy involving PI3K/AKT/mTOR and RAS/MEK/ERK pathways in patients with advanced cancer. Clin. Cancer Res. *18*, 2316–2325.

Shoelson, S.E. (1997). SH2 and PTB domain interactions in tyrosine kinase signal transduction. Curr. Opin. Chem. Biol. *1*, 227–234.

Sibilia, M., and Wagner, E. (1995). Strain-dependent epithelial defects in mice lacking the EGF receptor. Science (80-.). *8477*.

Sibilia, M., Steinbach, J.P., Stingl, L., Aguzzi, a, and Wagner, E.F. (1998). A strain-independent postnatal neurodegeneration in mice lacking the EGF receptor. EMBO J. *17*, 719–731.

Siegel, R., Miller, K., and Jemal, A. (2017). Cancer statistics , 2017 . CA Cancer J Clin *67*, 7–30.

Sipos, B., Frank, S., Gress, T., Hahn, S., and Klöppel, G. (2009). Pancreatic intraepithelial neoplasia revisited and updated. Pancreatology *9*, 45–54.

Slater, E.P., Langer, P., Fendrich, V., Habbe, N., Chaloupka, B., Matthäi, E., Sina, M., Hahn, S.A., and Bartsch, D.K. (2010). Prevalence of BRCA2 and CDKN2a mutations in German familial pancreatic cancer families. Fam. Cancer *9*, 335–343.

Smit, V.T.H.B.M., Boot, A.J.M., Smits, A.A.M., Fleuren, G.J., Cornelisse, C.J., and Bos, J.L. (1988). KRAS codon 12 mutations occur very frequently in pancreatic adenocarcinomas. Nucleic Acids Res. *16*, 10952.

Solomon, S., Das, S., Brand, R., and Whitcomb, D.C. (2012). Inherited pancreatic cancer syndromes. Cancer J. *18*, 485–491.

Soltoff, S.P., and Cantley, L.C. (1996). p120cbl is a cytosolic adapter protein that associates with phosphoinositide 3-kinase in response to epidermal growth factor in PC12 and other cells. J. Biol. Chem. *271*, 563–567.

Sordella, R., Bell, D.W., Haber, D.A., and Settleman, J. (2004). Gefitinib-sensitizing EGFR mutations in lung cancer activate anti-apoptotic pathways. Science (80-.). *305*, 1163–1167.

Soria, J.-C., Felip, E., Cobo, M., Lu, S., Syrigos, K., Lee, K.H., Göker, E., Georgoulias, V., Li, W., Isla, D., et al. (2015). Afatinib versus erlotinib as second-line treatment of patients with advanced squamous cell carcinoma of the lung (LUX-Lung 8): an open-label randomised controlled phase 3 trial. Lancet Oncol. *16*, 897–907.

Stephen, A.G., Esposito, D., Bagni, R.G., and McCormick, F. (2014). Dragging ras back in the ring. Cancer Cell *25*, 272–281.

Stocks, T., Rapp, K., Bjorge, T., Manjer, J., Ulmer, H., Selmer, R., Lukanova, A., Johansen, D., Concin, H., Tretli, S., et al. (2009). Blood glucose and risk of incident and fatal cancer in the metabolic syndrome and cancer project (Me-Can): Analysis of six prospective cohorts. PLoS Med. *6*.

Streicher, S.A., Yu, H., Lu, L., Kidd, M.S., and Risch, H.A. (2014). Case-Control Study of Aspirin Use and Risk of Pancreatic Cancer. Cancer Epidemiol. Biomarkers Prev. *23*, 1254–1263.

Su, G.H., Hruban, R.H., Bansal, R.K., Bova, G.S., Tang, D.J., Shekher, M.C., Westerman, A.M., Entius, M.M., Goggins, M., Yeo, C.J., et al. (1999). Germline and Somatic Mutations of the STK11/LKB1 Peutz-Jeghers Gene in Pancreatic and Biliary Cancers. Am. J. Pathol. *154*, 1835–1840.

Taipale, J., and Beachy, P.A. (2001). The Hedgehog and Wnt signalling pathways in cancer. Nature *411*, 349–354.

Thayer, S.P., di Magliano, M.P., Heiser, P.W., Nielsen, C.M., Roberts, D.J., Lauwers, G.Y., Qi, Y.P., Gysin, S., Fernández-del Castillo, C., Yajnik, V., et al. (2003). Hedgehog is an early and late mediator of pancreatic cancer tumorigenesis. Nature *425*, 851–856.

Theoharides, T.C., Alysandratos, K.D., Angelidou, A., Delivanis, D.A., Sismanopoulos, N., Zhang, B., Asadi, S., Vasiadi, M., Weng, Z., Miniati, A., et al. (2012). Mast cells and inflammation. Biochim. Biophys. Acta - Mol. Basis Dis. *1822*, 21–33.

Thomas, S.M., and Grandis, J.R. (2004). Pharmacokinetic and pharmacodynamic properties of EGFR inhibitors under clinical investigation. Cancer Treat. Rev. *30*, 255–268.

Threadgill, D.W., Dlugosz, a a, Hansen, L. a, Tennenbaum, T., Lichti, U., Yee, D., LaMantia, C., Mourton, T., Herrup, K., and Harris, R.C. (1995). Targeted disruption of mouse EGF receptor: effect of genetic background on mutant phenotype. Science (80-.). *269*, 230–234.

Tobita, K., Kijima, H., Dowaki, S., Kashiwagi, H., Ohtani, Y., Oida, Y., Yamazaki, H., Nakamura, M., Ueyama, Y., Tanaka, M., et al. (2003). Epidermal growth factor receptor expression in human pancreatic cancer: Significance for liver metastasis. Int. J. Mol. Med. *11*, 305–309.

Trevino, J.G., Verma, M., Singh, S., Pillai, S., Zhang, D., Pernazza, D., Sebti, S.M., Lawrence, N.J., Centeno, B.A., and Chellappan, S.P. (2013). Selective Disruption of Rb-Raf-1 Kinase Interaction Inhibits Pancreatic Adenocarcinoma Growth Irrespective of Gemcitabine Sensitivity. Mol. Cancer Ther. *12*, 2722–2734.

Tsai, J., Lee, J.T., Wang, W., Zhang, J., Cho, H., Mamo, S., Bremer, R., Gillette, S., Kong, J., Haass, N.K., et al. (2008). Discovery of a selective inhibitor of oncogenic B-Raf kinase with potent antimelanoma activity. Proc. Natl. Acad. Sci. U. S. A. *105*, 3041–3046.

Ueda, S., Ogata, S., Tsuda, H., Kawarabayashi, N., Kimura, M., Sugiura, Y., Tamai, S., Matsubara, O., Hatsuse, K., and Mochizuki, H. (2004). The correlation between cytoplasmic overexpression of epidermal growth factor receptor and tumor aggressiveness: poor prognosis in patients with pancreatic ductal adenocarcinoma. Pancreas *29*, e1-8.

Ullrich, A., Coussens, L., Hayflick, J., Dull, T., Gray, A., Tam, A., Lee, J., Yarden, Y., Libermann, T., and Schlessinger, J. (1984). Human epidermal growth factor receptor cDNA sequence and aberrant expression of the amplified gene in A431 epidermoid carcinoma cells. Nature *309*, 418–425.

Vogelstein, B., and Kinzler, K. (2004). Cancer genes and the pathways they control. Nat. Med. *10*, 789–799.

Waddell, N., Pajic, M., Patch, A., Chang, D.K., Kassahn, K.S., Bailey, P., Johns, A.L., Miller, D., Nones, K., Quek, K., et al. (2015). Whole genomes redefine the mutational landscape of pancreatic cancer. Nature *518*, 495–501.

Wagner, M., Weber, C.K., Bressau, F., Greten, F.R., Stagge, V., Ebert, M., Leach, S.D., Adler, G., and Schmid, R.M. (2002). Transgenic overexpression of amphiregulin induces a mitogenic response selectively in pancreatic duct cells. Gastroenterology *122*, 1898–1912.

Wahl, M.I., Nishibe, S., Kim, J.W., Kim, H., Rhee, S.G., and Carpenter, G. (1990). Identification of two epidermal growth factor-sensitive tyrosine phosphorylation sites of phospholipase C-gamma in intact HSC-1 cells. J. Biol. Chem. *265*, 3944–3948.

Wang, L., Heidt, D.G., Lee, C.J., Yang, H., Logsdon, C.D., Zhang, L., Fearon, E.R., Ljungman, M., and Simeone, D.M. (2009). Oncogenic Function of ATDC in Pancreatic Cancer through Wnt Pathway Activation and Beta-Catenin Stabilization. Cancer Cell *15*, 207–219.

Wang, S., Ghosh, R.N., and Chellappan, S.P. (1998). Raf-1 physically interacts with Rb and regulates its function: a link between mitogenic signaling and cell cycle regulation. Mol. Cell. Biol. *18*, 7487–7498.

Wang, Z., Zhang, L., Yeung, T.K., and Chen, X. (1999). Endocytosis deficiency of epidermal growth factor (EGF) receptor-ErbB2 heterodimers in response to EGF stimulation. Mol. Biol. Cell *10*, 1621–1636.

Whatcott, C.J., Han, H., and Von Hoff, D.D. (2015). Orchestrating the Tumor Microenvironment to Improve Survival for Patients With Pancreatic Cancer: Normalization, Not Destruction. Cancer J. *21*, 299–306.

Wilentz, R.E., Geradts, J., Maynard, R., Offerhaus, G.J.A., Kang, M., Goggins, M., Yeo, C.J., Kern, S.E., and Hruban, R.H. (1998). Inactivation of the p16 (INK4A) tumor-suppressor gene in pancreatic duct lesions: Loss of intranuclear expression. Cancer Res. *58*, 4740–4744.

Witkiewicz, A.K., McMillan, E. a., Balaji, U., Baek, G., Lin, W.-C., Mansour, J., Mollaee, M., Wagner, K.-U., Koduru, P., Yopp, A., et al. (2015). Whole-exome sequencing of pancreatic cancer defines genetic diversity and therapeutic targets. Nat. Commun. *6*, 6744.

Wood, L.D., and Hruban, R.H. (2012). Pathology and Molecular Genetics of Pancreatic Neoplasms. Cancer J. *18*, 492–501.

Wu, C.Y.C., Carpenter, E.S., Takeuchi, K.K., Halbrook, C.J., Peverley, L. V., Bien, H., Hall, J.C., Delgiorno, K.E., Pal, D., Song, Y., et al. (2014). PI3K regulation of RAC1 is required for KRAS-induced pancreatic tumorigenesis in mice. Gastroenterology *147*, 1405–1416.e7.

Xu, X., Gurski, L.A., Zhang, C., Harrington, D.A., Farach-Carson, M.C., and Jia, X. (2012). Recreating the tumor microenvironment in a bilayer, hyaluronic acid hydrogel construct for the growth of prostate cancer spheroids. Biomaterials *33*, 9049–9060.

Yamamoto, S., Tomita, Y., Hoshida, Y., Morooka, T., Nagano, H., Dono, K., Umeshita, K., Sakon, M., Ishikawa, O., Ohigashi, H., et al. (2004). Prognostic significance of activated Akt expression in pancreatic ductal adenocarcinoma. Clin. Cancer Res. *10*, 2846–2850.

Yamauchi, T., Ueki, K., Tobe, K., Tamemoto, H., Sekine, N., Wada, M., Honjo, M., Takahashi, M., Takahashi, T., Hirai, H., et al. (1997). Tyrosine phosphorylation of the EGF receptor by the kinase Jak2 is induced by growth hormone. Nature *390*, 91–96.

Yamauchi, T., Yamauchi, N., Ueki, K., Sugiyama, T., Waki, H., Miki, H., Tobe, K., Matsuda, S., Tsushima, T., Yamamoto, T., et al. (2000). Constitutive tyrosine phosphorylation of ErbB-2 via Jak2 by autocrine secretion of prolactin in human breast cancer. J. Biol. Chem. *275*, 33937–33944.

Yarden, Y., and Sliwkowski, M.X. (2001). Untangling the ErbB signalling network. Nat. Rev. Mol. Cell Biol. *2*, 127–137.

Ying, H., Elpek, K.G., Vinjamoori, A., Zimmerman, S.M., Chu, G.C., Yan, H., Fletcher-Sananikone, E., Zhang, H., Liu, Y., Wang, W., et al. (2011). PTEN is a major tumor suppressor in pancreatic ductal adenocarcinoma and regulates an NF-??B-cytokine network. Cancer Discov. *1*, 158–169.

Ying, H., Kimmelman, A.C., Lyssiotis, C.A., Hua, S., Chu, G.C., Fletcher-Sananikone, E., Locasale, J.W., Son, J., Zhang, H., Coloff, J.L., et al. (2012). Oncogenic kras maintains pancreatic tumors through regulation of anabolic glucose metabolism. Cell *149*, 656–670.

Ying, H., Dey, P., Yao, W., Kimmelman, A.C., Draetta, G.F., Maitra, A., and Depinho, R. a (2016). Genetics and biology of pancreatic ductal adenocarcinoma. Genes Dev. *30*, 355–385.

Yoon, S., and Seger, R. (2006). The extracellular signal-regulated kinase: Multiple substrates regulate diverse cellular functions. Growth Factors *24*, 21–44.

Yoshizawa, K., Nagai, H., Sakurai, S., Hironaka, M., Morinaga, S., Saitoh, K., and Fukayama, M. (2002). Clonality and K-ras mutation analyses of epithelia in intraductal papillary mucinous tumor and mucinous cystic tumor of the pancreas. Virchows Arch. *441*, 437–443.

Zandi, R., Larsen, A.B., Andersen, P., Stockhausen, M.T., and Poulsen, H.S. (2007). Mechanisms for oncogenic activation of the epidermal growth factor receptor. Cell. Signal. *19*, 2013–2023.

Zhang, C., Spevak, W., Zhang, Y., Burton, E.A., Ma, Y., Habets, G., Zhang, J., Lin, J., Ewing, T., Matusow, B., et al. (2015a). RAF inhibitors that evade paradoxical MAPK pathway activation. Nature *526*, 583–586.

Zhang, L., Wang, J.-C., Hou, L., Cao, P.-R., Wu, L., Zhang, Q.-S., Yang, H.-Y., Zang, Y., Ding, J.-P., and Li, J. (2015b). Functional Role of Histidine in the Conserved His-x-Asp Motif in the Catalytic Core of Protein Kinases. Sci. Rep. *5*, 10115.

8. Appendix

8.1. Elimination of c-Raf blocks and delays *K-Ras* driven PanIN and PDAC formation

To investigate the contribution of c-Raf in pancreatic tumorigenesis conditional floxed *c-Raf* alleles were introduced in our PDAC mouse model. Ablation of *c-Raf* in acinar cells of *ElasK-Ras*^{G12Vgeo} mice prevented the development of preneoplastic PanIN lesions even in the context of chronic pancreatitis (data not shown). However, deletion of *c-Raf* is not sufficient to inhibit PDAC tumor development in the absence of *p53* in the *embryonic protocol* (Figure 26A). Interestingly, *c-Raf* deletion prolonged survival of *ElasK-Ras*^{G12Vgeo};*p53*$^{Lox/Lox}$ mice in the *adult protocol* (Figure 26B). Efficient deletion of c-Raf alleles was verified by PCR of PDAC cells isolated from tumor specimens, ruling out the possibility that tumors developed due to incomplete c-Raf deletion (Figure 26C).

A

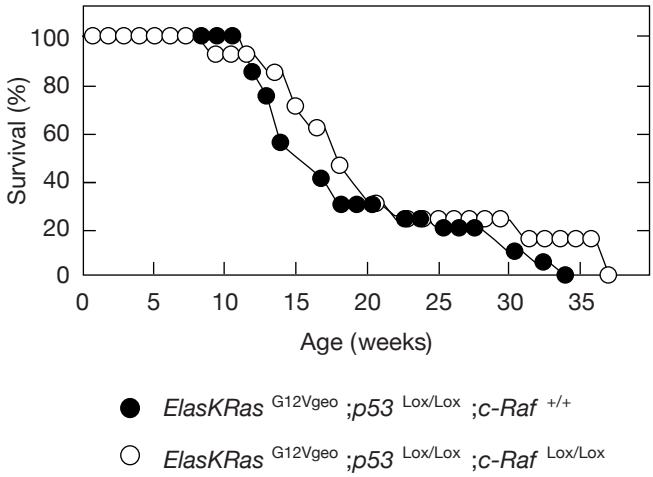

B

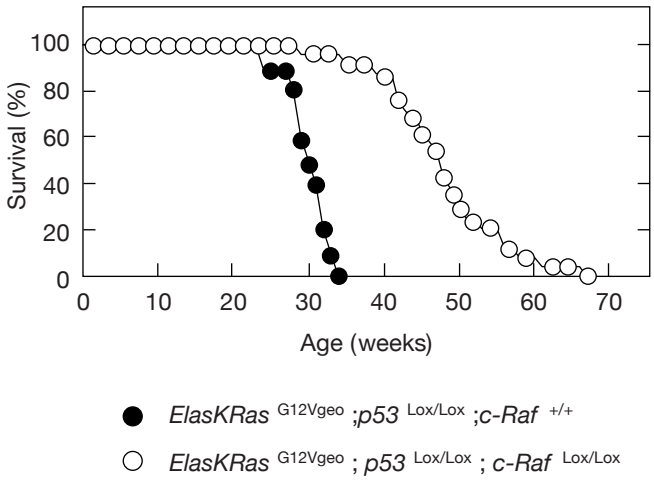

C

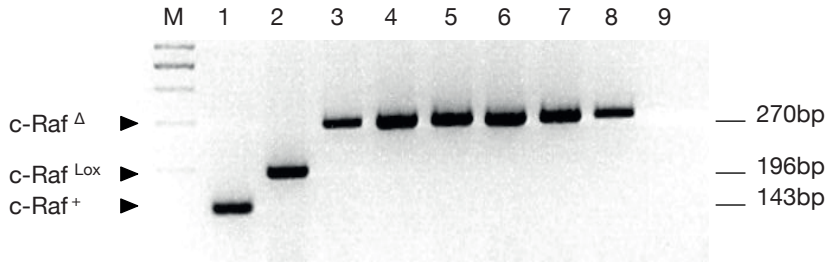

Figure 26. Deletion of *c-Raf* does not prevent PDAC development in a p53 deficient background. (A) Survival of dox-untreated *ElasK-Ras*^{G12Vgeo};*p53*$^{Lox/Lox}$;*c-Raf*$^{+/+}$ (solid circles, n=20) mice and *ElasK-Ras*^{G12Vgeo};*p53*$^{Lox/Lox}$;*c-Raf*$^{Lox/Lox}$ (open circles, n=13) mice. (B) Survival of *ElasK-Ras*^{G12Vgeo};*p53*$^{Lox/Lox}$;*c-Raf*$^{+/+}$; (solid circles, n=10) and *ElasK-Ras*^{G12Vgeo};*p53*$^{Lox/Lox}$;*c-Raf*$^{Lox/Lox}$ (open circles, n=24) mice in the adult protocol. Mice were exposed to doxycycline from conception until P60. At that time, Cre-recombinase leads to the concomitant expression of the resident K-Ras^{G12Vgeo} oncogene and the ablation of *p53* and *c-Raf* conditional alleles. Mice were treated with caerulein from P90 to P180. (C) PCR analysis of *c-Raf* alleles from tumor derived cell explants. Lanes 1, 2 and 3: *c-Raf*$^{+/+}$ (wt), *c-Raf*$^{Lox/Lox}$ and *c-Raf*$^{-/-}$ controls, respectively. Lanes 4, 5, 6, 7, 8: DNA extracted from five different cell explants obtained from *ElasK-Ras*^{G12Vgeo};*p53*$^{Lox/Lox}$;*c-Raf*$^{Lox/Lox}$ PDACs revealing complete deletion of *c-Raf* alleles. Lane 9: blank. Lane M: DNA ladder. Expected fragments for each allele are depicted.

8.2. Concomitant ablation of Egfr and c-Raf completely blocks PDAC initiation

Egfr and *c-Raf* floxed alleles were introduced in the *ElasK-Ras*^{G12Vgeo};*p53*$^{Lox/Lox}$ PDAC mouse model to produce simultaneous ablation of both targets concomitantly with *K-Ras*^{G12Vgeo} expression in acinar cells. Interestingly, the resultant strain *ElasK-Ras*^{G12Vgeo};*p53*$^{Lox/Lox}$;*Egfr*$^{Lox/Lox}$;*c-Raf*$^{Lox/Lox}$, did not develop PDAC after more than one year of age (Figure X). Furthermore, careful histological examination of their pancreas revealed even complete absence of PanIN lesions. In contrast, mice carrying either *Egfr* or *c-Raf* alleles in heterozygosis succumbed to the disease (Figure 27).

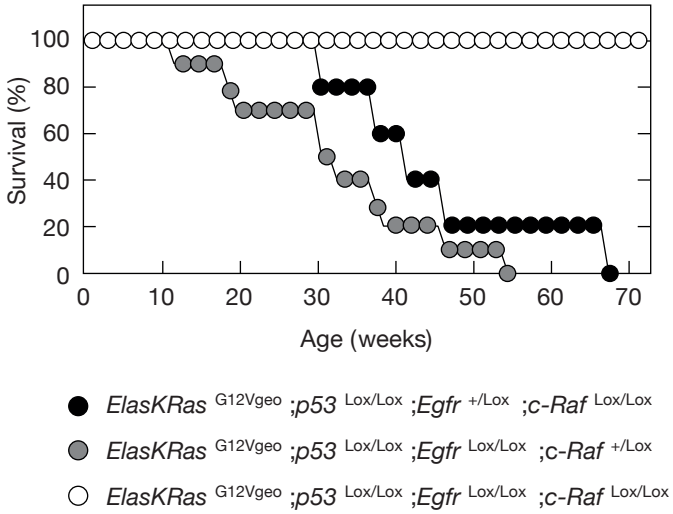

Figure 27. Simultaneous deletion of *Egfr* and *c-Raf* prevents PDAC formation in a p53 deficient background. Survival of dox-untreated *ElasK-Ras*^{G12Vgeo};*p53*$^{Lox/Lox}$;*Egfr*$^{+/Lox}$;*c-Raf*$^{Lox/Lox}$ (solid circles, n=5) mice, *ElasK-Ras*^{G12Vgeo};*p53*$^{Lox/Lox}$;*Egfr*$^{Lox/Lox}$;*c-Raf*$^{+/Lox}$ (grey circles, n=10) mice and *ElasK-Ras*^{G12Vgeo}; *p53*$^{Lox/Lox}$; *Egfr*$^{Lox/Lox}$; *c-Raf*$^{Lox/Lox}$ (open circles, n=14) mice.

9. Publications

Cancer Research

H-Ras and K-Ras Oncoproteins Induce Different Tumor Spectra When Driven by the Same Regulatory Sequences

Matthias Drosten[1], Lucía Simón-Carrasco[1], Isabel Hernández-Porras[1], Carmen G. Lechuga[1], María T. Blasco[1], Harrys K.C. Jacob[1], Salvatore Fabbiano[2,3], Nicoletta Potenza[4], Xosé R. Bustelo[2,3], Carmen Guerra[1], and Mariano Barbacid[1]

Abstract

Genetic studies in mice have provided evidence that H-Ras and K-Ras proteins are bioequivalent. However, human tumors display marked differences in the association of *RAS* oncogenes with tumor type. Thus, to further assess the bioequivalence of oncogenic H-Ras and K-Ras, we replaced the coding region of the murine K-Ras locus with H-Ras^{G12V} oncogene sequences. Germline expression of H-Ras^{G12V} or K-Ras^{G12V} from the K-Ras locus resulted in embryonic lethality. However, expression of these genes in adult mice led to different tumor phenotypes. Whereas H-Ras^{G12V} elicited papillomas and hematopoietic tumors, K-Ras^{G12V} induced lung tumors and gastric lesions. Pulmonary expression of H-Ras^{G12V} created a senescence-like state caused by excessive MAPK signaling. Likewise, H-Ras^{G12V} but not K-Ras^{G12V} induced senescence in mouse embryonic fibroblasts. Label-free quantitative analysis revealed that minor differences in H-Ras^{G12V} expression levels led to drastically different biological outputs, suggesting that subtle differences in MAPK signaling confer nonequivalent functions that influence tumor spectra induced by RAS oncoproteins. *Cancer Res; 77(3); 1–12. ©2016 AACR.*

Introduction

Mammals contain three *Ras* loci, H-*Ras*, K-*Ras*, and N-*Ras*, that encode highly related proteins (1–4). Ras proteins are small GTPases that function as mitogenic switches to control the transmission of extracellular signals to the nucleus (1). They share extensive homology at their N-terminal half, a region involved in nucleotide binding and interaction with downstream effectors (2). Their unique features reside in their carboxy-terminal half that includes the hypervariable region and a terminal domain known as the CAAX box (2). These structural motifs have been implicated in differential transport, posttranslational processing, and subcellular localization of the different Ras proteins (3, 4).

Early knockout data revealed significant functional differences for the three *Ras* loci. Whereas H- and N-*Ras* were dispensable for embryonic development, K-*Ras* was essential (5–7). These observations did not establish whether these differences were due to the intrinsic properties of their cognate Ras proteins or their patterns of expression. This issue was solved, at least in part, when Potenza and colleagues replaced mouse K-*Ras* alleles by chimeric K/H-*Ras* alleles encoding functional H-Ras proteins (8). These mice developed to adulthood despite the absence of K-Ras, indicating that the requirement for K-*Ras* alleles during embryonic development is primarily due to their pattern of expression. Yet, these mice displayed cardiovascular defects, thus raising the possibility that H-Ras and K-Ras proteins might have differential signaling properties, at least in certain tissues (8).

RAS genes have also attracted interest due to their involvement in tumor development (1, 2). The overall incidence of each *RAS* oncogene varies significantly among tumor types (9). Whereas *KRAS* is frequently mutated in pancreatic, colorectal, and lung adenocarcinomas, *HRAS* oncogenes are found in a limited percentage of tumors from the salivary gland, urinary track, cervix, or skin. On the other hand, *NRAS* oncogenes are present in melanomas and hematopoietic tumors. To date, the molecular basis for this incidence bias is still unresolved (9).

Mutant *RAS* genes also induce different phenotypes when expressed in the germline of patients suffering from RASopathies, a series of developmental defects that result from constitutive activation of RAS signaling pathways (10, 11). Oncogenic mutations in *HRAS* lead to relatively mild developmental defects in Costello syndrome patients (12, 13). In contrast, those *KRAS* mutations present in human tumors have not been found in RASopathy patients, suggesting that such mutations may cause embryonic lethality (14).

[1]Molecular Oncology Programme, Centro Nacional de Investigaciones Oncológicas (CNIO), Madrid, Spain. [2]Centro de Investigación del Cáncer and Instituto de Biología Molecular y Celular del Cáncer, CSIC-Universidad de Salamanca, Salamanca, Spain. [3]Centro de Investigación Biomédica en Red de Cáncer (CIBERONC), Salamanca, Spain. [4]Department of Environmental, Biological and Pharmaceutical Sciences and Technologies (DiSTABiF), Second University of Naples, Caserta, Italy.

Note: Supplementary data for this article are available at Cancer Research Online (http://cancerres.aacrjournals.org/).

Current address for S. Fabbiano: Department of Cell Physiology and Metabolism, Centre Médical Universitaire (CMU) and Diabetes Centre, Faculty of Medicine, University of Geneva, Geneva 1206, Switzerland.

Corresponding Authors: Matthias Drosten, Molecular Oncology Programme, Centro Nacional de Investigaciones Oncológicas, Melchor Fernández Almagro 3, Madrid 28029, Spain. Phone: 349-1732-8000; Fax: 349-1732-8033; E-mail: mdrosten@cnio.es; and Mariano Barbacid, mbarbacid@cnio.es

doi: 10.1158/0008-5472.CAN-16-2925

Similar results have been observed in mouse strains carrying genetically engineered *Ras* mutations. Whereas expression of resident K-Ras oncoproteins in the germline leads to early embryonic death, expression of an endogenous H-Ras oncogene is well tolerated and leads to developmental defects very similar to those observed in Costello patients (15–18). Likewise, germline expression of the partially activated K-Ras^{V14I}-mutant isoform results in phenotypic defects that closely resemble those of Noonan patients (19).

Here, we provide genetic evidence that the wild-type H-Ras and K-Ras proteins are bioequivalent in spite of their different structural and biological properties. We have also compared the spectrum of tumors elicited upon expression of the H-Ras^{G12V} and K-Ras^{G12V} oncoproteins from the same mouse K-*Ras* locus. These studies have revealed that these oncoproteins induce a different spectrum of tumors primarily due to differences in the intensity of MAPK signaling that results from subtle differences in their levels of expression.

Materials and Methods

Mouse strains

Generation of K-*Ras*$^{+/LSLH\text{-}RasG12V}$ mice ($K^{HRasV12}$) is described in Supplementary Information. KrasKI (8), HrasKI (8), H-*Ras*$^{-/-}$ (5), K-*Ras*$^{+/LSLG12Vgeo}$ (K^{V12}; ref. 16), and *p53*$^{lox/lox}$ (20) genetically engineered strains have been described. hUBC-CreERT2, *Elas*-tTA, and *tetO*-Cre transgenic strain have also been reported (21, 22). Activation of the inducible CreERT2 recombinase was achieved by feeding the mice with a tamoxifen-containing diet (Harlan Laboratories). For activation of H-Ras^{G12V} and K-Ras^{G12V} expression in lung tissue, mice were infected with Adeno-Cre particles as described previously (23). Trametinib (Mekinist) was purchased from Sellek Chemicals and was administered orally daily (1 mg/kg) for 8 weeks. All mice were maintained in a mixed 129Sv/J x C57BL/6j background and housed in a barrier facility according to standards established by the European Union. All animal experiments were approved by the CNIO, the Carlos III Health Institute (Madrid, Spain), and the Comunidad de Madrid Ethical Committees and performed in accordance with the ARRIVE (Animal Research: Reporting on In Vivo Experiments) guidelines.

Histopathology, IHC, and SA-β-Gal staining

Tissues were fixed in 10% buffered formalin and embedded in paraffin. Hematoxylin and eosin (H&E) staining and immunohistochemical analyses were performed on 3-μm paraffin sections. For IHC, the following antibodies were used: pErk1/2 (9101, Cell Signaling Technology), Active Caspase-3 (MAB835, R&D Systems), SPC (AB3786, Abcam), CC10 (T-18, Santa Cruz Biotechnology), and CD3e (clone 145-2C11, Abcam). Senescence-associated β-galactosidase (SA-β-Gal) activity in cultured mouse embryonic fibroblasts (MEF) as well as in cryosections of lungs was detected by X-Gal staining as described previously (24).

Southern and Western blot analysis

Southern blot analysis is described in Supplementary Information. Western blot analysis of protein extracts obtained from total lung tissue or MEFs was performed as described previously (25). Primary antibodies used included: Pan-Ras (OP40, Merck Millipore), H-Ras (clone 18, BD Transduction Laboratories), pErk1/2 (9101), p53 (2524), pAkt (9271), Akt (9272; all from Cell Signaling Technology), p19Arf (clone 5-C3-1, Upstate Biotechnology), Erk1 (C16), p16INK4a (M-156; all from Santa Cruz Biotechnology), and GAPDH (G8795, Sigma-Aldrich).

Statistical analysis

All statistical analyses were performed using an unpaired Student *t* test. *P* values <0.05 were considered to be statistically significant (* $P < 0.05$, *** $P < 0.001$).

Results

H-Ras and K-Ras are bioequivalent proteins

Germline ablation of K-*Ras* results in embryonic lethality (6, 7). Yet, expression of H-Ras proteins under the control of K-*Ras*–regulatory sequences results in viable mice, thus illustrating that H-Ras can replace K-Ras isoforms, for most biological activities (8). Yet, these mice, designated as HrasKI, displayed dilated cardiomyopathy and arterial hypertension when they reached adulthood (8). These cardiovascular defects were initially attributed to the absence of K-Ras proteins in heart tissue. Subsequent studies, however, revealed that germline expression of constitutively active H-Ras^{G12V} led to similar cardiovascular defects in a mouse model of Costello syndrome (17). Thus, we reasoned that these cardiovascular defects might be due to H-Ras overexpression due to the presence of four H-Ras–coding alleles (the knocked-in HrasKI alleles and the endogenous H-*Ras* alleles). To reduce the load of H-Ras expression, we crossed HrasKI mice with H-*Ras*$^{-/-}$ animals. HrasKI;H-*Ras*$^{-/-}$ mice displayed normal heart function and no hypertension (Fig. 1A and B). In addition, these mice displayed normal cardiomyocyte areas and did not accumulate fibrosis in their heart (Fig. 1C and D). These results indicate that the cardiovascular defects of HrasKI mice were due to H-Ras overexpression and not to differential activities between H-Ras and K-Ras proteins.

Germline expression of the H-Ras^{G12V} oncoprotein from the K-*Ras* locus results in embryonic lethality

Next, we interrogated whether their oncogenic isoforms, K-Ras^{G12V} and H-Ras^{G12V}, also have similar properties. To this end, we knocked in a cDNA encoding an H-*Ras*^{G12V} oncogene within the first coding exon of the K-*Ras* locus (Fig. 2A). We also knocked in a lox-STOP-lox (LSL) cassette upstream of the initiator codon to prevent expression of H-*Ras*^{G12V} (Supplementary Fig. S1A–S1C). Expression of the H-*Ras*^{G12V} cDNA clone and a genomic DNA fragment containing the four H-*Ras* coding exons resulted in similar expression levels, indicating that the H-*Ras* intronic sequences do not play a significant role in regulating H-Ras expression (Fig. 2B and C). For simplicity, the wild-type K-*Ras*$^{+/+}$ mice and the targeted K-*Ras*$^{+/LSLG12Vgeo}$ and K-*Ras*$^{+/LSLH\text{-}RasG12V}$ strains will be referred to hereafter as K^{+}, K^{V12}, and $K^{HRasV12}$, respectively.

Previous studies have indicated that expression of a K-*Ras*^{G12V} oncogene in the mouse germline results in embryonic lethality (16). In contrast, expression of the H-*Ras*^{G12V} oncogene, even in homozygosity, is well tolerated during embryonic development (17, 18). To determine whether this differential effect is an intrinsic property of the K-Ras^{G12V} and H-Ras^{G12V} oncoproteins, we crossed $K^{HRasV12}$ mice to EIIA-Cre transgenics (26) to express the H-Ras^{G12V} oncoprotein from the K-*Ras* locus in the germline. These embryos were no longer viable and died right after implantation, a time similar to that observed for embryos expressing an

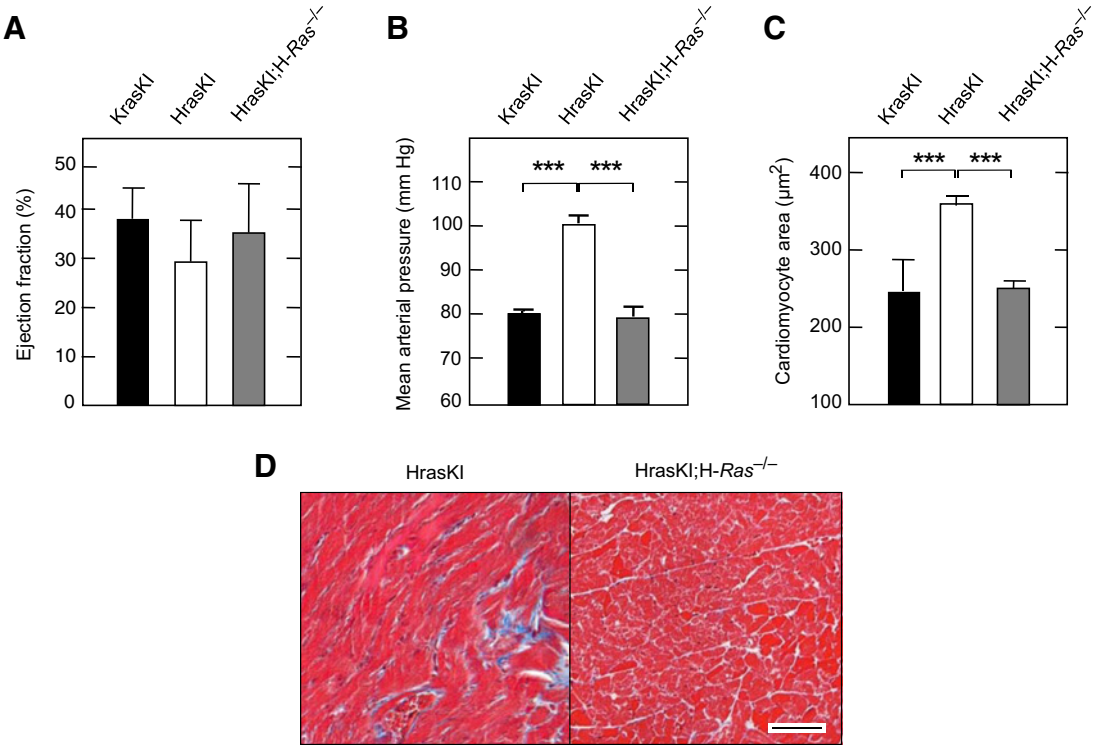

Figure 1.

H-Ras and K-Ras proteins are functionally bioequivalent. **A,** Heart function as determined by percentage of ejection fraction in the left ventricle of KrasKI ($n = 9$; solid bar), HrasKI ($n = 10$; open bar), or HrasKI;H-*Ras*$^{-/-}$ ($n = 9$; gray bar) mice. Data, mean ± SD. **B,** Mean arterial pressure of KrasKI ($n = 6$; solid bar), HrasKI ($n = 7$; open bar), or HrasKI;H-*Ras*$^{-/-}$ ($n = 7$; gray bar) mice. Data, mean ± SD. ***, $P < 0.001$ (unpaired Student *t* test). **C,** Cardiomyocyte area in the left ventricle of KrasKI ($n = 4$; solid bar), HrasKI ($n = 4$; open bar), or HrasKI;H-*Ras*$^{-/-}$ ($n = 5$; gray bar) mice. Data, mean ± SD. ***, $P < 0.001$ (unpaired Student *t* test). **D,** Masson trichrome staining for fibrosis in sections obtained from the left ventricle of representative HrasKI and HrasKI;H-*Ras*$^{-/-}$ mice. Scale bars, 200 μm.

endogenous K-Ras^{G12V} oncoprotein (16). Hence, the ability of mice, as well as of Costello syndrome patients, to tolerate expression of an oncogenic H-Ras^{G12V} protein during embryonic development is dictated by the expression pattern of the H-*Ras* locus.

Expression of H-Ras^{G12V} from the K-*Ras* locus in adult mice

Next, we explored the oncogenic properties of the K-Ras^{G12V} and H-Ras^{G12V} isoforms expressed from the K-*Ras* locus in adult mice. To this end, we inserted in the K^{V12} and $K^{HRasV12}$ strains a transgene encoding the inducible CreERT2 recombinase under the control of the human ubiquitin C promoter (21). We exposed K^{V12};hUBC-CreERT2$^{+/T}$ and $K^{HRasV12}$;hUBC-CreERT2$^{+/T}$ mice to a continuous tamoxifen diet to ensure efficient recombination of the targeted K-*Ras* alleles. Under these conditions, K^{V12};hUBC-CreERT2$^{+/T}$ mice had a median survival of 24 weeks (Fig. 2D). In agreement with previous studies (27), these mice displayed multiple lesions in their lungs as well as abundant gastric papillomas (Fig. 2E). No other tissue displayed significant alterations at the histopathologic level. $K^{HRasV12}$;hUBC-CreERT2$^{+/T}$ mice submitted to the same tamoxifen treatment died 4 to 5 weeks earlier (Fig. 2D). These mice did not develop detectable lesions in either lungs or stomach (Fig. 2E) despite expression of the mutant H-Ras^{G12V} protein in these tissues (Supplementary Fig. S1D). Instead, they displayed papillomas on their footpads after approximately 2 months of treatment (Supplementary Fig. S1E). Moreover, they had enlarged spleens and thymic tumors (Fig. 3). Tamoxifen-treated control K^{+};hUBC-CreERT2$^{+/T}$ mice did not display detectable lesions for up to one year of age. These observations indicate that oncogenic signaling initiated by K-Ras^{G12V} and H-Ras^{G12V} oncoproteins expressed under the same regulatory sequences has substantially different consequences on tumor formation.

Expression of H-Ras^{G12V} from the K-*Ras* locus in adult mice induces hematopoietic disorders

Postmortem characterization of tamoxifen-treated $K^{HRasV12}$;hUBC-CreERT2$^{+/T}$ mice at humane endpoint revealed enlarged spleens infiltrated with myeloid cell populations in 100% of the animals (Fig. 3A and B). This phenotype was not observed in K^{V12};hUBC-CreERT2$^{+/T}$ or K^{+};hUBC-CreERT2$^{+/T}$ mice. Flow cytometry analyses of these infiltrates revealed a dramatic expansion of CD11b^{+} and Gr1^{+}/CD11b^{+} double-positive cells indicative of myeloproliferative disease (Fig. 3C; Supplementary Fig. S2A). This increase in the myeloid cell compartment was accompanied by a concomitant decrease in CD3^{+} T cells and CD19^{+} B cells (Supplementary Fig. S2A). Analysis of committed progenitors in the bone marrow of mice exposed to the tamoxifen diet for 3 months revealed a significant increase in the common myeloid progenitors (CMP; Lin^{-}/IL7Rα^{-}/Sca-1^{-}/c-Kit^{+}/FcγR^{low}/CD34^{+}) as well as a slight expansion of the granulocyte–macrophage progenitor population (GMP; Lin^{-}/IL7Rα^{-}/Sca-1^{-}/c-Kit^{+}/FcγR^{high}/CD34^{+}; Supplementary Fig. S2B). The common lymphoid progenitors (CLP; Lin^{-}/IL7Rα^{+}/Sca-1^{low}/c-Kit^{low}), the megakaryocyte–erythroid progenitors (MEP; Lin^{-}/IL7Rα^{-}/Sca-1^{-}/c-Kit^{+}/FcγR^{low}/CD34^{-}), and

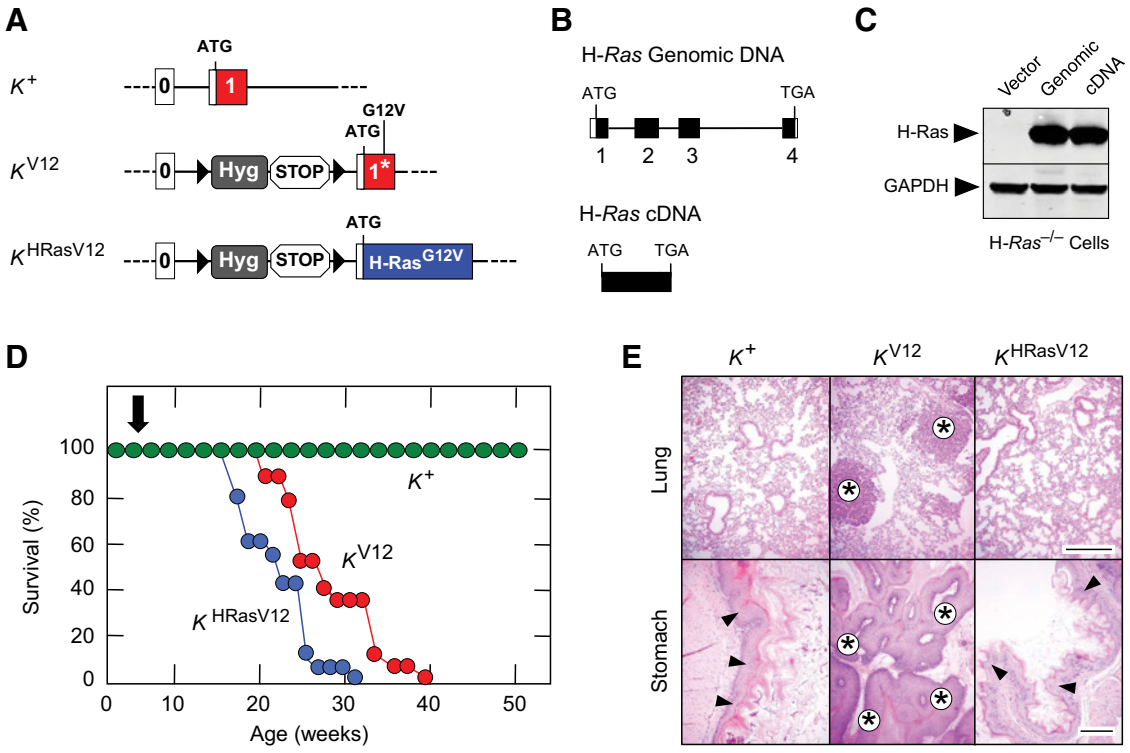

Figure 2.

Phenotypic consequences of the expression of H-Ras^{G12V} and K-Ras^{G12V} oncoproteins from the K-*Ras* locus in adult mice. **A,** Schematic representation of K-*Ras* wild-type (K^{+}), K-*Ras*^{LSLG12Vgeo} (*K*^{V12}), and K-*Ras*$^{LSLH\text{-}RasG12V}$ (*K*^{HRasV12}) alleles. The H-Ras^{G12V} cDNA (blue) was knocked-in into exon 1 of the endogenous K-*Ras* locus (red) along with transcriptional termination sequences (STOP) and a hygromycin-expressing selection cassette (Hyg) flanked by loxP sequences (closed triangles) upstream of exon 1, at the same location as in the *K*^{V12} allele. The exon 1 encoding the oncogenic G12V mutation is indicated by an asterisk. The three alleles share the same ATG initiator codon sequences. **B,** Schematic representation of the coding exons (1–4) present in the endogenous H-*Ras* locus and the H-Ras cDNA (cDNA). The noncoding domains of exons 1 and 4 are indicated by open boxes. **C,** Western blot analysis of H-Ras expression in H-*Ras*$^{-/-}$ MEFs infected with empty lentiviruses (vector), lentiviruses expressing the 1.6 kbp DNA fragment encompassing the H-*Ras* genomic sequences shown in **B** (genomic), or the H-*Ras* cDNA (cDNA). GAPDH expression served as a loading control. **D,** Survival of *K*$^{+}$;hUBC-CreERT2$^{+/T}$ (green dots; $n = 6$), *K*^{V12};hUBC-CreERT2$^{+/T}$ (red dots; $n = 19$), or *K*^{HRasV12};hUBC-CreERT2$^{+/T}$ (blue dots; $n = 16$) mice subjected to a continuous tamoxifen diet at 4 weeks of age (solid arrow). **E,** H&E staining of lung and stomach sections obtained from *K*$^{+}$;hUBC-CreERT2$^{+/T}$, *K*^{V12};hUBC-CreERT2$^{+/T}$, or *K*^{HRasV12};hUBC-CreERT2$^{+/T}$ mice treated for 4 months with tamoxifen diet. Asterisks indicate adenomas (lung) or papillomas (stomach) in *K*^{V12};hUBC-CreERT2$^{+/T}$ animals (*K*^{V12}). Arrowheads show the normal stratified epithelium of the forestomach in *K*$^{+}$;hUBC-CreERT2$^{+/T}$ (*K*$^{+}$) and *K*^{HRasV12};hUBC-CreERT2$^{+/T}$ (*K*^{HRasV12}) mice (scale bars, 200 μm).

LSK cells (Lin^{-}/Sca-1^{+}/c-Kit^{+}), a population enriched in hematopoietic stem cells, did not display significant changes. These observations indicate that H-Ras^{G12V}, but not K-Ras^{G12V}, is capable of inducing myeloproliferative disease in adult mice via expansion of a specific subset of committed progenitors in their bone marrow.

We also detected large tumor masses in the thymus in more than 85% of *K*^{HRasV12};hUBC-CreERT2$^{+/T}$ animals, a pathology not observed in *K*^{V12};hUBC-CreERT2$^{+/T}$ or *K*$^{+}$;hUBC-CreERT2$^{+/T}$ mice (Fig. 3D). Histopathologic characterization revealed the presence of T-cell lymphoblastic lymphoma (T-ALL), as determined by a uniform expansion of CD3^{+} T lymphocytes. Moreover, tumors displayed an increase in double-negative (DN) CD4/CD8^{-}, single-positive CD4^{+}, and single-positive CD8^{+} cells (Fig. 3E). In particular, when DN cells were further characterized, we detected elevated DN1 (CD44^{+}/CD25^{-}) and DN2 (CD44^{+}/CD25^{+}) populations (Supplementary Fig. S3A). The characteristic hyperactivation of the Notch pathway in T-ALL was also observed as demonstrated by immunostaining of Hes1 (Supplementary Fig. S3B; ref. 28). We also detected abundant lymphocyte infiltrates in a variety of organs, including lung, liver, kidney, and eye (Supplementary Fig. S3C). These data indicate that in addition to myeloproliferative disease, most mice expressing the H-Ras^{G12V} oncoprotein from the K-*Ras* locus also developed T-ALL, a tumor type not induced by the K-Ras^{G12V} isoform.

H-Ras^{G12V} driven from the *K-Ras* locus induces pancreatic tumors

Expression of a resident K-*Ras*^{G12V} oncogene during late embryonic development in pancreatic acinar cells results in pancreatic intraepithelial neoplasias (PanIN lesions) that occasionally progress to pancreatic ductal adenocarcinomas (PDAC; ref. 22). No such lesions were observed in H-*Ras*$^{+/G12V}$ or H-*Ras*$^{G12V/G12V}$ mice in which the H-Ras^{G12V} oncoprotein is expressed from its own locus (17). To determine whether H-Ras^{G12V} could induce pancreatic lesions when expressed from the K-*Ras* locus, we crossed *K*^{HRasV12} mice to *Elas*-tTA/*tetO*-Cre transgenic animals known to selectively express Cre recombinase in acinar cells from E16.5 onwards (22). Analysis of serial pancreatic tissue sections of *K*^{HRasV12};*Elas*-tTA/*tetO*-Cre animals at one year of age revealed the appearance of focal low- and high-grade PanIN lesions

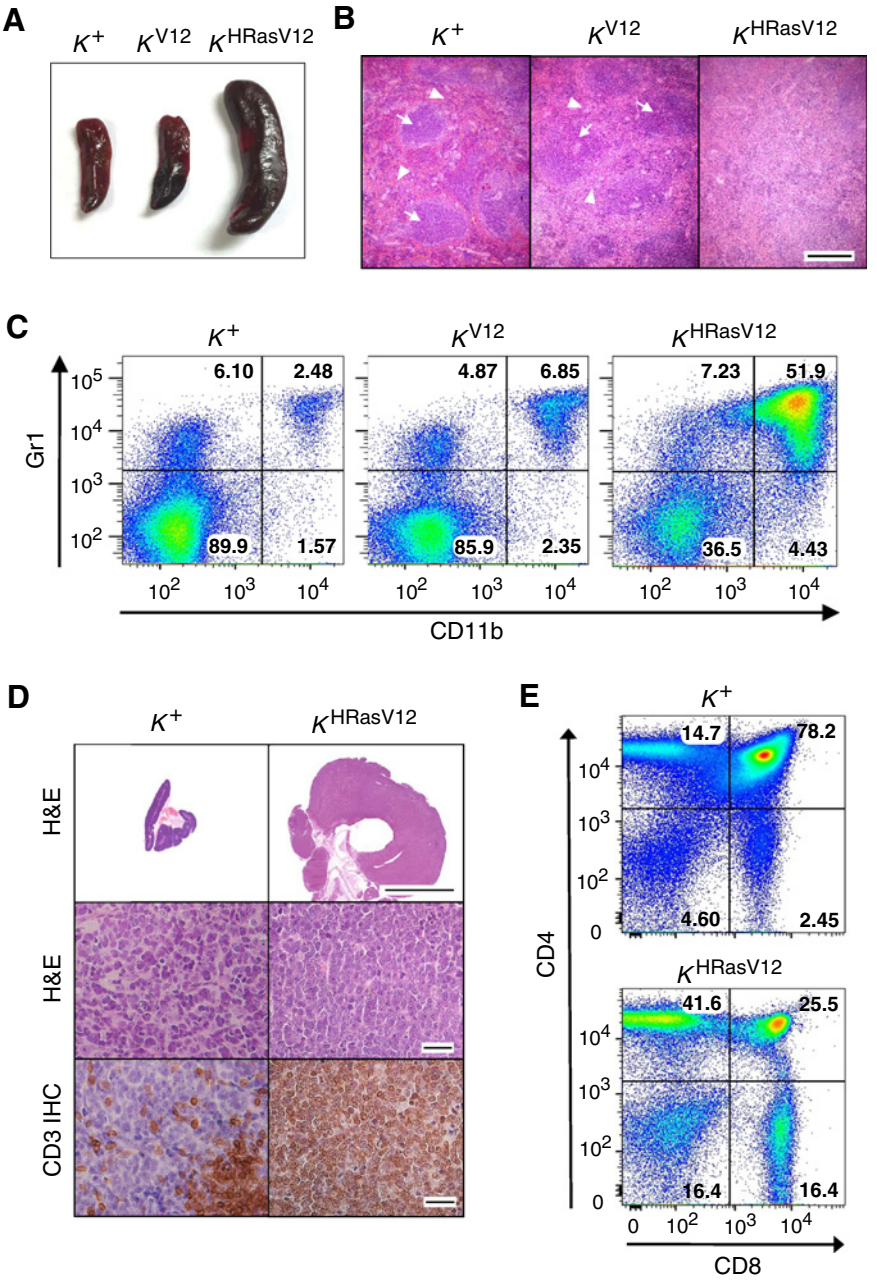

Figure 3.
H-Ras^{G12V}, but not K-Ras^{G12V}, induces hematopoietic tumors in adult mice. **A,** Representative images of spleens obtained from K^{+};hUBC-CreERT2$^{+/T}$, K^{V12};hUBC-CreERT2$^{+/T}$, or $K^{HRasV12}$;hUBC-CreERT2$^{+/T}$ mice treated for 4 months with tamoxifen diet. **B,** H&E staining of spleen sections obtained from K^{+};hUBC-CreERT2$^{+/T}$, K^{V12};hUBC-CreERT2$^{+/T}$, or $K^{HRasV12}$;hUBC-CreERT2$^{+/T}$ mice treated for 4 months with tamoxifen diet. White and red pulp are indicated by arrows and arrowheads, respectively (scale bars, 200 μm). **C,** Flow cytometry analysis of Gr1^{+} and CD11b^{+} cells in spleens obtained from K^{+};hUBC-CreERT2$^{+/T}$, K^{V12};hUBC-CreERT2$^{+/T}$, or $K^{HRasV12}$;hUBC-CreERT2$^{+/T}$ mice treated for 4 months with tamoxifen diet. **D,** H&E (top and middle) and CD3 immunohistochemical staining (bottom) in thymus sections obtained from K^{+};hUBC-CreERT2$^{+/T}$ or $K^{HRasV12}$;hUBC-CreERT2$^{+/T}$ mice treated for 4 months with tamoxifen diet. Scale bars, 5 mm (top), 25 μm (middle, bottom). **E,** Flow cytometry analysis of CD4^{+} and CD8^{+} cells in thymuses obtained from K^{+};hUBC-CreERT2$^{+/T}$ or $K^{HRasV12}$;hUBC-CreERT2$^{+/T}$ mice treated for 4 months with tamoxifen diet.

indistinguishable from those present in K^{V12};*Elas*-tTA/*tetO*-Cre mice (Supplementary Fig. S4A). However, the number of lesions was significantly lower than in similar mice expressing the K-Ras^{G12V} oncoprotein (Fig. 4A).

Loss of the tumor suppressor p53 accelerated tumor formation in $K^{HRasV12}$;*Elas*-tTA/*tetO*-Cre animals (22). These mice died of PDAC tumors, although they survived longer than those mice expressing the K-Ras^{G12V} oncoprotein (30 vs. 17 weeks average survival, a 75% increase; Fig. 4B; Supplementary Fig. S4A). Comparative analysis of $K^{HRasV12}$;p53$^{lox/lox}$;*Elas*-tTA/*tetO*-Cre and K^{V12};p53$^{lox/lox}$;*Elas*-tTA/*tetO*-Cre mice at 10 weeks of age revealed that the H-Ras^{G12V}-expressing animals displayed significantly fewer PanIN lesions and PDAC tumors than those expressing K-Ras^{G12V} (Fig. 4C). These quantitative differences are likely to be due to a reduction in the number of initiating events, as the number of acinar–ductal metaplasias was significantly higher in acinar cell explants of K^{V12} mice than in those derived from $K^{HRasV12}$ animals (Fig. 4D; Supplementary Fig. S4B).

H-Ras^{G12V} failed to induce lung adenocarcinomas due to excessive MAPK signaling

Systemic expression of H-Ras^{G12V} from the K-*Ras* locus did not yield lung lesions, including hyperplasias or benign adenomas. To rule out non–cell-autonomous effects, we infected $K^{HRasV12}$ and K^{V12} mice with Adeno-Cre particles to selectively induce oncogene expression in lung tissue. Six months after infection, none of the $K^{HRasV12}$ mice displayed detectable lesions in their lungs, whereas all K^{V12} animals had developed

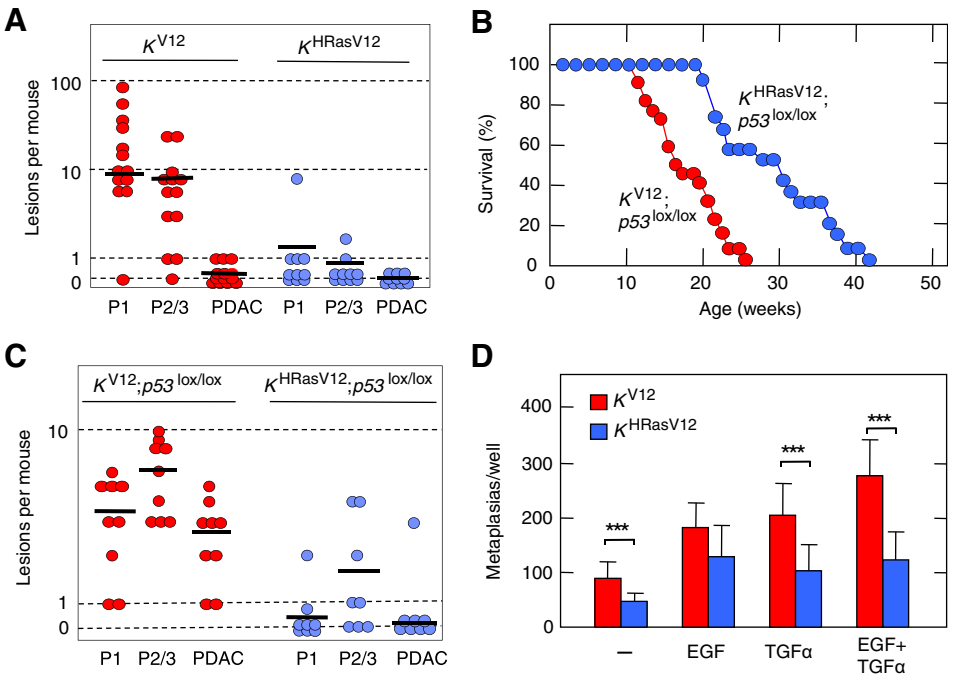

Figure 4.
K-Ras^{G12V} and H-Ras^{G12V} oncoproteins expressed from the K-*Ras* locus induce pancreatic lesions. **A,** Number of low (P1) and high (P2/3) grade PanINs as well as PDACs per mouse in 1-year-old K^{V12};*Elas*-tTA/*tetO*-Cre (red circles, $n = 13$) or $K^{HRasV12}$;*Elas*-tTA/*tetO*-Cre (blue circles; $n = 10$) mice. Data, mean (horizontal bars) ± SD. **B,** Survival of K^{V12};$p53^{lox/lox}$;*Elas*-tTA/*tetO*-Cre (K^{V12};$p53^{lox/lox}$; red dots; $n = 22$) or $K^{HRasV12}$;$p53^{lox/lox}$;*Elas*-tTA/*tetO*-Cre mice ($K^{HRasV12}$;$p53^{lox/lox}$; blue dots; $n = 19$). **C,** Number of low (P1) and high (P2/3) grade PanINs as well as PDACs per mouse in 10 week-old K^{V12};$p53^{lox/lox}$;*Elas*-tTA/*tetO*-Cre (red circles; $n = 9$) or $K^{HRasV12}$;$p53^{lox/lox}$;*Elas*-tTA/*tetO*-Cre (blue circles; $n = 8$) mice. Data, mean (horizontal bars) ± SD. **D,** Acinar cell explants isolated from pancreata of 6- to 8-week-old K^{V12};*Elas*-tTA/*tetO*-Cre (K^{V12}; red bars; $n = 6$) and $K^{HRasV12}$;*Elas*-tTA/*tetO*-Cre ($K^{HRasV12}$; blue bars; $n = 7$) mice were incubated in the absence or presence of the indicated growth factors. The number of metaplasias was determined after 5 days in culture. Data, mean ± SD. ***, $P < 0.001$ (unpaired Student *t* test).

multiple lesions, including lung adenocarcinomas (Supplementary Fig. S4C and S4D).

Tamoxifen treatment of K^{V12};hUBC-CreERT2$^{+/T}$ and $K^{HRasV12}$;hUBC-CreERT2$^{+/T}$ mice for short periods of time allowed us to analyze the immediate events that followed expression of the K-Ras^{G12V} and H-Ras^{G12V} oncoproteins in lung tissue. Four days after tamoxifen treatment, H-Ras^{G12V} induced phosphorylation of the downstream Erk1/2 kinases (pErk1/2) in more than 20% of the cells, whereas expression of K-Ras^{G12V} only resulted in pErk1/2 immunostaining in less than 5% of the cells (Fig. 5A). Similar results were obtained 7 days after treatment. These findings were not due to a differential number of cells expressing the K-Ras^{G12V} and H-Ras^{G12V} oncoproteins as the levels of Cre-mediated recombination in the lungs of K^{V12};hUBC-CreERT2$^{+/T}$ and $K^{HRasV12}$;hUBC-CreERT2$^{+/T}$ mice were similar (Supplementary Fig. S4E and S4F). More importantly, when mice were analyzed 2 weeks after tamoxifen treatment, the number of pErk1/2-expressing cells in the lungs of $K^{HRasV12}$ mice decreased dramatically, whereas those present in K^{V12} lungs displayed a modest increase (Fig. 5A). These results were further confirmed by Western blot analysis (Fig. 5B). These observations were selective for lung cells as we did not observe significantly differential numbers of pErk-expressing cells in other tissues with the possible exception of cells in the basal layer of the skin and in the white pulp of the spleen (Supplementary Fig. S5A). To determine whether these results were due to differential expression levels of the two mutant proteins, we compared their relative levels of expression in the lungs of K^{V12};hUBC-CreERT2$^{+/T}$ and $K^{HRasV12}$;hUBC-CreERT2$^{+/T}$ mice by a label-free quantification approach (29). This technique allowed us to determine their relative amounts based on the detection of the shared peptide (6-LVVVGAVGVGK-16) in which the underlined residue corresponds to the activating valine (Supplementary Fig. S5B). As illustrated in Fig. 5C, H-Ras^{G12V} is expressed at about 5-fold higher levels than K-Ras^{G12V}. The higher levels of H-Ras^{G12V} expression also resulted in increased levels of total GTP-bound active Ras complexes as determined by RBD pull-down assays (Fig. 5D).

Next, we examined whether the increased levels of GTP-bound H-Ras^{G12V} may have an effect on the proliferation of H-Ras^{G12V}-expressing cells that might prevent the appearance of hyperplastic lesions. To this end, we used the recombinant K-*Ras*$^{H\text{-}RasG12V}$ allele as a molecular marker for the presence of H-Ras^{G12V}-expressing lung cells. Exposure of 4-week-old $K^{HRasV12}$;hUBC-CreERT2$^{+/T}$ mice to a tamoxifen diet for 4 weeks resulted in the effective recombination of the K-Ras$^{LSLH\text{-}RasG12V}$ allele, thus indicating that a significant fraction of lung cells expressed the H-Ras^{G12V} oncoprotein (Fig. 6A). However, when these $K^{HRasV12}$;hUBC-CreERT2$^{+/T}$ mice were maintained in a diet lacking tamoxifen for an additional 8-week period, those cells that contained the recombined K-*Ras*$^{H\text{-}RasG12V}$ allele diagnostic of H-Ras^{G12V}

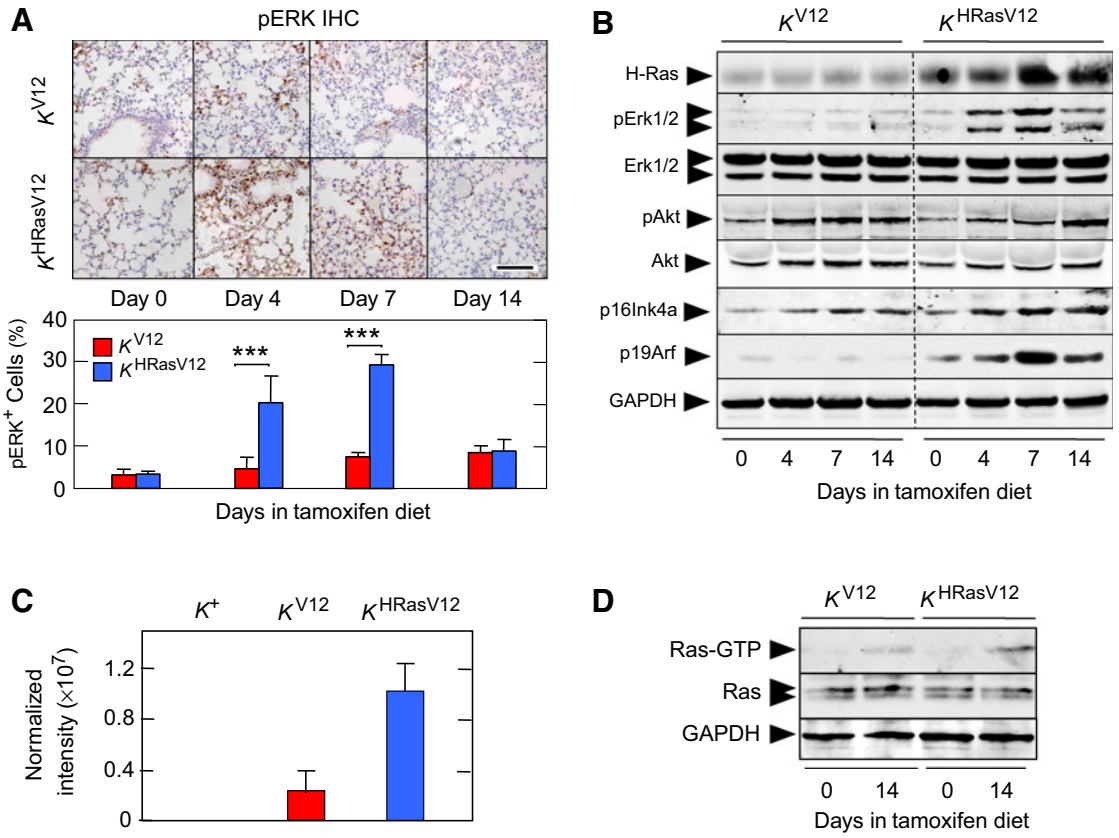

Figure 5.

H-Ras^{G12V} expressed from the K-*Ras* locus induces robust downstream signaling in lung tissue. **A,** Top, immunohistochemical staining for pErk^{+} cells in lung sections obtained from K^{V12};hUBC-CreERT2$^{+/T}$ or $K^{HRasV12}$;hUBC-CreERT2$^{+/T}$ mice subjected to tamoxifen diet for the indicated time (scale bars, 250 μm); bottom, quantification of the percentage of pERK^{+} cells in the lung sections shown above obtained from K^{V12};hUBC-CreERT2$^{+/T}$ (K^{V12}; red bars; $n = 3$) or $K^{HRasV12}$;hUBC-CreERT2$^{+/T}$ ($K^{HRasV12}$; blue bars; $n = 3$) mice. Data, mean ± SD. ***, $P < 0.001$ (unpaired Student t test). **B,** Western blot analysis of H-Ras, pErk1/2, Erk1/2, pAkt, Akt, p16Ink4a, and p19Arf expression in total lung extracts obtained from K^{V12};hUBC-CreERT2$^{+/T}$ or $K^{HRasV12}$;hUBC-CreERT2$^{+/T}$ mice exposed to tamoxifen diet for the indicated time. GAPDH expression served as a loading control. **C,** Relative quantification of the levels of expression of K-Ras^{G12V} and H-Ras^{G12V} oncoproteins by label-free quantification in lungs obtained from K^{+};hUBC-CreERT2$^{+/T}$ ($n = 6$), K^{V12};hUBC-CreERT2$^{+/T}$ ($n = 6$), or $K^{HRasV12}$;hUBC-CreERT2$^{+/T}$ ($n = 6$) mice treated for 2 months with tamoxifen diet. The tryptic peptide LVVVGAVGVGK was used to detect expression of both K-Ras^{G12V} and H-Ras^{G12V} proteins. Data, mean ± SD. **D,** Total Ras-GTP levels in lungs obtained from K^{V12};hUBC-CreERT2$^{+/T}$ or $K^{HRasV12}$;hUBC-CreERT2$^{+/T}$ mice treated with tamoxifen diet for the indicated time. GAPDH was used as a loading control.

expression completely disappeared (Fig. 6A). These results were selective for lung cells as the K-*Ras*$^{H\text{-}RasG12V}$ recombined allele remains present in other tissues, such as thymus, after the 8-week period in the absence of tamoxifen (Fig. 6A). To determine whether the disappearance of the lung cells was due to excessive H-Ras^{G12V} signaling, we treated $K^{HRasV12}$;hUBC-CreERT2$^{+/T}$ mice with a non-limiting dose (1 mg/kg) of trametinib, a MEK inhibitor known to effectively block MAPK signaling driven by Ras oncogenes (30). Trametinib was provided during the 8 weeks in which mice were no longer exposed to tamoxifen. As illustrated in Fig. 6A, these mice retained the K-*Ras*$^{H\text{-}RasG12V}$ recombined allele, indicating that expression of the H-Ras^{G12V} oncoprotein was no longer deleterious for lung cells in the presence of the MEK inhibitor.

H-Ras^{G12V} expression in lung cells induces a senescence-like arrest partially mediated by p53

The disappearance of H-Ras^{G12V}-expressing lung cells was not due to apoptosis, as we could not detect increased levels of active caspase-3 in the lungs of tamoxifen-treated $K^{HRasV12}$ mice (Supplementary Fig. S5C). Likewise, we did not detect SA-β-Gal expression, a standard marker for oncogene-induced senescence (OIS). Yet, we observed the induction of other senescence markers, such as p16Ink4a and p19Arf (Figs. 5B and 6B). These results suggest that H-Ras^{G12V} expression may induce some sort of noncanonical senescence-like state. Finally, we interrogated whether this phenomenon could be mediated by p53. To this end, we introduced *p53*^{lox} alleles into K^{V12} and $K^{HRasV12}$ mice. As illustrated in Supplementary Fig. S6A and S6B, $K^{HRasV12}$;*p53*$^{lox/lox}$ mice developed some hyperplasias and occasional adenomas in 30% of the animals, all of which stained positive for type II alveolar cell markers (Supplementary Fig. S6C). These results indicate that induction of a senescence-like phenotype in lung tissue by expression of the H-Ras^{G12V} oncoprotein from the K-*Ras* locus is only partially mediated by p53.

H-Ras^{G12V} expressed from the K-*Ras* locus induces OIS in MEFs

Finally, we decided to compare the effect of expressing the K-Ras^{G12V} and H-Ras^{G12V} oncoproteins from the same K-*Ras* locus

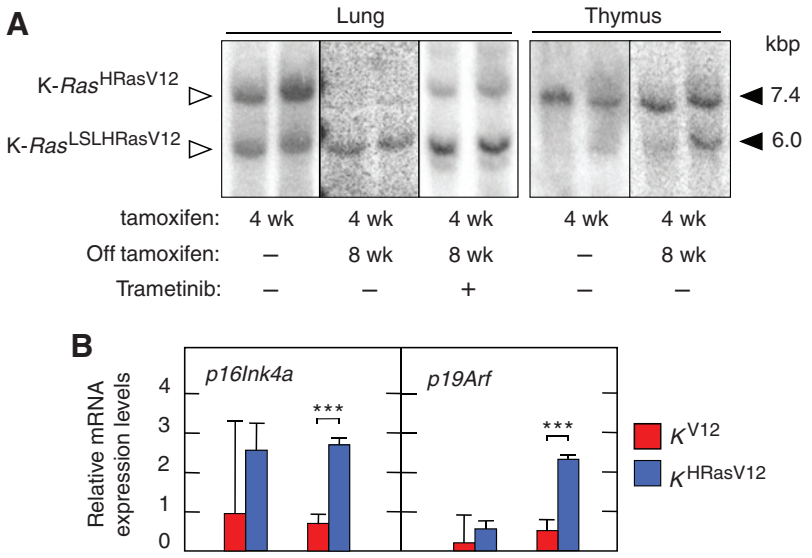

Figure 6.

H-Ras^{G12V} expressed from the K-*Ras* locus induces a senescence-like arrest in lung tissue that results in subsequent elimination of cells. **A,** Southern blot analysis of DNA isolated from lung tissue obtained from 4-week-old $K^{HRasV12}$;hUBC-CreERT2$^{+/T}$ mice exposed to a tamoxifen diet for 4 weeks either immediately ending the treatment (left) or after mice were maintained for 8 additional weeks in a regular diet (center and right). The latter mice were either left untreated during the additional 8-week period (center) or treated daily with 1 mg/kg of trametinib, a selective MEK inhibitor (right). DNA isolated from thymus tissue was used as control. The migration (open arrowheads) and sizes (solid arrowheads) of the diagnostic SphI + KpnI DNA fragments for the recombined K-*Ras*$^{H\text{-}RasG12V}$ allele that expresses the H-Ras^{G12V} oncoprotein and the nonrecombined K-*Ras*$^{LSLH\text{-}RasG12V}$ allele that does not allow H-Ras^{G12V} expression are indicated. Note the disappearance of the recombined K-*Ras*$^{H\text{-}RasG12V}$ allele in lung but not thymus tissue. Lung tissue from mice treated with trametinib also retains the recombined K-*Ras*$^{H\text{-}RasG12V}$ allele. **B,** Relative expression levels of *p16Ink4a* and *p19Arf* mRNAs in total lung extracts from K^{V12};hUBC-CreERT2$^{+/T}$ (K^{V12}; red bars; $n = 3$) or $K^{HRasV12}$;hUBC-CreERT2$^{+/T}$ ($K^{HRasV12}$; blue bars; $n = 3$) mice exposed to tamoxifen diet for the indicated time, as determined by qRT-PCR analysis. GAPDH expression levels were used for normalization. Data, mean ± SD. ***, $P < 0.001$ (unpaired Student *t* test).

in MEFs. Previous studies have shown that overexpression of these oncoproteins in MEFs readily induced OIS (31). However, when they were expressed from their own endogenous promoters, they failed to induce OIS (16, 17). We induced expression of either K-Ras^{G12V} or H-Ras^{G12V} oncoproteins by infecting immortalized K^{V12} and $K^{HRasV12}$ MEFs with Adeno-Cre particles, respectively. As expected, K-Ras^{G12V} expression did not cause significant changes in downstream signaling (Fig. 7A). In contrast, expression of H-Ras^{G12V} resulted in a sustained increase in the phosphorylation of the downstream substrates pErk and pAkt (Fig. 7A). Moreover, whereas K-Ras^{G12V} expression had no detectable effects on proliferation, expression of H-Ras^{G12V} effectively induced OIS, leading to complete cessation of cell proliferation and SA-β-Gal expression (Fig. 7B and C).

H-Ras^{G12V} expressing MEFs displayed increased levels of p53 (Fig. 7A). Yet, efficient depletion of p53 by short hairpin RNAs had no effect on cell-cycle arrest or induction of senescence, indicating that abrogation of p53 expression was not sufficient to overcome H-Ras^{G12V}–induced OIS (Supplementary Fig. S7AC). Likewise, we observed no significant increase in the expression levels of p16INK4a. However, ectopic expression of adenoviral E1A, an oncoprotein known to target the p53 and Rb pathways (32), was able to bypass OIS and to restore efficient proliferation of MEFs (Fig. 7B and C; Supplementary Fig. S7D). Furthermore, E1A cooperated with H-Ras^{G12V}, but not with K-Ras^{G12V}, to transform immortal MEFs (Fig. 7D; Supplementary Fig. S7E). In an effort to provide a mechanistic explanation for the dramatic differential effects induced by the K-Ras^{G12V} versus the H-Ras^{G12V} oncoproteins when expressed from the same locus, we established their relative levels of expression using label-free quantification techniques. As illustrated in Fig. 7E, H-Ras^{G12V} was more efficiently expressed (about 2.5-fold) than K-Ras^{G12V}.

To determine whether these minor differences might be responsible for the drastically differential outputs, we decided to explore how differential expression levels of the same oncoprotein, H-Ras^{G12V}, affected the biological behavior of MEFs. Whereas H-Ras^{G12V} expressed from its own promoter had no effect of MEF properties, including immortalization, proliferation, or senescence (17), H-Ras^{G12V} expression from the K-*Ras* promoter in $K^{HRasV12}$ led to rapid OIS (Fig. 7B and C). Western blot analysis revealed that the amount of H-Ras protein (both H-Ras and H-Ras^{G12V}) in $K^{HRasV12}$ MEFs was 3-fold higher than in H-*Ras*$^{G12V/G12V}$ MEFs (Fig. 7F). As $K^{HRasV12}$ MEFs also express a wild-type H-Ras protein from its endogenous locus, the amount of H-Ras^{G12V} expressed from the K-*Ras* locus in $K^{HRasV12}$ MEFs compared with that expressed from its own locus in H-*Ras*$^{G12V/G12V}$ MEFs is a mere 2-fold higher (1.9 ± 0.7) than that expressed from its own locus. These observations establish that relatively subtle increases in the levels of expression of the H-Ras^{G12V} oncoprotein can result in dramatically different biological consequences.

Discussion

Early genetic studies revealed that the three *Ras* loci have different biological properties. Whereas K-*Ras* is essential for embryonic development, H-*Ras* and N-*Ras* are dispensable (5–7). To determine whether these differences are due to the

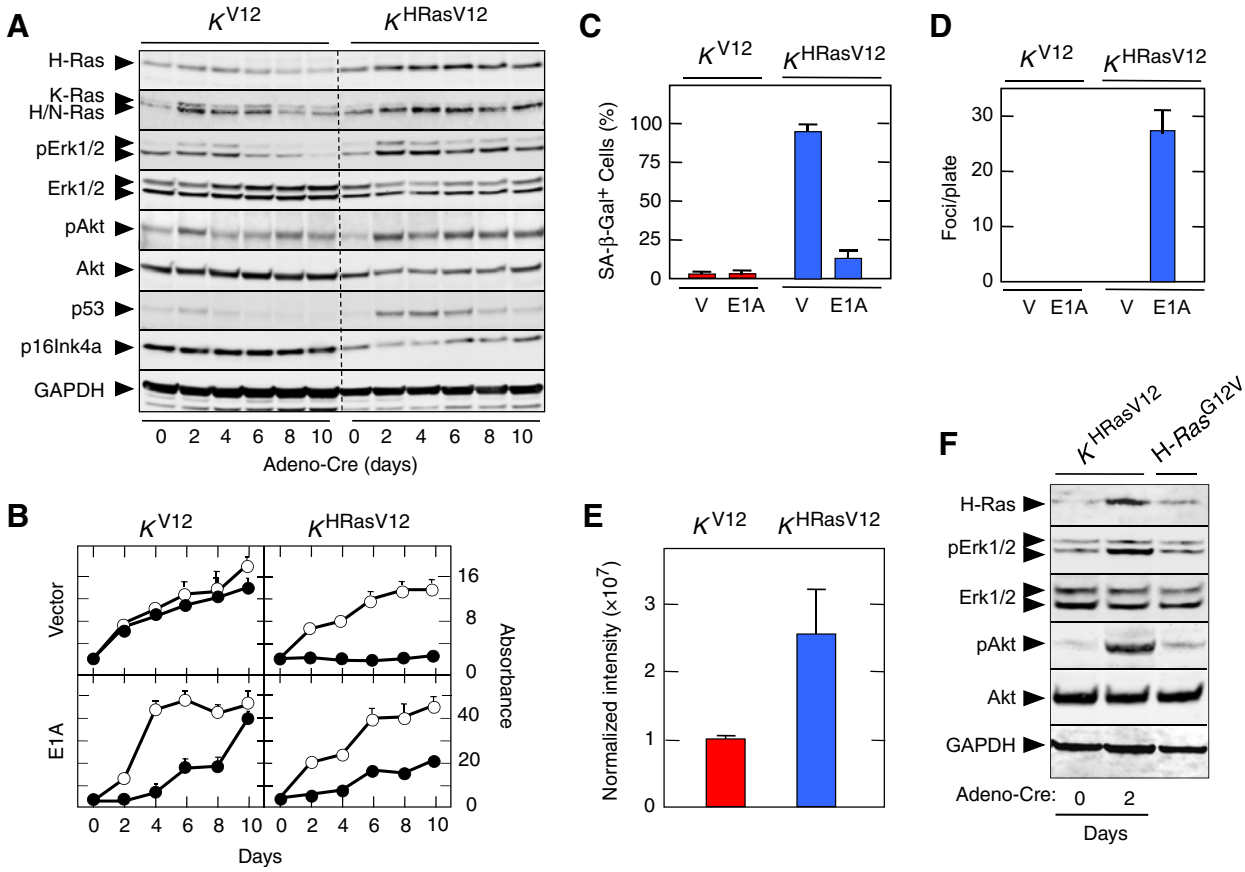

Figure 7.

H-Ras^{G12V}, but not K-Ras^{G12V}, expressed from the K-*Ras* locus induces senescence in MEFs. **A,** Western blot analysis of the indicated proteins expressed in K^{V12} or $K^{HRasV12}$ MEFs infected with Adeno-Cre particles for the indicated time. GAPDH expression served as a loading control. **B,** Growth curve of K^{V12} or $K^{HRasV12}$ MEFs infected with Adeno-GFP (open circles) or Adeno-Cre particles (closed circles) for the indicated time after stable infection with empty retroviruses (vector) or retroviruses expressing the Ad5 E1A oncoprotein (E1A). Data, mean ± SD. **C,** Percentage of SA-β-Gal–positive cells in K^{V12} or $K^{HRasV12}$ MEFs stably infected with empty retroviruses (V) or retroviruses expressing the Ad5 E1A oncoprotein (E1A) 4 days after infection with Adeno-Cre particles. Data, mean ± SD. ***, $P < 0.001$ (unpaired Student *t* test). **D,** Focus formation in K^{V12} or $K^{HRasV12}$ MEFs stably infected with empty retroviruses (V) or retroviruses expressing Ad5 E1A (E1A) 14 days after infection with Adeno-Cre particles. Data, mean ± SD. ***, $P < 0.001$ (unpaired Student *t* test). **E,** Relative quantification of the levels of expression of the K-Ras^{G12V} and H-Ras^{G12V} oncoproteins by label-free quantification in K^{V12};hUBC-CreERT2$^{+/T}$ (red bars; $n = 3$) or $K^{HRasV12}$;hUBC-CreERT2$^{+/T}$ MEFs (blue bars; $n = 3$) 4 days after infection with Adeno-Cre particles. The tryptic peptide LVVVGAVGVGK was used to detect expression of K-Ras^{G12V} and H-Ras^{G12V} proteins. Data, mean ± SD. **F,** Western blot analysis of H-Ras protein expression (H-Ras and H-Ras^{G12V}) driven by the K-*Ras* locus in $K^{HRasV12}$ MEFs upon infection with Adeno-Cre particles for the indicated time and by the H-*Ras* locus in H-*Ras*^{G12V} MEFs. Expression of Ras effector proteins pErk1/2, Erk1/2, pAkt, and Akt was also analyzed. GAPDH expression served as a loading control.

intrinsic properties of the different Ras protein isoforms or their pattern of expression, Potenza and colleagues modified the endogenous K-*Ras* alleles so they direct the synthesis of H-Ras instead of K-Ras proteins (8). These mice developed to adulthood, indicating that H-Ras could effectively compensate for the absence of the K-Ras proteins. Yet, these mice displayed cardiovascular defects, including dilated cardiomyopathy associated with arterial hypertension, attributed to the lack of K-Ras proteins in heart tissue (8). However, as illustrated in this study, these cardiovascular defects were a direct consequence of the overexpression of H-Ras proteins, as these mice carry four H-Ras–expressing alleles, two endogenous H-*Ras* alleles, and two HrasKI alleles. Indeed, elimination of the endogenous H-*Ras* alleles completely prevented these cardiovascular defects. Moreover, HrasKI;H-*Ras*$^{-/-}$ mice appear to be completely normal, indicating that the H-Ras and K-Ras proteins are fully bioequivalent, at least under normal homeostatic conditions. These observations are surprising considering the different properties of the H-Ras and K-Ras proteins in subcellular transport, posttranslational processing, and localization within the plasma membrane (3, 4). Whether their differential properties may play a role under stress conditions remains to be determined.

The intense focus on RAS biology is due, at least in part, to their involvement in human cancer. Over the years, scientists have been baffled by the distinct incidence of the various *RAS* oncogenes in tumors (9). In an attempt to shed some light on this issue, we expanded the early work of Potenza and colleagues (8), by generating a new conditional mouse strain, $K^{HRasV12}$, that expresses the H-Ras^{G12V} oncoprotein from the endogenous K-*Ras* locus. Germline expression of H-Ras^{G12V} from its own locus had no significant effect on embryonic development. Yet, these animals displayed facial and cardiovascular defects reminiscent of patients with

Costello syndrome (17, 18). However, germline expression of H-Ras^{G12V} from the endogenous K-*Ras* locus led to early embryonic death at a time similar to that observed for embryos expressing an endogenous K-Ras^{G12V} oncoprotein (16). Thus, expression of K-Ras and H-Ras oncoproteins from the K-*Ras* locus is equally deleterious for embryonic development. These observations illustrate that the viability of H-*Ras*$^{+/G12V}$ and H-*Ras*$^{G12V/G12V}$ mice must be due to a more restricted pattern of expression, lower expression levels or a combination of both (17, 18).

Expression of K-Ras^{G12V} in embryonic acinar cells resulted in the formation of low- and high-grade PanIN lesions and occasional PDAC tumors (24). Expression of the H-Ras^{G12V} oncoprotein from the K-*Ras* locus also resulted in the formation of low- and high-grade PanIN lesions albeit at lower frequencies, with no detectable PDAC tumors, at least by one year of age. Whether the high-grade PanINs will eventually progress to yield PDAC tumors in older animals remains to be determined. Recent studies have indicated that K-Ras^{G12V}, but not H-Ras^{G12V}, promotes tumor formation by suppressing noncanonical Wnt signaling (33). This property was used to repress the transforming activity of K-Ras^{G12V} in pancreatic xenograft tumor models with prostratin, a PKC activator (33). It will be interesting to explore whether this natural product has differential activity in pancreatic lesions driven by K-Ras^{G12V} and H-Ras^{G12V} oncoproteins.

Ubiquitous expression of H-Ras^{G12V} in adult $K^{HRasV12}$ mice led to a variety of tumors, mainly papillomas and hematopoietic malignancies. More importantly, the pattern of tumors observed in these mice was significantly different to that present in K^{V12} animals, thus indicating that H-Ras^{G12V} and K-Ras^{G12V} oncoproteins have different transforming capabilities in different tissues. Tamoxifen-treated adult $K^{HRasV12}$;hUBC-CreERT2$^{+/T}$ mice developed hematologic malignancies not observed in K^{V12};hUBC-CreERT2$^{+/T}$ animals, including myeloproliferative disease, a disease that resulted from expansion of the CMP population, as well as T-ALL. Previous studies have reported that expression of a resident K-*Ras*^{G12D} oncogene in the hematopoietic compartment caused fatal myeloproliferative disease (34, 35) as well as T-ALL upon bone marrow transplantation (36). In these studies, however, K-Ras^{G12D} expression was induced by an Mx1-Cre transgene known to express low levels of Cre recombinase activity during embryonic development. Thus, it is possible that these different results might be due to the differential susceptibility of embryonic hematopoietic precursors to K-Ras oncoproteins.

On the contrary, some tissues are susceptible to K-Ras^{G12V}, but not to H-Ras^{G12V}–induced neoplastic lesions, such as the lung alveoli and the stomach epithelium. The lack of lung tumors in $K^{HRasV12}$ mice appears to be a consequence of overactivation of the MAPK signaling cascade by the H-Ras^{G12V} oncoprotein. Indeed, H-Ras^{G12V} expression in type II alveolar cells of $K^{HRasV12}$ mice induced a significantly more robust phosphorylation of the Erk kinases than that observed upon induction of the K-Ras^{G12V} oncoprotein in K^{V12} animals. This increased signaling induced a noncanonical, senescence-like state that prevented proliferation of the H-Ras^{G12V}–expressing lung alveolar cells. Ablation of p53 in $K^{HRasV12}$ mice resulted in limited induction of hyperplastic lesions along with few adenomas, but not in overt lung tumor development, thus indicating that the senescence-like state was only partially mediated by p53. These senescent H-Ras^{G12V}–expressing cells are short lived as they could no longer be detected 8 weeks after the induction of H-Ras^{G12V} expression. Likewise, IHC examination of lung tissue of $K^{HRasV12}$ mice 2 weeks after the induction of H-Ras^{G12V} expression revealed a drastic reduction in the number of pErk-positive cells. The fate of these cells remains unclear, although the absence of active caspase-3 expression suggests that they did not undergo apoptosis. Finally, exposure of $K^{HRasV12}$ mice to the MEK inhibitor trametinib prevented elimination of the H-Ras^{G12V}–expressing cells, thus providing further evidence that the senescence-like state of these H-Ras^{G12V}–expressing lung cells was due to excessive MAPK signaling.

It has been proposed that the abundance of Ras isoforms can be affected by differences in protein translation efficiency (37). K-*Ras* mRNA is less efficiently translated than H-*Ras* due to the preferential usage of rare codons (37). Germline replacement of rare codons in the K-*Ras* locus resulted in mice that expressed higher levels of K-Ras proteins (38). Interestingly, these mice displayed increased resistance to urethane-mediated carcinogenesis, suggesting that increased levels of K-Ras oncoproteins had adverse effects on lung tumorigenesis (38). Whether these observations were due to the induction of a senescence-like state as described here for the H-Ras^{G12V} oncoprotein remains to be determined. Precise quantitative analysis of the relative amounts of H-Ras^{G12V} and K-Ras^{G12V} proteins in lung tissue revealed that H-Ras^{G12V} was present at 5-fold higher levels than K-Ras^{G12V}. Thus, it is possible that these oncoproteins may have similar signaling properties and their differential effects in lung tissue could be primarily due to quantitative differences in their levels of expression. Whether the differential results obtained in hematopoietic cells in which only H-Ras^{G12V} was capable of inducing tumors is also due to quantitative differences remains to be determined. For instance, it is possible that the hematopoietic precursors responsible for initiating myeloproliferative disease and T-ALL may require higher levels of MAPK signaling, such as those provided by H-Ras^{G12V} expression. Yet, at this time, we cannot rule out that the H-Ras^{G12V} and K-Ras^{G12V} oncoproteins may utilize differential signaling pathways in these hematopoietic cells.

Previous studies have illustrated the presence of H-*Ras* oncogenes in lung tumors of HrasKI mice exposed to urethane (39). Indeed, these mice developed more lung tumors than wild-type animals exposed to the same carcinogenic insult, a result attributed to the frequent activation of H-*Ras* oncogenes (39). This apparent conundrum could be explained by the presence of lower levels of H-Ras protein in H*ras*KI mice. Indeed, H*ras*KI is a chimeric allele made of H-*Ras* and K-*Ras* sequences that contains K-*Ras*–derived rare codons in two of the four coding exons. This fact may result in limited translation efficiency (9, 36, 37). Thus, H*ras*KI mice may express lower levels of H-Ras as compared with those present in $K^{HRasV12}$ animals that exclusively use H-*Ras*–derived codons. Alternatively, urethane may induce mutations and/or epigenetic alterations that prevent the development of the senescence-like state induced by H-Ras^{G12V} expression in $K^{HRasV12}$ mice.

Finally, *in vitro* studies also provided strong support for a direct relationship between H-Ras^{G12V}- and K-Ras^{G12V}–induced MAPK signaling and biological output. Expression of a resident K-Ras^{G12V} oncoprotein in primary MEFs led to immediate immortalization bypassing the replication-induced senescence characteristic of wild-type cells (16). In contrast, expression of the H-Ras^{G12V} oncoprotein from the K-*Ras* locus resulted in canonical OIS leading to complete cessation of cell proliferation and expression of SA-β-Gal. This senescence phenotype

was accompanied by a robust increase in the phosphorylation of Erk1/2 and Akt. Quantitative analysis of the relative levels of expression of the H-Ras^{G12V} and K-Ras^{G12V} oncoproteins in $K^{HRasV12}$ and K^{V12} MEFs, respectively, revealed 2.5-fold higher levels of expression of H-Ras^{G12V}, thus raising the possibility that differences other than levels of expression may account for the differential biological outputs induced by these oncoproteins. However, comparative analysis of the levels of expression of H-Ras^{G12V} in $K^{HRasV12}$ MEFs, which induces irreversible OIS versus H-Ras$^{G12V/G12V}$ MEFs in which there are no significant biological changes, revealed a meager 2-fold difference in its levels of expression. Thus, minor changes in the levels of expression of the H-Ras^{G12V} oncoprotein can induce significantly different outputs. These results, taken together, underscore the need to better understand the molecular mechanisms that regulate the intensity of MAPK signaling to control the detrimental effects induced by Ras oncoproteins during neoplastic development.

It is difficult to reckon why the wild-type H-Ras and K-Ras isoforms are bioequivalent in spite of their differential properties relating to cellular trafficking, posttranslational processing, and subcellular localization, whereas their oncogenic counterparts display differential transforming properties. It is conceivable that cells tolerate an ample range of Ras signaling during normal homeostasis providing that the differential signaling intensities between the different Ras isoforms stay below a critical threshold. In contrast, elevated signaling induced by Ras oncoproteins may activate "emergency" signals that either result in the activation of negative feedback loops or in the induction of OIS, ultimately leading to cell death. Activation of OIS and/or feedback loops might be cell type dependent, leading to the manifestation of different phenotypes ranging from senescence to malignant transformation. Finally, it should be noted that our observations do not eliminate the possibility that different oncogenic Ras isoforms may also engage differential signaling pathways. Understanding the differential outputs of H-*Ras* and K-*Ras* oncogenes in different cell types will require a more precise knowledge of the molecular mechanisms that control their key effector pathways.

Disclosure of Potential Conflicts of Interest

No potential conflicts of interest were disclosed.

Authors' Contributions

Conception and design: M. Drosten, X.R. Bustelo, C. Guerra, M. Barbacid
Development of methodology: M. Drosten, M.T. Blasco, H.K.C. Jacob, X.R. Bustelo, M. Barbacid
Acquisition of data (provided animals, acquired and managed patients, provided facilities, etc.): M. Drosten, L. Simón-Carrasco, C.G. Lechuga, S. Fabbiano, N. Potenza, X.R. Bustelo
Analysis and interpretation of data (e.g., statistical analysis, biostatistics, computational analysis): M. Drosten, L. Simón-Carrasco, I. Hernández-Porras, M.T. Blasco, H.K.C. Jacob, S. Fabbiano, X.R. Bustelo, C. Guerra, M. Barbacid
Writing, review, and/or revision of the manuscript: M. Drosten, X.R. Bustelo, C. Guerra, M. Barbacid
Study supervision: M. Drosten, X.R. Bustelo, C. Guerra, M. Barbacid
Other (designed and performed experimental work): I. Hernández-Porras
Other (mass spectrometric analyses): H.K.C. Jacob

Acknowledgments

We thank Alan Balmain (UCSF) for stimulating discussions and for critically reading the manuscript. We also thank Marta San Roman, Raquel Villar, Beatriz Jiménez, Nuria Cabrera, Patricia Villanueva, and Jennifer Condo for excellent technical assistance. We value the support of Juan Antonio Cámara and Francisca Mulero (Molecular Imaging Core Unit, CNIO) for the echocardiographic analyses, Alba de Martino (Histopathology Core Unit, CNIO) for her help with mouse histopathology, as well as Eduardo Zarzuela and Javier Muñoz (Proteomics Core Unit, CNIO) for mass spectrometric analyses.

Grant Support

This work was supported by grants from the European Research Council (ERC-AG/250297-RAS AHEAD), EU-Framework Programme (LSHG-CT-2007-037665/CHEMORES, HEALTH-F2-2010-259770/LUNG-TARGET, and HEALTH-2010-260791/EUROCANPLATFORM), Spanish Ministry of Economy and Competitiveness (SAF2011-30173 and SAF2014-59864-R), Autonomous Community of Madrid (S2011/BDM-2470/ONCOCYCLE to M. Barbacid), Castilla-León Autonomous Government (CSI101U13, BIO/SA01/15), the Spanish Ministry of Economy and Competitiveness (SAF2012-31371, RD12/0036/0002), Worldwide Cancer Research (14-1248), the Solórzano Foundation, and the Ramón Areces Foundation (X.R. Bustelo). Spanish government–sponsored funding to X.R. Bustelo is partially supported by the European Regional Development Fund. M. Barbacid is the recipient of an Endowed Chair from the AXA Research Fund.

The costs of publication of this article were defrayed in part by the payment of page charges. This article must therefore be hereby marked *advertisement* in accordance with 18 U.S.C. Section 1734 solely to indicate this fact.

Received October 27, 2016; accepted October 28, 2016; published OnlineFirst November 21, 2016.

References

1. Malumbres M, Barbacid M. RAS oncogenes: the first 30 years. Nat Rev Cancer 2003;3:459–65.
2. Karnoub AE, Weinberg RA. Ras oncogenes: split personalities. Nat Rev Mol Cell Biol 2008;9:517–31.
3. Cox AD, Der CJ, Philips MR. Targeting RAS membrane association: back to the future for anti-RAS drug discovery? Clin Cancer Res 2015; 21:1819–27.
4. Prior IA, Hancock JF. Ras trafficking, localization and compartmentalized signalling. Semin Cell Dev Biol 2012;23:145–53.
5. Esteban LM, Vicario-Abejón C, Fernández-Salguero P, Fernández-Medarde A, Swaminthan N, Yienger K, et al. Targeted genomic disruption of H-ras and N-ras, individually or in combination, reveals the dispensability of both loci for mouse growth and development. Mol Cell Biol 2001; 21:1444–52.
6. Johnson L, Greenbaum D, Cichowski K, Mercer K, Murphy E, Schmitt E, et al. K-ras is an essential gene in the mouse with partial functional overlap with N-ras. Genes Dev 1997;11:2468–81.
7. Koera K, Nakamura K, Nakao K, Miyoshi J, Toyoshima K, Hatta T, et al. K-ras is essential for the development of the mouse embryo. Oncogene 1997;15:1151–9.
8. Potenza N, Vecchione C, Notte A, De Rienzo A, Rosica A, Bauer L, et al. Replacement of K-Ras with H-ras supports embryonic development despite inducing cardiovascular pathology in adult mice. EMBO Rep 2005; 6:432–7.
9. Prior IA, Lewis PD, Mattos CA. A comprehensive survey of Ras mutations in cancer. Cancer Res 2012;72:2457–67.
10. Tidyman WE, Rauen KA. The RASopathies: developmental syndromes of Ras/MAPK pathway dysregulation. Curr Opin Genet Dev 2009; 19:230–6.
11. Aoki Y, Niihori T, Inoue S, Matsubara Y. Recent advances in RASopathies. J Hum Genet 2016;61:33–9.
12. Gripp KW, Lin AE. Costello syndrome: a Ras/mitogen activated protein kinase pathway syndrome (rasopathy) resulting from HRAS germline mutations. Genet Med 2012;14:285–92.

13. Aoki Y, Niihori T, Kawame H, Kurosawa K, Ohashi H, Tanaka Y, et al. Germline mutations in HRAS proto-oncogene cause Costello syndrome. Nat Genet 2005;37:1038–40.
14. Kratz CP, Schubbert S, Bollag G, Niemeyer CM, Shannon K, Zenker M. Germline mutations in components of the Ras signaling pathway in Noonan syndrome and related disorders. Cell Cycle 2006; 5:1607–11.
15. Tuveson DA, Shaw AT, Willis NA, Silver DP, Jackson EL, Chang S, et al. Endogenous oncogenic K-ras(G12D) stimulates proliferation and widespread neoplastic and developmental defects. Cancer Cell 2004;5:375–87.
16. Guerra C, Mijimolle N, Dhawahir A, Dubus P, Barradas M, Serrano M, et al. Tumor induction by an endogenous K-ras oncogene is highly dependent on cellular context. Cancer Cell 2003;4:111–20.
17. Schuhmacher A J, Guerra C, Sauzeau V, Cañamero M, Bustelo XR, Barbacid M. A mouse model for Costello syndrome reveals an Ang II-mediated hypertensive condition. J Clin Invest 2008;118:2169–79.
18. Chen X, Mitsutake N, LaPerle K, Akeno N, Zanzonico P, Longo VA, et al. Endogenous expression of HrasG12V induces developmental defects and neoplasms with copy number imbalances of the oncogene. Proc Natl Acad Sci USA 2009;106:7979–84.
19. Hernández-Porras I, Fabbiano S, Schuhmacher AJ, Aicher A, Cañamero M, Cämara JA, et al. K-RasV14I recapitulates Noonan syndrome in mice. Proc Natl Acad Sci USA 2014;111:16395–400.
20. Jonkers J, Meuwissen R, Van der Gulden H, Peterse H, van der Valk M, Berns A. Synergistic tumor suppressor activity of BRCA2 and p53 in a conditional mouse model for breast cancer. Nat Genet 2001;29:418–25.
21. Ruzankina Y, Pinzon-Guzman C, Asare A, Ong T, Pontano L, Cotsarelis G, et al. Deletion of the developmentally essential gene ATR in adult mice leads to age-related phenotypes and stem cell loss. Cell Stem Cell 2007;1: 113–26.
22. Guerra C, Schuhmacher AJ, Cañamero M, Grippo PJ, Verdaguer L, Pérez-Gallego L, et al. Chronic Pancreatitis is essential for induction of pancreatic ductal adenocarcinoma by K-Ras oncogenes in adult mice. Cancer Cell 2007;11:291–302.
23. Blasco RB, Francoz S, Santamaría D, Cañamero M, Dubus P, Charron J, et al. c-Raf, but not B-Raf, is essential for development of K-Ras oncogene-driven non-small cell lung carcinoma. Cancer Cell 2011; 19:652–63.
24. Itahana K, Campisi J, Dimri GP. Methods to detect biomarkers of cellular senescence: the senescence-associated β-Galactosidase assay. Methods Mol Biol 2007;371:21–31.
25. Drosten M, Sum EY, Lechuga CG, Simón-Carrasco L, Jacob HK, García-Medina R, et al. Loss of p53 induces cell proliferation via Ras-independent activation of the Raf/Mek/Erk signaling pathway. Proc Natl Acad Sci USA 2014;111:15155–60.
26. Lakso M, Pichel JG, Gorman JR, Sauer B, Okamoto Y, Lee E, et al. Efficient *in vivo* manipulation of mouse genomic sequences at the zygote stage. Proc Natl Acad Sci USA 1996;93:5860–5.
27. Mainardi S, Mijimolle N, Francoz S, Vicente-Dueñas C, Sánchez-García I, Barbacid M. Identification of cancer initiating cells in K-ras driven lung adenocarcinoma. Proc Natl Acad Sci USA 2014;111:255–60.
28. Wendorff AA, Koch U, Wunderlich FT, Wirth S, Dubey C, Brüning JC, et al. Hes1 is a critical but context-dependent mediator of canonical Notch signaling in lymphocyte development and transformation. Immunity 2010;33:671–84.
29. Cox J, Hein MY, Luber CA, Paron I, Nagaraj N, Mann M. Accurate proteome-wide label-free quantification by delayed normalization and maximal peptide ratio extraction, termed MaxLFQ. Mol Cell Proteomics 2014; 13:2513–26.
30. Wright CJ, McCormack PL. Trametinib: first global approval. Drugs 2013;73:1245–54.
31. Serrano M, Lin AW, McCurrach ME, Beach D, Lowe SW. Oncogenic ras provokes premature cell senescence associated with accumulation of p53 and p16INK4a. Cell 1997;88:593–602.
32. Frisch SM, Mymryk JS. Adenovirus-5 E1A: paradox or paradigm. Nat Rev Mol Cell Biol 2002;3:441–52.
33. Wang MT, Holderfield M, Galeas J, Delrosario R, To MD, Balmain A, et al. K-Ras promotes tumorigenicity through suppression of non-canonical Wnt signaling. Cell 2015;163:1237–51.
34. Braun BS, Tuveson DA, Kong N, Le DT, Kogan SC, Rozmus J, et al. Somatic activation of oncogenic Kras in hematopoietic cells initiates a rapidly fatal myeloproliferative disorder. Proc Natl Acad Sci U S A 2004;101:597–602.
35. Chan IT, Kutok JL, Williams IR, Cohen S, Kelly L, Shigematsu H, et al. Conditional expression of oncogenic K-ras from its endogenous promoter induces a myeloproliferative disease. J Clin Invest 2004;113:528–38.
36. Kindler T, Cornejo MG, Scholl C, Liu J, Leeman DS, Haydu JE, et al. K-RasG12D-induced T-cell lymphoblastic lymphoma/leukemias harbor Notch1 mutations and are sensitive to γ-secretase inhibitors. Blood 2008; 112:3373–82.
37. Lampson BJ, Pershing NL, Prinz JA, Lacsina JR, Marzluff WF, Nicchitta CV, et al. Rare codons regulate KRas oncogenesis. Curr Biol 2013;23:70–5.
38. Pershing NL, Lampson BL, Belsky JA, Kaltenbrun E, MacAlpine DM, Counter CM. Rare codons capacitate Kras-driven *de novo* tumorigenesis. J Clin Invest 2015;125:222–33.
39. To MD, Wong CE, Karnezis AN, Del Rosario R, Di Lauro R, Balmain A. Kras regulatory elements and exon 4A determine mutation specificity in lung cancer. Nat Genet 2008;40:1240–4.
40. Gao S, Ho D, Vatner DE, Vatner SF. Echocardiography in mice. Curr Protoc Mouse Biol 2011;1:71–83.